

INTERPARTICLE FORCES AND SUPERPLASTICIZERS IN CEMENT SUSPENSIONS

THÈSE N° 2040 (1999)

PRÉSENTÉE AU DÉPARTEMENT DE MATÉRIAUX

ÉCOLE POLYTECHNIQUE FÉDÉRALE DE LAUSANNE

POUR L'OBTENTION DU GRADE DE DOCTEUR ÈS SCIENCES

PAR

Robert Johann FLATT

Ingénieur chimiste diplômé EPF
de nationalité suisse et originaire de Bâle (BS)

acceptée sur proposition du jury:

Prof. H. Hofmann, directeur de thèse
Prof. L. Bergström, rapporteur
Prof. E. Brühwiler, rapporteur
Dr E. Gartner, rapporteur
Dr Y. Houst, rapporteur
Dr U. Mäder, rapporteur

Lausanne, EPFL
1999

<h2>Foreword</h2>

To my mother, for her courage in maintaining an outstanding moral and sense of humour, while suffering the constant progress of her PSP¹ over the past 15 years.

To my father and sister for the remarkable devotion and support they have shown during this period.

To my mother's family as well as to my father's family for their regular support and for their attitude in not judging our choices.

To the friends whose support has meant a lot to me. In particular: Alexandre, Brigitte, Catherine, Cathy, Eva, Fabian, Ion, Irina, Jérôme, Marilyn, Patrick, Olivier and Sandra.

And of course to Inma... my sunshine and personal expert art critic!

¹ Progressive Supranuclear Palsy, see http://www.ion.ucl.ac.uk/PSPeur/web_whatish.htm

Abstract

Placing of concrete requires much more water than the cement needs for its hydration. This results in a certain porosity in the hardened concrete, which facilitates chemical degradation of this material. By adding small amounts of polymeric admixtures, called superplasticizers, one can greatly decrease the amount of water required to obtain the desired workability and consequently the porosity, which improves durability.

Although these superplasticizers are widely used today, the mechanisms through which they act in concrete remain poorly understood. It nevertheless recognised that the origin of the effect, which superplasticizers have in concrete, comes from decreasing the attractive forces between cement particles. The effective volume of agglomerates and thereby the effective volume of solids in the suspension is decreased, which improves workability. Controlling and modifying interparticle forces has been for many years, and remains today, a topic of intense research in the field of colloids. Also, is it not surprising that many authors have attempted to apply this knowledge to explain the effect that superplasticizers have in concrete. They have thereby been able to identify different types of behaviour depending on the chemical nature of superplasticizers.

However, applying such concepts developed for colloids, to cement suspensions in which particle sizes are much larger presents many limitations. The main objective of this thesis has been to integrate these limitations, as rigorously as possible, while applying interparticle force concepts to cement suspensions.

In order to reach this objective, further development of current theoretical approaches had to be carried out. In particular, it was necessary to integrate the non-ideality of the thermodynamics of the aqueous phase of the cement suspension. These effects were integrated into the calculation of electrostatic and dispersion forces. In addition, we have taken into account the very large particle size distribution of cement, by determining the frequency of contacts between particles of different sizes. This allowed us to develop a quantitative relation between calculated interparticle forces and measured

yield stress of cement suspension. Although this approach still presents limitations, it is the first approach, at least for cement, which gives more than a qualitative link between rheology and interparticle forces.

These calculations could only be developed after experimental data had allowed attribution of the dispersing effect of superplasticizers exclusively to the adsorbed polymers. For this, we had to use, in addition to cement, inert model systems ($\text{Mg}(\text{OH})_2$ and MgO) in order not to superimpose to desagglomeration, the effect of modifying the on-going chemical reactions. The interest of these model systems over others is that they have a high isoelectric point (around pH 12) like cement. It is therefore possible to have both surface charge and pH similar to cement. This is important for adsorption and polymer conformation to be representative of cement suspensions.

We argue that the major effect of chemistry of cement suspensions is the coprecipitation or intercalation of the polymers during the formation of ettringite. This reaction reaches its maximum speed barely a few minutes after water is contacted with cement. It is why one observes much larger polymer consumption, when it is included in the mixing water. This has been often cited in literature, but was never developed in a satisfying way with respect to dispersion efficiency.

The calculation of interparticle forces, in a framework adapted to cement, as well as the identification of the reactions consuming superplasticizers, open new paths for the development of superplasticizers, which will offer higher performances for lower dosage. This should make the immediate cost of durable concrete more affordable, which is probably the best incentive to reduce the energy cost of the life service maintenance of concrete infrastructures.

Version abrégée

La mise en place d'un béton nécessite nettement plus d'eau que le ciment n'en requiert pour son hydratation. Il en résulte, dans le béton durci, une porosité finale qui facilite la dégradation chimique de ce matériau. En ajoutant de faibles quantités d'adjuvants polymériques, appelés superplastifiants, on peut nettement réduire la quantité d'eau nécessaire pour obtenir l'ouvrabilité désirée.

Bien qu'aujourd'hui les superplastifiants soient couramment utilisés, les mécanismes au travers desquels ils agissent dans le béton demeurent mal connus. On reconnaît néanmoins que l'origine de l'effet des superplastifiants dans le béton, vient d'une diminution des forces attractives entre les grains de ciment. Le volume effectif des agglomérats et donc le volume effectif de solide dans la suspension s'en trouve diminué, ce qui améliore la fluidité. L'étude du contrôle et la modification des forces interparticulaires est depuis nombreuses années, et encore aujourd'hui, l'objet d'intenses études dans le domaine des colloïdes. Aussi n'est-il pas étonnant que divers auteurs aient tentés d'appliquer ces notions à l'effet qu'on les superplastifiants dans le béton. Ils ont ainsi pu identifier différents types de comportement selon la nature chimique des superplastifiants.

Cependant, l'application de ces notions, développées pour des colloïdes, à des suspensions de ciments dans lesquelles les particules sont nettement plus grandes, présente de nombreuses limitations. L'objectif principal de cette thèse a été précisément d'intégrer, le plus rigoureusement possible, ces limites lors de l'application des concepts de forces interparticulaires aux suspensions de ciment.

Pour cela de nombreux développements ont dû être effectués sur le plan théorique. En particulier il a fallu intégrer la non-idéalité de la thermodynamique de la phase aqueuse de la suspension de ciment. Ces effets ont été intégrés dans les calculs des forces électrostatiques ainsi que dans les forces de dispersion. De plus, nous avons pris en compte la très large distribution de taille des particules de ciment, en déterminant la fréquence de contact en particules de tailles différentes. Cela nous a permis de développer une relation quantitative entre les forces interparticulaires calculées et les seuils d'écoulement mesurés des suspensions de ciment. Bien que présentant encore de nombreuses

limitations, ceci est la première approche, au moins pour le ciment, qui donne plus qu'une relation qualitative entre forces interparticulaires et rhéologie.

Ces calculs n'ont pu être développés qu'après qu'un travail expérimental ait permis d'attribuer l'effet dispersant des superplastifiants de manière exclusive aux polymères adsorbés. Pour cela nous avons dû utiliser, en plus du ciment, des systèmes modèles inertes ($\text{Mg}(\text{OH})_2$ et MgO) afin de ne pas superposer à la désagglomération, la modification des réactions chimiques en cours. L'intérêt de ces systèmes modèles, par rapport à d'autres, est qu'ils ont un point isoélectrique élevé (environ pH 12), comme le ciment. Il est donc possible d'obtenir à la fois des charges de surface et des potentiels de surface similaires à ceux du ciment. Ceci est important pour que l'adsorption et la conformation des polymères soient représentatives de celles dans les suspensions de ciment.

Nous argumentons qu'un effet majeur de la chimie dans les suspensions de ciment est la coprécipitation ou l'interacallage du polymère lors de la formation d'ettringite. Cette réaction atteint sa vitesse maximale à peine quelques minutes après le contact entre l'eau et le ciment. C'est pourquoi on observe une consommation nettement plus importante de polymère, lorsque celui-ci est ajouté dans l'eau de gâchage. Cet effet a été souvent mentionné dans la littérature antérieure, mais n'a jamais été développé de manière satisfaisante par rapport à l'efficacité de dispersion.

Le calcul des forces interparticulaires, dans un cadre adapté au ciment, ainsi que l'identification de réactions de consommation des superplastifiants, ouvrant de nouvelles voies pour le développement de superplastifiants qui pourront offrir des performances accrues à des dosages inférieurs. Cela devrait réduire le coût immédiat d'un béton durable, ce qui est probablement le meilleur moyen de réduire le coût énergétique de la maintenance des ouvrages en béton.

Acknowledgements

I would like to thank the following people for their contributions to this work:

- Professor Heinrich Hofmann, my thesis supervisor, for his very open attitude, for making it possible for me to present my work in international conferences. These were very intellectually stimulating experiences, which have opened me many doors for the future. I also want to express my gratitude to Professor Hofmann for trusting my judgement, when I suggested setting up undergraduate projects for developing repair materials, including superplasticizers, for the roman mosaics I had worked on prior to starting my thesis.
- Dr. Yves Houst for the confidence he placed in my work and the help he brought in particular from his wide knowledge of cement as well as for his great availability and for inciting me to submit my work for international conferences. I must also thank him for thinking up a project in which it was possible to perform very interesting fundamental work with practical relevance.
- Dr. Paul Bowen for numerous very challenging discussions, for his insightful remarks always straight to the point. His excellent understanding of colloidal science and constant encouragement for me to lead a fundamental study have undoubtedly brought an additional dimension to my thesis.
- Mr. Fred Girardet from the Expert Center for Conservation of the Built Cultural Heritage, for his extreme availability, the immense help he brought for the projects applying superplasticizers to repair materials, for his incredible capacity of asking immediately the most pertinent questions whatever the subject may be.
- Mr. Theodore Bürge, Dr. Urs Maeder, Mr. Ueli Sulser and Dr. Jürg Widmer from Sika A.G. for the fruitful discussions during meetings. In particular, I would like to thank Mr. Ueli Sulser for all the time he spend while we were setting up the use of HPLC to analyse the adsorption of polymers.

-
- LTP members for much help in different tasks. In particular: Dr. Devrim Akyüz for the hot press, Ms. Elisabeth Burdet for settling administration issues, Dr. Raymond Houriet for FTIR, Ms. Estelle Pingoud for FTIR and zeta potential, Mr. Carlos Morais for zeta potential and polymer adsorption, Mr. Raymond Oesch for specific surfaces and polymer adsorption, Mr. Christian Pittet for mechanical testing, Dr. Martin Staiger for particle size determination, Mr. Stéphane Terrazzoni for spray drying, Dr. Pascale van Landuyt for rheology and of course Ms. Cécile Grace for livening up the weakly coffee club, croissant, pig-outs, breaks !
 - Dr. Olivier Renaud for spending many hours helping me to develop the most appropriate statistical treatment of my experimental data.
 - Mr. Christian Pignat for programming the identification of the frequency of interactions between particles of different sizes.
 - Dr. Parviz Navi for many fruitful discussions on the possibility of using computer simulations for cementitious systems.
 - The staff of the Material Science Department for assistance in many occasions and in particular: Mr. Louis-Henri Masson for the producing some special pieces for the rheometer, Dr. Moeckli for XRD use and interpretation and Mr. Jean-Daniel Neuvecelle for atomic absorption spectroscopy and XRF. Mr. Brian Senior from the interdepartmental centre for electron microscopy for SEM pictures.
 - Dr. Clarissa Ferraris from the NIST who brought a wind of enthusiasm into the lab and also stimulated much thought through discussions during her stay at LTP.
 - Professors Lennart Bergström from YKI, Jacob Klein from Weizmann Institute, Bill Russel from Princeton University and Wolfgang Sigmund from the University of Florida, who all contributed through discussion and email to my deeper understanding of colloidal science.
 - The following students for their great motivation, excellent work and intellectually stimulating questions and observations during their undergraduate projects: Mr. Jean François Despois and Mr. Collin Sanctuary (Determination of the optimal conservation conditions for the roman mosaics of Orbe), Mr. Stéphane Essade and Mr. Vincent von Niderhausern (*In Situ* conservation of the roman mosaics at the villa of Boscéaz {Orbe, Switzerland}: preparation if an injectable repair mortar), Mr. Yannick Huet and Mr. Benoit Petit (Elaboration of an injectable mortar for the

restoration of a roman mosaic of the IIIrd century) and Mr. Luciano Perez (Synthesis of a γ - $2\text{CaO}.\text{SiO}_2$ powder).

- Dr. Denis Weidmann, archeologist for the État de Vaud, for supporting the development on tailored repair mortars for the mosaics of Orbe; Mathias Kaufmann and Verena Fischbacher for assistance with the *in situ* testing of the products.
- Dr. Bertrand Fritz from the *Centre de Géochimie de la Surface*, CNRS, Strasbourg, for giving me access to the thermodynamic simulation code KINDIS developed in his group.
- Sika A.G., the Swiss Commission for Technology and Innovation (CTI) and the EPFL for financial support.

The whole LTP deserves a round of applause for working through *Colloidal Dispersions*, week after week!

Finally, I would like to thank the members of my thesis Jury for reviewing this work: Professor Lennart Bergström from YKI (Stockholm, Sweden), Dr. Ellis Gartner from Lafarge S.A. (St. Quentin Fallavier, France), Dr. Urs Mäder from Sika A.G. (Zürich, Switzerland), Professor Eugen Brühwiler from MCS-DGC at EPFL, Professor Heinrich Hofmann and Dr. Yves Houst from LTP. I am also thankful to Professor Andreas Mortensen, from LMM at EPFL, who was the president of this Jury.

Table of Contents

FOREWORD	3
ABSTRACT	5
VERSION ABRÉGÉE	7
ACKNOWLEDGEMENTS	9
TABLE OF CONTENTS	13
CHAPTER 1 INTRODUCTION	1
CHAPTER 2 STRATEGY	9
2.1 EXPECTED MECHANISMS	9
2.2 MODEL SUSPENSIONS	10
2.3 ADSORPTION	12
2.4 RHEOLOGY	13
2.5 STABILITY CALCULATIONS	14
2.6 CHEMICAL EFFECTS	15
CHAPTER 3 THEORETICAL CONSIDERATIONS	17
3.1 CHEMISTRY OF CEMENTICIOUS SUSPENSIONS	18

3.1.1	<i>Composition</i>	18
3.1.2	<i>Chemical description of hydration</i>	20
3.1.3	<i>Supersaturation regions</i>	22
3.1.4	<i>Ion activity models</i>	23
3.1.5	<i>Ionic species</i>	24
3.1.6	<i>Implications for cement suspensions</i>	26
3.2	HYDRODYNAMICS.....	26
3.2.1	<i>The Navier-Stokes equation</i>	27
3.2.2	<i>Stokes flow</i>	29
3.2.3	<i>Single sphere dynamics</i>	30
	Steady state motion of single sphere.....	30
	Transient motion of single sphere.....	31
3.2.4	<i>Dynamics of two spheres</i>	32
	Shearing motion of rigid surfaces.....	33
	Squeezing motion of rigid spheres.....	34
3.3	RHEOLOGY	35
3.3.1	<i>Basis of rheology</i>	35
3.3.2	<i>Shear rate and shear controlled rheometers</i>	36
3.3.3	<i>Some rheological behaviours</i>	37
3.3.4	<i>Rheology of viscoelastic fluids</i>	38
3.3.5	<i>Other testing methods</i>	40

3.3.6	<i>Selection of a rheometer for measuring cement pastes.....</i>	40
3.4	BROWNIAN MOTION.....	41
3.5	SEDIMENTATION.....	42
3.5.1	<i>General realtions</i>	42
3.5.2	<i>Sedimentation in cement suspensions.....</i>	43
3.6	DISPERSION FORCES.....	44
3.6.1	<i>Origin of dispersion forces</i>	44
3.6.2	<i>Microscopic theory.....</i>	44
3.6.3	<i>Continuum theory.....</i>	45
	Formulation.....	45
	Geometry	46
	Dielectric Properties.....	47
	Screening and Retardation in cement suspensions	49
	Summary of continuum theory implications.....	50
3.6.4	<i>Cement like suspensions</i>	50
	Effective Hamaker constants.....	50
3.6.5	<i>Expression for dispersion force.....</i>	53
3.7	ELECTROSTATIC FORCES.....	60
3.7.1	<i>Situation in vacuum</i>	60
3.7.2	<i>Situation in a dielectric.....</i>	61
3.7.3	<i>Origin of surface charge and Boltzmann distribution.....</i>	61

3.7.4	<i>Gouy-Chapman double layer</i>	63
3.7.5	<i>Double layer at the surface of a spherical surface</i>	64
3.7.6	<i>Non-ideality of cement suspension</i>	65
	Potential dependent activity coefficients.....	65
	Non-ideal form of Poisson-Boltzmann equation.....	68
3.7.7	<i>Charge-Potential relation</i>	71
3.7.8	<i>Surface potential regulation</i>	72
3.7.9	<i>Electrostatic force between flat plates</i>	74
	Relation between pressure gradients and local electrostatic field.....	74
	Electrostatic force between two parallel flat plates with identical potentials.....	75
	Electrostatic force between two parallel flat plates with different potentials.....	76
3.7.10	<i>Electrostatic force between spheres</i>	77
	General expression for electrostatic force between spheres with constant potential.....	77
	Electrostatic force between equally charged spheres.....	79
	Electrostatic force between spheres with different potentials.....	80
3.7.11	<i>Summary of electrostatics for cement suspensions</i>	81
3.8	FORCES LINKED TO POLYMERS.....	82
3.8.1	<i>Adsorbing polymers</i>	82
	Adsorption modes.....	82
	Electrostatic forces.....	84
	Steric forces.....	85

<u>Interpenetrational energy model</u>	85
<u>Scaling theory</u>	87
3.8.2 <i>Non adsorbing polymers</i>	88
Air entrainment.....	88
Modification of capillary forces	88
Depletion flocculation.....	89
Depletion stabilisation.....	89
3.8.3 <i>Adsorbed and non-adsorbed polymers</i>	90
CHAPTER 4 MATERIALS	91
4.1 MODEL POWDERS.....	91
4.2 CEMENTS.....	93
4.3 POLYMERS.....	95
CHAPTER 5 EXPERIMENTAL METHODS	101
5.1 ADSORPTION	101
5.1.1 <i>High Performance Liquid Chromatography (HPLC)</i>	101
Principles.....	101
Operation conditions.....	102
5.1.2 <i>Model suspensions</i>	104
5.1.3 <i>Cements</i>	105
5.2 RHEOLOGY.....	106
5.2.1 <i>Model suspensions</i>	106

5.2.2	<i>Cement suspensions</i>	107
5.3	ZETA POTENTIAL	107
5.3.1	<i>Principle of the acoustophoresis</i>	107
5.3.2	<i>Model suspensions</i>	108
5.3.3	<i>Cement suspensions</i>	108
CHAPTER 6 RESULTS WITH MODEL SUSPENSIONS.....		109
6.1	CHEMICAL STABILITY OF SUSPENSIONS.....	109
6.2	ZETA POTENTIAL.....	109
6.3	ADSORPTION.....	111
6.3.1	<i>Calibration Data</i>	111
	PCA-2 calibration line	111
	PCA-1 calibration line	112
	PCE-1 calibration line.....	113
6.3.2	<i>Adsorption onto MgO</i>	115
	Adsorption of PCA-2 onto MgO.....	115
	Adsorption of PCA-1 onto MgO.....	120
	Adsorption of PCE-1 onto MgO.....	124
	Compilation of adsorption data onto MgO.....	128
6.3.3	<i>Adsorption onto Mg(OH)₂</i>	129
6.4	RHEOLOGY	132
6.4.1	<i>General Trends</i>	133

6.4.2	<i>Effect of Solid Volume Fraction</i>	136
CHAPTER 7 DISCUSSION OF MODEL SUSPENSIONS		139
7.1	ZETA POTENTIAL.....	139
7.2	ADSORPTION	140
7.2.1	<i>Links between adsorption and zeta potential</i>	140
7.2.2	<i>Adsorption onto magnesium hydroxide</i>	143
	Adsorption differences with Mg(OH) ₂	143
	Effect of temperature for adsorption onto Mg(OH) ₂	143
7.2.3	<i>Adsorption onto magnesium oxide</i>	144
	Adsorption differences with MgO.....	144
	Effect of temperature for adsorption onto MgO	145
7.2.4	<i>Interpretation of the temperature effect on adsorption</i>	146
7.3	SURFACE COVERAGE.....	149
7.4	RHEOLOGY.....	149
7.4.1	<i>Effect of Solid Volume Fraction</i>	150
7.5	IMPLICATIONS FROM MODEL SUSPENSION BEHAVIOUR.....	151
CHAPTER 8 RESULTS WITH CEMENT SUSPENSIONS		153
8.1	ADSORPTION	153
8.1.1	<i>General trends</i>	153
8.1.2	<i>PCA-2</i>	155
8.1.3	<i>PCA-1</i>	155

Global adsorption.....	157
Adsorption of individual polymeric fractions	159
Effect of polymeric fraction.....	159
Effect of addition time.....	162
Effect of Grinding Aid	163
8.2 RHEOLOGY	164
8.2.1 <i>General trends</i>	164
8.2.2 <i>Yield Stress</i>	166
CHAPTER 9 DISCUSSION OF CEMENT SUSPENSIONS	171
9.1 ADSORPTION.....	171
9.1.1 <i>Effect of polymeric fraction</i>	171
9.1.2 <i>Effect of Hydration Time</i>	173
9.1.3 <i>Effect of grinding aid (triethanol amine acetate)</i>	174
9.2 RHEOLOGY	174
9.2.1 <i>Effect of dosage</i>	174
9.2.2 <i>Origin of dispersion force</i>	175
9.3 CONCLUSIONS.....	175
9.3.1 <i>Adsorption</i>	175
9.3.2 <i>Rheology</i>	177
9.4 IMPLICATION OF THE BEHAVIOUR OF CEMENT SUSPENSIONS.....	177
CHAPTER 10 INTERPARTICLE FORCES AND YIELD STRESS.....	179

10.1	PROBLEM OF ENERGY NORMALISATION.....	179
10.1.1	<i>Brownian motion</i>	180
10.1.2	<i>Shear forces</i>	180
10.2	INTERPARTICLE FORCES.....	181
10.2.1	<i>Dispersion force</i>	181
10.2.2	<i>Electrostatic force</i>	182
10.2.3	<i>Steric force</i>	184
10.2.4	<i>Total interaction</i>	184
10.2.5	<i>Maximum interparticle force</i>	185
10.3	PROBLEM OF WIDE PARTICLE SIZE DISTRIBUTION OF CEMENT.....	185
10.4	YIELD STRESS CALCULATIONS.....	191
10.4.1	<i>Force balances</i>	192
	Projection of interparticle force.....	192
	Movement under shear	194
	Rupture Stress per doublet.....	195
	Fraction of broken bonds.....	196
	Effective volume	197
	Maximum packing fraction of solids.....	201
	Estimation of polymer layer thickness.....	202
	Limitations.....	204
10.4.2	<i>Hydrodynamic interactions</i>	204

10.4.3	<i>Experimental data for estimating of layer thickness</i>	211
10.5	IMPLICATIONS OF INTERPARTICLE FORCE CALCULATIONS	215
CHAPTER 11 GENERAL DISCUSSION		217
11.1	A BRIEF OVERVIEW	217
11.2	ROLE OF PHYSICO-CHEMICAL EFFECTS	219
11.2.1	<i>Agglomeration</i>	219
	Electrostatic forces.....	219
	Dispersion forces.....	219
	Steric Forces.....	220
	Electrosteric forces.....	221
	Total interaction.....	222
	Effect of particle size	223
11.2.2	<i>Desagglomeration</i>	223
11.3	ROLE OF CHEMICAL EFFECTS	225
	Grinding aid effect.....	225
	Ettringite a chemical sink for superplasticizers.....	226
	Role of sulphates and alkalis.....	228
	Reactivity towards superplasticizers	231
CHAPTER 12 CONCLUSIONS		235
12.1	ADSORPTION.....	236
	Results.....	236

Perspectives.....	237
12.2 RHEOLOGY.....	238
Results.....	238
Perspectives.....	238
12.3 INTERPARTICLE FORCES.....	240
Results.....	240
Perspectives.....	241
12.4 CHEMICAL EFFECTS.....	243
Interpretation.....	243
Perspectives.....	243
12.5 PERSPECTIVES FOR DURABILITY.....	243
REFERENCES.....	245
ANNEX A CEMENT NOMENCLATURE.....	251
ANNEX B NOTATIONS.....	253
ANNEX B.1 GREEK SYMBOLS.....	253
ANNEX B.2. LATIN SYMBOLS.....	253
ANNEX C HAMAKER CONSTANT CALCULATIONS.....	255
ANNEX D STATISTICAL TREATMENT OF DATA.....	265
ANNEX D.1 TESTING THE IDENTITY OF LINES.....	265
<i>Annex D.1.1 Use of the macros.....</i>	<i>266</i>
<i>Annex D.1.2. Microsoft Excell Macro listing.....</i>	<i>267</i>

ANNEX D.2.	TESTING AN EFFECT ON A SERIES OF VALUES, ALL HAVING THEIR OWN UNCERTAINTY.....	277
	<i>Annex D.2.2 Listing of Microsoft Excell macro.....</i>	<i>278</i>
ANNEX E	INTERPARTICLE FORCE PARAMETERS.....	283
ANNEX E.1	NUMERICAL VALUES.....	283
ANNEX E.2	MICROSOFT EXCELL MACRO LISTING.....	289
ANNEX F	DISTRIBUTION OF INTERACTION DIAMETERS.....	295
ANNEX G	INTERPARTICLE FORCE PARAMETERS.....	297
ANNEX H	ADDITIONAL EFFECTIVE VOLUMES.....	299
CURRICULUM.....		303

Chapter 1 Introduction

Concrete is a composite material in which aggregates (gravel and sand) are bound by hydrated cement paste. The amount of water required for the reaction of hydration represents about 25% of the mass of cement. However, in order to obtain flowing concrete, which can be either cast or pumped, much more water is required (about double). In the long term, this excess water evaporates, leaving voids in the concrete. The associated porosity decreases both the mechanical strength and the durability. Such concrete does not reach the optimal properties it could have if it were produced as a more compact material.

This is where superplasticizers, also known as High Range Water Reducers (HRWRs), are of interest. Superplasticizers are polymeric dispersants, which when added in small amounts to concrete (typically less than 0.5% of the mass of cement), allow high water reduction for the same workability [Aïtcin et al (1994), Ramachandran et al (1998)]. Also, they allow efficient incorporation of industrial by-products such as silica fume, fly-ash or slag. Because cement production consumes a lot of energy, this leads to substantial energy savings [Mehta (1998)].

So the use of superplasticizers to increase durability and incorporate industrial by-products represents a major environmental issue. In order to emphasise the importance of this technology, some figures are presented below.

Producing clinker, which once ground with added gypsum gives portland cement, requires about 5 MJ/kg [Ramchandran et al (1998)²], for only the high temperature calcination step. In Switzerland, the total cement production has been about constant at 3.9 million tons over recent years [WEB site of Holderbank]. Because transporting cement farther than about 150 km is not economical, unless it is done by boat, we can consider that all this cement is used in Switzerland. Therefore, we can

² Given as 1'100-1'400 kCal/g (should be kCal/kg)

normalise this production by the population of Switzerland, which is about 7 million inhabitants [WEB site Federal Office of Statistics³]. This gives, per year, an energy for clinker formation of 2.8 GJ /inhabitant.

Let us convert this into an amount of octane, which is the main component of the fuel used by private motor vehicles. Combustion of octane provides about 39 MJ /litre [CRC Handbook of Physics and Chemistry (1977-78)]. So, clinker formation requires 71 litres of octane per inhabitant. For a small car, consuming more or less 7 litres over 100 km, this corresponds to a distance of 1'020 km.

In order to reduce the environmental impact of cement production, much industrial waste is burnt in the cement kilns in order to recover the thermal capacity of this waste. However, this industry remains a very energy consuming one.

But this is not the only problem linked to cement production. During clinkerisation, calcium carbonate is converted to calcium oxide (in various solid solutions with other minerals) and this emits substantial amounts of CO₂. The production of 1 kg of portland cement requires 1.5 kg of raw material with about 75% calcium carbonate [Swiss society for cement, lime and gypsum producers (1988)]. So the production of 1 kg of cement requires 1.13 kg of CaCO₃ (100 g/mol), which will liberate 0.52 kg of CO₂ (46 g/mol). An equivalent emission of CO₂ is produced by the combustion of 0.26 litres of octane per kg of cement. So, in Switzerland, the emission of CO₂ linked to cement production per inhabitant per year represents about 145 litres of octane. This is equivalent 2'080 km with our reference car.

These figures show that the biogenic release of CO₂ by cement is important. Let us now consider its importance with respect to the other sources of CO₂ in Switzerland. In 1995 the total release of biogenic CO₂ in Switzerland was of 43.5 million tons [WEB site Federal Office of Statistics]. It is spread as follows: transport 14.5 million tons, industry 17 million tons and households 12 million tons (Figure 1-1). In the transport, private vehicles account for 9.5 million tons, which is 22% of the total CO₂ emissions. The CO₂ emitted by the calcination step in cement production (2.0 mio t /year) is therefore about 21% of the CO₂ released by private traffic. Note that this also represents 12% of the total emissions by the industry and 4.5% of the total biogenic CO₂ emitted in Switzerland.

³ The most recent compiled data accessible on this site is for 1995, which corresponds to the value given.

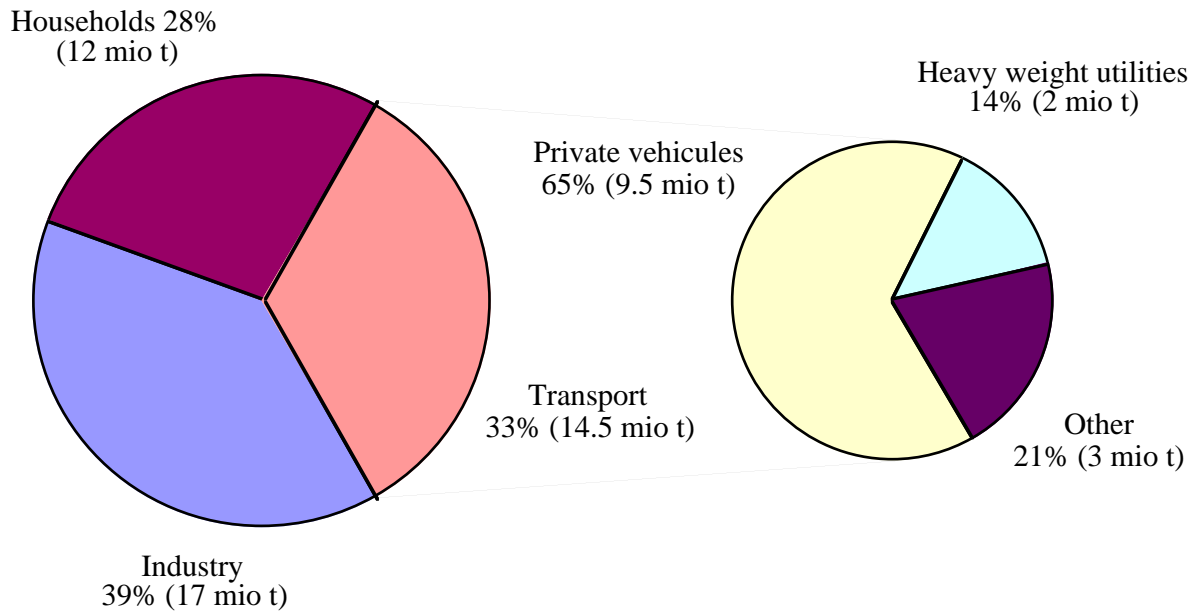


Figure 1-1. Biogenic release of CO₂ in Switzerland in 1995, according to data accessible on the WEB page of the Swiss Federal Office of Statistics.

If we now consider, the amount of concrete structures, which will be built over the next decades in developing countries, very alarming figures concerning energy consumption and CO₂ emissions are obtained [Mehta (1998)]. It is therefore paramount to have a technology allowing production of more durable concrete containing less cement. Superplasticizers have a unique place in this technology, since they are essential for the preparation of concrete with low porosity. In addition, without their use, it is almost impossible to efficiently integrate certain industrial by-products, silica fume in particular.

For these reasons, the use of superplasticizers will still grow because of their ability to allow the production of concrete exhibiting high durability. Nowadays, superplasticizers are most widely used in Japan, where it is estimated that almost no concrete is produced without superplasticizers.

Currently, very good performances can be obtained with a wide range of superplasticizers. However, the time during which these are active remains short, which causes practical problems on site. In addition, many unexplained incompatibilities subsist between some superplasticizers and cement combinations [Aïtcin et al (1994) and Ramachandran et al (1998)]. The risk of encountering such incompatibilities increases with the chemical variability of the materials used. This implies is higher

risk of problems, when incorporating industrial by-products into concrete. In order to make the use of superplasticizers more robust to the end users and to orient the development of superplasticizers more performant at lower dosages, it is necessary to understand correctly the way by which these molecules act.

Table 1-1. Summary of data used to discuss ecological impact of cement production.

Energy Clinker production Octane combustion	5 MJ / kg 39MJ / litre	Ramachandran et al (1998) ² Handbook of Physics and Chemistry
Population Switzerland in 1995	7 million	WEB site Federal Office of Statistics
Cement Production in Switzerland in 1998 Raw material required CaCO ₃ content of raw material CO ₂ release by CaCO ₃ calcination	3.9 million tons 1.5 ton / ton cement 75% 0.52 t / ton cement	WEB site of Holderbank Swiss society for cement, lime and gypsum producers, 1988
Biogenic CO₂ releases in Switzerland (1995) Industry Households Transport Private vehicles Heavy weight utilities Other transport	17 million tons 12 million tons 14.5 million tons 9.5 million tons 2 million tons 3 million tons	WEB site Federal Office of Statistics

In this task, we are aided by the fact that such molecules are not only of interest to the concrete industry. They have a much larger scale of application, particularly in ceramic processing. Traditional ceramics (whitewear, sanitary appliances, insulators, etc.), refractories (crucibles, engine components, supports for catalysts, etc.), bioceramics, biocements, watchmaking (watch bodies) are just some of the examples of products which include the use of such molecules in their production scheme.

The mechanisms of action of these molecules are largely recognised to be linked to a change in interparticle forces. Much has been learned from the field of colloidal science, where surface forces and their role on interparticle interactions has been a subject of ongoing research for many years. Evans and Wennerström (1994), and Israelachvili (1990) present clear treatments of colloidal, surface and interparticle forces. Horn (1990) shows how these concepts can be applied to ceramic processing. Russel *et al* (1991) give an extensive treatment of these effects, illustrating how these effects are the regulating factors of the rheology of colloidal dispersions.

In cementitious materials, the time dependence due to on-going chemical reactions complicates the understanding [Aïtcin *et al* (1994)]. Nevertheless, intensive work over the past years has brought significant progress in the understanding of this field. In particular, the design of polymers having a backbone containing carboxylic groups and onto which side chains are grafted has allowed much better performances than with the conventional polymers, such as sulfonated naphthalene formaldehyde condensate (SNFC). Uchikawa *et al* (1997a,b) showed by Atomic Force Microscopy (AFM) that polymers with long side chains can be much more efficient than the ones with shorter or no side chains. Yoshioka *et al* (1997) and Sakai and Daimon (1997) calculated the importance of steric contribution to the stabilization of alite by such polymers. The effect of such polymers on the rheology of cement suspensions was studied for instance by Matsuyama *et al* (1997).

So far however, all attempts to calculate interparticle forces have been based on assumptions, of which the validity in cement suspensions is highly debatable. Speculations on such results can therefore lead to misinterpretation of underlying mechanisms and orient research and development in irrelevant directions.

A proper understanding of the dominant mechanisms has major implications for the design of polymers with increased performances. It is also essential to optimise the use of current polymers. It is the object of this thesis to take a closer look at the mechanisms underlying the action of superplasticizers in concrete, and more specifically, the interaction of these polymers with cement

suspensions. It has been carried out within the framework of a European Eureka framework⁴, for which a number of cements and superplasticizers of different chemical nature were selected. From the multiple possible combinations, only a few have been selected for detailed investigation in this thesis.

This document is structured as follows. Chapter 2 describes the strategy, which has been adopted in order to investigate the complex system. In particular, we argue about choosing an appropriate inert model system in order to determine the effects without interfering chemical reactions. In Chapter 3, we develop the theoretical background necessary for interpretation of results. Cement hydration is considered under the viewpoint of thermodynamics of non-ideal systems. Then, we present much knowledge from colloidal science, with the constant effort to relate this specifically to cementitious systems. Subchapters deal successively with hydrodynamics, rheology, Brownian motion, sedimentation, dispersion forces, electrostatic forces and forces linked to added polymers. Chapters 4 and 5 present respectively the methods and materials used in the experimental work. Chapters 6 to 9 give the results and discussions of both model systems and cementitious systems. These sections lead to the conclusion that for the polymers under investigation, only the adsorbed fractions are relevant to interparticle force modifications. This orients the theoretical developments in chapter 10, which attempt a pragmatic integration of interparticle force calculation into a model for the directly determining of yield stresses in poly-dispersed systems such as cement. This leads to the general

⁴ „Interaction of High Range Water Reducers with Cements“.

Participants: EPFL – Lausanne, Switzerland
Sika A.G. – Zürich, Switzerland
University of Innsbruck - Innsbruck, Austria
Deisl A.G. – Austria
ZAG – Lubliana, Slovenia

discussion, in chapter 11, of the implications of both experimental and theoretical results of this thesis. It is followed by chapter 12, which gives the general conclusions.

Chapter 2 Strategy

In this chapter, a brief overview is given of the way by which the problem of studying, understanding and explaining cement / superplasticizer interactions has been approached.

2.1 Expected Mechanisms

At the beginning of the project, we have first considered a priori a series of known dispersion mechanisms. Consideration of their mode of action has oriented choices of the experiments to perform. Extending the terminology introduced by Jolicoeur et al (1994), we classify these mechanisms as:

- Physical effects: for the effects linked mainly to the modification of the surface tension of the aqueous phase.
- Chemical effects: for the effects linked to the way by which superplasticizers can modify the hydration reactions.
- Physico-chemical effects: for the modification of interparticle forces

The polymers we have chosen to study do not significantly modify the surface tension of the aqueous phase, so physical effects should be negligible (measurements performed by Sika A.G.).

As discussed later, the use of model inert systems provides a way to study only physico-chemical effects above. A more complete description of these effects will be given later. Here we will just mention that these effects can be classified as:

- Linked to adsorbed polymers: for the effect linked only to the adsorbed polymers. Mechanisms involved here are steric or electrostatic repulsion.
- Linked to non-adsorbed polymers: for the effects only linked to the polymers remaining in solution. This would involve the still debated depletion stabilisation or the surface tension modifications.
- Linked to both adsorbed and non-adsorbed polymers: for effects linked both to the polymers adsorbed and those remaining in solution.

Model suspensions allow us to work independently of chemical effects. A proper determination of adsorption versus dispersion performance should therefore determine whether the effects are linked to adsorbed and/or non-adsorbed polymers. Differentiation between the identified categories will be done by calculation of interparticle forces. The importance of chemical effects will then be addressed as the reason for any unanticipated behaviour.

2.2 Model suspensions

Cement suspensions have an inherent complexity, which constitutes both a challenge and an obstacle to understanding cement/superplasticizer interactions. Indeed, cements are reactive multimineral powders, the surfaces of which evolve in time. Mineralogical and chemical compositions of the different granulometric fractions can be different. Some cements also contain mineral additions, like silica fume, fly ash, slag or filler. Grinding aids are generally used in the production route and remain on cement grains. Cements have variable C_3A content, the reactivity of which can also vary. The importance of the C_3A reactivity on the rheology of cement slurries is well known. The dissolution of sulfate ions must be balanced with the reactivity of C_3A [Aïtcin et al (1994)]. Not only do the surfaces of the hydrating minerals evolve in time, but also the chemical composition of the solution is changing in the period between the mixing and placing of concrete.

Because of this complexity, superplasticizers and other dispersing agents have often been studied using model suspensions of inert powders [Chapuis (1986,1990), Girod et al (1988), Jolicoeur et al (1994), Pierre et al (1988)]. The information that such experiments provide is an indication of the initial interaction of superplasticizers with cement particles.

We need these model suspensions to provide chemical inertness, while nevertheless being able to represent as well as possible the interactions between cement surfaces and superplasticizers. A major factor is to ensure that the polymers adsorb onto the particles in a similar way and maintain a similar configuration.

Most if not all superplasticizers are polyelectrolytes and their adsorption is strongly influenced by the surface charge of particles. Nkinamubanzi (1994) and Pierre et al (1988) found that the adsorption of SNFC on TiO_2 strongly depends on the pH of the suspension. It has a maximum at pH 3 and does not adsorb in the alkaline region. This behaviour is rationalised by taking into account the change in surface charge of TiO_2 with pH. Titanium dioxide has an isoelectric point at pH 5.5-6. Below this value, its zeta potential is positive and above it, negative. This explains the pH dependent adsorption of the SNFC, which is an anionic polymer as are the large majority of superplasticizers. Because of this important role of electrostatic interactions, it would be beneficial for our model suspensions to have a surface charge similar to that of cement.

Getting exact values of surface potentials of cement is a tedious task. This is because most systems do not allow measurements at volume concentrations representative of cement, which alters the ion distribution between the surface and solution. Another common limitation is the particle size. Because of either intrinsic limitations or sedimentation, it is often not possible to determine the potential of the largest cement particles. Bearing these limitations in mind, we should discuss the zeta potential values of dilute suspensions reported in the literature.

It is interesting that both slightly positive and negative zeta potentials are reported. For what we are concerned with however, it suffices to state that cement suspensions have a very small surface charge. This can be attributed to the fact that cement suspensions are very close to their isoelectric point (pH of zero charge) and therefore have a very small surface charge even though they are in a highly alkaline suspension (most particles are strongly negative at these pHs).

If we only consider the surface charge criteria, it would be possible to use any powder as long as one chooses to operate close to its isoelectric point. However, pH can influence the polymer conformation. It also influences the hydrolysis rate of polymers. For these reasons, we also wish to have model systems at high pH.

So it is intended to use model powders, having an isoelectric points at a high pHs. Suspensions such as those containing titanium dioxide can not simultaneously fulfil both conditions (high pH and positive zeta potential). Though they can provide some information on adsorption, it would not be wise to use such data to differentiate the effects involved in the superplasticizing of concrete. As a matter of fact,

very few systems can satisfy simultaneously the above mentioned conditions and conserve the essential inertness required for a model system. To the best of our knowledge, no adsorption experiments have been carried out at pH around 12 with model powders that are positively charged.

The powders used in our study: dead burnt magnesium oxide and magnesium hydroxide have nominal isoelectric points respectively at pH 12.4 and 12 [Parks (1965)]. They were studied in suspensions at pH 12 and 11.3 (pH reached in suspensions prepared with NaOH 0.01M), giving in both cases a zeta potential positive by a couple mV.

Magnesium, which lies above calcium in the periodic table, has a similar outer electronic shell and a smaller radius than calcium. This makes its bonding to oxygen much stronger than that of calcium. This stronger bond makes magnesium oxide almost insoluble. Its rate of dissolution can be further decreased by *dead burning*. This produces a very interesting model powder. The main cement phases (calcium silicates and calcium aluminates) contain calcium oxide, which is probably the dominant surface leading to the probably positive zeta potential of cement [Sakai and Daimon (1995)]. It is therefore possible that the initial effects involved in superplasticizing will be closely linked to the adsorption of superplasticizers on calcium oxide-like surfaces. This makes magnesium oxide an even more interesting model powder. As for magnesium hydroxide it offers a surface expected to provide many similarities to that of the hydrated cement phases.

We must point out that it is possible to add electrolytes to these model suspensions in order to obtain very similar ionic compositions of the aqueous phases to those encountered in cementitious suspensions. However, in the experiments we have performed, the suspensions were only prepared in 0.01 M NaOH in order to work at a pH close to the isoelectric point of the suspensions. Though losing a little of the cement specificity, we believe however that such suspensions maintain the three major features of interest, low zeta potential, high pH and inertness.

2.3 Adsorption

Adsorption of superplasticizers is a major step in many dispersions mechanisms, which can be expected to be responsible for the dispersion of cement. It is therefore important to identify correctly the relation between the amount of superplasticizer adsorbed and the amount remaining in solution. At a given temperature, the relation between these two entities is termed an adsorption isotherm.

It is well known that the molar mass of polymers strongly influences adsorption. On the other hand, the fact that these polymers are always polydisperse has received little attention. Studies relative to this issue usually just identify differences between monomers, dimers and the polymeric fraction. The polydispersity within the polymeric fraction is often overlooked.

High Performance Liquid Chromatography (HPLC) is a method, which allows an efficient separation of polymeric fractions. This tool provides the ability to identify effects of polydispersity. However, it requires a detector compatible with the choice of elution gradients needed to separate the fractions. At the time this project was started, a UV-visible diode array detector was the best choice. This however, limits the choice of polymers to those having a sufficient amount of UV or visible light absorbing groups. We chose to study only the polymers, which could clearly be identified by HPLC. This is because the project was oriented towards understanding mechanisms and that in absence of a good knowledge of the role of polydispersity in adsorption, many of the conclusions drawn could be incorrect.

2.4 Rheology

Rheology was measured with a concentric cylinder geometry. Because the gap between the cylinders is small, it is possible to assume a constant velocity gradient is established through the sheared fluid. This is very important, because it allows to obtain real viscosity values. Many systems used to measure concentrated dispersions can only provide comparative values [Ferraris (1996)].

So, the selected geometry, will allow us to attempt to establish a quantitative relation between rheological data and interparticle forces.

Another geometry leading to real viscosity determination is the cone and plate. In this case, however, the minimum gap between the pieces can be a limiting factor because it is of the order only a few diameters of the larger cement particles. In addition, the concentric cylinder geometry is much less sensitive to sedimentation and evaporation than the cone-plate system. So, it appears to be a more robust geometry for quantitative results.

Many fluids exhibit a yield stress. This is the stress, which must be applied to a fluid in order to pass from a solid to a liquid behaviour. This yield stress is strongly linked to the magnitude and spatial distribution of interparticle forces, which must be overcome to produce the solid to liquid transition. Up to this limit, the behaviour of the liquid is viscoelastic.

Viscoelastic properties can be determined by oscillation measurements [Schultz and Struble (1993)]. Because of cement hydration the frequency range applicable is limited. In addition, it turns out that the linear viscoelastic regime, which is relevant for determining measurement condition independent parameters, is at the limit of current instruments. The most important viscoelastic effects have been measured in a vessel with an oscillating paddle in the first minutes after water addition [Nachbaur (1997)]. However, it is not clear whether this is a consequence of mixing.

With regard to this, the choice was made to determine precisely yield stress and behaviour at shear rate above yield stress, as a function of superplasticizer dosages.

2.5 Stability calculations

In chapter 3, the background for calculating interparticle forces and determining the stability of suspensions is presented. Particular attention is taken to stress to what extent the usual approximations can or cannot be used in the case of cement suspensions. We have attempted, as much as possible, to account for the characteristics of cement suspensions, in particular, particle size distribution and non ideal thermodynamics of the concentrated aqueous phase.

Normalising the interaction energy is a key aspect in discussing stability of suspensions. Brownian motion is usually used in colloidal science, but does not appear a valid criterion for cement suspensions, due to the large size of the particles. On the other hand, large particles, due to their inertia, are more susceptible to viscous forces.

After determining the number of interactions between particles of different sizes, the interaction forces are calculated and used in an attempt to directly calculate the yield stress of cement suspensions. The critical step of this procedure is the identification of the number of interparticle bonds, which should be broken in order for the suspension to pass from a solid-like to a liquid-like form. The other critical parameter of the modelling of interparticle forces is the thickness of the adsorption layer. Despite these two difficulties, the modelling leads to measured yield stresses of cement suspensions, with realistic values of adsorbed layer thickness and number of interparticle bonds to break. This approach is then taken a step further by integrating a simplified treatment of hydrodynamic interactions between pairs of particles, leading to a reevaluation of the adsorbed layer thickness 30% on average higher than the previous one.

2.6 Chemical effects

The predictions of the stability calculations allow the interpretation of cement specific effects. The interpretation we present is supported by some of our own results, but most of all by a selection of recent data from the literature [Uchikawa (1999), Kim et al (1999) and Pagé et al (1999)]. The importance of coprecipitation or micellisation of superplasticizers with aluminates during the formation of ettringite will be emphasised.

It appears that such reactions, studied by for instance by Fernon et al (1997) in the case of SNFC, play an important role in the consumption of superplasticizer. Therefore they play an important role in consumption/performance studies. However, at sufficiently high dosages the effect of this consumption seems to be minor on performance. We present a simplified model for understanding such effects. Nevertheless, we have the impression that it provides interesting perspectives for the development of superplasticizers of higher performance either at lower dosage or at lower W/C ratios.

This model also allows some discussions concerning the use of current superplasticizers and the future development of new superplasticizer for increased performance.

Chapter 3 Theoretical considerations

The addition of superplasticizers to cement suspensions changes the nature and magnitude of interparticle forces. However, it also modifies the rates of the ongoing hydration reactions. Nucleation rates are influenced as well as crystal shapes. The object of this chapter is to develop the theoretical background, which will be necessary in later chapters in order to develop a mechanistic understanding of the effect of the action of superplasticizers.

In the first section the chemistry of cement is presented. We develop ion activity calculations, which are necessary to give a thermodynamic description of the aqueous phase of these suspensions, which are highly concentrated in electrolytes. These results serve later in the development of dispersion and electrostatic forces, in a framework relevant to cement suspensions.

The other sections of this chapter deal with the wide range of colloidal forces. We successively address hydrodynamics, rheology, Brownian motion, sedimentation, dispersion forces, electrostatic forces and polymer induced forces. Most of these sections follow the treatment used by Russel et al (1991). However, the presentation is led with the constant objective of relating basic colloidal phenomena to cement suspensions. For instance, many developments are carried out in order to account specifically for the high electrolyte concentration, the large particle size and wide particle size distribution of cement suspensions.

To clarify the objective of this chapter, we will recall here that: the basis of the theory of colloidal stability is that the total interaction force between macroscopic bodies can be obtained by summation of the individual forces. A proper energy normalisation (Brownian motion, shear, etc.) should then allow prediction of whether these bodies will attract one another or not. If they do, this will lead to agglomeration and reduced flowability. The object of using superplasticizers is precisely to avoid this type of situation. Therefore, this subchapter by describing the nature and quantification of these interparticle forces, provides the tools which are used subsequently to develop a quantitative prediction of the performance of superplasticizers.

3.1 Chemistry of cementitious suspensions

3.1.1 Composition

The widest used cement in construction is portland cement. The clinker is obtained by successively grinding and calcining a mixture of limestone and clay. The portland cement, a fine powder, is the result of the grinding of the clinker with a small amount of gypsum. Schematically the process of clinkerisation can be written as follows:

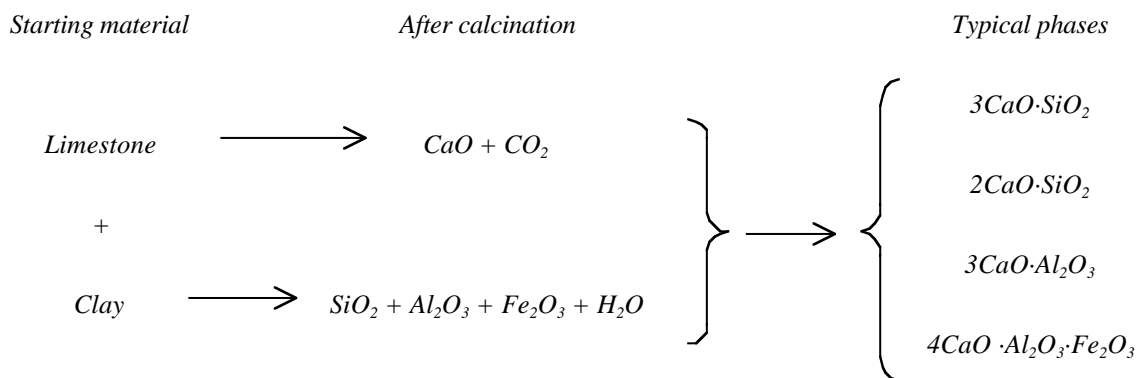


Table 3-1 gives a wider range of the compounds formed, along with their abbreviation in the cement field nomenclature. Note that in cement all these phases are not pure. For instance, the C_3S and β - C_2S phases, which represent about 75% of the mass of portland cement, invariably contain small amounts of magnesium, aluminium, iron, potassium and sulphur ions [see for instance Mehta (1986), chapter 6]. The impure C_3S and β - C_2S phase in cement are termed alite and belite respectively. Characteristics of the main phases in portland cement are given in Table 3-2.

Once in contact with water, these phases hydrate and form highly insoluble hydrates. Hydration of the pure phases C_3S and C_2S both lead to calcium silicate hydrate and calcium hydroxide. The hydration of these pure phases provides useful information about the hydration of alite and belite phases. In cement, their hydration leads to impure calcium silicate hydrates with varying C/S ratios.

Concerning the effect of hydration on the rheology at early ages, let us note that the hydration of the aluminate phases can be extremely fast, leading to a premature loss of workability. In order to avoid this problem, calcium sulphates are added. This allows the coprecipitation of the dissolved calcium aluminates and calcium sulphates as crystals of ettringite ($6CaO \cdot Al_2O_3 \cdot 3SO_3 \cdot 32H_2O$), before forming

the rigidifying calcium aluminate hydrate. This takes place very quickly after water is added (minutes) and is therefore one of the main reactions with which superplasticizers could be interfering.

Table 3-1. Formulas for the pure phases of the compounds found in portland cement and corresponding nomenclature.

Compound	Abbreviation	Abbreviation	Name
CaO	C	C_3S	Tri-calcium Silicate
SiO ₂	S	C_2S	Di-calcium Silicate
Al ₂ O ₃	A	C_3A	Tri-calcium Aluminate
Fe ₂ O ₃	F	C_4AF	Tetra-calcium aluminoferrite
MgO	M	$C_3S_2H_3$	Calcium Silicate hydrate
SO ₃	\bar{S}	$C\bar{S}H_2$	Gypsum
H ₂ O	H	$C_6A\bar{S}_3H_{32}$	Calcium aluminate tri-sulphate (Ettringite)
		$C_4A\bar{S}H_{18}$	Calcium aluminate mono-sulphate (Monosulfate)

Table 3-2. Principle compounds of portland cement and their characteristics [after Mehta (1986)].

Approximate composition	$3CaO \cdot SiO_2$	$2CaO \cdot SiO_2$	$3CaO \cdot Al_2O_3$	$4CaO \cdot Al_2O_3 \cdot Fe_2O_3$
Abbreviated formula	C_3S	$\beta-C_2S$	C_3A	C_4AF
Common name	Alite	Belite	—	Ferrite phase, Fss
Principal impurities	MgO, Al ₂ O ₃ , Fe ₂ O ₃	MgO, Al ₂ O ₃ , Fe ₂ O ₃	SiO ₂ , MgO, alkalies	SiO ₂ , MgO
Proportion of compounds present (wt%)				
Range	35-65	10-40	0-15	5-15
Average	50	25	8	8
Contribution to early strength				
Early age (days)	Good	Poor	Good	Good
Ultimate (years)	Good	Excellent	Medium	Medium
Heat of hydration	Medium	Low	High	Medium
Typical (J/g)	500	250	1340	420

In what follows we present, thermodynamically based descriptions of cement hydration. The non-ideality of systems is equated for pure phases and some ideas concerning possible effects of

admixtures are briefly presented and discussed. Results of activity coefficient calculations will be used in the calculation of electrostatic repulsion.

3.1.2 Chemical description of hydration

Many studies have attempted to relate the evolution of the solution's chemistry to the rates of the on-going hydration reactions. Pure cement phases especially calcium aluminates and calcium silicates have been studied in detail. These studies however seemed to have failed in explaining rationally the transition from the dormant period to hydration.

More recently, Damidot et al. (1997) developed phase diagrams for such cement systems, using an adequate thermodynamic description for the aqueous phase, which is a very concentrated electrolyte. The idea is that cement suspensions attempt simultaneously to reach equilibrium between aqueous species and reactive minerals, as well as the equilibria between aqueous species. For C_3S let us write:



At equilibrium, chemical potentials of the reactants are equal to those of the aqueous species:

$$\mu_{3\text{CaO}\cdot\text{SiO}_2} + 4\mu_{\text{H}_2\text{O}} = 3\mu_{\text{Ca}^{2+}} + 5\mu_{\text{OH}^-} + \mu_{\text{H}_3\text{SiO}_4^-} \quad [3-2]$$

The chemical potential of species k is given by:

$$\mu_k = \mu_k^0 + k_B T \ln(a_k) = \mu_k^0 + k_B T \ln(\gamma_k c_k) \quad [3-3]$$

μ_k^0 is the standard chemical potential of species k

a_k is the activity of species k

γ_k is the activity coefficient of species k

c_k is the concentration of species k

k_B is the Boltzmann constant

T is the temperature in °K

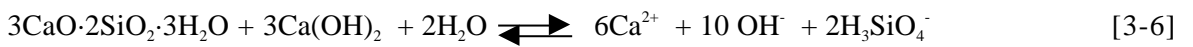
Equations [3-2] and [3-3] lead to the equilibrium constant :

$$K_{3CaO \cdot SiO_2} = \frac{a_{Ca^{2+}}^3 \cdot a_{OH^-}^5 \cdot a_{H_3SiO_4^-}}{a_{3CaO \cdot SiO_2} \cdot a_{H_2O}^4} \quad [3-4]$$

Where:

$$K_{3CaO \cdot SiO_2} = \exp\left(\frac{\mu_{3CaO \cdot SiO_2}^0 + 4\mu_{H_2O}^0 - 3\mu_{Ca^{2+}}^0 - 5\mu_{OH^-}^0 - \mu_{H_3SiO_4^-}^0}{k_B T}\right) \quad [3-5]$$

On the other hand, for the hydrated phase we have:



With:

$$K_{3CaO \cdot 2SiO_2 \cdot 3H_2O} \cdot K_{Ca(OH)_2} = \frac{a_{Ca^{2+}}^6 \cdot a_{OH^-}^{10} \cdot a_{H_3SiO_4^-}^2}{a_{3CaO \cdot 2SiO_2 \cdot 3H_2O} \cdot a_{Ca(OH)_2}^3 \cdot a_{H_2O}^2} \quad [3-7]$$

Dividing [3-7] by [3-4] and taking the activities of the solid phases to be unity, we get:

$$\frac{K_{3CaO \cdot 2SiO_2 \cdot 3H_2O} \cdot K_{Ca(OH)_2}}{K_{3CaO \cdot SiO_2}^2} = a_{H_2O}^6 \quad [3-8]$$

Because the solubility products of hydrates is smaller than that of reactants, we have:

$$K_{CaO \cdot SiO_2 \cdot H_2O} \cdot K_{Ca(OH)_2} < K_{3CaO \cdot SiO_2} \quad [3-9]$$

Therefore, in order for both the hydrate and the reactant to reach equilibrium with the solution, the activity of water must be inferior to unity, which can be the case in presence of deliquescent salts. Nevertheless, the ratio [3-8] is large enough to avoid in principle this possibility (the lowest activity attainable with a deliquescent salt is around 0.3). In addition the dissolved ions must satisfy electrical neutrality.

So, in the majority of cases of interest, the system is unable to satisfy simultaneously both equilibrias. Before equilibrium is reached for the reactants, the system becomes supersaturated with respect to the products. This means that precipitation becomes possible. The rate at which it will take place then depends on the degree of supersaturation and the possibilities of (heterogeneous) nucleation.

Finally, let us note that if more than one hydration reaction is to take place, giving the same hydration product, then the system will mathematically be unable to satisfy simultaneously all equilibria.

3.1.3 Supersaturation regions

Damidot et al (1997) have mapped out regions in which precipitation can take place. In addition, they have mapped out what they call the critical supersaturation regions. These regions correspond to regions in which supersaturation is sufficient to induce an *immediate* precipitation (immediate refers to a timescale of a human observer, seconds or fraction of seconds). Two important cases can then be distinguished. The first one leads to a rapid precipitation. It requires that the concentrations needed for the critical supersaturation be smaller than those obtained once the reactants are in equilibrium with the solution. On the other hand, if the critical supersaturation concentrations are larger than equilibrium concentrations of the reactants, then the system will not be able to dissolve enough to reach the conditions of immediate precipitation. In such a situation, the precipitation is kinetically hindered by the equilibrium reached by the reactants with the aqueous phase.

It is important to note that the aqueous phase is a concentrated electrolyte. Therefore, the ion activities are not independent of one another. Presence of uncommon ions, as well as changing different relative or absolute compositions are therefore liable to alter the regions of saturation (if these are described by concentration) as well as regions of critical supersaturation. In particular, the addition of a superplasticizer was found to substantially modify supersaturation requirements for nucleation of CH.

For instance if we refer to the development in the previous section, altering the activity of water by adding a deliquescent salt, could in principle alter saturation domains and thereby also critical supersaturation domains.

Modification of critical supersaturation zones must also be a way through which superplasticizers can and certainly do affect cement chemistry and consequently rheology. Jolicoeur et al (1994) terms this the chemical effect, in opposition to the physical effect which he relates to a modification a interparticle forces.

3.1.4 Ion activity models

Determining supersaturation regions remains an experimental task, because of the system's complexity. Modelling the zones of saturation follows from thermodynamics. In order to relate these zones with experimentally accessible data such as elemental composition, a valid thermodynamic description is required to relate concentrations to activities.

For dilute solutions, activity coefficients are equal to unity, and concentrations suffice. However, this description fails for ionic strengths of the order of 10^{-3} M.

Debye and Hückel first proposed the calculation of ion activities using :

$$\text{Log}_{10}(\gamma_k) = -\frac{A_{D-H} z_k^2 \sqrt{I}}{1 + a_k^0 B_{D-H} \sqrt{I}} \quad [3-10]$$

$$I = \frac{1}{2} \sum_k z_k^2 c_k$$

z_k is the charge number of the ion k

c_k is the concentration of the ion k

a_k^0 is the Debye - Hückel radius of the ion k

A_{D-H}, B_{D-H} are the Debye - Hückel constants

I is the ionic strength of the solution

This description is valid up to about an ionic strength of 10^{-2} M.

Introducing a third parameter allows us to extend the use of this description up to about 10^{-1} M.

$$\text{Log}_{10}(\gamma_k) = -\frac{A_{D-H} z_k^2 \sqrt{I}}{1 + a_k^0 B_{D-H} \sqrt{I}} + C_{D-H} \sqrt{I} \quad [3-11]$$

C_{D-H} is a third Debye - Hückel parameter

For further extension, a species specific parameter must be used for C_{D-H} . This allows predictions to be made up to 1 M (at 25°C):

$$\text{Log}_{10}(\gamma_k) = -\frac{A_{D-H} z_k^2 \sqrt{I}}{1 + a_k^0 B_{D-H} \sqrt{I}} + C_k \sqrt{I} \quad [3-12]$$

C_k is an ion specific parameter

For higher concentrations, the Pitzer model should be used [Pitzer (1991)]. This model is semi-empirical and is based on a parameterisation of all the specific pair interactions, as well as the three ion interactions. This method is certainly the most powerful, but is also the one, which requires the most detailed description of the system. In addition, it does not account for some species found at high pH such as $\text{Ca}(\text{OH})^+$, for instance. For most purposes of relating aqueous phase chemistry to bulk composition, this is not a problem. These species are indirectly accounted for in the experimental data for the interaction parameterisation. However, for discussing electrostatic forces in the system, it is important in order to validate the theory to have an accurate description of the distribution of such species.

For this reason, we resort to the second version of the extended Debye-Hückel model. As it turns out, its range of validity falls within the ionic strengths of the cement suspensions considered below.

3.1.5 Ionic species

In order to illustrate the distribution of ionic species in an aqueous phase we perform ion activity calculations on data reported by Yang et al. (1997) for water/cement ratios of 0.35 and 0.45. Their data are reported in Table 3-3.

Table 3-3. Ionic concentrations for two cement suspensions as reported by Yang et al (1997). Ionic strength is 266.3 and 268.9 mM.

W:C	K^+	Na^+	Ca^{2+}	SO_4^{2-}	Si^{4+}	Mg^{2+}	Al^{3+}	OH	pH
0.35	123.94	28.14	18.31	58.72	0.05	0.04	0.07	70.79	12.85
0.45	119.60	27.12	22.28	50.34	0.4	0.02	0.09	93.3	12.97

Because the main aim in presenting these ion activity calculations is to obtain the distribution of the different aqueous species in order to perform correct calculations of electrostatic interactions between particles, we will neglect the species associated with Mg, Al and Si, because their concentration are low and contribute little to the ionic strength.

In order to perform the activity calculations, we have used the initial equilibration step included in the program KINDIS initially developed by Fritz (1975). In doing these calculations, it turns out that for the indicated pH, the solution is not electrically neutral. The solution bears an excess of anions. This is attributed to an over-evaluation of the pH. The pH, which leads to electric neutrality, has therefore

been recalculated (with an accuracy of 0.01 pH units). After this calculation, the program automatically balances any remaining small charge excess by adding Na^+ .

Table 3-4. Recalculated distributions of species in a cement suspension at 25°C. W/C = 0.35. Ionic strength is 211.6.

	K^+	Na^+	Ca^{++}	OH^-	SO_4^{--}	KSO_4^-	NaSO_4^-	$\text{Ca}(\text{OH})^+$	CaSO_4	pH
Concentration [mmol / kg H_2O]	115.75	25.11	8.68	67.86	41.28	8.19	3.08	3.45	6.17	12.69
Activity coefficient	0.695	0.745	0.347	0.717	0.255	0.717	0.736	0.729	1.052	
Total [mmol / kg H_2O]	123.94	28.19	18.31	71.31	58.72	—	—	—	—	
% of total ion in dissociated form	93%	89%	47%	95%	70%	—	—	—	—	

Table 3-5. Recalculated distribution of species in cement suspension at 25°C. W/C = 0.45. Ionic strength is 211.2.

	K^+	Na^+	Ca^{++}	OH^-	SO_4^{--}	KSO_4^-	NaSO_4^-	$\text{Ca}(\text{OH})^+$	CaSO_4	pH
Concentration [mmol / kg H_2O]	112.91	25.77	10.82	87.40	34.56	6.69	2.65	5.54	6.45	12.8
Activity coefficient	0.695	0.745	0.348	0.717	0.256	0.717	0.736	0.729	1.052	
Total [mmol / kg H_2O]	119.60	28.42	22.80	92.94	50.34	—	—	—	—	
% of total ion in dissociated form	94%	91%	47%	94%	69%	—	—	—	—	

The last line in the above table indicates the percentage of the elements found in their fully dissociated state. It is seen for instance that less than half the calcium is found in its divalent form. In addition, a substantial amount of sulphate forms pairs with the cations present in solution. All these ion associations reduce the ionic strength.

Let us consider solutions in which no ion-pairs are formed. If we then calculate the ionic strength we find that this leads to an over-evaluation of 26%.

It is also important to observe that the activity coefficients of all ions are substantially different from unity. This clearly points to the non-ideal nature of the aqueous phase of cement suspensions.

3.1.6 Implications for cement suspensions

The chemistry of the aqueous phase of cement suspensions must be described by the thermodynamics of non-ideal solutions. In this framework all ions are not independent one of another. Setting rates of cement must involve a complex synergy between dissolution and precipitation, in which the concentration of ions in the aqueous phase plays an important role. Because these, through their activities are not independent one of another, we can expect modifications of setting rates by addition of ions which in principle would not alter these rates in dilute solutions. In the case where these reactions can alter the rheology of cement suspensions at very early ages, they can decrease rapidly the fluidifying effect of a superplasticizer.

Another implication of these couplings is that addition of superplasticizers can also affect the solution chemistry. In particular if a large amount of these polymers remain in solution and do not adsorb onto the various particle surfaces.

The ion pair associations substantially modify the distribution of calcium, since less than 50% of this element is found under its divalent form. These facts will be taken into account when discussing the calculation of the electrostatic force between two cement particles.

3.2 Hydrodynamics

The rheology of suspensions is governed not only by the properties of its liquid and its solid phase but also by interactions between these phases. For instance, the nature of the liquid phase has an effect on the interparticle forces.

The effects, which are addressed here, are linked to hydrodynamics. The basic knowledge needed to account for such interactions will be presented. As a first description we may state that the movement of a particle induces a fluid movement, which in turn effects the displacement of other particles in the suspension, and so forth.

The first part of this section is strongly based on the presentation of hydrodynamics made by Russel et al (1991, chapter 2).

3.2.1 The Navier-Stokes equation

The forces encountered in a fluid can be divided into body forces and contact forces. Here we consider gravity as the only body force. Electrostatic and dispersion forces are dealt with later.

$$\mathbf{F}_g = \int_V \rho \mathbf{g} dV \quad [3-13]$$

ρ is the fluid density

\mathbf{g} is the gravitational acceleration vector

For contact forces, we consider the stress exerted at the infinitesimal stress exerts at the surface element dS of the surface S enclosing volume V .

$$\mathbf{F}_c = \int_S \mathbf{t} dS = \int_S (\boldsymbol{\sigma} \cdot \mathbf{n}) dS = \int_V \nabla \cdot (\boldsymbol{\sigma} \cdot \mathbf{n}) dV \quad [3-14]$$

Where :

\mathbf{t} is the stress vector acting on dS

\mathbf{n} is the unit vector normal to dS

$\boldsymbol{\sigma}$ is the stress tensor

$$\boldsymbol{\sigma} = \begin{bmatrix} \sigma_{xx} & \sigma_{xy} & \sigma_{xz} \\ \sigma_{yx} & \sigma_{yy} & \sigma_{yz} \\ \sigma_{zx} & \sigma_{zy} & \sigma_{zz} \end{bmatrix} \quad [3-15]$$

The sum of the body and surface forces is equated to the momentum change of volume V .

$$\frac{\partial(\rho \mathbf{u})}{\partial t} + \nabla \cdot (\rho \mathbf{u} \mathbf{u}) = \rho \mathbf{g} + \nabla \cdot \boldsymbol{\sigma} \quad [3-16]$$

\mathbf{u} is the vector of the local fluid velocity

For constant density fluids, this becomes

$$\rho \frac{\partial(\mathbf{u})}{\partial t} + \rho \nabla \cdot (\mathbf{u}\mathbf{u}) = \rho \mathbf{g} + \nabla \cdot \boldsymbol{\sigma} \quad [3-17]$$

$$\rho \frac{\partial(\mathbf{u})}{\partial t} + \rho \{ \mathbf{u} \cdot (\nabla \mathbf{u}) + \mathbf{u} (\nabla \cdot \mathbf{u}) \} = \rho \mathbf{g} + \nabla \cdot \boldsymbol{\sigma}$$

We can set up a mass conservation balance:

$$\frac{\partial(\rho)}{\partial t} + \nabla \cdot (\rho \mathbf{u}) = 0 \quad [3-18]$$

Which for constant density fluids leads to

$$\nabla \cdot \mathbf{u} = 0 \quad [3-19]$$

So, the momentum balance becomes :

$$\rho \left(\frac{\partial \mathbf{u}}{\partial t} + \mathbf{u} \cdot (\nabla \mathbf{u}) \right) = \rho \mathbf{g} + \nabla \cdot \boldsymbol{\sigma} \quad [3-20]$$

For Newtonian fluids, there is a linear relation between the stress tensor and the rate of strain tensor:

$$\boldsymbol{\sigma} = -P\boldsymbol{\delta} + \mu \left[\nabla \mathbf{u} + (\nabla \mathbf{u})^T \right] \quad [3-21]$$

Where:

P is the isotropic pressure

μ is the shear viscosity of the fluid

$(\nabla \mathbf{u})^T$ indicates the transpose of a matrix $\nabla \mathbf{u}$

$\boldsymbol{\delta}$ is the unity matrix

Substitution into the momentum balance leads to:

$$\begin{aligned} \rho \left(\frac{\partial \mathbf{u}}{\partial t} + \mathbf{u} \cdot (\nabla \mathbf{u}) \right) &= -\nabla \cdot (P\boldsymbol{\delta}) + \rho \mathbf{g} + \mu \nabla \cdot \left[\nabla \mathbf{u} + (\nabla \mathbf{u})^T \right] \\ &= -\nabla \cdot (P\boldsymbol{\delta}) + \rho \mathbf{g} + \mu \left[\nabla^2 \mathbf{u} + \nabla (\nabla \cdot \mathbf{u}) \right] \end{aligned} \quad [3-22]$$

Which after defining a dynamic pressure p such that:

$$\nabla p = \nabla \cdot (P\boldsymbol{\delta}) - \rho \mathbf{g} \quad [3-23]$$

And for a constant density fluid leads to:

$$\rho \left(\frac{\partial \mathbf{u}}{\partial t} + \mathbf{u} \cdot (\nabla \mathbf{u}) \right) = -\nabla p + \mu \nabla^2 \mathbf{u} \quad [3-24]$$

This is the Navier Stokes equation, which is the governing equation for an incompressible Newtonian fluid.

3.2.2 Stokes flow

For most colloidal systems, the inertia is negligible, so the Navier-Stokes equation [3-24] can be simplified. With [3-19], which defines incompressible fluids, we get the Stokes equations:

$$\begin{aligned} \nabla p &= \mu \nabla^2 \mathbf{u} \\ \nabla \cdot \mathbf{u} &= 0 \end{aligned} \quad [3-25]$$

These equations are the basis for most of the equations characterising the flow of colloidal systems. However, because cement particles are significantly larger than 1 μm , which is usually considered the upper bound of colloidal systems, it is important to consider whether or not inertia may be neglected.

The Navier-Stokes equation can be written in its dimensionless form as:

$$\text{Re} \left(\frac{\partial \bar{\mathbf{u}}}{\partial \bar{t}} + \bar{\mathbf{u}} \cdot (\nabla \bar{\mathbf{u}}) \right) = -\nabla \bar{p} + \mu \nabla^2 \bar{\mathbf{u}} \quad [3-26]$$

Where :

$$\begin{aligned} \bar{x} &= x / L \\ \bar{\mathbf{u}} &= \mathbf{u} / U \\ \bar{t} &= t / (L / U) \\ \text{Re} &\equiv \frac{\rho U L}{\mu} \\ \bar{p} &\equiv \frac{p L}{\mu U} \end{aligned} \quad [3-27]$$

The Reynolds number Re expresses the ratio of inertia forces versus viscous forces. For spherical particles, the characteristic distance L is the particle diameter 2a. For $\text{Re} \ll 1$, inertia is negligible.

Let us consider the maximum velocity U that a cement particle can experience in the concentric cylinder rheometer (see subchapter 3.3) used in this work. The gap d and maximum shear rate $\dot{\gamma}_{\max}$ are respectively 0.85 mm and 640 1/s. So, the maximum fluid velocity is $U_{\max} = \dot{\gamma}_{\max} d = 0.544$ m/s. In pure water, the particle size giving a Re of 0.1 would be about 0.2 μm . Therefore in pure water, the behaviour of isolated cement particles cannot be accounted for by the Stokes equations.

However, the situation is somewhat different in more concentrated suspensions, which are of interest for studying superplasticizers. In this case, viscosity values at the maximum shear rate are of the order of 0.2 Pa s for well dispersed cement suspensions having 48% volume of cement particles. The average fluid density would be 2512 kg/m³. So the maximum particle size about 15 μm , which is about the volume average particle size of most cements. This calculation was done using the maximum fluid velocity. However, both the particles and the aqueous phase are in movement and it is the relative velocity, which is most relevant for calculations. This will extend the maximum particle size and certainly include all cement particles. **The inertia can therefore be neglected in concentrated suspensions and the Stokes equations can be used for cement suspensions.**

Note that most cement suspensions are shear thinning. This means that at low shear rates, the viscosity is higher than at high shear rates. So, provided a yield stress is present more dilute suspensions could be described by the Stokes equations at lower shear rates (this effect should overbalance the viscosity decrease due to lower solid volume fractions).

Note that if Stokes equations appear to be relevant for cement suspensions at low shear rates, they are most likely not applicable to large agglomerates of cement particles, which in concentrated suspensions could have equivalent sizes much larger than cement particles (possibly one order of magnitude larger).

3.2.3 Single sphere dynamics

Steady state motion of single sphere

The Stokes equations are linear. This means that it is often possible to describe complicated situations by superimposition of solutions to simpler problems. For single sphere dynamics, important results can be derived by superimposition of solutions to point force problems.

Russel et al (1991, §2.5) show that the application of a point force induces both a fluid motion and pressure in any point of this fluid:

$$\mathbf{u}(\mathbf{x}) = \frac{1}{4\pi\mu} \left(\frac{\boldsymbol{\delta}}{x} + \frac{\mathbf{x}\mathbf{x}}{x^3} \right) \cdot \mathbf{f} \quad [3-28]$$

$$p(\mathbf{x}) = \frac{1}{4\pi x^3} \mathbf{x} \cdot \mathbf{f}$$

Where:

$$\mathbf{x} \text{ is the position vector of point at which velocity and pressure are evaluated} \quad [3-29]$$

$$x \text{ is the norm of } \mathbf{x}$$

$$\mathbf{f} \text{ is the point force applied at the origin } (\mathbf{x} = 0)$$

These solutions allow the construction of the dynamics of an isolated sphere (Russel et al (1991, §2.6). For creeping flow, the force on a sphere can be written:

$$\mathbf{F} = 6\pi\mu a \left[\left(\mathbf{u}_\infty + \frac{1}{6} a^2 \nabla^2 \mathbf{u}_\infty \right)_0 - \mathbf{U}_0 \right] \quad [3-30]$$

Where:

$$\mathbf{u}_\infty \text{ is the velocity the fluid would have in absence of the sphere} \quad [3-31]$$

$$(\)_0 \text{ indicates that the expression is evaluated at the sphere centre}$$

$$\mathbf{U}_0 \text{ is the velocity of the translating sphere}$$

So, at steady state, the viscous force on a sphere translating through a fluid otherwise at rest is given by:

$$\mathbf{F} = 6\pi\mu a \mathbf{U}_0 \quad [3-32]$$

Transient motion of single sphere

Another expression for single sphere dynamics, which will be of interest to us is the time scale of unsteady state motion. In cases where inertia can not be neglected, but where Re number remains sufficiently small to neglect inertial accelerations ($\mathbf{u} \cdot \nabla \mathbf{u} = 0$), show that the velocity of a sphere subjected to a force impulse $\mathbf{F}(t) = \mathbf{M}_0 \delta(t)$ decays as:

$$U(t) = \frac{1}{9\sqrt{\pi}} \frac{3M_0}{4\pi a^3 \rho} \left(\frac{\rho a^2}{\mu t} \right)^{3/2} + \dots \quad [3-33]$$

Integration of this expression shows that the impulse propels the particle over a finite distance $\frac{M_0}{6\pi\mu a}$.

Equation [3-33] indicates that steady state expressions assume that the time scale of observation is much larger than that of this transient motion, $t \gg \rho a^2 / \mu$. The time scale for neglecting this transient effect in water for a large 50 μm particle would be about 0.6 ms, while for a small 1 μm particle, it would be 0.25 μs . Again, approximations valid for colloid particles seem doubtful for cement particles in very dilute suspensions. In more concentrated suspensions however, the viscosity increase makes the approximation more acceptable.

3.2.4 Dynamics of two spheres

We have seen that a force applied in a point of a fluid influences the velocity of all other points of the fluid. So a sphere under translation induces a velocity field of all other points of the fluid. This fluid velocity influences the motion of all other spheres within the suspension. In turn, their motion influences the motion of the first sphere. This phenomena is termed hydrodynamic interaction.

In this section, we will only consider the hydrodynamic interactions of two spheres. In addition, as is discussed below, we are primarily concerned with measuring yield stress because this parameter is related to the interparticle forces. Our interest is to determine how much hydrodynamic interactions effect the determination of the yield stress of a cement suspension.

A suspension can be considered to yield once the applied shear has overcome a given number of interparticle forces (Russel et al (1991), subchapter 14.7). **So, the main interest is to determine the hydrodynamic interactions of spheres in close contact.**

The equations presented below are taken from Kim and Karrila (1991) (chapter 9).

Shearing motion of rigid surfaces

We consider two spheres of S_1 and S_2 with their radii respectively a_1 and a_2 . S_2 is stationary while S_1 is in motion. As shown in Figure 3-1, a Cartesian coordinate system is chosen so that its z axis is the line between the sphere centers and its origin is at the closest point of S_2 to S_1 . S_1 moves with a velocity U in the positive x direction.

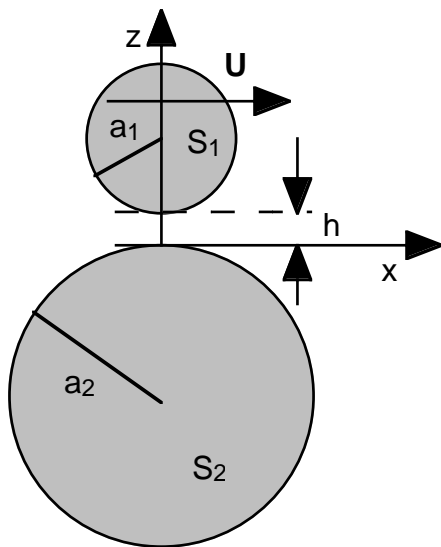


Figure 3-1. Flow produced by shearing one sphere S_1 past another sphere S_2 , which is fixed.

Defining:

$$\beta = \frac{a_2}{a_1} \quad [3-34]$$

$$\varepsilon = \frac{h}{a_1}$$

h is the gap between both spheres

Kim and Karrila (1991) show that the force F_x exerted on S_1 is given by:

$$\begin{aligned}
\frac{F_x}{6\pi\mu a_1 U} &= V_{(\beta,\varepsilon)} & [3-35] \\
&= -\frac{4\beta(2+\beta+2\beta^2)}{15(1+\beta)^3} \ln\left(\frac{1}{\varepsilon}\right) + A(\beta) \\
&\quad - \frac{4(16-45\beta+58\beta^2-45\beta^3+16\beta^4)}{375(1+\beta)^4} \varepsilon \ln\left(\frac{1}{\varepsilon}\right) + O(\varepsilon)
\end{aligned}$$

Evaluation of the $O(1)$ term $A(\beta)$ and of the $O(\varepsilon)$ term is beyond the scope of this work. So we will only be considering the leading term, bearing in mind that numerical solutions would be needed for more accurate predictions.

Squeezing motion of rigid spheres

Using the same coordinate system as above, we now consider S_1 to approach S_2 with a velocity along the line of centers (Figure 3-2). In this case, Kim and Karilla (1991), (§9.3) find the force along the line of centers to be:

$$\begin{aligned}
\frac{F_z}{6\pi\mu a_1 U} &= W_{(\beta,\varepsilon)} & [3-36] \\
&= -\frac{\beta^2}{(1+\beta)^2} \varepsilon^{-1} - \frac{(1+7\beta+\beta^2)}{5(1+\beta)^3} \ln\left(\frac{1}{\varepsilon}\right) + K(\beta) \quad ^5 \\
&\quad - \frac{(1+18\beta-29\beta^2+18\beta^3+\beta^4)}{21(1+\beta)^4} \varepsilon \ln\left(\frac{1}{\varepsilon}\right) + O(\varepsilon)
\end{aligned}$$

Again, proper evaluation of the force would require fitting with numerical solutions to obtain $K(\beta)$ and $O(\varepsilon)$ terms.

⁵ Note Kim and Karrila (1991) falsely write this the equation with F_x instead of F_z .

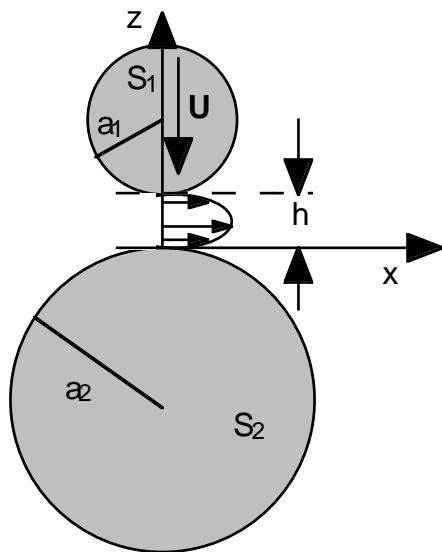


Figure 3-2. Flow produced by approaching a sphere S_1 from a fixed sphere S_2 .

3.3 Rheology

3.3.1 Basis of rheology

Rheology measurements seek to define a characterising equation as [3-21], which describes the relation between the local stress tensor $[\sigma]$ and the local rate of strain tensor $[\nabla\mathbf{u} + (\nabla\mathbf{u})^T]$ within a fluid. For Newtonian fluids there is a linear relation and a single parameter μ , the viscosity. For non-Newtonian fluids more parameters are needed.

Viscoelastic fluids are characterised by the fact that at low shear they exhibit a solid like behaviour, while at high shear they exhibit a liquid like behaviour. In the low shear regime, oscillation measurements are applicable for determining the rheological behaviour of the fluid. At high shear it is shear stress or shear rate controlled experiments which are not suitable.

3.3.2 Shear rate and shear controlled rheometers

The principle of many rheometers is to submit a fluid to either controlled stress or controlled shear rate and measure the resulting shear rate or shear stress respectively. The geometry is selected in order to simplify the form of the shear stress and rate of strain tensors. This is done by putting the fluid in motion between two walls separated by only a small distance, so that a uniform velocity gradient can be assumed over the separation gap (Figure 3-3).

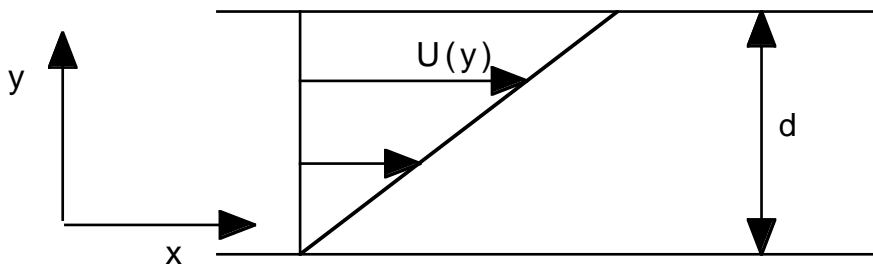


Figure 3-3. Flow representation in a shear stress or shear rate controlled rheometer.

Under such conditions, and assuming a no slip boundary condition, the Navier Stokes equation leads to:

$$u_y = U \frac{y}{d} \quad [3-37]$$

Where:

$$u_y \text{ is the velocity along } x \text{ at distance } y \text{ from the fixed wall} \quad [3-38]$$

U is the velocity of the moving wall

d is the separation between both walls

In absence of pressure differences, the relation between shear stress and shear rate becomes

$$\sigma = \mu \begin{bmatrix} 2 \frac{\partial}{\partial x} u_x & \frac{\partial}{\partial x} u_y + \frac{\partial}{\partial y} u_x \\ \frac{\partial}{\partial x} u_y + \frac{\partial}{\partial y} u_x & 2 \frac{\partial}{\partial y} u_y \end{bmatrix} = \mu \begin{bmatrix} 0 & \frac{\partial}{\partial y} u_x \\ \frac{\partial}{\partial y} u_x & 0 \end{bmatrix} = \mu \frac{U}{d} \begin{bmatrix} 0 & 1 \\ 1 & 0 \end{bmatrix} \quad [3-39]$$

Typical geometries of rheometers, which satisfy the constant shear rate conditions are either concentric cylinders or cone and plate setups.

3.3.3 Some rheological behaviours

Equation [3-39] is valid for Newtonian fluids. We rewrite this with:

$$\tau = \mu \dot{\gamma} \quad [3-40]$$

Bingham fluids, have the relation:

$$\tau = \tau_0 + \mu_{Bi} \dot{\gamma} \quad [3-41]$$

Where τ_0 is the yield stress and μ_{Bi} the intrinsic viscosity. Yield Stress is defined as the critical stress at which the fluid has a transition between a solid-like and a liquid-like behaviour. However, this parameter remains relatively poorly defined, since this transition is not as sudden as predicted by the Bingham model.

Yield stress as expressed in the Bingham model is also found in the model of Herschel-Buckley. In this case, the shear stress is assumed to increase as a power law of shear rate, above yield stress.

$$\tau = \tau_0 + \mu_{H-B} \dot{\gamma}^n \quad [3-42]$$

Note that the very sharp transition between the solid-like and the liquid-like assumed in both the Bingham and the Herschel-Buckley model is a clear simplification.

Figure 3-4 shows flow curves for these different fluids. In this figure, the intrinsic viscosity of the Bingham fluid μ_{Bi} is the same as the true viscosity of the Newtonian fluid η (0.2 Pa s). The Bingham and the Herschel-Buckley fluids have the same yield stress τ_0 (10 Pa). In addition, the parameters are taken so that the apparent viscosity of the Herschel-Buckley fluid is the same as the Newtonian at a shear rate of 200 s^{-1} . These parameters were chosen because, the high shear viscosity of our most studied cement was 0.2 Pa s and the yield stress was between 6 and 10 Pa, for the optimal effect of added superplasticizers. The Herschel-Buckley exponent is chosen so that the behaviour is inbetween the Newtonian and the Bingham fluid.

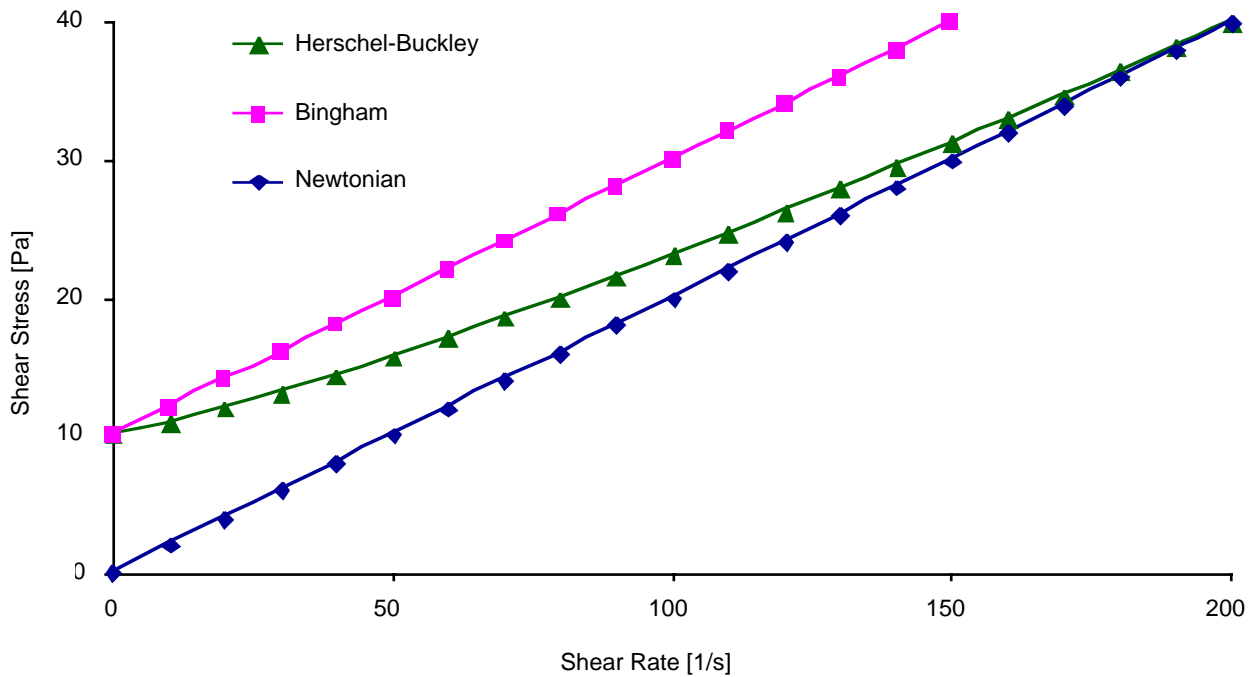


Figure 3-4. Example of different flow curves.

3.3.4 Rheology of viscoelastic fluids

Oscillation rheology is a way of obtaining information on the viscoelastic behaviour of fluids. The equivalent of shear stress and shear rate are respectively deformation and frequency. One usually fixes one of the parameters and sweeps values of the other.

For cement suspensions, the hydration avoids long measuring times, so frequency sweeps are avoided. Measurements were done by Schultz et al (1993) and Nachbaur et al (1997) using amplitude sweeps at a frequency of 1Hz. They find that the smallest deformations already induce a breakdown of the microstructure. This means that almost no data can be acquired in the linear viscoelastic region. This raises a problem of data interpretation because beyond this region, leaving interpretation at best non-trivial if not impossible.

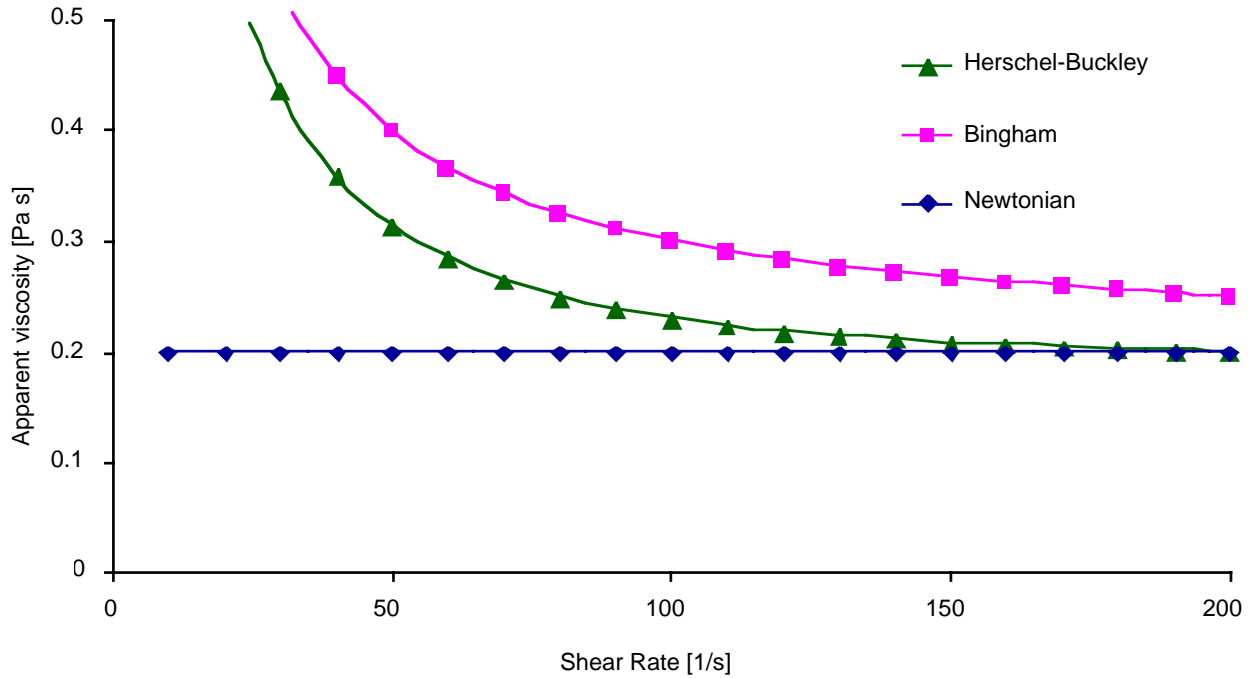


Figure 3-5. Viscosity curves for the same conditions as in Figure 3-4.

An important factor is that the inertial effects must be negligible, in order for the velocity gradient to follow:

$$u_x = \gamma \sin(\omega t) \quad [3-43]$$

Let us consider small amplitude oscillations. Their characteristic time $1/\omega$ must be longer than the characteristic time of transient effects $\rho d^2/\mu$ (subchapter 3.2.3). Here h is the gap between both walls. For the concentric cylinder used the gap is 0.85 mm. For a suspension with $W/C = 0.35$ the density ρ is 2512 kg/m^3 . If the suspension is Newtonian and its viscosity is 0.2 Pa s (the intrinsic viscosity of the Bingham behaviour measured on well dispersed 0.35 W/C suspensions), the frequency would have to be smaller than 9 mHz . So, the period would be about 110 seconds . This is much too long considering the hydration of cement paste. We can calculate the minimum viscosity μ_{\min} required for a 1 Hz oscillation frequency to be: 550 Pa s . If the viscosity follows a Bingham model with a 0.2 Pa s intrinsic viscosity μ_{Bi} , then the maximum shear rate can be written:

$$\dot{\gamma}_{\max} = \frac{\tau_0}{\mu_{\text{Bi}}} - \mu_{\min} \cong \frac{\tau_0}{\mu_{\text{Bi}}} \quad [3-44]$$

For 10 Pa yield stress, the maximum shear rate is 0.02 1/s. Note the Bingham model is not appropriate for describing oscillation measurements. It is just used here to evaluate the equivalent maximum shear rate up to which 1Hz oscillation might induce transient effect perturbing the measurement of a well-dispersed 0.35 W/C cement suspension. So, we expect oscillation at 1Hz, to be relevant only for determining behaviour below shear rate of 0.02 1/s. Above it shear stress or shear rate controlled measurements would be more relevant.

Another measurement of viscoelastic fluids is creep compliance. In this case one measures the response of the material to a sudden loading or unloading of stress or strain. Struble and Schultz (1993) have used this method to determine yield stress. **Values turn out to be consistent with shear controlled experiments.**

3.3.5 Other testing methods

Probably the most widely used method for measuring the rheology of concrete is the slump test. It consists filling a cone with the concrete, placing this cone over a table and removing the cone. The concrete spreads onto the table. One then measures the difference between the initial height of the cone and of the spread concrete. This is a practical and simple way of comparing the rheology of different suspensions, but does not provide any insight into the microstructural origin of the differences. Most of the other methods, such as flow table spread, cone test etc. suffer the same problem.

Some rheometers measure the torque necessary to mix a sample at a given rotation rate, usually with vanes. In such systems, the flow patterns are not known and it is not possible to derive a physically meaning relation between shear stress and shear strain.

3.3.6 Selection of a rheometer for measuring cement pastes

One of the concerns of this work is to determine the mechanism of action of superplasticizers in cement paste. We are primarily concerned with obtaining information on pastes flowing with only low applied shear. So, it is mainly the region of transition between liquid and solid behaviours which is of interest. This is precisely the region where the interpretation of both oscillation and shear controlled measurements falls down. The oscillation is certainly relevant for studying cement hydration, since it

will not perturb the microstructure. On the other hand stress or strain controlled experiments is more relevant for high shear situations. Because of the limitations in deformation of cement previously mentioned, it appears a better choice to use shear controlled experiments.

This is chosen rather than creep and compliance since work by Struble and Schultz (1993) has shown values consistent with shear controlled experiments and that it is a faster method also providing reliable information of high shear behaviour.

So, we have determined yield stress by shear stress ramps. This provides us with a parameter mainly linked to the magnitude of interparticle forces. Our objective, bearing in mind the limitations of its experimental determination, is to relate this yield stress to the effect of superplasticizers on the magnitude of interparticle forces.

A possible limitation with this method is slip at the walls of the rheometer, generally referred to as wall-slip. Under such conditions, the boundary conditions assumed for the Navier-Stokes equation solution are no longer valid and the fluid resistance is underestimated.

3.4 Brownian motion

A particle in a suspension undergoes incessant impacts from the fluid molecules. These impacts impart an energy of $3/2 k_B T$, partitioned equally among the three translational degrees of freedom. Over time, this allows a particle, on average, to move away from an arbitrary initial position.

In the absence of interparticle forces and in an unbounded fluid, Brownian motion will lead over time, to an increased averaged separation between a pair of particles. However, due to hydrodynamic interactions, the displacement of both particles are not independent one of the other [Russel et al (1991), subchapters 3.5-3.6].

In the presence of an attractive force between the particles, the dynamics will be strongly modified. Most discussions regarding colloidal stability (i.e, the facility to prevent agglomeration), is based on a comparison between interparticle interaction energies and the thermal energy, which can lead to particle agglomeration or separation.

It is not the purpose of this section to develop the notions or equations further to describe these phenomena. Indeed, as will be argued in chapter 10, Brownian forces are insignificant with respect to

viscous forces in cementitious systems. Therefore, stability of cement suspensions can be discussed with respect to viscous forces only.

3.5 Sedimentation

3.5.1 General realtions

Under the effect of gravity all particles have a tendency to sediment. However, the rate at which this takes place is highly dependent on the particle radius (a), and to a lesser extent on the viscosity (μ) of the surrounding fluid and the difference between the density of the particle (ρ_p) and the fluid (ρ_f).

In a Newtonian fluid, the steady state sedimentation velocity is obtained by balancing the viscous drag against the gravitational force. For spheres, we get:

$$m\mathbf{g} = \frac{4}{3}\pi a^3(\rho_p - \rho_f)\mathbf{g} = 6\pi\mu a\mathbf{U}_s \quad [3-45]$$

Which leads to :

$$\mathbf{U}_s = \frac{2a^2}{9\mu}(\rho_p - \rho_f)\mathbf{g} \quad [3-46]$$

This equation indicates that the sedimentation velocity increases strongly with particle size. Note that one assumption here is the Newtonian behaviour of the fluid. In presence of a yield stress, sedimentation will be at least strongly hindered.

Again, for several particles the movement is coupled through the hydrodynamic interactions. The term hindered settling is often used to indicate that at higher volume fractions of solid the sedimentation rate is hindered. This term can be somewhat misleading, since it suggests a hard sphere exclusion effect. A prediction by Batchelor (1972) was recently confirmed for suspensions containing up to 15% volume of solids. The major hindering is due to the fact that the settling of the lower spheres induces an upstream current, which imparts a vertical velocity to the other spheres. At higher volume fractions other effects come into account and the term hindered settling might become less misleading about the reasons behind the reduced settling rates.

3.5.2 Sedimentation in cement suspensions

For cement suspensions, due to the large size of particles, the sedimentation rates for the majority of the particles are very high in dilute suspensions. An effect often observed when adding superplasticizers is segregation. This is the result of the superplasticizers dispersing space filling flocs and allowing sedimentation of smaller sub-units into a smaller volume. It can also be viewed as inducing a yield stress decrease and thereby strongly modifying sedimentation rates.

Assume we start with a viscous suspension of cement. As superplasticizer is added, this suspension becomes more fluid. However, there is a point beyond which segregation (sedimentation) of the particles takes place. To prevent this settling, more solids can be introduced. However, they do not only increase viscosity through hydrodynamic interactions, but also through added interparticle forces. This second contribution can be decreased by adding superplasticizers. Again, as this is done, a point will be reached beyond which segregation appears. The procedure can then be repeated until the highest volume fraction is obtained for the desired workability. At this point, it will be the pure volume effect hindering the settling of cement particles and the optimum dispersion ability of the superplasticizer. Note that in such concentrated suspensions, it might become relevant to study interparticle frictions.

In practice, there is a constant play between solids loading and superplasticizer dosage in order to obtain a fluid suspension without sedimentation. The optimum solid loading, which superplasticizers can allow is probably rarely exploited and a degree of agglomeration is maintained in order to hinder settling brought about by sedimentation.

In self-compacting concrete, thickeners are usually added. Thus, it is no longer necessary at solid loadings lower than the maximum loading to maintain a certain degree of agglomeration to hinder segregation. This means that the suspension can have almost zero yield stress without segregation. Therefore, the viscosity at the low shear rates attainable in self-compacting concrete will remain low enough for compaction, while high enough to hinder settling.

3.6 Dispersion forces

3.6.1 Origin of dispersion forces

Dispersion forces between two particles “arise because local fluctuations in the polarisation within one particle induce, via propagation of electromagnetic waves, a correlated response in the other” [Russel et al (1991)]. For two particles made of the same isotropic matter, this interaction is always attractive. The terminology *of dispersion forces* can therefore be somewhat confusing. In fact, it arises from the fact that the equations used to describe the phenomena are similar to those which describe light scattering (light dispersion). This force can become repulsive for particles of different composition or between different faces of anisotropic particles. This aspect might carry some important implications in cementitious systems.

The range of this dispersion force is much larger than that of the individual dipoles. It is the summation of the interaction of these dipoles, which leads to this “long distance” interaction. The way this summation has been performed has changed over the years, both as a result of a better physical description of the phenomena and of an increased ability to deal numerically with the most complete description.

3.6.2 Microscopic theory

The microscopic theory was the first to lead to a description of the dispersion force between particles. It is based on a pair-wise summation of the interacting dipoles. The interaction reduces to the product of two terms: the Hamaker constant A and the geometric factor H . The Hamaker constant depends on the optical properties of the particles and of the intervening material. The geometric factor accounts for the dependence on the morphology of the interacting particles. In what follows, we limit our description to the case of spherical particles with different radii. The interaction potential, Φ , of two spherical particles (i.e. the energy involved in bringing the surfaces of two particles of radius a_1 and a_2 from an infinite separation to a distance h from each other) is given by:

$$\Phi = -A H_{(a_1, a_2, h)}$$

Where :

$$H_{(a_1, a_2, h)} = -\frac{1}{6} \left(\frac{2a_1 a_2}{2(a_1 + a_2)h + h^2} + \frac{2a_1 a_2}{4a_1 a_2 + 2(a_1 + a_2)h + h^2} + \text{Ln} \left(\frac{2(a_1 + a_2)h + h^2}{4a_1 a_2 + 2(a_1 + a_2)h + h^2} \right) \right)$$

[3-47]

The dispersion force is equal to the derivative with respect to separation distance of interaction potential.

$$F = \frac{d\Phi}{dh} = -A \frac{dH_{(a_1, a_2, h)}}{dh} \quad [3-48]$$

In the microscopic description, the Hamaker constant is independent of separation distance.

3.6.3 Continuum theory

Formulation

The continuum theory takes the microscopic theory a step further in describing dispersion forces. Instead of treating the interaction as a summation of individual dipoles interactions, the continuum theory considers the fluctuating electromagnetic fields, which exist in each particle. These fields extend beyond their boundaries in the form of travelling waves and standing waves.

Since the original treatment of the continuum theory by Lifshitz (1956), it has been realised that standing waves alone suffice to quantify dispersion forces. Another important step in simplifying the treatment of the continuum theory was made by Mahanty and Ninham (1976, §2.7) who showed that these interactions could be described by a discrete series of equally spaced imaginary frequencies, instead of having to evaluate the interaction over the whole electromagnetic spectrum.

This leaves the description of the interaction potential as function of the normal modes associated with a particular geometry the specific dielectric properties of the materials (particles and intervening medium).

Geometry

The interaction between flat plates leads to an analytical solution, which can be expressed in a similar way as the result from the microscopic theory. However, in this case, the Hamaker constant is an effective Hamaker constant, which depends also on the separation distance. This distance dependence accounts for the fact that, although correlation of the fluctuating dipoles takes place at the speed of light, it requires a finite time. With increasing separation, this time becomes comparable to the time scale of the fluctuations, leading to a lower of correlation, and a decrease in the effective Hamaker constant. This effect is termed retardation.

For spheres retardation is much more complicated. Its adequate numerical description by Langbein (1974), is renowned for its extremely slow convergence. Pailthorpe and Russel (1982) have proposed an algorithm giving good precision for much less numerical effort. They express the dispersion potential in a similar way as for the microscopic theory, the product between the geometrical factor for spheres and an effective Hamaker constant. This effective Hamaker constant is calculated as follows:

$$A_{eff} = \frac{3}{2} k_B T \sum_{N=1}^{\infty} \left(\frac{\xi_N}{\xi_C} \right)^2 \int_1^{\infty} dp p \operatorname{Ln} \left[\left(1 - \left(\frac{S_1 \epsilon_0 - p \epsilon_1}{S_1 \epsilon_0 + p \epsilon_1} \right)^2 \exp \left(- \frac{\xi_N}{\xi_C} p \right) \right) \left(1 - \left(\frac{S_1 - P}{S_1 + P} \right)^2 \exp \left(- \frac{\xi_N}{\xi_C} p \right) \right) \right]$$

Where : [3-49]

$$\xi_C = \frac{c}{2h\sqrt{\epsilon_0}}$$

$$\xi_N = N \frac{4\pi^2 k_B T}{h} \text{ is the infinite set of discrete frequencies}$$

$$S_1^2 = p^2 - 1 + \frac{\epsilon_1}{\epsilon_0}$$

$$\epsilon_j = \epsilon_j(i\xi_N) \text{ is the the dielectric response function of material j}$$

c is the speed of light

h is the distance of closest contact between the spheres

h is Planck's constant

They tested this approach for equal spheres and found a good correlation with the full calculations using Langbein (1974) formulation. In what follows, we extend the use of this approach to the case of unequal spheres.

It should be pointed out here, that the dispersion interaction comprises a static term ($N = 0$), which is non-retarded (does not decrease with separation). The above description does not include this term.

Other approaches used to calculate retarded dispersion interactions have been proposed, however they tend to rely on an extended simplification of spectroscopic data. In the case of water, which has complicated spectral features, this has led to large errors in the evaluation of non-retarded Hamaker constants as discussed below. Therefore we have not adopted these methods and use the somewhat more complicated method outlined above.

Dielectric Properties

One important part of the evaluation of the dispersion interaction is to obtain a valid description of the dielectric properties of the particles and the intervening fluid. Bergström (1997) showed the importance of using a detailed dielectric representation for water, as recently published by Roth and Lenhoff (1996). The function is based on the representation of a damped oscillator and is given by:

$$\varepsilon(i\xi_m) = 1 + \frac{B}{1 + \xi \tau} + \sum_j \frac{C_j}{1 + g_j \left(\frac{\xi}{\omega_j} \right) + \left(\frac{\xi}{\omega_j} \right)^2} \quad [3-50]$$

$i\xi_m$ is the set of discrete imaginary frequencies for which:

$$\xi_m = m \left(\frac{4\pi k_B T}{h} \right)$$

$$m = 0, 1, 2, 3, 4, \dots$$

Orientation of permanent dipoles accounts for the second term. The summation is linked to infrared and ultraviolet absorption peaks. B and g_j relate to the oscillator strength in the microwave range and damping coefficient of the oscillator respectively. C_j is linked to the oscillator strength f_j and to the relaxation frequency ω_j by :

$$C_j = \frac{2 f_j}{\pi \omega_j} \quad [3-51]$$

Parameters calculated by Bergström(1997) in order to obtain, with [3-50], the best fit to experimental data compiled from various sources are given in Table 3-6.

At the moment, accurate dielectric data are not available for the pure phases of cement. Therefore, we evaluate a series of minerals believed to be relatively close to these cement phases. For these materials, the spectral features require a less elaborate description than water [Bergström (1997)]:

$$\epsilon(i\xi_m) = 1 + \frac{C_{IR}}{1 + \left(\frac{\xi}{\omega_{IR}}\right)^2} + \frac{C_{UV}}{1 + \left(\frac{\xi}{\omega_{UV}}\right)^2} \quad [3-52]$$

Where C_{IR} and C_{UV} are the absorption strengths (IR or UV) and ω_{IR} and ω_{UV} are the characteristic absorption frequency (IR or UV). Values for the minerals considered are given in Table 3-7.

Table 3-6. Spectral parameters for water, from Bergström (1997)

C_{UV}	$\omega_{UV} \times 10^{16}$ rad/s	$g_{UV} \times 10^{15}$ rad/s	C_{IR}	$\omega_{IR} \times 10^{14}$ rad/s	$g_{IR} \times 10^{15}$ rad/s
0.0484	1.25	0.957	1.46	0.314	2.29
0.0387	1.52	1.28	0.737	1.05	5.78
0.0923	1.73	3.11	0.152	1.40	4.22
0.344	2.07	5.92	0.0136	3.06	3.81
0.360	2.70	11.1	0.0751	6.46	8.54
0.0383	3.83	8.11			

$$B = 76.8 \text{ and } 1/\tau_{\mu\text{-wave}} = 1.08 \times 10^{11} \text{ rad/s}$$

Table 3-7. Parameters for dielectric representation of some minerals, from Bergström (1997)

	Structure	C_{UV}	$\omega_{UV} \times 10^{16}$ rad/s	C_{IR}	$\omega_{IR} \times 10^{14}$ rad/s
CaCO ₃ (Calcite)	Average*	1.516	1.897	5.7	2.691
α -Al ₂ O ₃	Hexagonal	2.072	2.00	7.03	1
MgO	Cubic	1.946	1.71	6.85	1.0
SiO ₂ (quartz)	Trigonal	1.359	2.032	1.93	2.093
SiO ₂ (silica)	Amorphous	1.098	2.034	0.829	0.867
MgAl ₂ O ₄	Cubic	1.887	1.87	5.41	1.0

* Average of the different orientations for this mineral which is anisotropic.

It is important to remark that the calculations of the non-retarded Hamaker constant done with a less precise dielectric description of water can lead to an over-evaluation of about 40%. It seems that up to the work of Bergström (1997), all calculations were relying on the same imprecise dielectric description of water. In other words, up to 1997, all Hamaker constants reported in the literature for aqueous systems are over-evaluated.

Screening and Retardation in cement suspensions

An important issue for cement suspensions is whether the high ionic concentration can effect the magnitude of the dispersion force. It turns out that only the static term ($N=0$) is affected by the presence of electrolytes. At high concentrations, this term is totally screened and does therefore not contribute to the total dispersion interaction [Russel et al (1991)].

In addition, we recall that only this static term is non-retarded. Therefore, at large separations, in water, the effective Hamaker constant is greater than zero, while in a concentrated electrolyte it will be equal to zero.

Because the aqueous phase of cement suspensions is a very concentrated electrolyte, the Hamaker constant can be calculated without the static term. The equation presented above for calculating the contribution to the retarded Hamaker constants can therefore be used directly to evaluate the effective Hamaker constant.

Summary of continuum theory implications

The main points of interest for cement suspensions are:

- Due to the wide use of inadequate dielectric representation of the dielectric spectra of water, Hamaker constants for aqueous suspensions published up to 1997 are over-evaluated by about 40%.
- In suspensions containing high concentrations of electrolytes, the static term of the Hamaker constant need not be taken into account.
- Retardation increases for long interaction distances and can be evaluated by the product of an effective Hamaker constant (function of separation and dielectric properties of the particles and liquid) and a geometric term (function of particle sizes and separation).

3.6.4 Cement like suspensions

Effective Hamaker constants

Numerical calculations were performed to obtain retarded and screened Hamaker constants as a function of separation distance up to 3000 nm, for the materials listed in Table 3-7. A listing of the macros used to perform these calculations with Microsoft Excel is given in Annex C. Results were then fitted in order to obtain an equation for Hamaker constant as a function of separation distance.

At large separations, the retarded Hamaker constant decays exponentially:

$$\lim_{h \rightarrow \infty} A_{(h)} = a_{\infty} \exp(-b_{\infty} h) \quad [3-53]$$

Where: a_{∞} and b_{∞} are fitted parameters

A regression performed over data at large separations allows us to determine a_{∞} and b_{∞} . Then the difference between the calculated Hamaker constant and this long-range decay function were evaluated over the whole range of separation distances:

$$\Delta A_{(h)} = A_{(h)} - A_{\infty(h)} \quad [3-54]$$

We found that this difference could be adequately represented by:

$$\Delta A_{(h)} = (m_1 h^2 + m_2 h + m_3) \exp(-m_4 h) \quad [3-55]$$

Where: $m_{1,2,3,4}$ are fitted parameters

Leading to the following description of the effective Hamaker constant:

$$A_{(h)} = (m_1 h^2 + m_2 h + m_3) \exp(-m_4 h) + a_\infty \exp(-b_\infty h) \quad [3-56]$$

Values for the minerals considered are reported in Table 3-8. Comparison between the retarded Hamaker constant versus separation are given in Figure 3-6 and Figure 3-7. For convenience of the representation, values are only shown down to 1 nm. However, the smallest separation calculated was 0.05 nm.

Table 3-8. Parameters for fitted effective Hamaker constant. The last line gives the non-retarded static term. This term is totally screened in cement suspensions.

	Calcite	Alumina (α -Al ₂ O ₃)	Magnesium Oxide	Quartz	Amorphous Silica	Spinel (Al ₂ MgO ₄)
a_∞	0.276	0.191	0.166	0.059	0.004	0.143
$b_\infty \times 10^3$	2.028	2.185	2.166	2.009	2.116	2.193
$m_1 \times 10^4$	3.449	18.740	5.691	3.000	0.476	8.661
$m_2 \times 10^2$	-1.636	-7.256	-2.695	-1.495	-0.335	-3.893
m_3	1.000	3.378	1.918	0.717	0.163	2.149
$m_4 \times 10^2$	3.955	5.107	4.019	4.288	3.821	4.471
$A_{\text{nr}} \times 10^{20}$	0.227	0.205	0.208	0.283	0.306	0.226

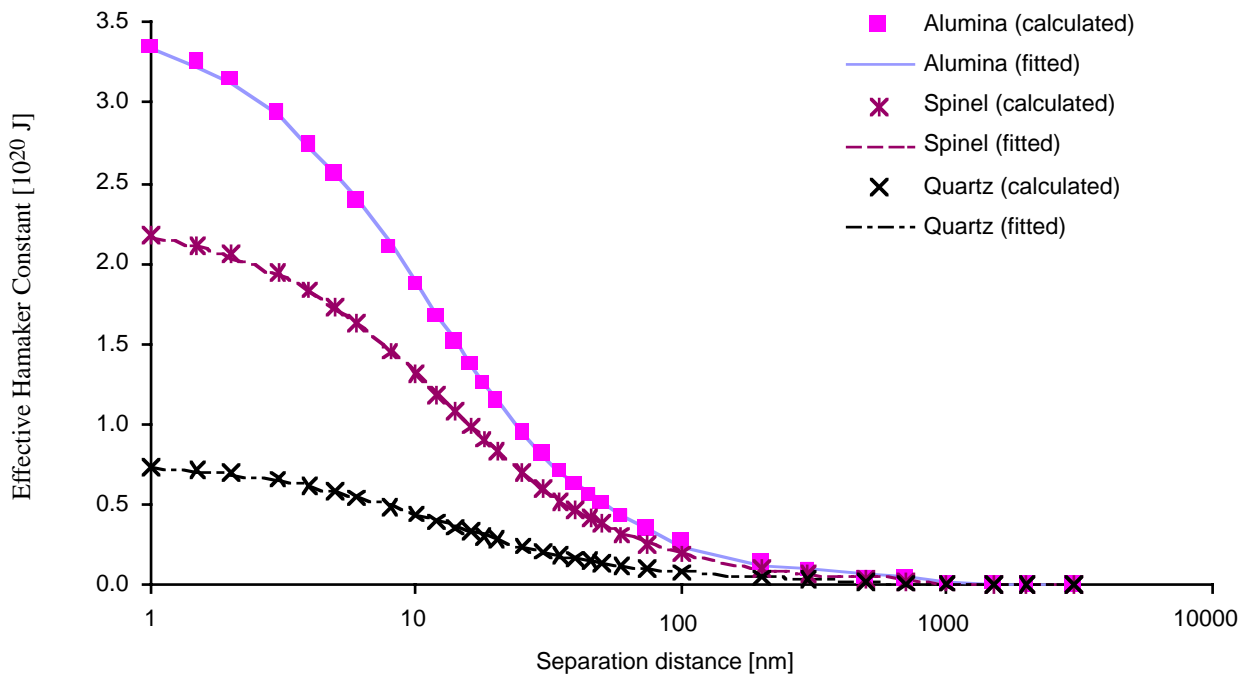


Figure 3-6. Comparison between discrete values of calculated effective Hamaker constants and suggested fits.

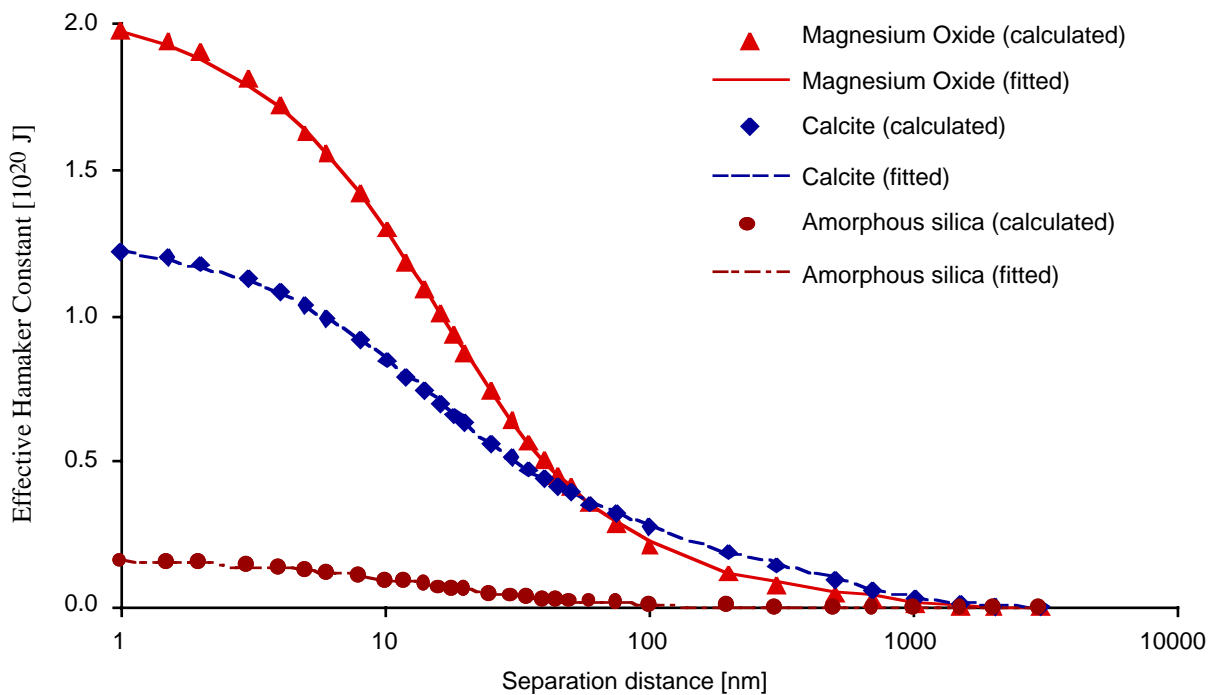


Figure 3-7. Comparison between discrete values of calculated effective Hamaker constants and suggested fits.

The computation of these Hamaker constants with retardation and screening is important for cement suspensions, and has not previously been carried out. In order to evaluate the consequence of neglecting either retardation or screening or both, the errors induced are shown in Figure 3-8.

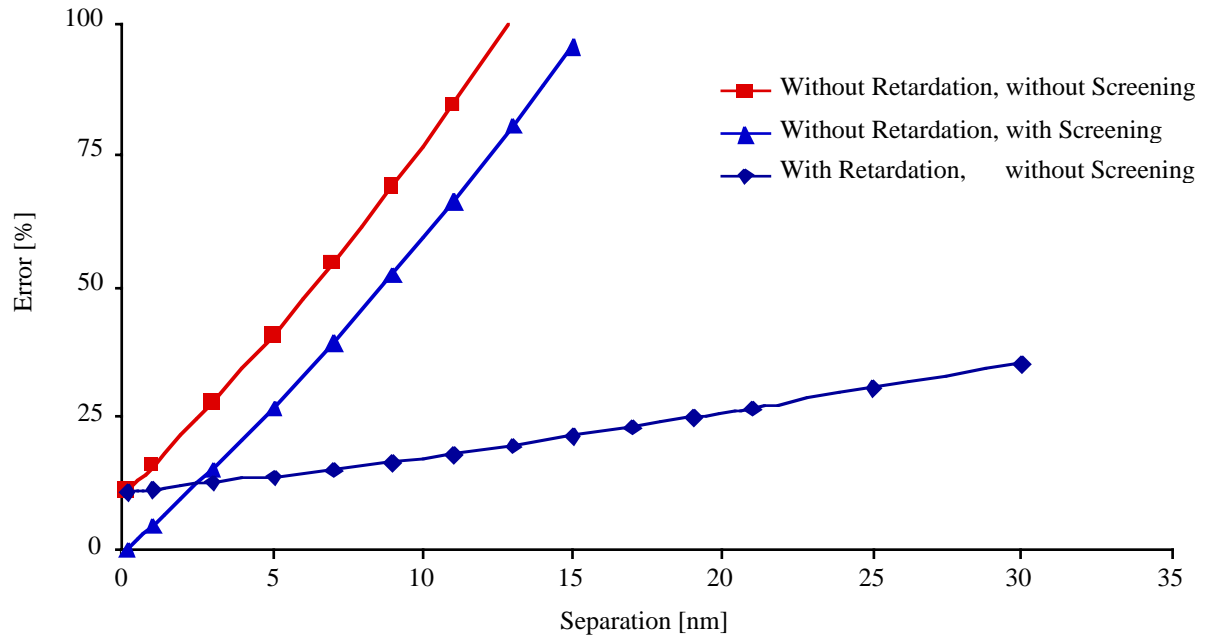


Figure 3-8. Comparison of the various errors, which can be made in calculating the Hamaker constant for a cement suspension when either screening or retardation, or both are not taken into account.

3.6.5 Expression for dispersion force

As previously mentioned [3-48], the dispersion force is given by the derivative of the dispersion potential:

$$F_{(a_1, a_2, h)} = \frac{d\Phi}{dh} = \frac{d}{dh} \left(A_{(h)} H_{(a_1, a_2, h)} \right) = A_{(h)} \frac{dH_{(a_1, a_2, h)}}{dh} + H_{(a_1, a_2, h)} \frac{dA_{(h)}}{dh} \quad [3-57]$$

With:

$$A_{(h)} = (m_1 h^2 + m_2 h + m_3) \exp(-m_4 h) + a_\infty \exp(-b_\infty h)$$

$$\frac{dA_{(h)}}{dh} = (2m_1 h + m_2) \exp(-m_4 h) - m_4 (m_1 h^2 + m_2 h + m_3) \exp(-m_4 h) - a_\infty b_\infty \exp(-b_\infty h)$$

$$H_{(a_1, a_2, h)} = -\frac{1}{6} \left(\frac{2a_1 a_2}{2(a_1 + a_2)h + h^2} + \frac{2a_1 a_2}{4a_1 a_2 + 2(a_1 + a_2)h + h^2} + \text{Ln} \left(\frac{2(a_1 + a_2)h + h^2}{4a_1 a_2 + 2(a_1 + a_2)h + h^2} \right) \right)$$

$$\frac{dH_{(a_1, a_2, h)}}{dh} = -\frac{1}{6} \left(\frac{-4a_1 a_2 [(a_1 + a_2) + h]}{[2(a_1 + a_2)h + h^2]^2} + \frac{-4a_1 a_2 [(a_1 + a_2) + h]}{[4a_1 a_2 + 2(a_1 + a_2)h + h^2]^2} \right. \\ \left. + \frac{8a_1 a_2 [(a_1 + a_2) + h]}{[4a_1 a_2 + 2(a_1 + a_2)h + h^2][2(a_1 + a_2)h + h^2]} \right)$$

The importance of using a retarded Hamaker constant is illustrated in Figure 3-9 for two identical particles having a radius of 1 μm . The retarded and non-retarded force are plotted as a function of separation distance. The ratio between both values is also indicated. It illustrates that at 15 nm an error of 100% is already made in the non-retarded case.

In fact, it turns out that up to very large separations, where in any case the force becomes negligible, the slope of the geometric term is much sharper than the one of the Hamaker constant. So the Force can be written as:

$$F_{(a_1, a_2, h)} \cong A_{(h)} \frac{dH_{(a_1, a_2, h)}}{dh} \quad [3-58]$$

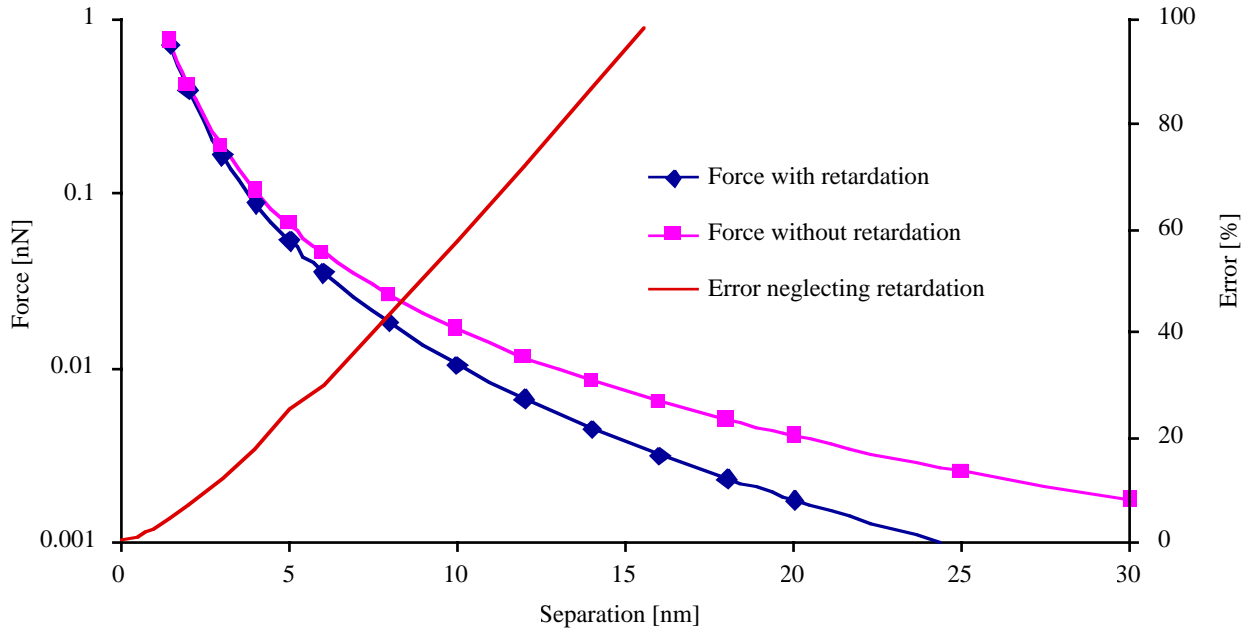


Figure 3-9. Force dependence on separation distance for two spherical particles of magnesium oxide, with a $1 \mu\text{m}$ radius. The graph illustrates the importance of including retardation effects.

In addition, we will consider cement suspensions with particle sizes (diameters) ranging from $0.4 \mu\text{m}$ to $50 \mu\text{m}$. For this size range, we will evaluate the validity of the approximations that can be made for $a \gg h$. In this situation we can simplify the geometric terms to:

$$\frac{dH_{(a_1, a_2, h)}}{dh} \cong \frac{dH_{(a_1, a_2, h)}^*}{dh} = -\frac{1}{6} \left(\frac{-\bar{a}}{2h^2} + \frac{-1}{2\bar{a}} + \frac{1}{h} \right) \quad [3-59]$$

$$\text{With: } \bar{a} = \frac{2a_1 a_2}{a_1 + a_2}$$

Giving:

$$F_{(a_1, a_2, h)} \cong A_{(h)} \frac{dH_{(a_1, a_2, h)}^*}{dh} \quad [3-60]$$

$$= -\frac{1}{6} \left[(m_1 h^2 + m_2 h + m_3) \exp(-m_4 h) + a_\infty \exp(-b_\infty h) \right] \left(\frac{-\bar{a}}{2h^2} + \frac{-1}{2\bar{a}} + \frac{1}{h} \right)$$

Errors linked to this approximation increase with separation as the averaged radius is no longer much larger than the separation. If the validity of this approximation is evaluated by calculating the relative error, an expression independent of the Hamaker constant is obtained:

$$\frac{F_{(a_1, a_2, h)} - F_{(a_1, a_2, h)}^*}{F_{(a_1, a_2, h)}} = \frac{A_{(h)} \frac{dH_{(a_1, a_2, h)}}{dh} - A_{(h)} \frac{dH_{(a_1, a_2, h)}^*}{dh}}{A_{(h)} \frac{dH_{(a_1, a_2, h)}}{dh}} = \frac{\frac{dH_{(a_1, a_2, h)}}{dh} - \frac{dH_{(a_1, a_2, h)}^*}{dh}}{\frac{dH_{(a_1, a_2, h)}}{dh}} \quad [3-61]$$

This means that the relative error made by using this approximation is the same for each material.

In discussing the dispersion of cement agglomerates, the force at close contact is going to be an important factor. For this reason, the separation for which the above approximation leads to a relative error inferior to 10 % has been evaluated.

Different particle size ratios have been considered and are plotted in Figure 3-10. As the ratio between the radii of both particles increases, the distance over which the approximation can be used decreases. However, we must consider that the particle size distribution has finite upper and lower bounds. This puts a limitation onto the particle size ratios, which can be encountered in the cement suspension. The discontinuous line in this figure shows this limit. In any case, it appears that the approximation can be used with good accuracy for separations below 50 nm.

Another important result is to see that the dispersion force depends on the following average radius, which will be termed the equivalent colloidal radius :

$$\bar{a} = \frac{2a_1a_2}{a_1 + a_2} \quad [3-62]$$

\bar{a} is the equivalent colloidal radius

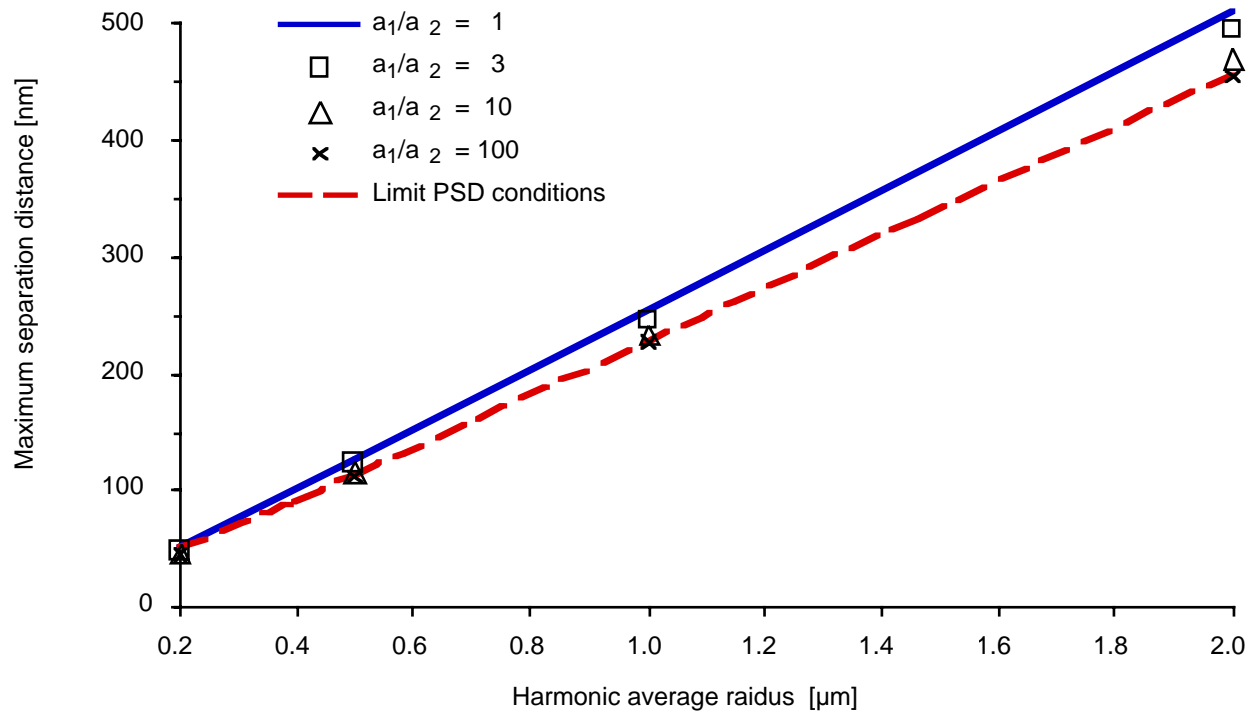


Figure 3-10. Separation in nm beyond which the approximation $a_1, a_2 \gg h$, leads to errors larger than 10%. The various curves are for different ratios a_1/a_2 . Note errors are independent of the material considered, as indicated in [3-61].

We note that this reduces to the equivalent colloidal radius only for two identical particles. In all other cases, this radius is smaller. However, it would be incorrect to describe the interaction by two spheres having the same radius, given by the arithmetic mean $(a_1+a_2)/2$. The error that this assumption would induce is calculated for a separation of 50 nm. Results are given for five different particle size ratios as a function of \bar{a} in Figure 3-11. They express the ratio between the value obtained with an arithmetic mean or with \bar{a} . In this way, the distance dependence of the Hamaker constant cancels out, as appears in [3-63]. We can write:

$$\begin{aligned}
\frac{F\left(\frac{a_1+a_2}{2}, h\right)}{F\left(\frac{2a_1a_2}{a_1+a_2}, h\right)} &= \frac{\left(\frac{-a^2 - h^2 + ha}{2ah^2}\right)}{\left(\frac{-\bar{a}^2 - h^2 + h\bar{a}}{2\bar{a}h^2}\right)} = \frac{\left(\frac{-\left(\frac{a_1+a_2}{2}\right)^2 - h^2 + h\frac{a_1+a_2}{2}}{2\frac{a_1+a_2}{2}h^2}\right)}{\left(\frac{-\left(\frac{2a_1a_2}{a_1+a_2}\right)^2 - h^2 + h\frac{2a_1a_2}{a_1+a_2}}{2\frac{2a_1a_2}{a_1+a_2}h^2}\right)} \quad [3-63] \\
&= \frac{\left(\frac{-(a_1^2 + 2a_1a_2 + a_2^2) - 4h^2 + 2h(a_1 + a_2)}{4(a_1 + a_2)h^2}\right)}{\frac{-4a_1^2a_2^2 - h^2(a_1^2 + 2a_1a_2 + a_2^2) + h(2a_1^2a_2 + 2a_1a_2^2)}{4a_1a_2(a_1 + a_2)h^2}} \\
&= \frac{a_1a_2\left(-(a_1 + a_2)^2 - 4h^2 + 2h(a_1 + a_2)\right)}{-4a_1^2a_2^2 - h^2(a_1 + a_2)^2 + 2a_1a_2h(a_1 + a_2)} \\
&\cong \frac{(a_1 + a_2)^2}{4a_1a_2}
\end{aligned}$$

Note that the approximation made in the last step is valid only at very small separations. It is equivalent to a $1/h^2$ dependence of the derivative of the geometric term. For the non-retarded case, this corresponds to a $1/h$ dependence of the dispersion potential. At these small separations this also implies the dispersion force to be proportional to \bar{a} . This point is illustrated in Figure 3-12, where the dispersion force is plotted as a function of \bar{a} for various separations. The symbols indicate calculated values, while the lines correspond to a linear fit having a zero intercept. The very good fit these lines provide indicates that the dispersion force is proportional to the equivalent colloidal radius at least up to separations of 4 nm.

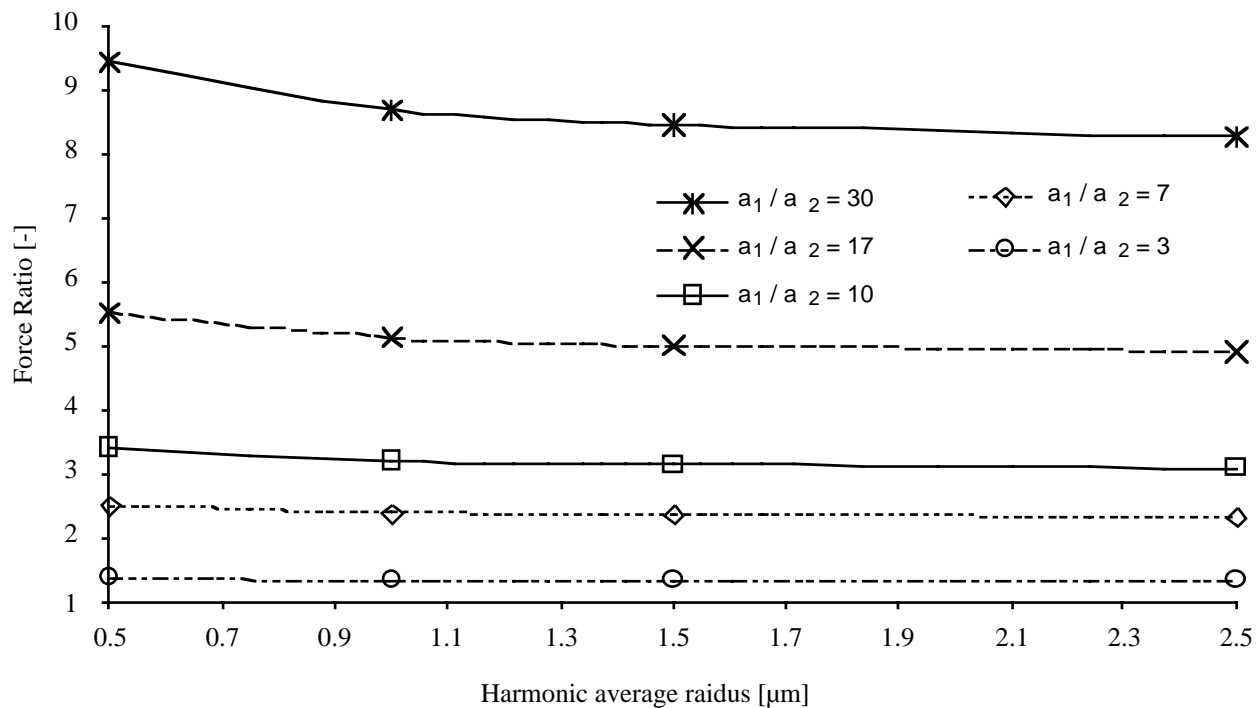


Figure 3-11. Ratio between dispersion force evaluated with an arithmetic averaged radius, versus the force evaluated with the harmonic average radius $2a_1a_2/(a_1+a_2)$.

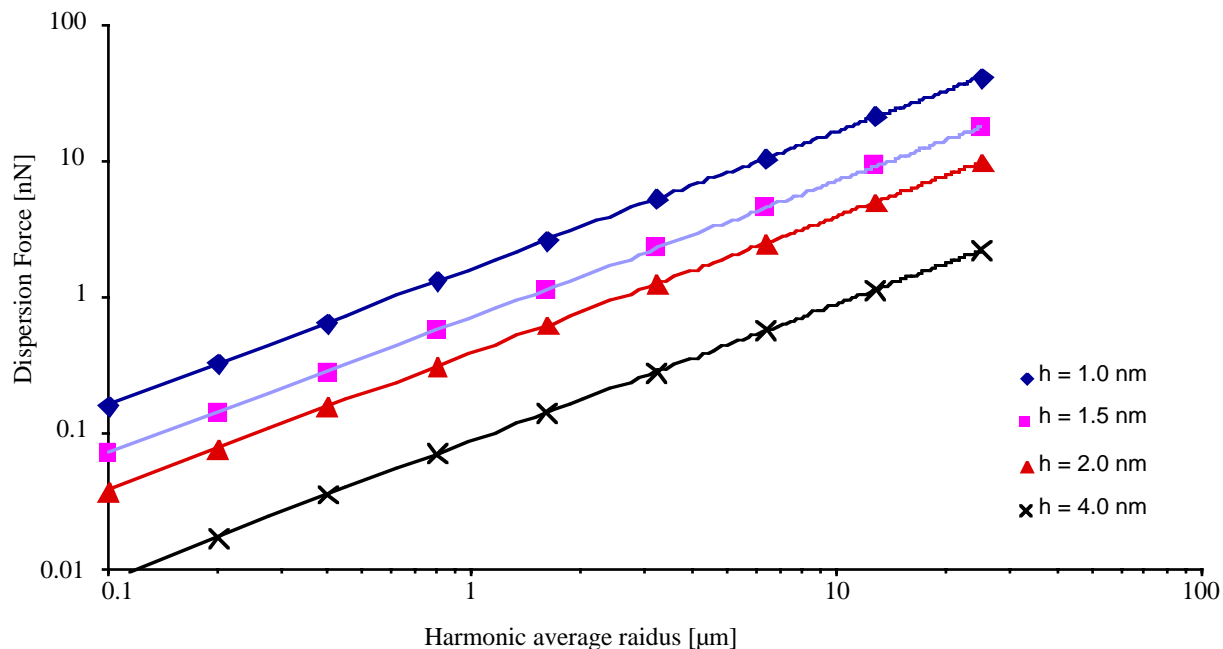


Figure 3-12. MgO dispersion force for different separation distances as a function of the harmonic average radius $2a_1a_2/(a_1+a_2)$. Symbols are calculated data and lines are linear fits for zero intercepts.

3.7 Electrostatic forces

3.7.1 Situation in vacuum

For electrostatics, two simplified version of Maxwell's equations can be used.

$$\epsilon_0 \nabla \cdot \mathbf{E} = \rho^{(e)} \quad [3-64]$$

\mathbf{E} is the electrostatic field

$\rho^{(e)}$ is the total density of charges

$$\nabla \times \mathbf{E} = 0 \quad [3-65]$$

Equation [3-65] indicates that the curl product of the electrostatic field is equal to zero. On the other hand, it is known that curl product of a divergence is zero. It follows that there exists a function termed potential and of which the divergence is equal to the electrostatic field.

$$\mathbf{E} = -\nabla \psi \quad [3-66]$$

ψ is the electrostatic potential

Rather than potentials it is potential differences which are relevant. An electrostatic potential difference between two points 1 and 2 in space corresponds to the work which must be done to bring a charge e (magnitude of the electron charge) from one of these points to the other.

$$\int_1^2 \mathbf{F}_{(r)} d\mathbf{r} = \int_1^2 e \mathbf{E}_{(r)} d\mathbf{r} = - \int_1^2 e \nabla \psi d\mathbf{r} = e(\psi_1 - \psi_2) \quad [3-67]$$

For a spherical particle bearing a charge Q , we define the potential at an infinite distance as equal to zero, which leads to an expression of the electrostatic potential of a sphere:

$$\psi_s = \frac{Q}{4\pi\epsilon_0 r} \quad [3-68]$$

In fact this potential is the factor by which one must multiply e in order to obtain the work needed to bring this charge e from an infinite distance up to the surface of the particle bearing the charge Q .

With the first Maxwell equation, the relation between potential and field gives the Poisson equation for vacuum:

$$\varepsilon_0 \nabla^2 \psi = -\rho^{(e)} \quad [3-69]$$

3.7.2 Situation in a dielectric

So far, we have a relation between the electrostatic potential and the surface charge of a particle in vacuum. This relation is linked to the work needed to bring a charge q from infinite distance to the surface of this particle. In a dielectric, this work will be altered because of the polarisability of the medium.

The following relation is obtained between potential and charge for a particle in a dielectric:

$$\psi_s = \frac{Q}{4\pi\varepsilon_0 a(1+\chi)} = \frac{Q}{4\pi\varepsilon_0 \varepsilon a} \quad [3-70]$$

Where:

$\varepsilon = (1 + \chi)$ is the relative dielectric constant of the dielectric

$\chi = (N\alpha)$ is the electric susceptibility

α is the polarisability of the individual dipoles

N is the number density of dipoles

The dielectric constant gives the extent to which the work for bringing a charge to the surface of charged particle can be decreased due to the polarisability of the continuous medium.

3.7.3 Origin of surface charge and Boltzmann distribution

Surface charges originate from a preference of some electrolytes to be at the surface of a particle rather than in solution or vice versa. Surface charge can therefore originate from dissociation of surface groups, specific adsorption of ions or ionic polymers.

The distribution of ionic species away from a surface is calculated by assuming that the suspension is at equilibrium. This means that for each specie, the electrochemical potential will be the same, whatever its distance from the charged surface.

$$\Delta\mu_k^* = \Delta\mu_k + ez_k\Delta\psi = \mu_k^0 + \Delta k_B T \ln(a_k) + ez_k\Delta\psi = 0 \quad [3-71]$$

$$\Delta \ln(a_k) = -\frac{ez_k}{k_B T} \Delta\psi$$

$$d \ln(a_k) = -\frac{ez_k}{k_B T} d\psi$$

$$\nabla \ln(a_k) = -\frac{ez_k}{k_B T} \nabla\psi$$

Where:

μ_k^* is the electrochemical potential of species k

μ_k is the chemical potential of species k

a_k is the activity of species k

z_k is the number of unit charges born by species k

ψ is the electrostatic potential at the point where μ_k^* is evaluated

At an infinite distance from the surface, it is assumed that the activity of all species is given by their bulk activity.

$$d \ln a_k = -\frac{ez_k}{k_B T} d\psi \quad [3-72]$$

$$\ln a_k = -\frac{ez_k}{k_B T} \psi + cte \quad [3-73]$$

$$a_k = \exp\left(-\frac{ez_k}{k_B T} \psi\right) \exp(cte) \quad [3-74]$$

$$a_k = a_k^b \exp\left(-\frac{ez_k}{k_B T} \psi\right) \quad [3-75]$$

a_k^b is the activity of species k in the bulk

Note that at infinity the potential is equal to zero and the concentration is effectively the bulk concentration.

For ideal solutions, in which activity is given by concentration, this leads to the Boltzmann distribution, which for a given point from a charged surface, relates the ionic concentration of species with the local electrochemical potential.

$$a_k = n_k \gamma_k = n_k^b \gamma_k^b \exp\left(-\frac{e z_k}{k_B T} \psi\right) \quad [3-76]$$

$$n_k = n_k^b \exp\left(-\frac{e z_k}{k_B T} \psi\right)$$

Where :

n_k is the concentration of species k

γ_k is the activity coefficient of species k

n_k^b is the concentration of species k in the bulk

γ_k^b is the activity coefficient of species k in the bulk

3.7.4 Gouy-Chapman double layer

A charged interface attracts ions of opposite sign. On the other hand, Brownian motion will oppose this process, acting as a rehomogenising force. The double layer model of Gouy-Chapman distinguishes between two zones.

A first layer called either the Stern layer or the compact layer defines the thickness of adsorbed ions which are linked to the surface sufficiently strongly to be unaffected by Brownian motion. This layer can be considered as a capacitor in which the potential varies linearly with separation. The outer-bound of this layer is considered to carry the charge, which is relevant for describing the next layer.

A second layer called the diffuse layer covers the region from the outer-bound of the Stern layer to the bulk solution, in which ions are affected both by Brownian motion and by the charged interface. The Stern layer and the diffuse layer are called the double layer.

In an electrolyte, the Poisson equation takes the form:

$$\epsilon \epsilon_0 \nabla^2 \psi = -\rho^{(f)} \quad [3-77]$$

$\rho^{(f)}$ is the volume density of free charges

For electrolyte concentrations smaller than 1 M, and potentials smaller than 200 mV, the electrostatic potentials in the Poisson equation and the Boltzmann distribution can be considered identical [Russell et al (1991), subchapter 4.6].

Since the volume density of free charges is given by:

$$\rho^{(f)} = \sum_{k=1}^N e z_k n_k \quad [3-78]$$

Substitution into the Poisson and the Boltzmann equations leads to the Poisson-Boltzmann equation:

$$\nabla^2 \psi = -\frac{e}{\epsilon \epsilon_0} \sum_{k=1}^N z_k n_k^b \exp\left(-\frac{e z_k}{k_B T} \psi\right) \quad [3-79]$$

Note that potential and concentration, which are linked through in this equation, both depend on the distance from the charged interface.

3.7.5 Double layer at the surface of a spherical surface

While the Poisson-Boltzmann equation can be solved analytically for parallel planes, the situation is different for spheres. Indeed the curvature leads to another expression of the left hand term which complicates the resolution.

Different approximations exist, most of which are concerned with symmetric electrolytes ($n_+ = n_-$; $z_+ = -z_-$). Because most approximations allowing us to calculate the electrostatic repulsion force assume electrolytes to be symmetric, we show how the P-B equation can be rewritten for a symmetric electrolyte:

$$\begin{aligned} \nabla^2 \psi &= -\frac{e}{\epsilon \epsilon_0} \left[z_+ n_+^b \exp\left(-\frac{e z_+}{k_B T} \psi\right) + z_- n_-^b \exp\left(-\frac{e z_-}{k_B T} \psi\right) \right] \quad [3-80] \\ &= -\frac{e}{\epsilon \epsilon_0} \left[z_+ n_+^b \exp\left(-\frac{e z_+}{k_B T} \psi\right) - z_+ n_+^b \exp\left(+\frac{e z_+}{k_B T} \psi\right) \right] \\ &= \frac{e z_+ n_+^b}{\epsilon \epsilon_0} \left[\exp\left(+\frac{e z_+}{k_B T} \psi\right) - \exp\left(-\frac{e z_+}{k_B T} \psi\right) \right] \\ &= 2 \frac{e z_+ n_+^b}{\epsilon \epsilon_0} \sinh\left(+\frac{e z_+}{k_B T} \psi\right) \end{aligned}$$

Linearisation of this expression, valid for small values $\frac{ez_+}{k_B T} \psi$, leads to:

$$\nabla^2 \psi \cong \frac{2e^2 z_+^2 n_+^b}{\epsilon \epsilon_0 k_B T} \psi = \kappa^2 \psi \quad [3-81]$$

Which introduces the Debye length κ^{-1} :

$$\kappa^{-1} = \sqrt{\frac{\epsilon \epsilon_0 k_B T}{2e^2 z_+^2 n_+^b}} \quad [3-82]$$

For a non-symmetric electrolyte, the Debye length is written:

$$\kappa^{-1} = \sqrt{\frac{\epsilon \epsilon_0 k_B T}{\sum_k e^2 z_k^2 n_k^b}} \quad [3-83]$$

3.7.6 Non-idealality of cement suspension

Potential dependent activity coefficients

As mentioned above, most of the approximations allowing us to calculate the repulsive electrostatic force between charged spherical particles assume that the intervening medium is composed of a symmetric electrolyte with a characteristic Debye length. In the aqueous phase of cement suspensions, many electrolytes are present. They are essentially non-symmetric (see chapter 3, page 25).

In addition, the derivation of the P-B equation includes the assumption that ion activities can be given by ion concentrations. This is no longer a good approximation for the concentrated aqueous phase of cement suspensions (see 3.1.5, page 24).

Let us recall that the exact form of the Poisson equation is written:

$$a_k = n_k \gamma_k = n_k^b \gamma_k^b \exp\left(-\frac{ez_k}{k_B T} \psi\right) \quad [3-84]$$

In section 3.1.5, we have already calculated bulk activity coefficients for two cement suspensions having water to cement ratios of 0.35 and 0.45. The values obtained are those of the bulk, where the

potential is equal to zero and the exponential term is equal to unity. Using this information on the bulk it is possible to calculate the activity of all the species as a function of the electrostatic potential.

An iterative procedure is then required to obtain both concentration and activity potential. First the ionic strength is calculated with bulk concentration of electrolytes:

$$I = \frac{1}{2} \sum_k z_k^2 n_k \quad [3-85]$$

With this ionic strength and the data in Table 3-9, a first approximation of activity coefficients can be obtained with the Debye-Hückel relationship :

$$\text{Log}_{10}(\gamma_k) = -\frac{A z_k^2 \sqrt{I}}{1 + a_k^0 B \sqrt{I}} + C_k \sqrt{I} \quad [3-86]$$

Table 3-9. Parameters for calculating ion activities of selected aqueous species.

	K ⁺	Na ⁺	Ca ⁺⁺	OH ⁻	SO ₄ ⁻	KSO ₄ ⁻	NaSO ₄ ⁻	Ca(OH) ⁺	CaSO ₄
a _k ⁰	3.0	4.0	6.0	3.5	4.0	3.5	4.3	4.0	4.0
C _k	0.0163	0.0867	0.1546	0.041	-0.04	0.041	0.041	0.041	0.041

A new set of concentrations can be obtained:

$$n_k = \frac{a_k}{\gamma_k} \quad [3-87]$$

The procedure is then repeated with this new set of concentrations until sufficient convergence is obtained. This has been done for many potentials to obtain a variation of less than 0.1% between two consecutive steps.

The evolution of ionic strength is shown in Figure 3-13 as a function of the local electrostatic potential.

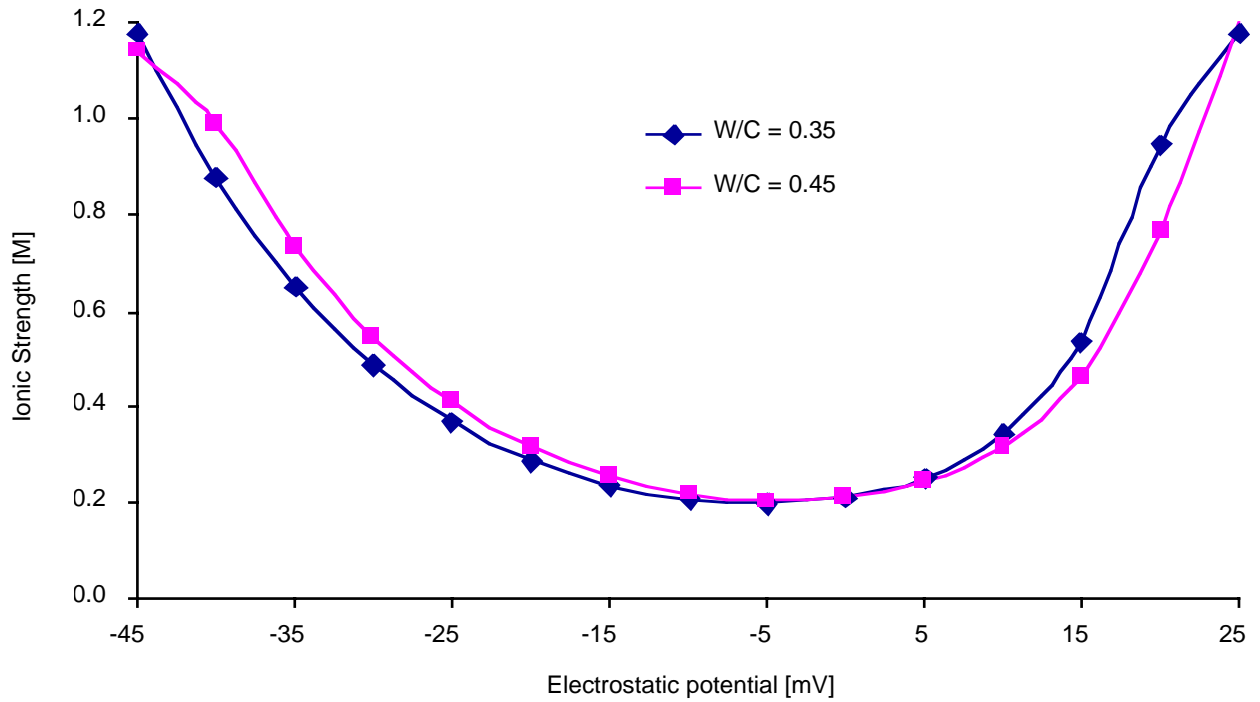


Figure 3-13. Variation of ionic strength as a function of local electrostatic potential.

For the suspension with $W/C = 0.35$, we report in Figure 3-14 the error induced if ideal solutions are assumed in order to calculate ionic distributions as a function of the local electrostatic potentials. For the purpose of this comparison, the total concentrations of the primitive ions are given. In addition, only values for opposite ion sign and surface potential are shown. Indeed, when ion and potential have the opposite sign, the local ion concentration goes to zero and the relative error diverges. In this figure, it appears that it is mainly the concentration of the divalent ions, which is biased if an ideal solution is assumed.

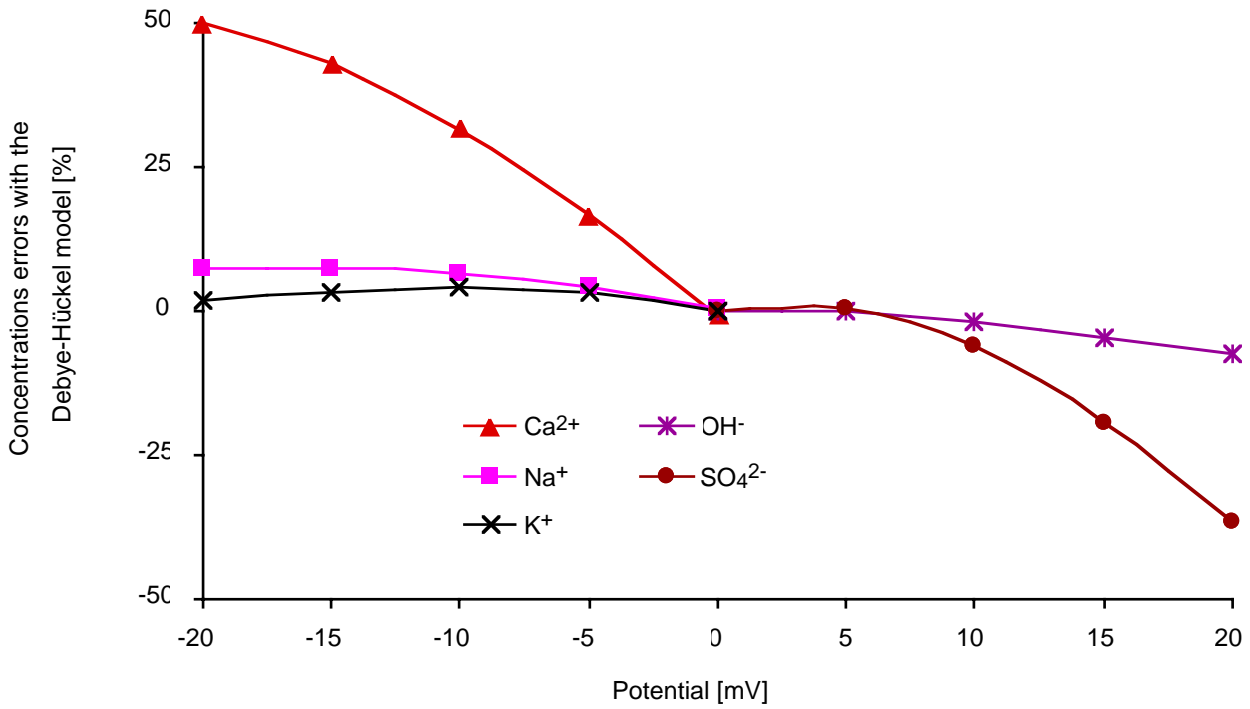


Figure 3-14. Relative error made if an ideal solution is assumed to calculate the ion distribution of cement suspension with $w/c = 0.35$.

Non-ideal form of Poisson-Boltzmann equation

The Poisson-Boltzmann (P-B) equation is obtained by combining the Boltzmann distribution with the Poisson equation, giving for non-ideal electrolytes:

$$\nabla^2 \psi = -\frac{e}{\epsilon \epsilon_0} \sum_{k=1}^N z_k n_k^b \frac{\gamma_k^b}{\gamma_k} \exp\left(-\frac{e z_k}{k_B T} \psi\right) \quad [3-88]$$

The object in this section to see whether the right hand side of this equation can be equated to that of a symmetric electrolyte having the same Debye length but a non unit charge. In addition, we wish this equivalent electrolyte to behave as an ideal solution (activity coefficient effects can be neglected).

Let us first equate the Debye length of a symmetric electrolyte with that of a non symmetric electrolyte:

$$\sqrt{\frac{\epsilon \epsilon_0 k_B T}{2e^2 z_+^2 n_+^b}} = \sqrt{\frac{\epsilon \epsilon_0 k_B T}{\sum_k e^2 z_k^2 n_k^b}} \quad [3-89]$$

$$z_+^2 n_+^b = \frac{\sum_k z_k^2 n_k^b}{2} \quad [3-90]$$

In order to describe the P-B equation by an equivalent symmetric electrolyte, we equate [3-80] and [3-89]. This leads to:

$$2 \frac{ez_+ n_+^b}{\epsilon \epsilon_0} \sinh\left(+\frac{ez_+}{k_B T} \psi\right) = -\frac{e}{\epsilon \epsilon_0} \sum_{k=1}^N z_k n_k^b \frac{\gamma_k^b}{\gamma_b} \exp\left(-\frac{ez_k}{k_B T} \psi\right) \quad [3-91]$$

$$z_+ n_+^b \sinh\left(+\frac{ez_+}{k_B T} \psi\right) = -\frac{1}{2} \sum_{k=1}^N z_k n_k^b \frac{\gamma_k^b}{\gamma_b} \exp\left(-\frac{ez_k}{k_B T} \psi\right)$$

By substituting [3-90] into [3-91], we get:

$$\frac{\sinh\left(+\frac{ez_+}{k_B T} \psi\right)}{z_+} = \frac{-\sum_{k=1}^N z_k n_k^b \frac{\gamma_k^b}{\gamma_b} \exp\left(-\frac{ez_k}{k_B T} \psi\right)}{\sum_k z_k^2 n_k^b} \quad [3-92]$$

At this point we must point out that we must distinguish the positive from the negative potential, since the essentially non-symmetric character of the liquid phase has been shown.

To solve equation for the charge number z , a mean square minimisation was used for a series of values spaced by 5 mV. Computations were performed over the range found to fall within the limit of ionic strengths inferior to unity (0 to 20 mV and 0 to -35 mV). Results are shown in Table 3-10.

Table 3-10. Characteristics of fitted symmetric electrolytes over potentials for which the ionic strength is inferior to 1M.

		Potential	
		0 \diamond 20	-35 \diamond 0
Fitted Electrolyte	z	1.16	3.52
	κ^{-1} [nm]	0.67	0.67
Debye-Hückel 1:1	z	1	1
	κ^{-1} [nm]	0.60	0.60

A graphic comparison of the values for the right hand term of P-B equation is shown for positive potentials in Figure 3-15 and for negative potentials in Figure 3-16.

Open triangles show exact values. The dashed line shows the fitted symmetric electrolyte. Closed triangles show values obtained if a non-ideal solution is assumed, but the effect of potential is not considered. Finally, the continuous line shows the Debye-Hückel approximation assuming the solution to be ideal and not calculating the distribution of ion pairs.

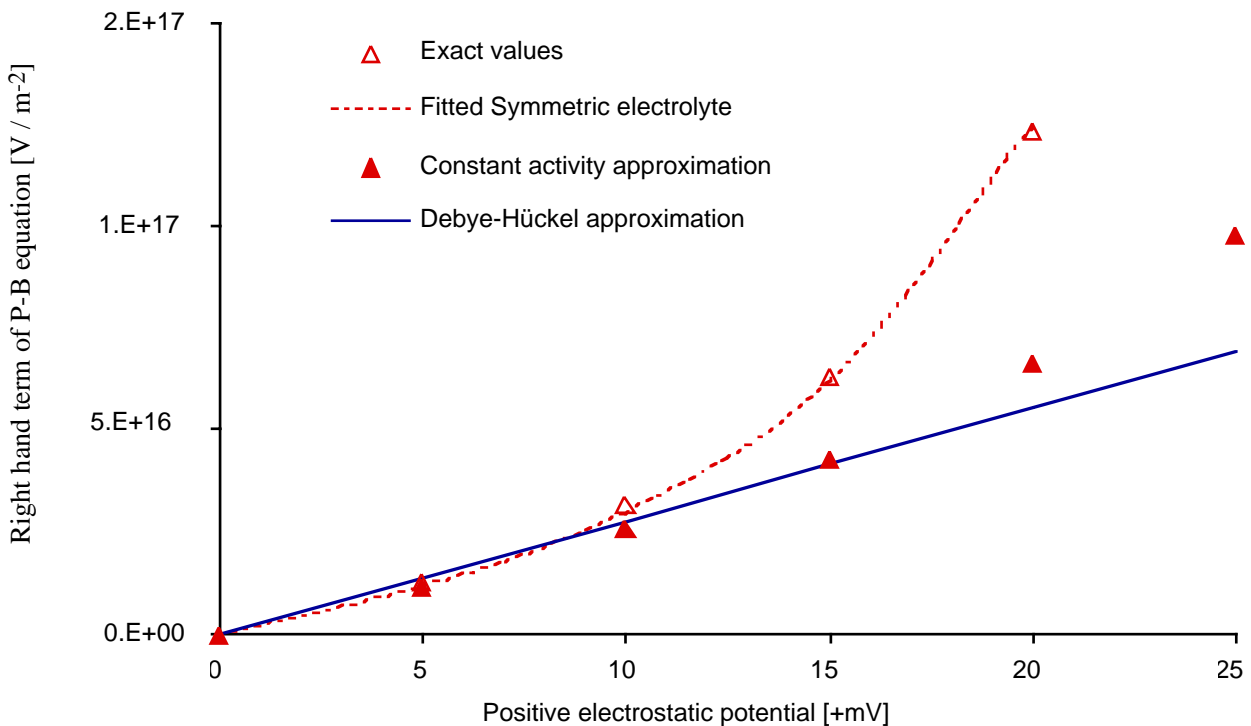


Figure 3-15. Comparison of right hand term of P-B equation for positive potentials.

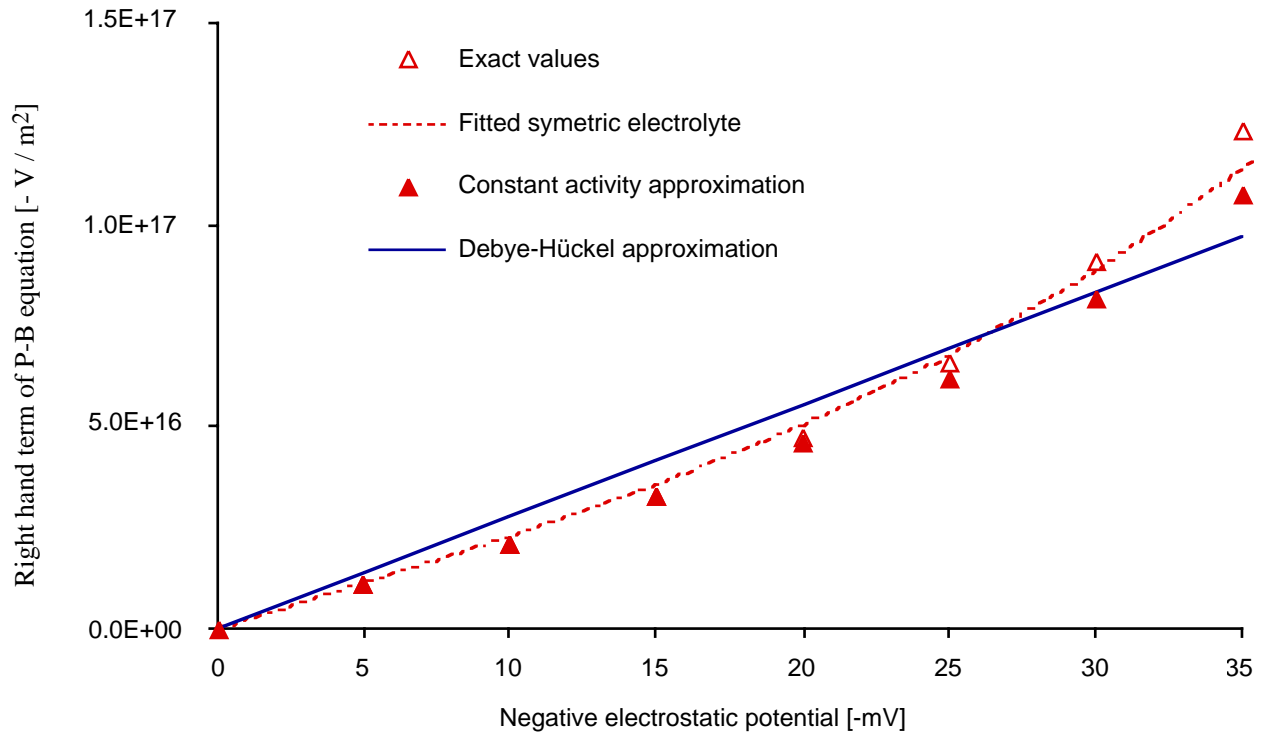


Figure 3-16. Comparison of right hand term of P-B equation for negative potentials.

For negative surface potentials, it appears that the Debye-Hückel approximation applied to the P-B equation in which ideal solution is assumed, induces minor errors down to -30 mV. On the other hand, this approximation fails above 10 mV for positive surface potentials.

3.7.7 Charge-Potential relation

For values of $\kappa a > 0.5$, there is a relationship between the charge density and the surface potential, which gives less than 5% error [Russel et al (1991), subchapter 4.8].

$$q = \frac{Q}{4\pi a^2} = \frac{\epsilon \epsilon_0 k_B T}{ez} \kappa \left[2 \sinh\left(\frac{1}{2} \Psi_s\right) + \frac{4}{\kappa a} \tanh\left(\frac{1}{4} \Psi_s\right) \right] \quad [3-93]$$

$$\text{where: } \Psi = \frac{ez\psi}{k_B T}$$

This expression includes a dependence on particle size. However, for the range of particle sizes of interest in cement, this dependence is not significant. This leads to:

$$q = \frac{Q}{4\pi a^2} \cong 2 \frac{\epsilon \epsilon_0 k_B T}{e z} \kappa \sinh\left(\frac{1}{2} \Psi_s\right) \quad [3-94]$$

The error induced by this approximation is inferior to 0.5% for particles with radii between 0.1 and 25 μm and for surface potentials up to 50 mV.

3.7.8 Surface potential regulation

So far, we have looked at relations between local electrostatic potential in the aqueous phase of a dielectric. Through the Boltzmann distribution this local potential could be related to the local composition of the solution, which has been described as a non-ideal electrolyte.

In this section we try to relate the surface potential to the bulk composition of the electrolyte, based on the assumption that particle surface has ionisable groups. The extent of their ionisation will dictate the value of the surface potential. It is also assumed, that these groups are in equilibrium with the solution.

For the purpose of discussing the effect of adsorbed superplasticizers, let us consider an adsorbed polymer having sodium sulfonate groups. We have:



With:

$$K_{\text{R-SO}_3\text{Na}} = \frac{a_{\text{R-SO}_3^-} \cdot a_{\text{Na}^+}^\circ}{a_{\text{R-SO}_3\text{Na}}} \quad [3-96]$$

The superscript $^\circ$ indicates that the activity of Na^+ is evaluated at the surface. In addition to association-dissociation equilibrium of sodium with sulfonate groups, other counter ions must also be considered. We therefore have:





To simplify the argument, only monovalent interactions are considered for calcium. Rearranging the equilibrium constants, and taking the sum for all counter ions, we can write:

$$\frac{\sum_X a_{\text{R-SO}_3\text{X}}}{a_{\text{R-SO}_3^-}} = \sum_X \frac{a_X^o}{K_{\text{R-SO}_3\text{X}}} \quad [3-100]$$

At this step, we approximate the activities of the surface species to their surface concentrations. The total number of sulfonate groups $[n_{\text{R-SO}_3}]$ per unit area, is therefore given by:

$$[n_{\text{R-SO}_3}] = a_{\text{R-SO}_3^-} + \sum_X a_{\text{R-SO}_3\text{X}} \quad [3-101]$$

Substituting into the previous equation leads to:

$$\frac{[n_{\text{R-SO}_3}] - a_{\text{R-SO}_3^-}}{a_{\text{R-SO}_3^-}} = \sum_X \frac{a_X^o}{K_{\text{R-SO}_3\text{X}}} \quad [3-102]$$

$$a_{\text{R-SO}_3^-} = \frac{[n_{\text{R-SO}_3}]}{1 + \sum_X \frac{a_X^o}{K_{\text{R-SO}_3\text{X}}}}$$

Using the Boltzmann equation to calculate the ion potentials at the interface, and multiplying by the electron charge yields the surface charge:

$$q = -e a_{\text{R-SO}_3^-} = \frac{-e [n_{\text{R-SO}_3}]}{1 + \sum_X \frac{a_X^o \exp\left(\frac{-ez_X}{k_B T} \psi_s\right)}{K_{\text{R-SO}_3\text{X}}}} \quad [3-103]$$

This provides an additional relation between surface charge q and surface potential ψ_s . Equating both [3-103] and [3-94], we obtain:

$$2 \frac{\epsilon \epsilon_0 k_B T}{e z_+} \kappa \sinh \left(\frac{1}{2} \frac{e z_+}{k_B T} \psi_s \right) = \frac{-e [n_{R-SO_3}]}{1 + \sum_X \frac{a_X^b \exp \left(\frac{-e z_X}{k_B T} \psi_s \right)}{K_{R-SO_3 X}}} \quad [3-104]$$

Note that the left hand term is calculated from the data for the equivalent symmetric electrolyte, while the term on the right side must be calculated with all counter ions. This development leaves two unknowns, the surface concentration of sulfonate groups and the surface potential. From adsorption measurements, it is possible to know how much polymer is present at the surface of the cement particles. This allows us to calculate the surface concentration of sulfonate groups. The above equation remains then to be solved for the surface potential. Note that the potential obtained is the one at the outer bound of the Stern layer. This potential should be equal or superior to the experimentally measurable zeta potentials as will be discussed later.

Use of adequate thermodynamic data, along with adsorption data, solution composition analysis and a model for describing a non ideal aqueous phase should therefore allow us to calculate the surface potential of superplasticizer coated cement particles. The other important aspect is that the surface potential in such a case is not dependent on the distance from other particles. This is important for setting proper boundary conditions when calculating the repulsive force for electrostatic repulsion. In other words, during approach, if chemical equilibrium can remain in the system, the particles would maintain a constant surface potential.

3.7.9 Electrostatic force between flat plates

Relation between pressure gradients and local electrostatic field

To describe the repulsive force between two bodies, an expression is required for the local stress. The derivation [see for instance Russel et al (1991)] is based on the fact that, at equilibrium, the body forces induced by the electrostatic field in a charged dielectric must be balanced by a pressure gradient. This leads to the following equation:

$$-\nabla \left[p - \frac{1}{2} \epsilon_0 \rho \left(\frac{\partial \epsilon}{\partial \rho} \right)_T \right] - \frac{1}{2} \epsilon_0 \mathbf{E} \cdot \nabla \epsilon + \rho^{(f)} \mathbf{E} = 0 \quad [3-105]$$

For rigid bodies, in incompressible fluids, the term

$$-\frac{1}{2} \varepsilon_0 \rho \left(\frac{\partial \varepsilon}{\partial \rho} \right)_T$$

can be absorbed into a modified pressure. We get:

$$-\nabla p - \frac{1}{2} \varepsilon_0 \mathbf{E} \cdot \nabla \varepsilon + \rho^{(f)} \mathbf{E} = 0 \quad [3-106]$$

If the dielectric properties are homogeneous throughout the fluid, we get:

$$-\nabla p + \rho^{(f)} \mathbf{E} = 0 \quad [3-107]$$

Recalling the Maxwell equation rewritten for a dielectric, this becomes:

$$-\nabla p + (\varepsilon \varepsilon_0 \nabla \mathbf{E}) \mathbf{E} = 0 \quad [3-108]$$

$$\Delta p = \varepsilon \varepsilon_0 \Delta \mathbf{E} = -\varepsilon \varepsilon_0 \Delta (\nabla \psi) \quad [3-109]$$

From the Poisson-Boltzmann equation:

$$\nabla^2 \psi = 2 \frac{e z_+ n_+^b}{\varepsilon \varepsilon_0} \sinh \left(\frac{e z_k}{k_B T} \psi \right) \quad [3-110]$$

We get:

$$\nabla \psi = 2 \frac{k_B T n_+^b}{\varepsilon \varepsilon_0} \cosh \left(\frac{e z_k}{k_B T} \psi \right) \quad [3-111]$$

Which leads to the following expression for the pressure difference between the bulk and point x:

$$\begin{aligned} \Delta p_{x,b} &= 2 k_B T n_+^b \left[\cosh \left(\frac{e z_k}{k_B T} \psi_b \right) - \cosh \left(\frac{e z_k}{k_B T} \psi_x \right) \right] = \\ &= 2 k_B T n_+^b \left[1 - \cosh \left(\frac{e z_k}{k_B T} \psi_x \right) \right] \end{aligned} \quad [3-112]$$

Electrostatic force between two parallel flat plates with identical potentials

In the case of parallel plates of equal charges, there is symmetry at mid-plane, which cancels out contribution from the terms linked to the electric stress. Only pressure differences are relevant and the

above equation describes the repulsive force. The force per unit area is therefore given by the above equation.

Electrostatic force between two parallel flat plates with different potentials

However, in the case on plates with unequal charges the electric stress does not vanish due to a lack of symmetry. An important implication of this is that, two plates with constant but different charge of the same sign will undergo an attraction at short distances.

This certainly could be very important in the agglomeration of cement particles. It may be expected that calcium is a potential determining ion for most of the cement phases. Suppose sufficient calcium is present to induce positive potentials on these phases. These potentials however will only be equal if their dissociation constants are equal. If the dispersion force is sufficient to bring bodies together, then an additional attractive force will arise whenever these phases do not have the same dissociation constants.

In addition, we note that this force is infinite at zero separation and that at very small separations y , it decreases as:

$$\frac{\Delta\psi_s^2}{\sinh^2(\kappa y)}$$

In order to evaluate the importance of this effect, let us compare two parallel flat plates with surface charges +2 and +12 mV, $A_{\text{eff}(0)} = 2.04 \times 10^{-20}$ J (MgO), for the equivalent symmetric electrolyte of our cement suspension. Note that since we assume the particles are of different nature, a more adequate Hamaker constant would have to be calculated. Nevertheless, for these conditions, we find that the ratio between the electrostatic force and the dispersion force becomes significant below 0.2 nm. In other words, below this separation, the attraction force between both surfaces contains an important part due to the non-identical surface potentials (Figure 3-17). The situation for spheres is discussed below.

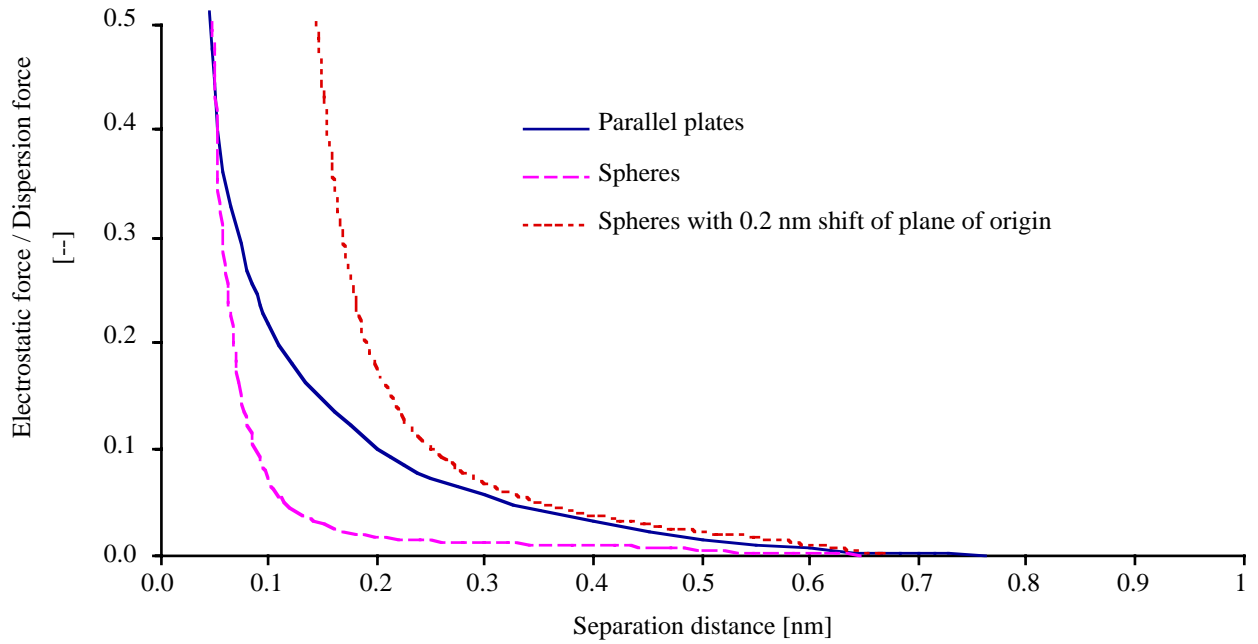


Figure 3-17. Ratio of electrostatic force to dispersion force for bodies with $A_{\text{eff}(0)} = 2.04 \times 10^{-20} \text{ J}$ (MgO), surface potentials of +2 mV and +12 mV, in the equivalent symmetric electrolyte. In the case of spheres we also show the case where the plane of origin for the electrostatic potential is 0.2 nm away from the one for the dispersion force.

3.7.10 Electrostatic force between spheres

General expression for electrostatic force between spheres with constant potential

In the case of spheres, the curvature introduces an electric stress, much as the lack of symmetry did for plates of different charge. The force expression for two charged spheres is given by:

$$\mathbf{F} = 2k_B T n_+^b \int_S \left[1 - \cosh\left(\frac{ez_k}{k_B T} \psi_x\right) \right] \mathbf{n} dS + \epsilon \epsilon_0 \int_S [\mathbf{E}\mathbf{E} - \frac{1}{2} \mathbf{E} \cdot \mathbf{E} \mathbf{d}] \mathbf{n} dS \quad [3-113]$$

Because we assume the potential to be regulated by dissociation equilibrium, either of surface groups or of adsorbed ionic polymers, we consider only constant potential boundary conditions.

The following approximation can be used to obtain the electrostatic force between two spheres in a symmetric electrolyte. It is the method used by Vellegrol (1997) to compare his direct measurements

of interparticle forces between latex particles bearing different surface potentials and values predicted by DLVO theory.

$$\Phi^{ES} = \Phi_1 + \Phi_2 + \Phi_3 \quad [3-114]$$

Where:

$$\Phi_1 = \frac{2\pi\epsilon\epsilon_0 k_B^2 T^2}{z_+^2 e^2} \bar{a} \left[Y_+^2 \ln(1 + e^{-2\kappa\delta}) + Y_-^2 \ln(1 - e^{-2\kappa\delta}) \right] \quad [3-115]$$

$$\begin{aligned} \Phi_2 = & \frac{2\pi\epsilon\epsilon_0 k_B^2 T^2}{z_+^2 e^2} \bar{a} \left[-\frac{1}{48} (Y_+^4 + 3Y_+^2 Y_-^2) (\kappa\delta) (1 - \tanh \kappa\delta) \right. \\ & + \frac{1}{48} (Y_-^4 + 3Y_+^2 Y_-^2) (\kappa\delta) (\coth \kappa\delta - 1) \\ & \left. - \frac{1}{96} Y_+^4 \left(\frac{1 - \kappa\delta \tanh \kappa\delta}{\cosh^2 \kappa\delta} \right) - \frac{1}{96} Y_-^4 \left(\frac{\kappa\delta \coth \kappa\delta - 1}{\sinh^2 \kappa\delta} \right) \right] \quad [3-116] \end{aligned}$$

$$\begin{aligned} \Phi_3 = & \frac{2\pi\epsilon\epsilon_0 k_B^2 T^2}{z_+^2 e^2} \bar{a} \left[-\frac{1}{5760} Y_+^2 \left\{ Y_+^4 + \frac{15}{8} Y_-^2 (7Y_+^2 + Y_-^2) \right\} (\kappa\delta) (1 - \tanh \kappa\delta) \right. \\ & + \frac{1}{5760} Y_-^2 \left\{ Y_-^4 + \frac{15}{8} Y_+^2 (7Y_-^2 + Y_+^2) \right\} (\kappa\delta) (\coth \kappa\delta - 1) \\ & + Y_+^6 \left(\frac{17 + 4\kappa\delta \tanh \kappa\delta}{46080 \cosh^2 \kappa\delta} \right) - Y_-^6 \left(\frac{4\kappa\delta \coth \kappa\delta + 17}{46080 \sinh^2 \kappa\delta} \right) \\ & + Y_+^4 Y_-^2 \left(\frac{1 + \kappa\delta \tanh \kappa\delta}{1024 \cosh^2 \kappa\delta} \right) - Y_+^2 Y_-^4 \left(\frac{\kappa\delta \coth \kappa\delta + 1}{1024 \sinh^2 \kappa\delta} \right) \\ & - Y_+^6 \left(\frac{1 - 11 \kappa\delta \tanh \kappa\delta}{15360 \cosh^4 \kappa\delta} \right) + Y_-^6 \left(\frac{11 \kappa\delta \coth \kappa\delta - 1}{15360 \sinh^4 \kappa\delta} \right) \\ & \left. + \frac{1}{1536} (\kappa\delta)^2 \left\{ \frac{Y_+^2}{\cosh^2 \kappa\delta} - \frac{Y_-^2}{\sinh^2 \kappa\delta} \right\}^3 \right] \quad [3-117] \end{aligned}$$

And:

$$Y_+ = \frac{z_+ e}{2k_B T} (\psi_1 + \psi_2) \quad [3-118]$$

$$Y_- = \frac{z_+ e}{2k_B T} (\psi_1 - \psi_2) \quad [3-119]$$

$$\delta = \frac{y}{2} \quad \text{is half the separation distance between the particles} \quad [3-120]$$

A very interesting aspect in these formulas is that they predict that the electrostatic potential is proportional to the reduced average radius. For very small separations the same result had been obtained for the dispersion force. For slightly larger separations, the relevant size parameter remained this reduced radius. This parameter therefore seems the most adequate for evaluating the interaction between particles.

Electrostatic force between equally charged spheres

Using this expression for the force, we calculate the repulsive electrostatic force. We consider two calcite particles with 1 μm radius, 30mV surface potentials and an aqueous phase similar to a cement suspension. In such a situation, as discussed previously, we must use different equivalent symmetric electrolytes to distinguish the positive from the negative potential situations. In addition, we use the Debye-Hückel approximation for a 1:1 electrolyte and neglect any effect of the non-ideal thermodynamics. In this case, the repulsive force is predicted to be the same whether both surfaces are positive or negative.

Values for all three situations are compared in Figure 3-18. The first observation is that whatever the situation, the order of magnitude is well predicted by the Debye-Hückel approximation. At contact this approximation tends to over-evaluate the force for the negative potential by about 15%. On the other hand for the positive potentials, errors are greater at intermediate separations.

If values are compared to those in Figure 3-9, we see that values of electrostatic repulsion are much smaller, than the attractive forces for similar separation distances.

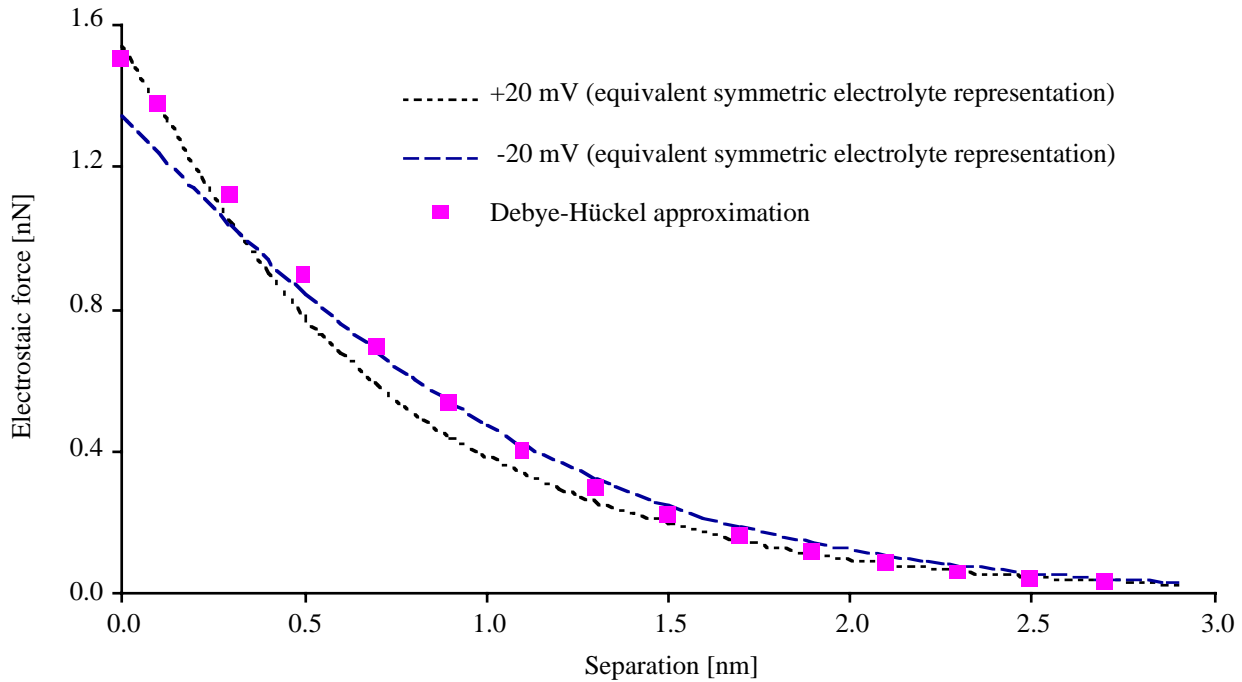


Figure 3-18. Electrostatic force between particles having $1\mu\text{m}$ radius and 20 mV surface charges. Debye-Hückel approximation is compared with exact results for the equivalent symmetric electrolyte determined for thermodynamics of the non-ideal cement suspension.

Electrostatic force between spheres with different potentials

As was done for flat plates, the attractive force arising from different potentials can be calculated. For the same conditions as discussed previously (two calcite particles with $+2$ and $+12\text{ mV}$), we see this force becomes important only for separations smaller than $0.1\ \mu\text{m}$ (Figure 3-7).

This is valid provided the plane of origin of the dispersion forces and the electrostatic forces are identical. In fact, surface force measurements have shown that the repulsive electrostatic force is larger than expected at small separation for silica surfaces. This has been explained by the fact that there is a small hydration layer at the surface of which are located the charges relevant for calculating the repulsive force. The main problem in this case is to evaluate the thickness of this layer. In any case, this layer will be too small to change the balance between the dispersion and the repulsive force in the case of spheres with identical surface potentials. On the other hand, for spheres with different surface potentials, this layer will increase the probability of getting a significant electrostatic attraction. This is shown in Figure 3-17, where a 0.1 nm thick layer is compared with a 0 nm layer.

3.7.11 Summary of electrostatics for cement suspensions

1) The distribution of species in the non-ideal suspension can be taken into account to calculate the concentration and unit charge (non-integer) of an equivalent symmetric electrolyte. The condition for this approach to be valid is that the solution of the Poisson-Boltzmann equation of this electrolyte and of the cement suspension to be identical. This provides a more simple description of the local electrostatic potential at a certain distance from cement particles.

The interest of defining a symmetric electrolyte is that well established approximations for electrostatic force can then be used. It turns out the potential can not be described in the same way owing to the fact that the cement suspension is not a symmetric electrolyte. In fact for the region of negative potentials, which is of particular interest for cement suspensions, is almost equivalent to that of a 1:1 electrolyte. On the other hand in the positive potential range, the situation resembles that of a 3:3 electrolyte. These effects however are only of second and higher orders in the expression of the electrostatic force. **It turns out that the repulsive force is relatively well described by the Debye-Hückel approximation, for the cement suspensions used in this study.**

2) An important aspect, which to our knowledge has so far been over-looked is the electrostatic attraction which can take place between non superplasticizer coated cement particles. For constant potential boundary conditions, with potentials not equal in intensity, then at small separations the electrostatic force becomes attractive, even for like charges.

Force dissociation regulated potentials, either different dissociation constants or different amounts of ionizable groups per unit area can induce different surface potentials. To a first approximation, these parameters are mineral specific. Since cement is a multimineral powder, it is therefore highly probable to find surfaces interacting with different surface potentials.

Although, the above mentioned attraction only occurs at very small separations, these distances can be met within agglomerates. **Therefore, within a cement agglomerate, an additional attractive force probably exists due to the multimineral nature of cement.**

Imagine coating these particles with a zero thickness molecule, the purpose of which is to give a homogeneous surface potential. Then although remaining agglomerated at rest, the particles will required less external energy to be separated. The nature of this energy can be Brownian or hydrodynamic and was the object of previous sections.

3) Probably the most important remark, regarding all dispersion and electrostatic calculations made up to now for cement suspensions, is the following. All these calculations have been for identical spheres, arbitrarily using a particle radius much smaller than the average radius of particles in cement. It turns out that the harmonic average radius is consistent with this choice. For more consistency in the choice of this value, the frequency of pair interactions in a cement powder must be considered. This is done in chapter 10.

3.8 Forces linked to polymers

3.8.1 Adsorbing polymers

Adsorption modes

We will distinguish between two modes of adsorption.

In the first situation, the polymer is in contact only by one of its extremities with the surface. This can be for grafted polymers or co-block polymers. As illustrated in Figure 3-19, the conformation of the polymers at the surface depends on the amount of adsorbed polymers. In a dilute situation (Figure 3-19a), the adsorption layer will correspond more or less to the radius of gyration of the polymer in solution. In the semi-dilute situation (Figure 3-19b), the polymer molecules are stretched out and the adsorbed layer thickness is increased. This mode of adsorption can be used to describe to repulsion induced by comb-type copolymers [Yoshioka et al (1997). Russel et al (1991, subchapter 6.3)] develop a model allowing the calculation of the interaction between such layers. For the polymers used in this study however, this mode of adsorption is not expected to be relevant.

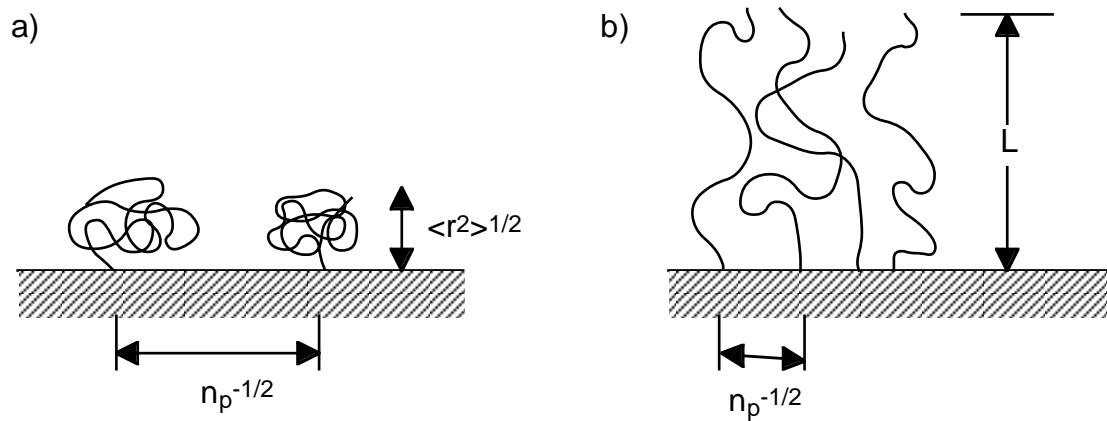


Figure 3-19. Schematic representation of the conformation of grafted polymers or polymers adsorbed as brushes. Parameters n_p , $\langle r^2 \rangle^{1/2}$, and L represent respectively the lateral distance fixation points, the radius of gyration and the length of the adsorbed layer.

In the second situation, the polymers adsorb in the so-called train and loop mode, in which the polymer has many contact points with the surface (Figure 3-20), because of the multifunctional nature of the polymer. We believe this is the adsorption mode, which predominates in this study. The discussion of forces induced by adsorbed polymers will therefore focus on this mode of adsorption.

The adsorption energy of a monomer is not very large, typically of the order of the thermal energy $k_b T$, which does not make this a very favourable process. Polymers however have many interactions per molecule with the surface. Their molar adsorption energy is therefore much larger. Polymer parts in contact with the surface are those designed by the term trains.

Desorption is therefore an unfavourable process, because of the large adsorption energy. Another way of understanding this is that all trains would have to desorb simultaneously in order for the polymer to leave the surface. However, the polymer can exchange with polymer in the bulk solution. This was shown by Pfefferkorn et al (1982) [cited by de Gennes (1987)], who adsorbed labelled polymers onto grains and then washed the system with a solution containing identical unlabelled polymers. The kinetic law for the decay of radioactivity is proportional to the coverage by labelled polymers Γ^* and to the bulk concentration of unlabelled polymers, c_b .

$$\frac{d\Gamma^*}{dt} = -k\Gamma^*c_b \quad [3-121]$$

As discussed by de Gennes (1987), this law indicates an exchange process and confirms the existence of a restoring force leading to a constant surface coverage Γ . Below this surface coverage, the conformation of the polymers is much more stretched out over the surface. Above it, the excess polymers tend to be spilled out into the solution.

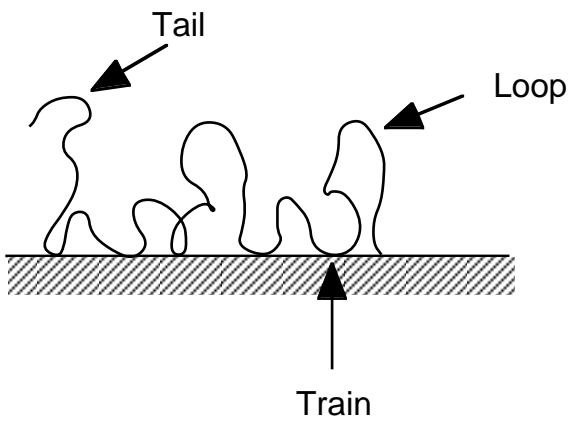


Figure 3-20. Schematic representation of the train and loop adsorption mode.

Electrostatic forces

The adsorption of ionic polymers onto surfaces modifies the surface charge/potential of these surfaces. The adsorption of most superplasticizers onto cement particles induces negative zeta potentials. These are larger in magnitude than the zeta potential of the initial cement. Therefore, provided zeta potential measurement may be used in place of the Stern potential, the electrostatic repulsion is increased. Let us note that this repulsion is linked to the gain in entropy from the dissociation of the counter ions of these polymers.

The adsorption of an anionic polymer onto a positive surface is illustrated schematically in Figure 3-21, for the train-loop adsorption mode.

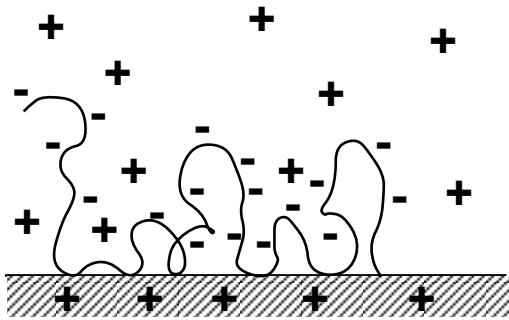


Figure 3-21. Schematic representation of the train and loop adsorption mode for an anionic polymer.

Steric forces

There has been debate as to whether polymer adsorption induces attraction or repulsion between particles. If chemical equilibrium is assumed, theory leads to the conclusion that the net force should be attractive [de Gennes (1987)].

Indeed, upon approach, some of the polymers will be compressed and excluded while others will cross-link the particles. Cross-linking is a process which is expected at low surface coverage, but which should also take place if the system remains at equilibrium.

However, practical evidence is found that adsorbed polymers can stabilise colloids. In addition, direct force measurements detect definite repulsive forces between surfaces with adsorbed polymers.

The difference between the theoretical expectation and the experimental evidence lies in the time scales, which are required for the system to reach equilibrium. Indeed, since desorption is a very slow process, one can consider that the surfaces maintain a given surface coverage upon approach.

Interpenetrational energy model

Naper (1983, subchapter 12.2) presents some pragmatic theories allowing determination of interaction energy between adsorbed layers. We will consider the model developed by Fischer (1958), which leads to the following relation for the interaction energy:

$$\Delta U_{ster}(a_k, a_k) = \pi a_k \frac{N_a}{\bar{v}_3} \left(\frac{\Gamma}{\rho_2 \delta} \right)^2 k_B T \left(\frac{1}{2} - \kappa_1 \right) (2\delta - h)^2 \quad [3-122]$$

Where:

- a_k is the radius of the particle
- N_a is Avogadro's number
- Γ is the weight of stabilizing moieties attached to the surface per unit area
- ρ_2 is the density of the attached polymer chains
- \bar{v}_3 is the molar volume of the dispersion medium
- δ is the thickness of the adsorbed layer
- h is the minimum surface to surface separation between both particles

Note that using the relations:

$$\bar{\phi}_2 = \frac{\Gamma}{\delta \rho_2}, \quad \text{for the volume fraction of polymer in the adsorbed layer} \quad [3-123]$$

$$D = h + 2a_k, \quad \text{for distance between the sphere centers}$$

$$\bar{V}_3 = \frac{\bar{v}_3}{N_a}, \quad \text{for the partial molar volume of the dispersing medium}$$

equation [3-122] can be rewritten in the form used by Bergström et al (1992) in a study of the consolidation behaviour of alumina. More recently it was used by Sakai and Daimon (1996) and Yoshokui et al (1997) to calculate steric hindrance induced by superplasticizers:

$$\Delta U_{ster}(a_k, a_k) = \frac{\pi a_k k_B T}{\bar{V}_3} \bar{\phi}_2^2 \left(\frac{1}{2} - \kappa_1 \right) (2\delta + 2a_k - D)^2 \quad [3-124]$$

These equations are valid in the interpenetrational region defined by:

$$\delta < h < 2\delta$$

Naper (1983, subchapter 12.3.1.2) reports the relationship for determining the interaction between unequal spheres:

$$\Delta U_{ster}(a_k, a_l) = \frac{2a_l}{a_k + a_l} \Delta U_{ster}(a_k, a_k) \quad [3-125]$$

Together with [3-122] we get for two unequal spheres:

$$\begin{aligned} \Delta U_{ster}(a_k, a_l) &= \pi \frac{2a_l a_k}{a_l + a_k} \frac{N_a}{\bar{v}_3} \left(\frac{\Gamma}{\rho_2 \delta} \right)^2 k_B T \left(\frac{1}{2} - \kappa_1 \right) (2\delta - h)^2 \\ &= \pi \bar{a} \frac{N_a}{\bar{v}_3} \left(\frac{\Gamma}{\rho_2 \delta} \right)^2 k_B T \left(\frac{1}{2} - \kappa_1 \right) (2\delta - h)^2 \end{aligned} \quad [3-126]$$

We recall that the force is given by the derivative of the potential with respect to distance, so that from [3-122], we obtain the following expression for the steric force in the interpenetrational region:

$$F_{ster}(a_k, a_l) = 2\pi \bar{a} \frac{N_a}{\bar{v}_3} \left(\frac{\Gamma}{\rho_2 \delta} \right)^2 k_B T \left(\frac{1}{2} - \kappa_1 \right) (2\delta - h) \quad [3-127]$$

Note we have changed the sign. To make the norm positive, since we know the direction in which the force is exerted.

Scaling theory

The scaling theory developed by de Gennes (1987) provides an expression for the force due to the compression as the layers begin to interpenetrate. It assumes either a mushroom or a brush conformation of the adsorbed polymers. For vinylic superplasticizers on cement, we have mentioned above that we would expect train and loop conformation. It seems that assuming a mushroom conformation would therefore lead to a better approximation than assuming a brush conformation.

Because this model provides good correlation with surface force measurements, and because its use is more simple than self-consistent field calculations, its use is increasing [Klein (1993), Peterson and Bergström (1999), Sigmund et al (1999)].

The steric force is zero before overlap begins. Then it progressively rises to reach infinity once the maximum compression thickness δ is reached. The functionality of this increase is given by:

$$F_{ster}(a_k, a_l) = 2\pi\bar{a} \frac{3k_B T}{5s^2} \left[\left(\frac{2L}{h} \right)^{5/3} - 1 \right] \quad [3-128]$$

Where:

s is the centre to centre distance between neighbouring mushrooms.

L is the thickness of the adsorbed layer

h is the minimum separation between the surfaces of the spheres. It can also be written as $D+2\delta$, where D would be the distance between the spheres each covered by a compressed layer of polymer.

3.8.2 Non adsorbing polymers

Air entrainment

When a molecule decreases the surface tension of a liquid phase, the result is that air bubbles can be entrained. These entrained bubbles can substantially modify the rheologic behaviour of a suspension.

Modification of capillary forces

When a powder is introduced into a liquid, some air can remain entrapped in between particles. The presence of these air bubbles can lead to a capillary force, which would resist particle separation.

A decrease of the surface tension of the liquid phase will increase the wettability of the powder and release the entrapped air.

Depletion flocculation

As two particles approach, free polymers in the interstitial liquid are compressed instead of interacting with the particles [Russel et al (1991), subchapter 6.4]. This increases the internal energy of these polymers (Figure 3-22). The polymer is therefore excluded from the gap. Further approach of the particles is driven because the solvent excluded dilutes the bulk system where the polymers are, which decreases the overall energy of the system. This process is described as depletion flocculation. It is increased when a clear repulsion exists between the polymer and the surface.

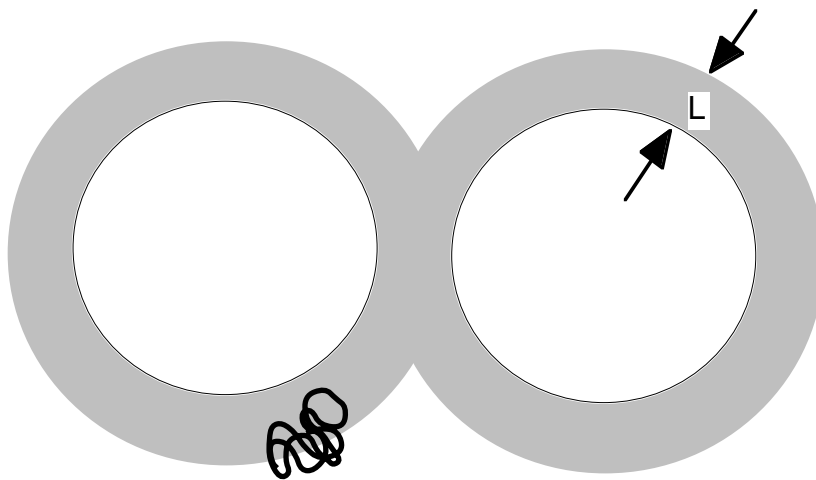


Figure 3-22. Schematic illustration two particles interacting due to depletion layers of thickness L .

Depletion stabilisation

The existence of a repulsive interparticle force induced by non-adsorbing polymers, is still a much debated topic [Ogden and Lewis (1996), Russel et al (1991), subchapter 6.6]. Experimental data indicates an oscillating force giving successively repulsive barriers and attractive wells as surfaces are approached in the presence of non-adsorbing polymers. An illustration of such force is given in Figure 3-23. The force barriers are attributed to the difficulty of the polymers to be excluded from the interstitial region as particles are approached. The overall force is therefore attractive, but kinetic effects might be slowing the process down. Note that unlike in adsorption where surface polymer interactions were hindering exclusion, this would be a purely transport limited process.

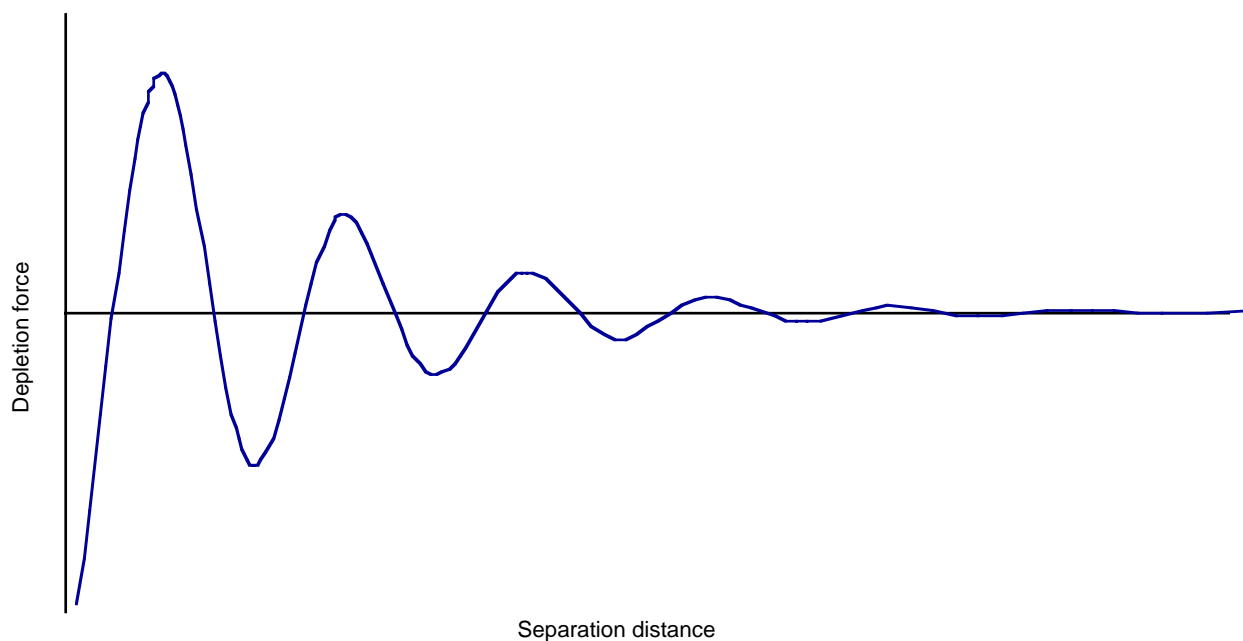


Figure 3-23. Schematic illustration of the force-distance relation, which has been measured between surfaces in presence of non-adsorbing polymers.

3.8.3 Adsorbed and non-adsorbed polymers

A word of caution must be made with regards to the situation in which both adsorbed and non-adsorbed polymers are present. The following effects will complicate interpretation.

- Segregation of molar masses during adsorption.
- Finalising of the surface coverage made possible by an excess of non-adsorbed polymer.
- Superposition of individual effects of adsorbed and non-adsorbed polymers.
- Additional mechanism for stabilisation by non-adsorbed polymers requiring the presence of an adsorbed layer.

Chapter 4 Materials

4.1 Model powders

MgO dead burnt and $\text{Mg}(\text{OH})_2$ from Martin Marietta Magnesia Specialties Inc. (type: P-98 and MH-10 respectively; Baltimore, USA) were carefully sampled. A representative part of the MgO was then sieved. The fraction below $50\ \mu\text{m}$ was sampled and used in all experiments with MgO.

The particle size was determined either by laser diffraction (Malvern Mastersizer; Malvern, GB) or with an apparatus from Micromeritics based on X-Ray absorption (mod. Sedigraph 5100; Norcross, USA). Both results for MgO (Figure 4-1) and $\text{Mg}(\text{OH})_2$ (Figure 4-2) indicate important differences in the distribution, while the mass average values remain relatively similar.

The BET specific surface area was determined by adsorption of N_2 (Micromeritics Gemini III 2375; Norcross, USA). No impurities were detected in the XRD data collected on the MgO. The $\text{Mg}(\text{OH})_2$ contained a small amount of MgO, possibly formed at the surface by excess drying during the production. The powder characteristics are given in Table 4-1.

Figure 4-3 and Figure 4-4 show SEM pictures of these powders. MgO has a morphology relatively close to that of cement. $\text{Mg}(\text{OH})_2$ is a solid aggregate of small crystallites and was found by N_2 adsorption/desorption measurements to contain a non negligible porosity (Micromeritics Asap 2010). About 50% of the surface area is contained in pores smaller than 1 nm (part of this can however be due to small surface asperities).

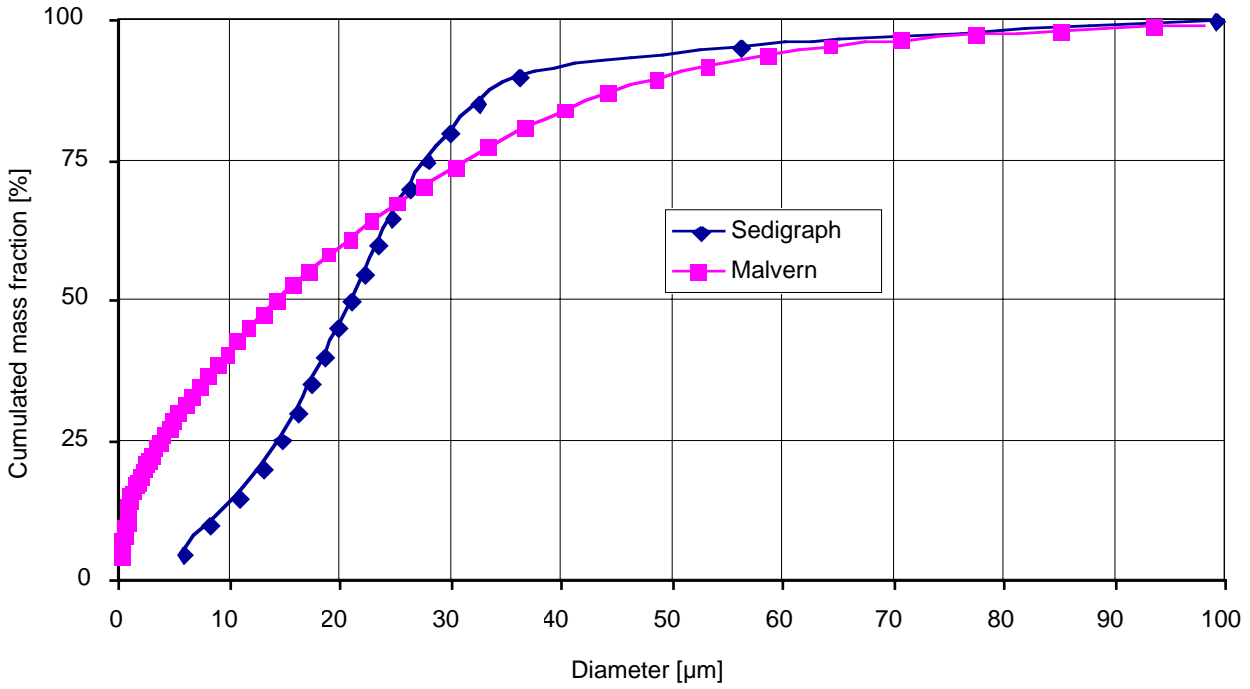


Figure 4-1. Particle size distribution of sieved MgO determined both by Malvern Mastersizer and Sedigraph.

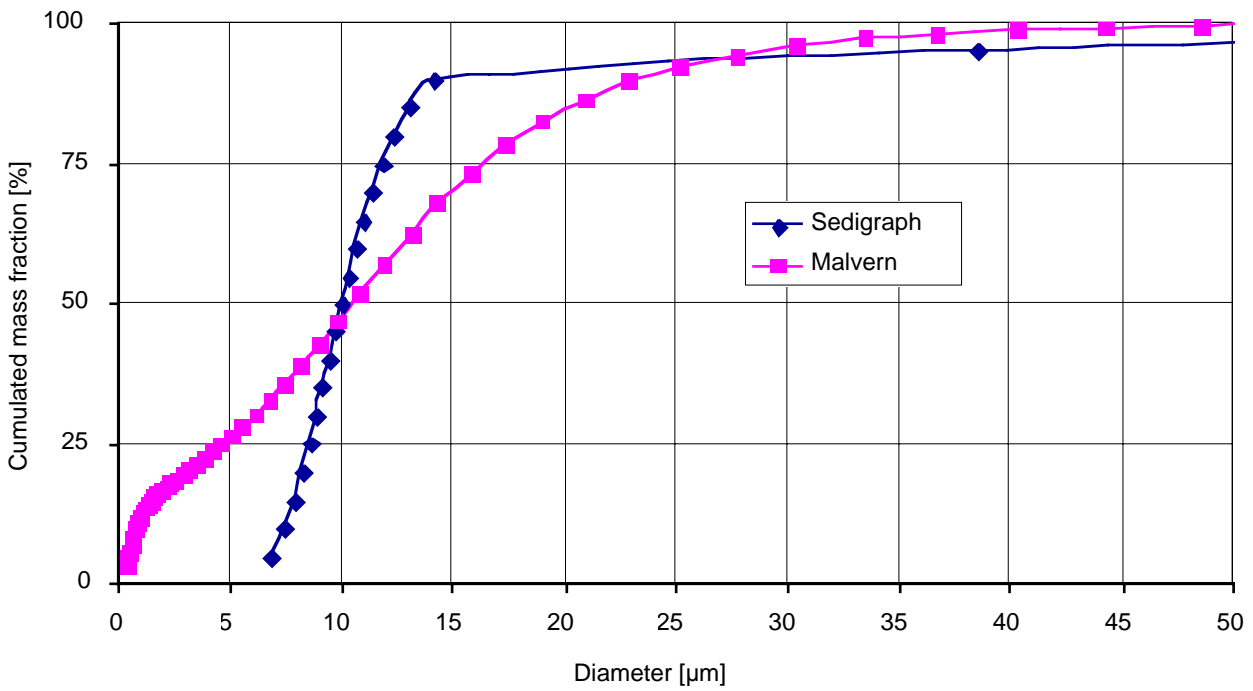


Figure 4-2. Particle size distribution of sieved Mg(OH)₂ determined both by Malvern Mastersizer and Sedigraph.

Table 4-1. Powder characteristics. Chemical analysis is given by the producer. Particle size and specific surface was measured at LTP.

mass %	Mg(OH) ₂	MgO
Mg(OH) ₂	98.6	
MgO	68.1 (equivalent)	98.5
CaO	0.55	0.69
SiO ₂	0.25	0.13
Fe ₂ O ₃	0.10	0.48
Al ₂ O ₃	0.07	0.06
Cl	0.2	----
SO ₃	0.15	----
K ₂ O	----	----
Na ₂ O	----	----
SiC	----	----
Loss on ignition	30.5	----
Free moisture	0.5	----
BET Specific surface area	11.8 ± 0.5 m ² g ⁻¹	0.77 ± 0.03 m ² g ⁻¹
Mass average diameter*	10.5 ± 0.5 μm	15.0 ± 0.5 μm
Mass average diameter**	9.9 μm	21.0 μm

* Determined by Malvern Mastersizer, ** Determined by Sedigraph

4.2 Cements

Two normal portland cements (CEM I) obtained from the same clinker (Olten, Switzerland), were used. The first was ground without any grinding aid. The second was ground in presence of a couple ppm of a triethanol amine acetate, a common grinding aid. Grinding times were adjusted so as to obtain two cements with the same specific surface areas.

The BET specific surface area of both powders was determined by N₂ adsorption (Micromeritics Gemini III 2375). Three samples were measured for each cement. Bulk chemical compositions and specific surfaces of both cements are given in Table 4-2.

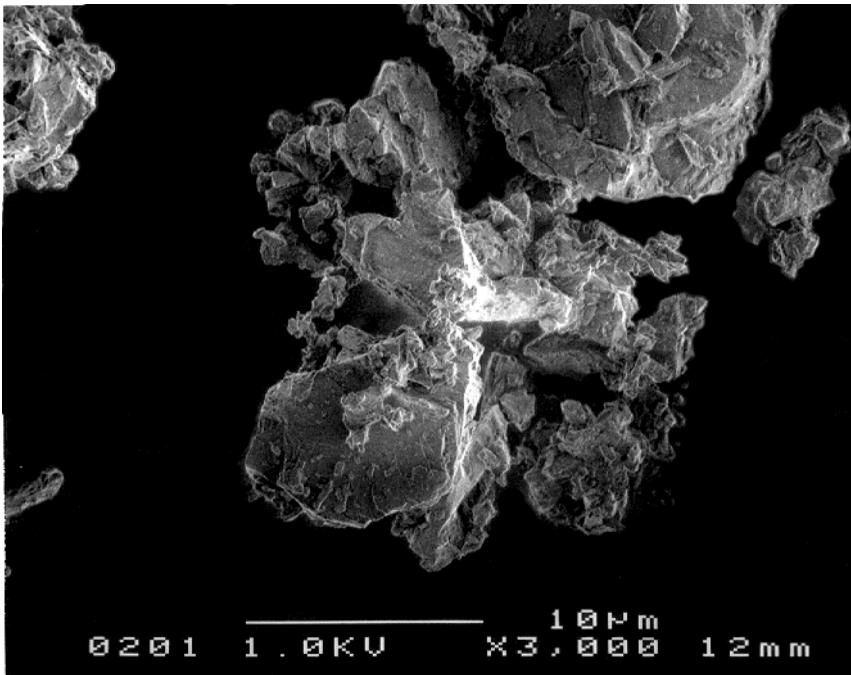


Figure 4-3. SEM picture of MgO.

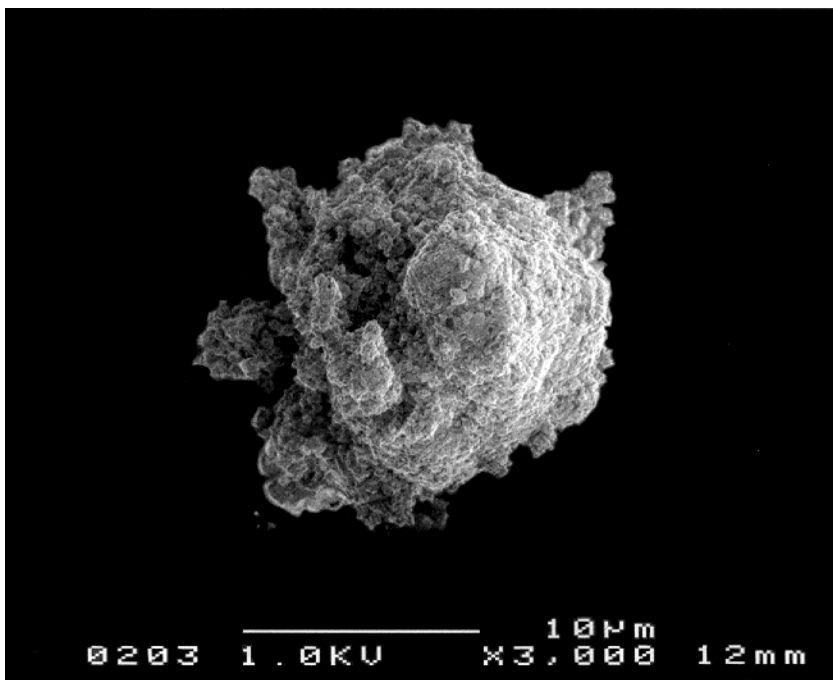


Figure 4-4. SEM picture of Mg(OH)₂.

To obtain a more reliable particle size distribution of the cements, we used X-ray disk centrifuge from Brookhaven (mod. BI-XDC; Holtsville NJ, U.S.A.), operated in sedimentation mode. To slow down sedimentation, the continuous phase used was ethylene glycol at 25°C. The distributions almost perfectly superimpose. In Figure 4-5, we show an Olten cement and a finer cement used in the Eureka project. Its particle size distribution only, will be used later.

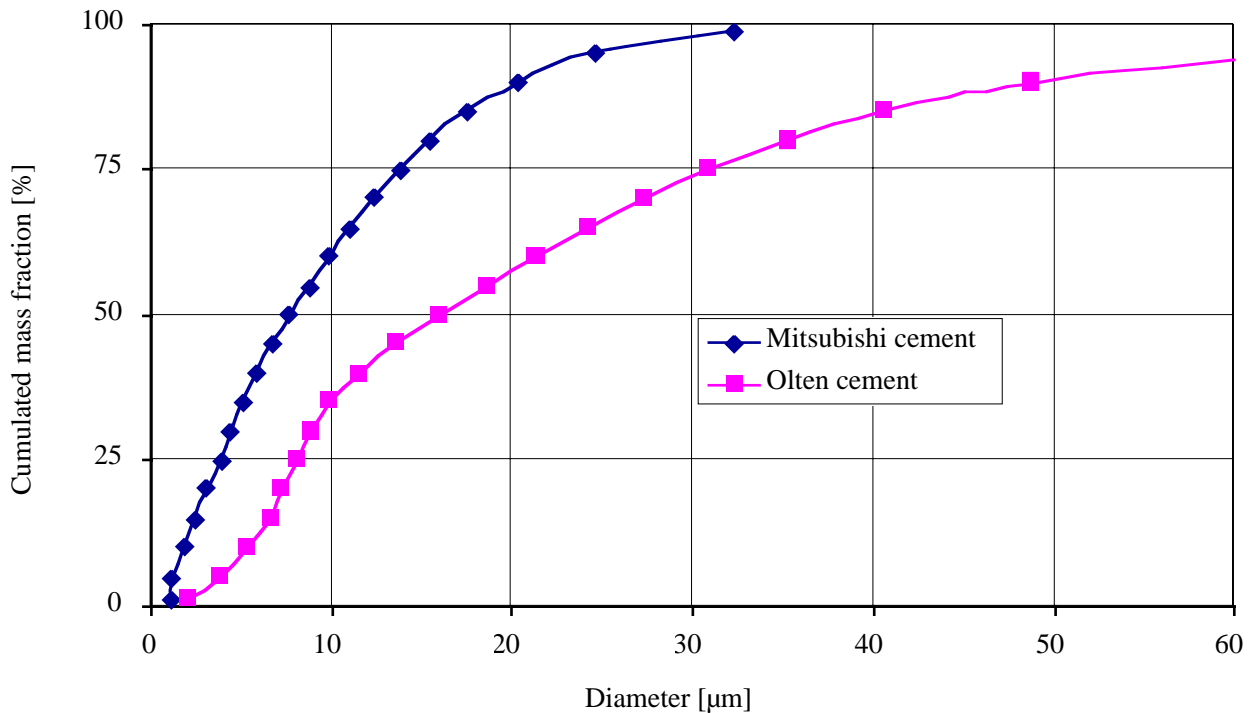


Figure 4-5. Particle size distribution of one Olten cement and a finer Mitsubishi cement, measured by X-ray disk centrifuge.

4.3 Polymers

Seven structurally different polymers which are representative for most of the superplasticizers used today have been chosen in this study. They are listed in Table 4-3. This table also contains average molar masses determined by Sika A.G by exclusion chromatography. A combination of 3 coupled columns of hydrophilized hydroxyethyl methacrylate gel (100 + 30 + 10 nm) was used. Samples of Na-polystyrene sulfonates of different molar masses each having very narrow molar mass distributions ($M_w/M_n = 1.10-1.25$) were used as calibration standards for the columns. The detectors used were either UV or light scattering.

Table 4-2. Characteristics of studied cements⁶.

	Cement With Grinding Aid	Cement Without Grinding Aid
LOI (1000°C)	2.89	2.65
CO ₂	2.61	2.29
SiO ₂	20.35	20.51
Al ₂ O ₃	5.26	5.28
Fe ₂ O ₃	2.92	2.91
CaO	63.19	63.18
SO ₃	2.25	2.20
MgO	1.52	1.58
K ₂ O	1.10	1.11
Na ₂ O	0.26	0.28
MnO	0.05	0.05
TiO ₂	0.24	0.25
CaO (free)	0.07	0.07
Specific Surface Blaine [m ² g ⁻¹]	0.327	0.349
Specific Surface BET [m ² g ⁻¹]*	0.96 ± 0.09	0.95 ± 0.18

* Values are an average of three measurements. Errors given correspond to the 95% confidence interval.

Four of these polymers, PCA-1, PCA-2, PCE-1 and PCE-2, are laboratory test products [Bürge et al (1992)]. The other three, PCE-3, PCA-3 and SNFC-1, are commercially available. Apart from the SNFC-1, these polymers are found as concentrated aqueous solutions, with a solid content of about 30-40% by mass. Apart from PCE-3 and PCA-3, molecular structures of these polymers are given below.

⁶ Chemical compositions were determined by the *Institut für Baustofflehre und Materialprüfung* of the University of Innsbruck, Austria. Blaine specific surface was determined by ZAG, the Slovenian Center for Materials testing in Ljubljana, Slovenia.

Table 4-3. Characteristics of the polymers used. Molar mass errors are estimated by Sika. We have chosen to consider this estimate as the error for a 95% confidence intervals, following a normal distribution.

Designation	Chemical Type	Number Average Molar Mass [g mol ⁻¹]	Mass Average Molar Mass [g mol ⁻¹]	Polydispersity Coefficient Mw / Mn [-]
PCA-1	Na-polycarboxylate-polysulfonate	15'600 ± 2'000	40'500 ± 5'000	2.6 ± 0.5
PCA-2	Na-polycarboxylate-polysulfonate	11'500 ± 2'000	24'500 ± 5'000	2.1 ± 0.5
PCE-1	Na-polycarboxylate-polysulfonate, containing PEG-ester	9'500 ± 1'500	30'000 ± 5'000	3.2 ± 0.8
PCE-2	PEG-ester containing polymer, weakly ionic	15'000 ± 5'000	45'000 ± 10'000	3.0 ± 1.0
PCE-3	Na-polymethacrylic acid, containing PEG-ester, weakly ionic		10'000 ± 2'000	
PCA-3	Na-polyacrylate		2'500 ± 500	
SNFC-1	Sulfonated naphtalene formaldehyde polycondensate, Na-salt		6'000 ± 1'000	

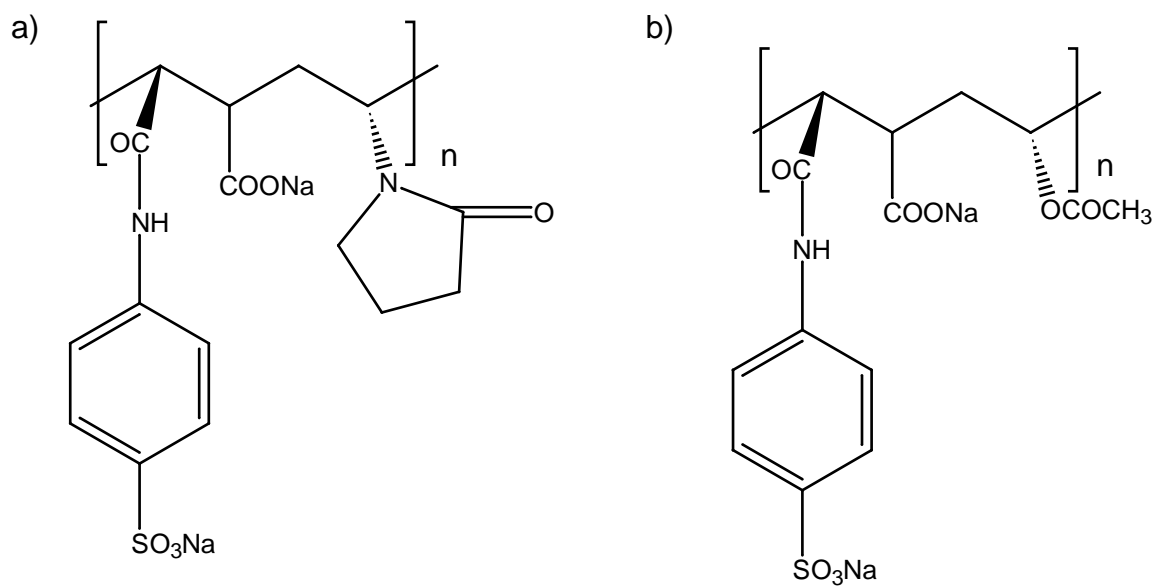


Figure 4-6. Molecular structure of PCA-1 (a) and PCA-2 (b)

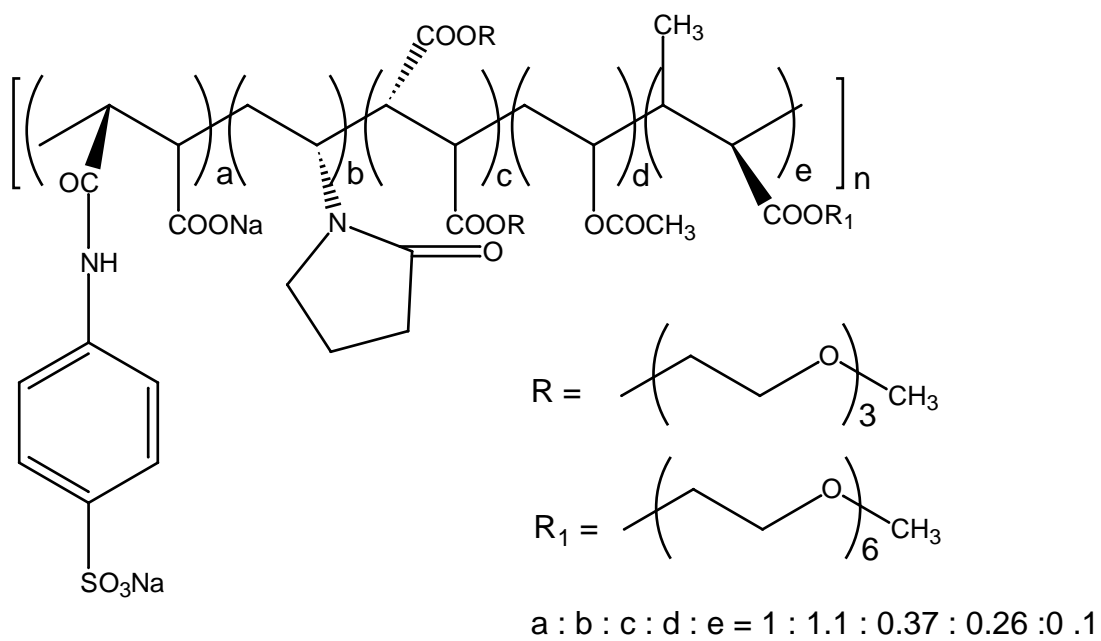
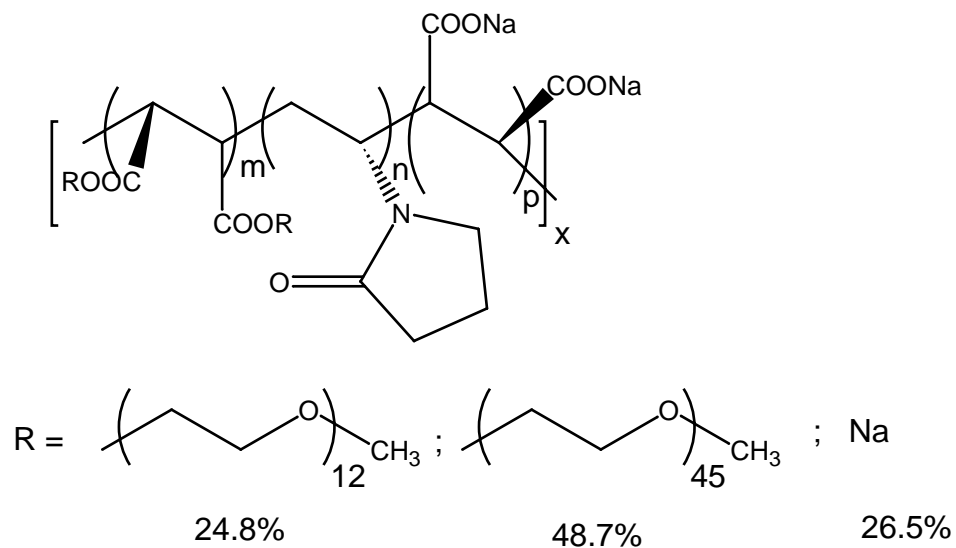


Figure 4-7. Molecular structure of PCE-1



$$M : n : p = 1 : 2 : 1$$

Figure 4-8. Molecular structure of PCE-2.

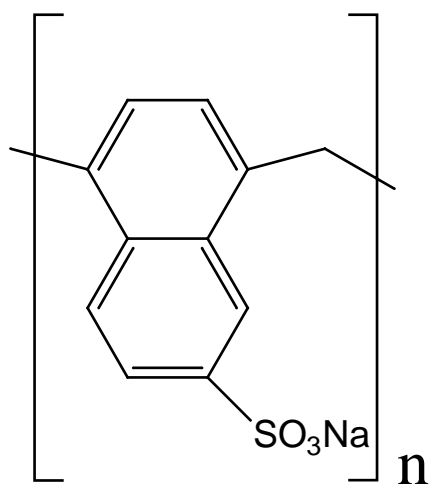


Figure 4-9. Molecular structure of SNFC-1.

Chapter 5 Experimental methods

5.1 Adsorption

5.1.1 High Performance Liquid Chromatography (HPLC)

Principles

High performance liquid chromatography allows the separation of molecules according to their chemical nature. A mobile phase (liquid), passes continuously through a column filled with a stationary phase (a gel). At a given time, a known volume of the sample to analyse is injected into the mobile phase, prior to its entering the column. Molecules with a poor affinity for the stationary phase will go through the column fast, while molecules with a higher affinity will take much longer.

At the outlet of the column is a detector, which produces a signal related to the concentration of molecules eluted. An HPLC analysis is therefore the combination of a separation and an analytical technique.

Some molecules, due to a high affinity for the stationary phase, can have excessively long times residence times in the column. Changing the mobile phase can solve this problem. However, with mixtures, this often results in a poor separation of the different molecules to be analysed. In such cases, one can use a mixture of two solvents and change the fraction over time. The result is a progressive elution of well-separated molecules within reasonable time. The term for this procedure is elution gradient chromatography.

Reverse phase chromatography uses a stationary phase made hydrophobic by grafting alkyl groups onto the stationary phase. In such situations, the elution time of polymers increases with their molar mass. HPLC provides one of the best separation techniques for analysing polymeric fractions [Piotte et al (1995)]. It overpasses gel permeation chromatography (GPC) in this respect. This technique

however can provide molar masses, provided sufficiently similar molecules of well defined masses are available for calibration. Obtaining a proper molar mass from HPLC is a more complicated task as discussed by Piotte et al (1995).

Operation conditions

The HPLC used was from Waters (mod. Alliance; Milford, U.S.A.) equipped with a diode array detector. The column was an RP-18 from Merck. Elution of the samples was obtained by applying gradients specially developed by Sika. The elution gradient uses H_2SO_4 0.01N and acetonitrile from Fluka (grade. HPLC; Basel, Switzerland) from Merck (grade. Gradient; Darmstadt, Germany). The same gradient is used for polymers PCA-1 and PCA-2. The chromatogram of PCA-1 (Figure 5-1) clearly indicates a polydispersity within the polymeric fraction. Both the hand PCA-2 (Figure 5-2) and the PCE-1 (Figure 5-3) appear to be relatively monomodal. These figures give arbitrary absorption units (AU). The magnitude of the scale depends both on the amount of polymer analysed and on the polymers specific absorption at the wave length used.

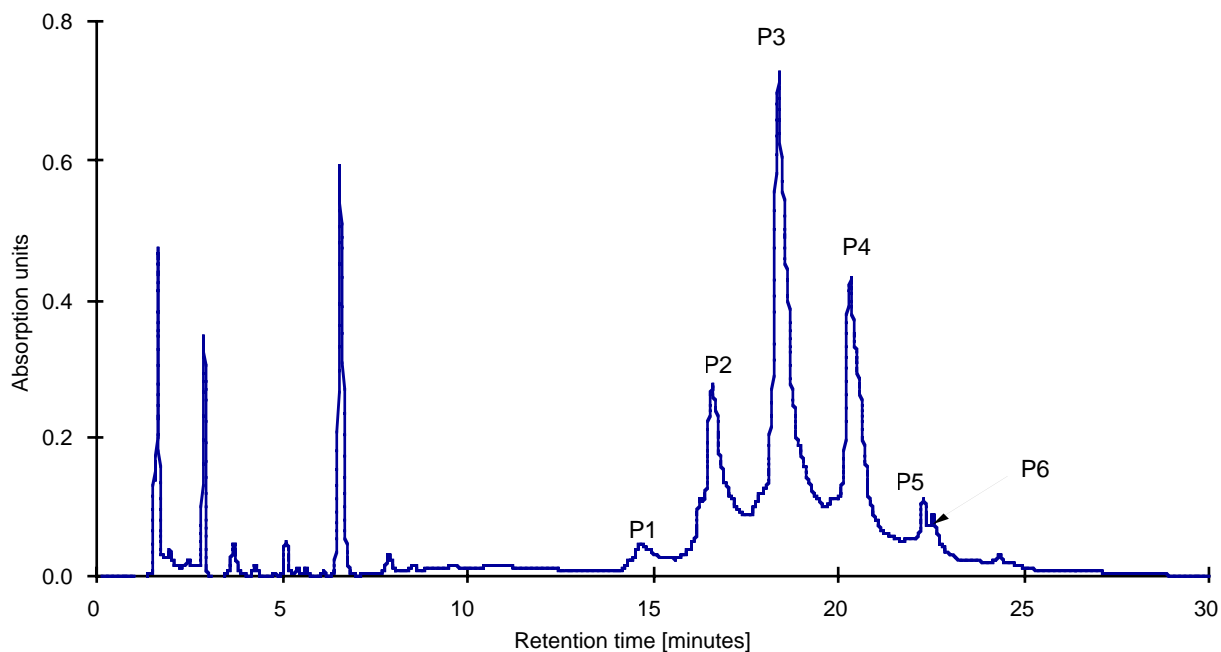


Figure 5-1 . HPLC Chromatogram for polymer PCA-1.

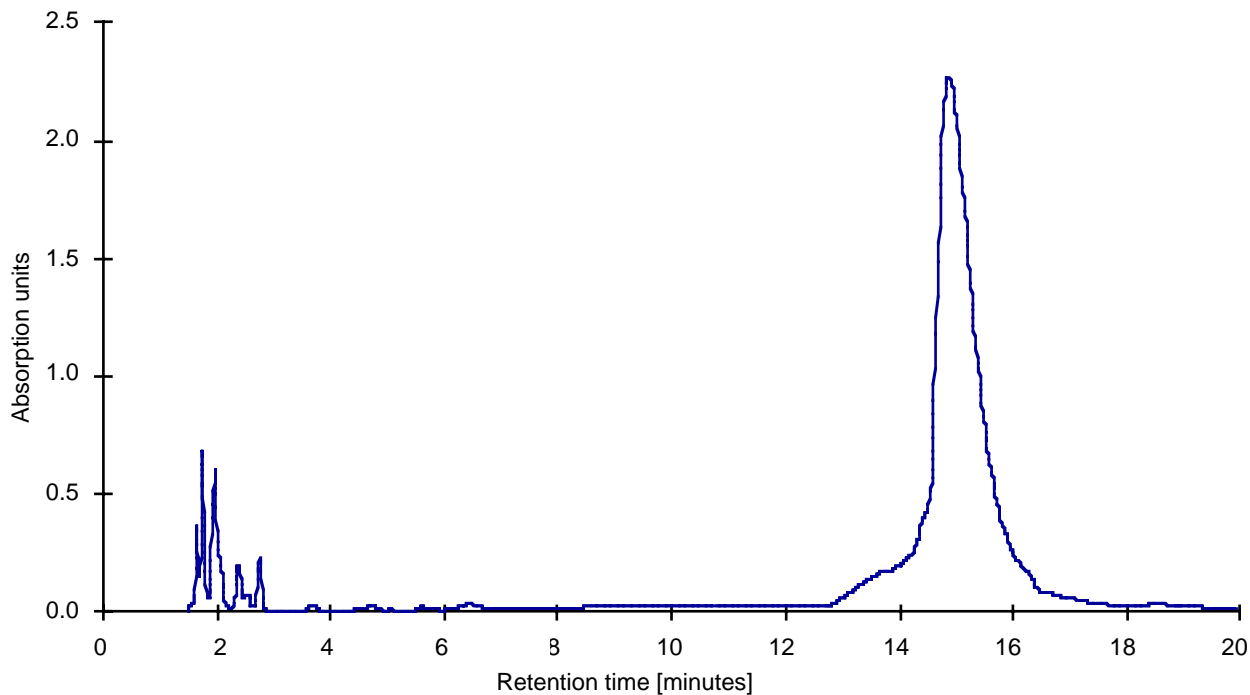


Figure 5-2. HPLC Chromatogram for PCA-2.

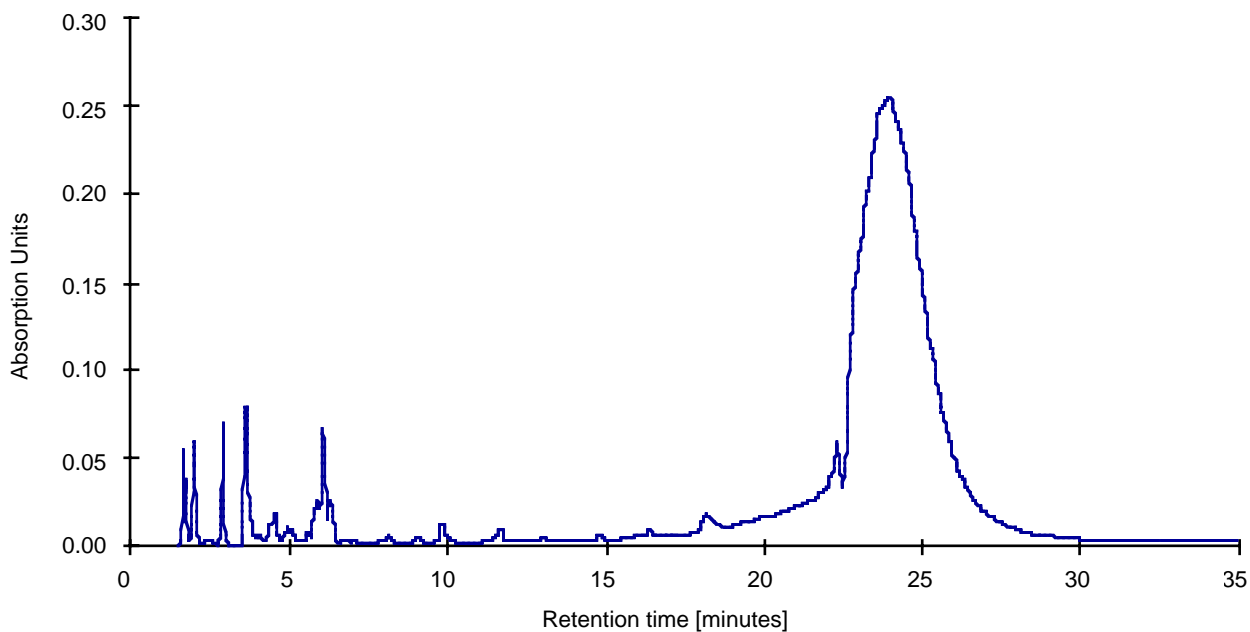


Figure 5-3. HPLC Chromatogram for PCE-1.

For PCE-1, spectroscopy grade acetonitrile from Merk (grade. Uvasol) was used in later experiments to obtain a better baseline. This is because the elution gradient for PCE-1 goes to higher fractions of acetonitrile and that each polymer contains less UV absorbing groups (benzene sulfonates) than either PCA-1 or PCA-2.

5.1.2 Model suspensions

It was found by high performance liquid chromatography (HPLC) that excessive residence of the superplasticizers in a solution at pH around 12 can lead to a partial hydrolysis of the polymer (about 1–2 hours). The adsorption experiments were designed to minimise the necessary residence time of the polymer in solution, while achieving complete adsorption.

Adsorption measurements were performed in suspensions of 10 g of MgO or 5 g of Mg(OH)₂ in 20 ml NaOH 0.01M (pH 12.0 ± 0.1 at 20°C), previously thermostated in a rotary bath at 200 rpm (different masses were taken to achieve similar volume fractions). In all cases water was obtained from a purifying system by Seral (mod. Seralpur; Ransbach-Baumbach, Germany) giving conductivity inferior to 0.055µS/m. In later experiments the water was also boiled to ensure complete elimination of CO₂.

The suspensions were kept in closed 125 ml polyethylene flasks to avoid change in concentration by evaporation. Superplasticizers were added as concentrated aqueous solutions (10-15% solid content by mass) with a microdispenser. This concentration range allows a viscosity small enough to obtain a precise dosage with microdispensers, while keeping added volumes sufficiently small not to change the systems behaviour due to dilution. Nevertheless, the dilution was taken into consideration when calculating the adsorption mass balance.

After 30 min in the rotary bath, the suspensions were centrifuged 5 min at 3'000 rpm, in a thermostatable table centrifuge from Jouan (mod. CR-412; St-Nazaire, France) regulated at the same temperature as the adsorption experiments were carried out. From the supernatant, 5 ml, buffered with 25 µl of CH₃COOH (30% V/V), were filtered through a 0.45 µm filter mounted on a dispensable syringe. The first 2 ml were discarded and the rest was analysed by reverse phase HPLC.

The calibration standards contained no powder and were therefore not centrifuged. Apart from this, they were treated in the same way as the other samples. Each sample was analysed at least twice.

The temperatures at which these measurements were carried out were 25, 32 and 40 °C. For MgO and polymer PCE-1, adsorption was also measured at 11 and 18°C in order to confirm an unexpected temperature effect on adsorption. For PCA-2 on MgO the behaviour was also measured at 18°C.

The diode array detector, which only allows one to study products which absorb in the UV or visible range, has limited the number of polymers whose adsorption could be studied to PCA-1, PCA-2, PCE-1 and SNFC. Because already extensively studied, the SNFC polymer has been studied in less detail. Its adsorption onto the model powders was not measured.

5.1.3 Cements

The suspensions of cement were prepared by dispersing 10 g of cement in 20 ml demineralised water (conductivity < 0.05 µS/m). The temperature was 25°C.

In a first set of experiments, the polymer was predissolved in the water. In a second set of experiments, polymers were added as concentrated solutions (10-15% solid content by mass) with a microdispenser after 30 min hydration. The added amount was weighed.

The adsorption time was varied, leaving either 5 or 30 min. Longer adsorption times were not studied because of the risk of hydrolysis of the polymers.

After adsorption, the supernatant was obtained as described above. For the neutralising step 30 µl of CH₃COOH (Merck; pro analysis) had to be used. Indeed, the alkalinity of the suspensions is even higher than that of the model suspensions.

Because dissolved impurities from cement can alter the polymers, standards were not prepared in pure water. Instead, they were prepared in solutions having the same composition as the liquid phase of the cement suspensions. These were obtained as follows. Conductivity measurements showed that, after less than 10 min, the liquid phase was stable. Large volumes of suspensions having the same solid/liquid ratio were mixed 10 min and then centrifuged and filtered (0.2 µm). The solutions obtained were kept in closed bottles. Longer storage times were avoided because of the risk of carbonating the solution. These calibration samples, apart from containing no powder and not being centrifuged, were treated in the same way as the other samples.

5.2 Rheology

5.2.1 Model suspensions

Only rheology of $\text{Mg}(\text{OH})_2$ are reported, because it was more convenient for these measurements (smaller average particle size and narrower distribution, smaller density, little or no effect of temperature on adsorption).

Small volumes of concentrated superplasticizer solutions were pipetted into 50 mL PE flasks and weighed. With a macrodispenser, NaOH 0.01 M was added to complete the total desired liquid volume (volumes were considered additive). The added mass of NaOH was weighed. This procedure, by reducing contact time of superplasticizers in the alkaline solution, renders their hydrolysis negligible.

$\text{Mg}(\text{OH})_2$ and silica fume were then separately weighed into separate sample holders before being added to the PE flasks. The added mass of each powder was also weighed. $\text{Mg}(\text{OH})_2$ was always added first.

Samples were then mixed by hand with a spatula from 1-5 minutes depending on the solid/liquid ratios (higher ratios required more mixing). They were then inserted into the sample holder of a coaxial cylinder device (Z20 DIN) mounted on a rheometer (Haake mod. RS100; Karlsruhe, Germany), thermostated at 25°C. The gap between both cylinders is 0.85 mm. Over this gap, the velocity gradient is assumed to be constant.

One commonly mentioned condition for cement rheology measurements to be reproducible is to complete irreversible breakdown of a critical fraction of the agglomerates. High mixing achieves this purpose and one can consider that when a paste is submitted to constant high shear rate, the breakdown is complete at the latest once the viscosity reaches a constant value. To fulfill this condition, the samples were initially mixed for 45 s at the maximum shear rate of the instrument (640 s^{-1}). After that, stress was ramped down from 20 Pa (50 Pa for the more concentrated suspensions) to 1 Pa. The sample was then held at 1 Pa for 30s, before ramping back up to the initial stress. Both stress ramps lasted 5 min during which 15 data points were collected at logarithmic time intervals.

5.2.2 Cement suspensions

Rheology measurements were all performed at 0.35 W/C. Solutions of known superplasticizer composition (7 ml) were weighed into 50 ml PE flasks. Cements (20 g) were weighed separately into sample holders and then added into the PE flasks.

Samples were then mixed by hand with a spatula from 1-3 minutes depending on the polymer dosage (lower dosages required more mixing). They were then inserted into the sample holder.

For all our cement samples, 160 s at the maximum shear rate of the instrument (640 s^{-1}) was applied. This was sufficient to reach stationary viscosity of the most viscous samples.

During this initial mixing (160s; 640 s^{-1}), 5 points are taken at equal intervals. Then, the samples were left to rest 5 min. After that, the stress was ramped up from 1 Pa to 100 Pa in 8 minutes, taking 20 points logarithmically spaced. Stress ramps are most adequate for directly measuring a yield stress (Schramm (1994), pp. 195-196). If the shear rate reached 640 s^{-1} , before 100 Pa, the step was interrupted. After that, the samples were held 3 min at 640 s^{-1} , taking one point each minute. Finally, the shear rate was reduced to the minimum value possible.

5.3 Zeta Potential

5.3.1 Principle of the acoustophoresis

In acoustophoresis, a periodic sound wave is used to induce a periodic velocity difference between the continuous media and colloidal particles provided they do not have the same density. When particles are charged, this periodic velocity difference induces a periodic electrical potential. The amplitude of the macroscopic potential measured in the suspension is called the colloid vibration potential (CVP) and is linked to the zeta potential of the colloid particles.

There is debate in the literature as to the exact way by which this potential should be calculated [Scales and Jones (1992)]. However, not being aware of a definitive study on the question, the standard method proposed by the manufacturer and outlined by Marlow et al (1988) was used.

5.3.2 Model suspensions

Zeta potential was measured at 23-25° C by acoustophoresis (Penkem, system 7000; Bedford Hills, USA). In this method, particles are put into movement by an acoustic wave. A slight vacuum was maintained in the measuring cell to avoid bubble formation, which attenuates the signal. The suspensions were prepared by dispersing 20 g of powder in 300 ml NaOH 0.01M (pH 12.0 ± 0.1 at 20°C) under vigorous agitation and sonification for 15 min (150 W, 20 kHz). Prior to measuring, they were degassed for 5 min (≈ 20 torr). The superplasticizers were progressively added as concentrated aqueous solutions with a microdispenser.

5.3.3 Cement suspensions

One of the limitations linked to the calculation mode of zeta potential is the particle size distribution. In particular, very large particles induce a smaller signal than the smaller particles. This becomes a major problem for cement suspensions. We have developed a procedure to take into account particle size distribution effects. These results will be the object of a publication with Clarissa Ferraris (NIST, Washington) but are not presented here.

Chapter 6 Results with model suspensions

6.1 Chemical stability of suspensions

The pH of the $\text{Mg}(\text{OH})_2$ suspensions dropped to 11.3, while it remained at 12.0 ± 0.1 with MgO . The pH change of the $\text{Mg}(\text{OH})_2$ suspensions is believed to result from the precipitation of hydroxides by dissolved impurities. A further pH decrease is limited by the following equilibria:



6.2 Zeta potential

The influence that superplasticizers have on zeta potentials of $\text{Mg}(\text{OH})_2$ suspensions is shown in Figure 6-1. Potentials are plotted as a function of superplasticizer added, given in mg of their dry mass by m^2 of $\text{Mg}(\text{OH})_2$ in suspension. Results show that the polymers PCA-1, 2, 3 and SNFC-1 induce the largest final potentials (around -23 mV), while the polymers PCE-1, 2, 3 induce lower potentials ranging from -5 to -18 mV.

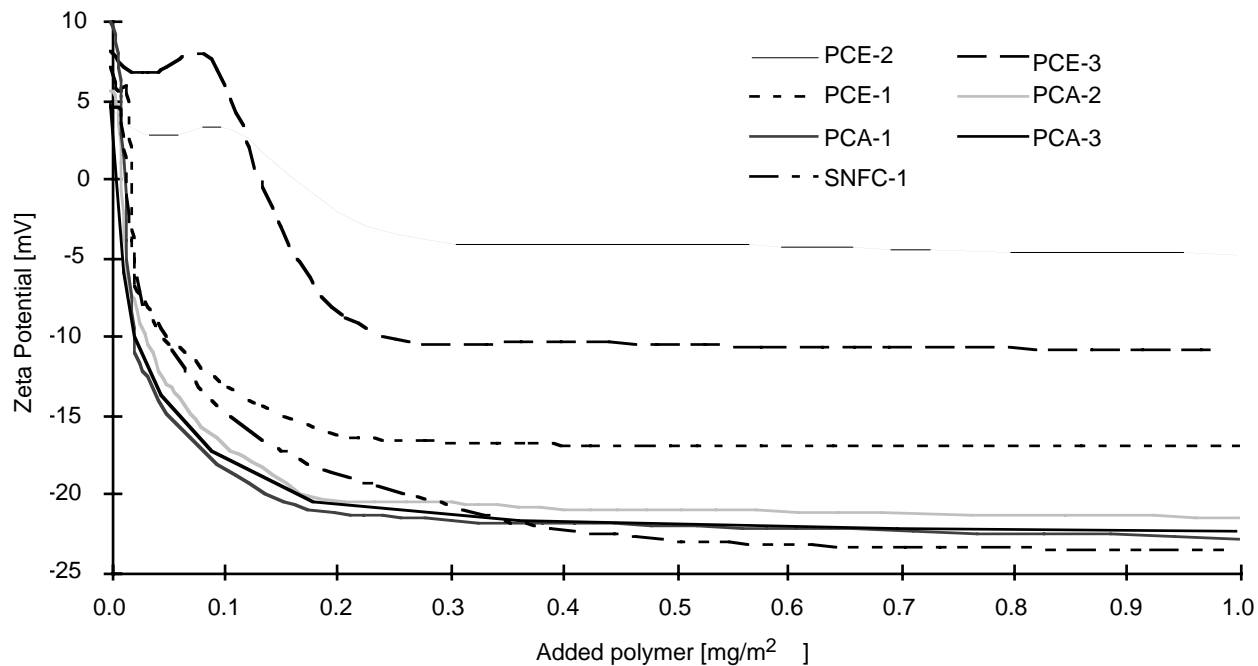


Figure 6-1. Zeta potential of magnesium hydroxide suspensions plotted as a function of the added mass of superplasticizers.

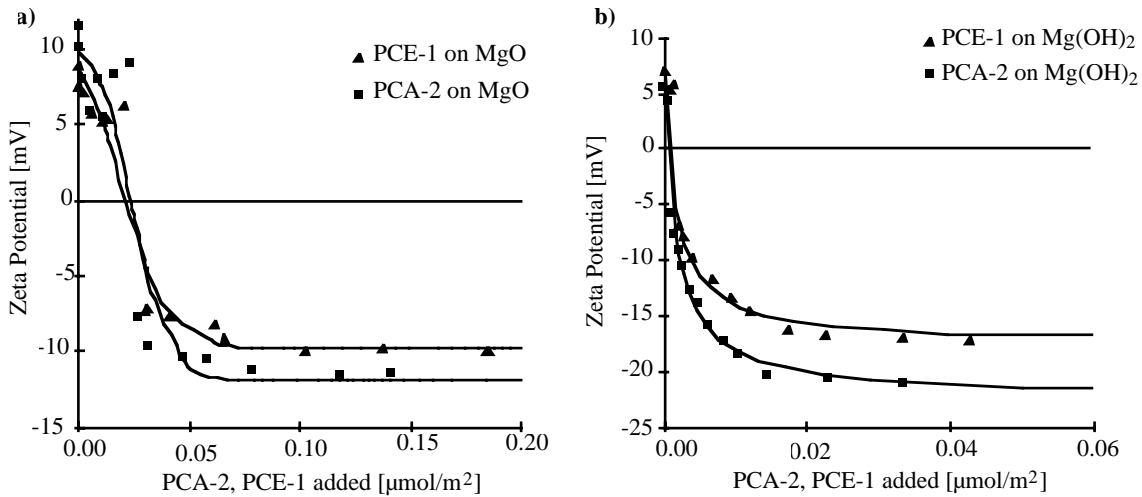


Figure 6-2. Zeta potential measured of PCE-1 and PCA-2. a) with MgO. b) with Mg(OH)₂. Fitted curves are S-functions for MgO and hyperbolas for Mg(OH)₂.

Figure 6-2 a and b show the change in zeta potential that both polymers PCA-2 and PCE-1 induce respectively on MgO and Mg(OH)₂. Here, the superplasticizer added is given in molar units instead of mass of solids content. Both figures show similar differences between the potentials induced by the PCA-2 and the PCE-1, though the potentials of the saturated powders are smaller (in absolute value) on MgO than on Mg(OH)₂.

6.3 Adsorption

In this section we present a rather detailed description of adsorption data. The purpose of this is to obtain a statistical testing of an unexpected result, where the amount of adsorbed polymer can increase with temperature, depending on the nature of the surface and the polymer.

The first subchapter examines for each polymer whether the calibration data is correlated with temperature. Having done this, it is possible to calculate more accurately the amount of polymer, which remains in the supernatant of the model suspensions.

The statistical data analysis used here is presented in more detail in Annex D. It is based on linear regressions performed on different data sources. We compare both ordinates at the origin and slopes. What can be obtained is a degree of confidence, which allows rejection of the hypothesis that the sets of data compared produce the same parameters (ordinate at the origin, slope or both). If this degree of confidence is high, the parameters are not all identical. If the degree of confidence is low, the parameters might not be identical, but it is not possible to prove so within experimental error.

6.3.1 Calibration Data

PCA-2 calibration line

For the PCA-2 polymer, it appears that all calibration lines pass through the origin. So, regressions at each temperature were performed with this requirement. We obtain a series of slopes and now wish to know whether their values are correlated with temperature. So, we calculate the confidence level to reject the absence of a temperature effect. This turns out to be 75%, a value considered too low to reject this hypothesis.

Having admitted the slopes to be independent of temperature, we now wish to know whether all these slopes can be considered identical. Again, we must proceed by calculating the degree of confidence to reject the fact that there is at least one slope different from the others. The degree of confidence for rejecting this hypothesis is 60%. So, we conclude that all the calibration lines can be considered as defining a single line through the origin. Therefore, all data can be used to compute a more precise regression line (Figure 6-3).

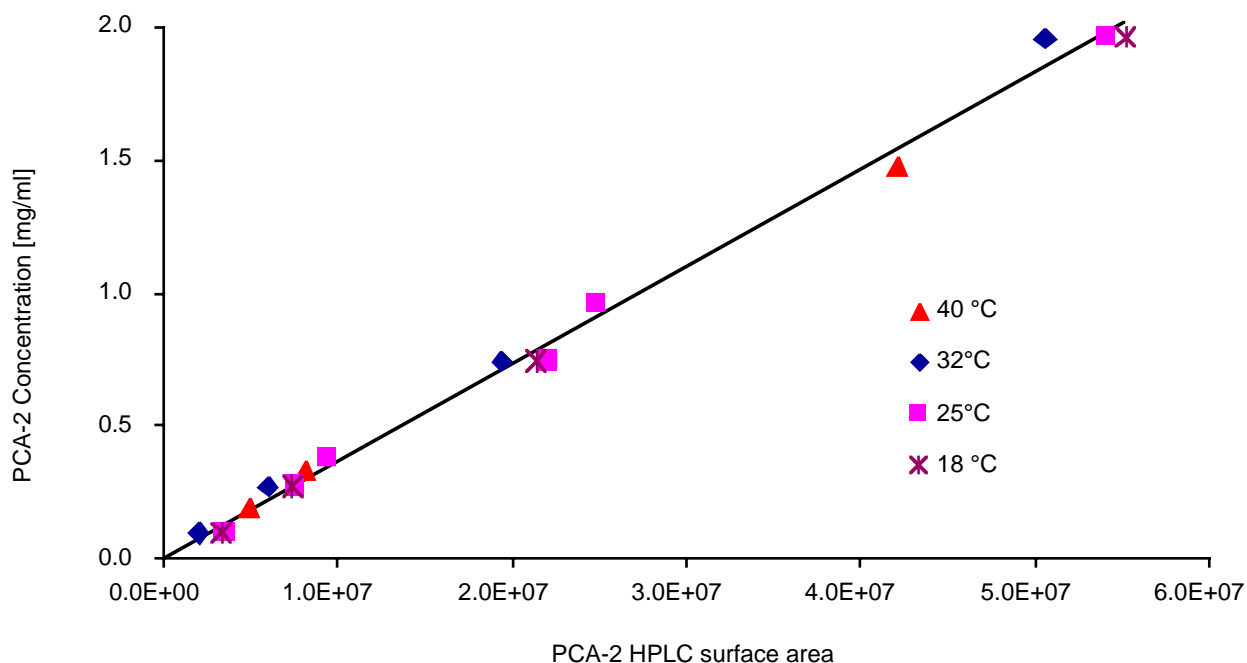


Figure 6-3. Calibration data of PCA-2 at 18°C, 25°C, 32°C and 40°C. The line shows the regression line passing through the origin.

PCA-1 calibration line

As for PCA-2, PCA-1 regression lines appear to pass through the origin. We test a temperature effect on slopes and ordinates at the origin and obtain a confidence level for rejecting the absence of such an effect of 66% and 83% respectively. For regressions passing through the origin the level for rejecting the absence of an effect of temperature on the slope is 51%. These results lead us to assume that all series are identical. As previously it is then possible to use all data together to obtain one common regression line. Testing whether this line passes through the origin gives a rejection level of

49%. So, we accept the hypothesis that this regression line passes through the origin and recalculate the appropriate line (Figure 6-4).

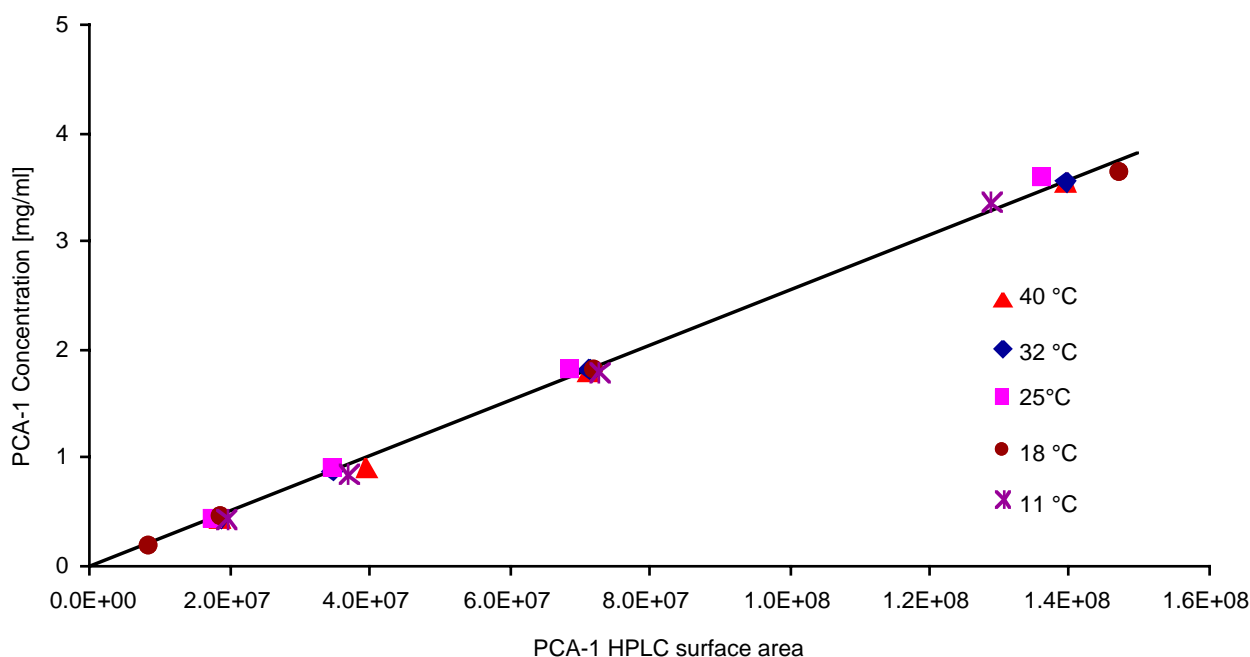


Figure 6-4. Calibration data for PCA-1 at 11°C, 18°C, 25°C, 32°C and 40°C. The regression line passes through the origin.

PCE-1 calibration line

A first serie of measurements was performed at temperatures of 25°C, 32°C and 40°C [Flatt et al (1986a)]. Later additional data were acquired at 11°C and 18°C to complete the description of the behaviour of PCE-1 in presence of MgO [Flatt et al (1986b)]. In the first serie of measurements, the following problem was encountered. The acetonitrile of HPLC grade contained some impurity, which accumulated in the column and only eluted at the same time as the polymer. For this reason calibration curves have non-zero ordinates at the origin. To avoid this problem we later chose to use spectroscopy grade acetonitrile when measuring PCE-1. This was the case at the moment of measuring samples acquired at 11°C and 18°C. For this reason, there is a clear difference for the ordinate at the origin. In the second case, this ordinate can be taken to be equal to zero. In addition, the column had been changed. Both sets of calibration data must be considered separately.

For the second set of data, we compare both regression lines and calculate the degree of confidence with which it is possible to reject the hypothesis that either both ordinates at the origin or both slopes are identical (Annex D). If this level of confidence is high, it is possible to conclude that the parameters (ordinate at the origin or slope) are different. In the opposite situation, one concludes that if there is a difference, it is too small to be detected within experimental error. For the slopes this level is 22% and for the ordinates 17%. These values are very low, so we cannot conclude that the lines are different. Therefore, data at both temperatures are used to calculate a common regression line.

With the regression data, a new test is performed to test whether the ordinate at the origin is equal to zero. This bimodal test leads to a confidence level of 63% to reject that hypothesis. So we admit the slope to pass through the origin and recalculate the regression line, which is plotted Figure 6-5.

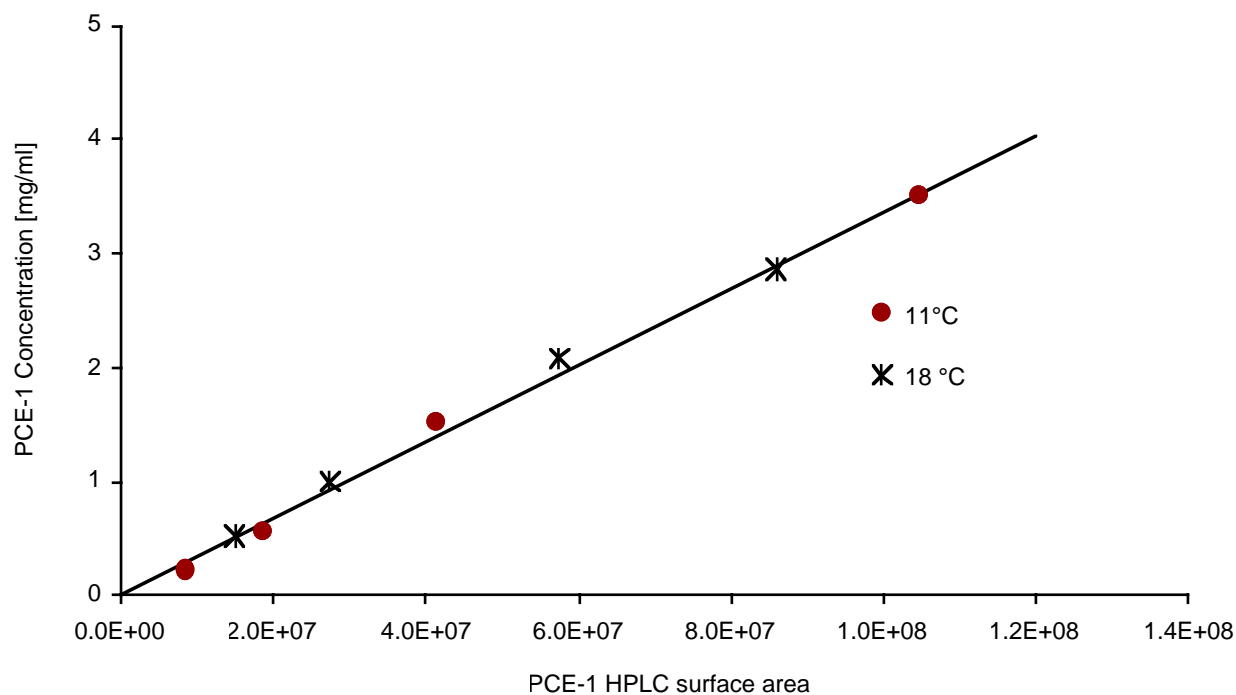


Figure 6-5. Calibration data for polymer PCE-1 at temperature of 11°C and 18°C. The line represents the linear regression performed over all data. The ordinate at the origin is zero.

For the first series of data, these confidence levels are 30% and 21%. Here again the values are low. However, in this situation we must take into account the fact that we are dealing with three different temperatures. For this reason, we must test whether temperature has an effect on either the slope or the

ordinate at the origin (Annex D). The confidence intervals for rejecting this hypothesis are respectively 50% and 55%. Though higher, than the previous, these values remain sufficiently low to not conclude on a temperature effect on these calibration lines. All data at these three temperatures are therefore used to calculate a common regression line. Performing a test to determine whether the line passes through the origin gives a degree of confidence to reject this hypothesis of 100%. The regression line is shown in Figure 6-6.

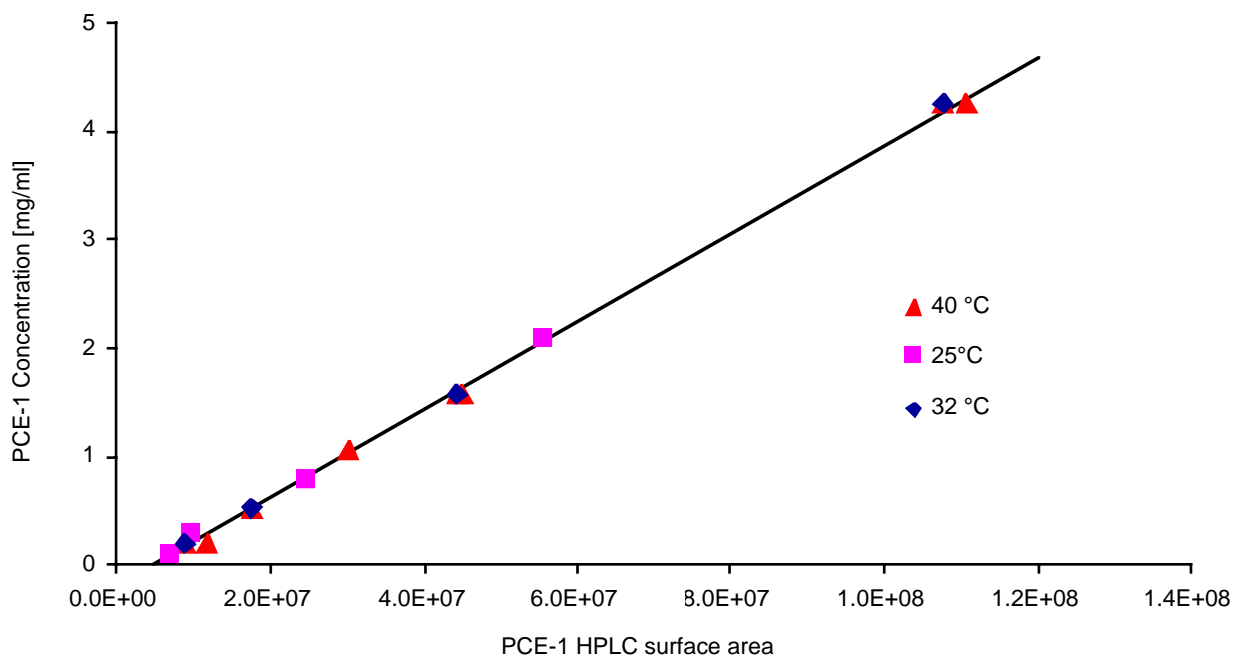


Figure 6-6 -Calibration data for polymer PCE-1 at temperature of 25°C, 32°C and 40°C. The line represents the linear regression performed over all data. The ordinate at the origin is not zero.

6.3.2 Adsorption onto MgO

Adsorption of PCA-2 onto MgO

The following general behaviour was observed for adsorption experiments onto magnesium oxide. Up to a given concentration, all the polymer added was adsorbed. No polymer was measured in solution at the end of the experiment.

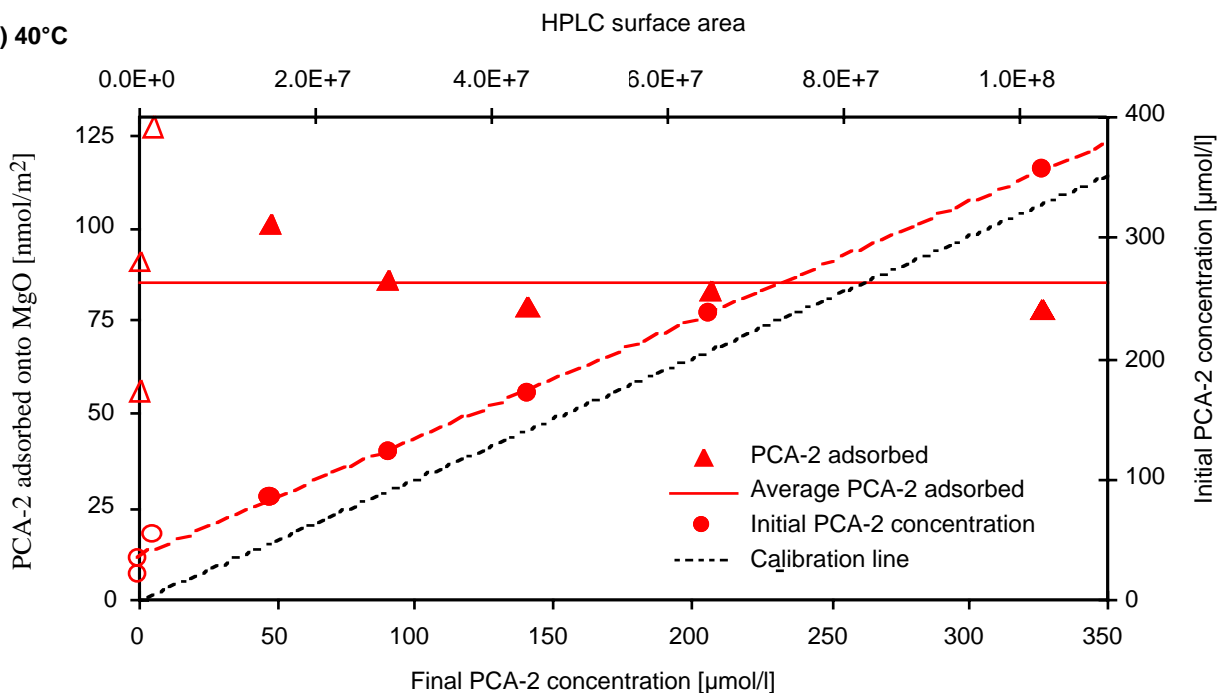
Above this point, the amount of polymer adsorbed does not increase significantly for higher initial concentrations. This behaviour will be termed step-like adsorption. We can divide the data in two sets.

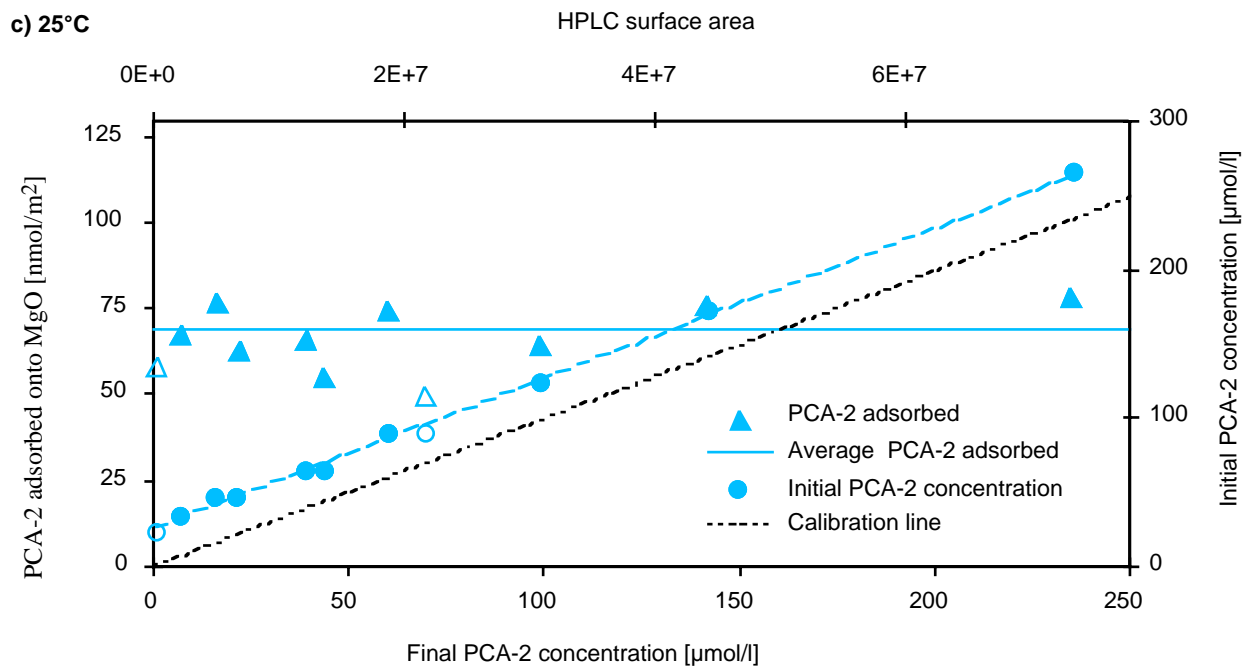
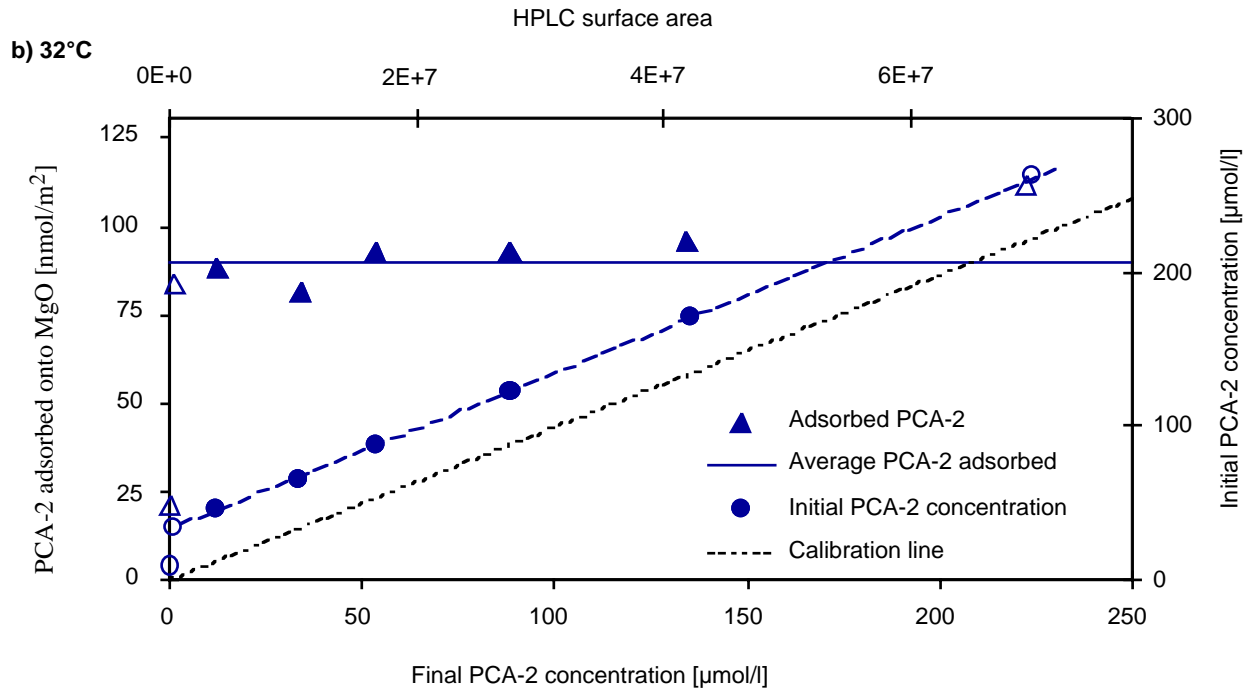
The first leads to incomplete coverage, with no excess polymer in solution. The second leads to maximum coverage and the excess polymer remains in the solution. If initial concentrations of the second set of data are plotted versus the HPLC surface measured at the end of the experiment, we obtain a line parallel to the calibration line. The ordinate at the origin indicates the initial concentration leading to full coverage.

For each temperature we have plotted on the same graph the adsorption isotherms (primary x,y axis). The symbols for the adsorption isotherm plots are triangles. Full triangles were used to compute the adsorption plateau. Open triangles were omitted. The continuous horizontal lines indicate this adsorption plateau.

The secondary axis gives the initial polymer concentration versus the HPLC surface measured in the supernatant. These data are plotted as circles. A discontinuous line shows the linear regression performed with the filled circles, open circles being omitted. The dotted line is the calibration line computed from the standards. When both lines are parallel, this is an indication that the adsorption indeed has a step like functionality.

a) 40°C





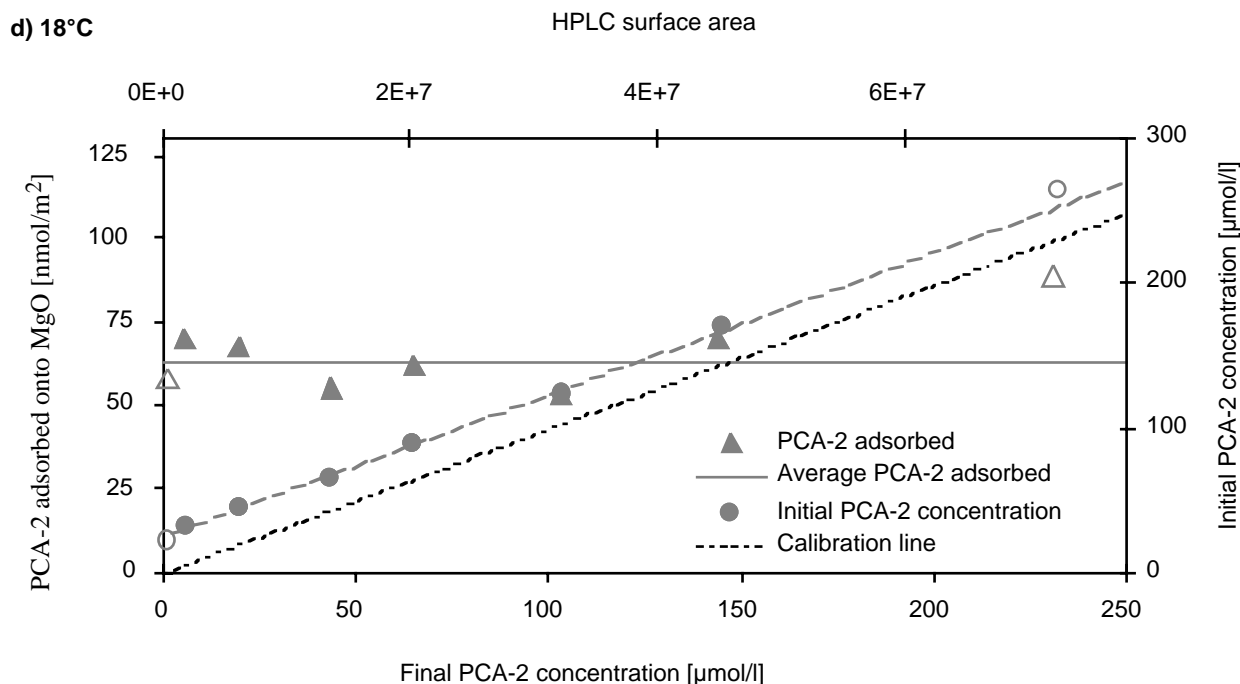


Figure 6-7. Adsorption data of PCA-2 in MgO suspensions at 40°C (a), 32°C (b), 25°C (d) and 18°C (d). Open symbols indicate data omitted in regressions.

At all temperatures, linear regressions have been calculated. In Figure 6-8, the slopes of these regressions are plotted versus temperature. Using the individual slope errors, it is possible to calculate the temperature effect from a general linear regression (Annex C). Using the associated errors determines whether or not this effect lies within experimental error. The confidence interval for rejecting the absence of an effect is 84%. Thus, we admit there is no effect of temperature on the slope determined from the samples in contact with MgO.

In Figure 6-9, the amount of PCA-2 adsorbed, determined by the standard solution depletion calculation are plotted with filled squares. The continuous lines indicate the effect that temperature has on these values, as well as the 95% confidence interval for predicting this effect. The confidence interval for rejecting the absence of it is 100%. Therefore, we conclude that adsorption of PCA-2 onto MgO increases with temperature.

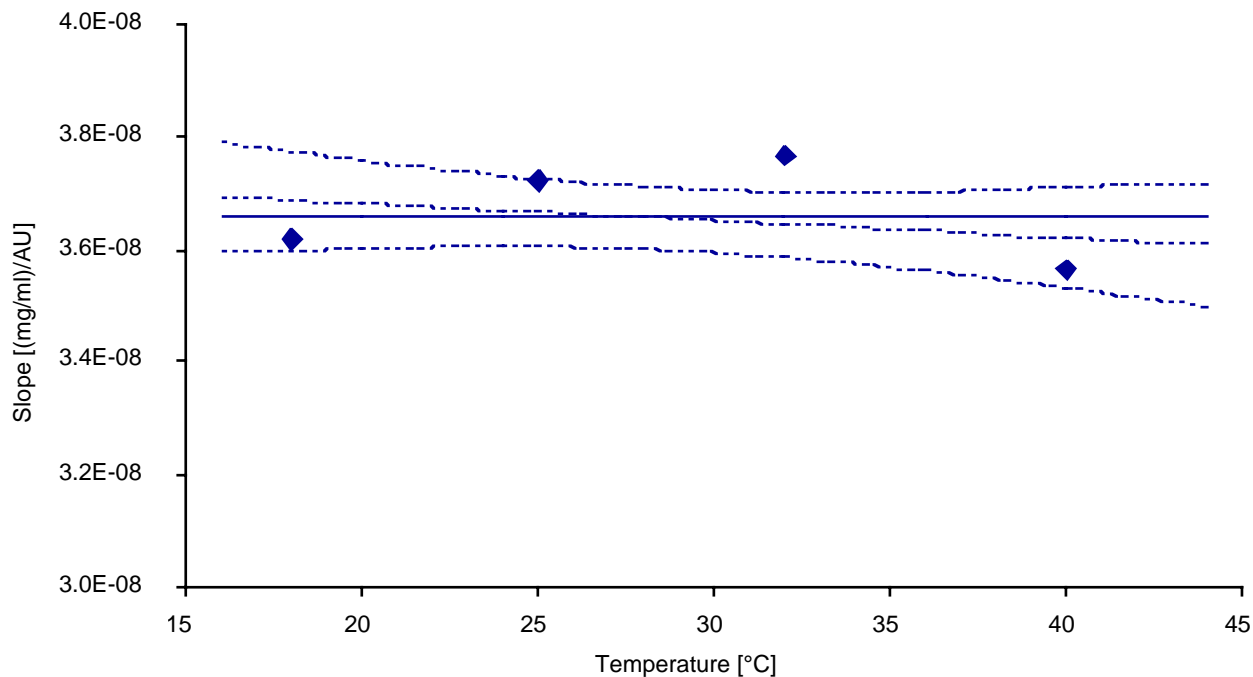


Figure 6-8. Slopes of the regressions of initial concentration versus HPLC surface are shown as a function of temperature. The continuous line shows the slope of the calibration line. The dotted show the linear temperature dependence calculated by weighted linear regression as well as 95% confidence intervals. Polymer is PCA-2.

At this point, we recall that saturation concentrations are also given by the ordinate at the origin obtained from the regression of initial PCA-2 concentration versus HPLC surface. Using values computed at each temperature leads to the data plotted in Figure 6-9, by the open squares. Continuous lines indicate the temperature effect and its 95% confidence interval.

In order to perfect the above procedure, we can use all the data in order to compute a common slope and obtain a more accurate ordinate at the origin. The values are plotted as crosses in Figure 6-9. They fall exactly on the data obtained by the normal procedure.

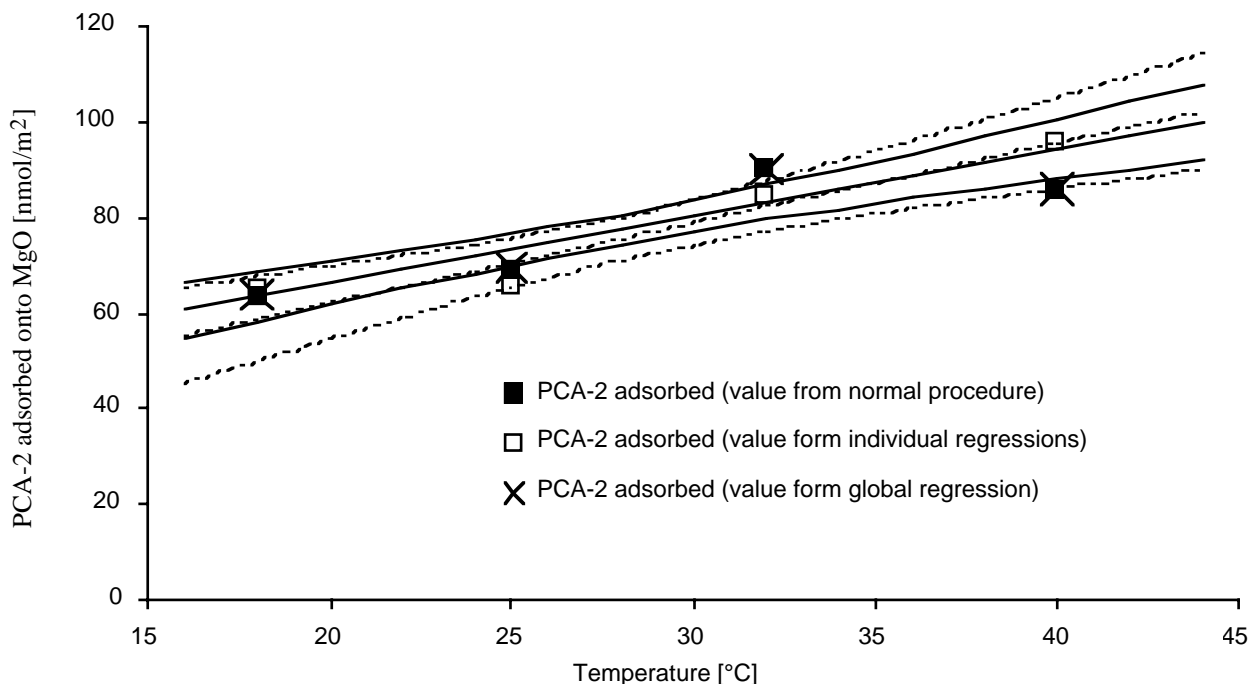


Figure 6-9. Effect of temperature on adsorption. Three series of data are plotted together. Data calculated from the standard solution depletion procedure (filled squares). Data calculated from the ordinate at the origin of the regression lines at each temperature, not using the calibration curve (open squares). Data obtained by using all data to obtain the best slope (crosses).

Adsorption of PCA-1 onto MgO

The behaviour of polymer PCA-1 is somewhat less ideal than the one of PCA-2. The first main difference is that there seems to be an alteration of the samples while they await HPLC analysis.

Let us recall that all samples discussed here are submitted to three HPLC analyses. The samples are injected one after another, in increasing order of concentrations. Then a series of blank samples are injected in order to make sure the column does not contain any remaining impurities. This procedure is the same for the standards and adsorption samples. After all samples and blanks have been analysed, the procedure is carried out a second and a third time. So, the time between each analysis of the same sample is the same. The time elapsed between the end of adsorption and the first measurement is longer for the samples with the highest concentration. However, the difference would be much longer if each sample was analysed three times before moving onto the next sample.

The deviation of the first injection result to the average of the three injections appears proportional to the amount of polymer in solution.

In addition, the deviation between injections 2 and 3 is small (about 2%). Therefore, we use the results of these last two injections, as values for the stabilised solution. We bear in mind that a fraction of the signal has been lost and that this loss is proportional to the amount of PCA-1 in solution.

Unlike with PCA-2, the calibration data does not provide a curve parallel to the one of the adsorption samples. In fact the calibration curve is systematically steeper than the calibration one.

On the other hand all slopes from the adsorption data are equal (rejection is 0.5%) and no temperature effect is apparent (rejection only 81%).

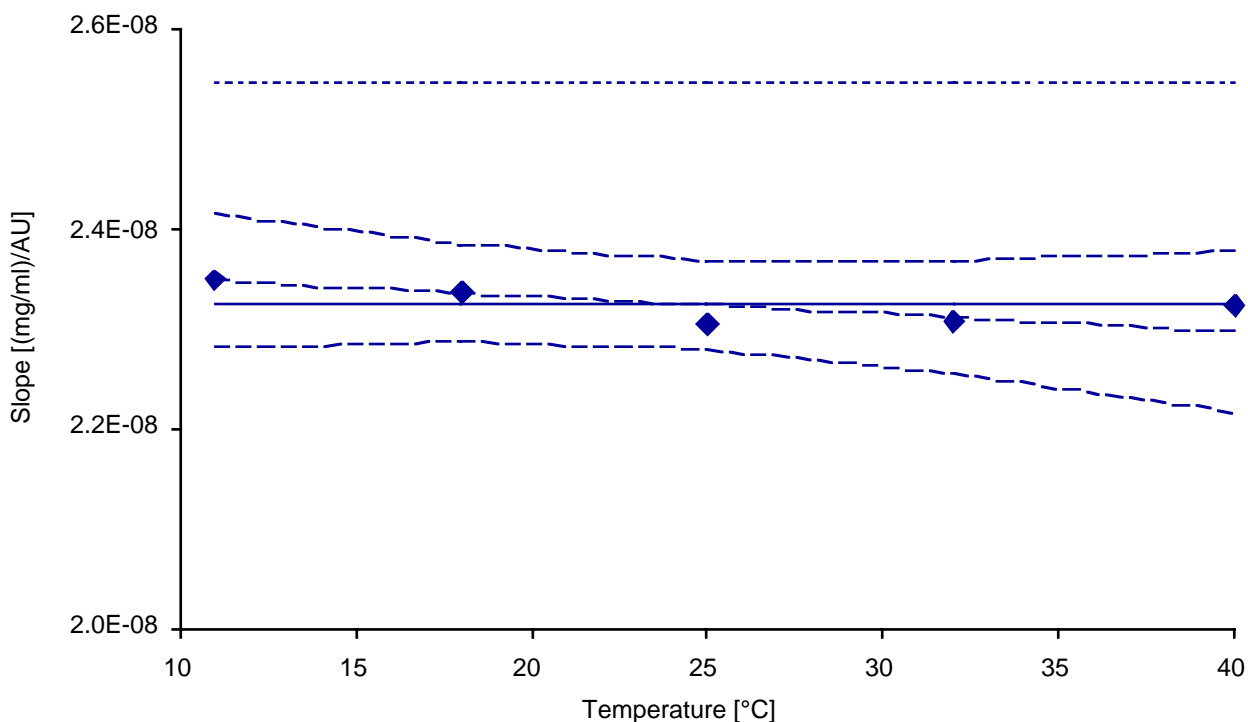
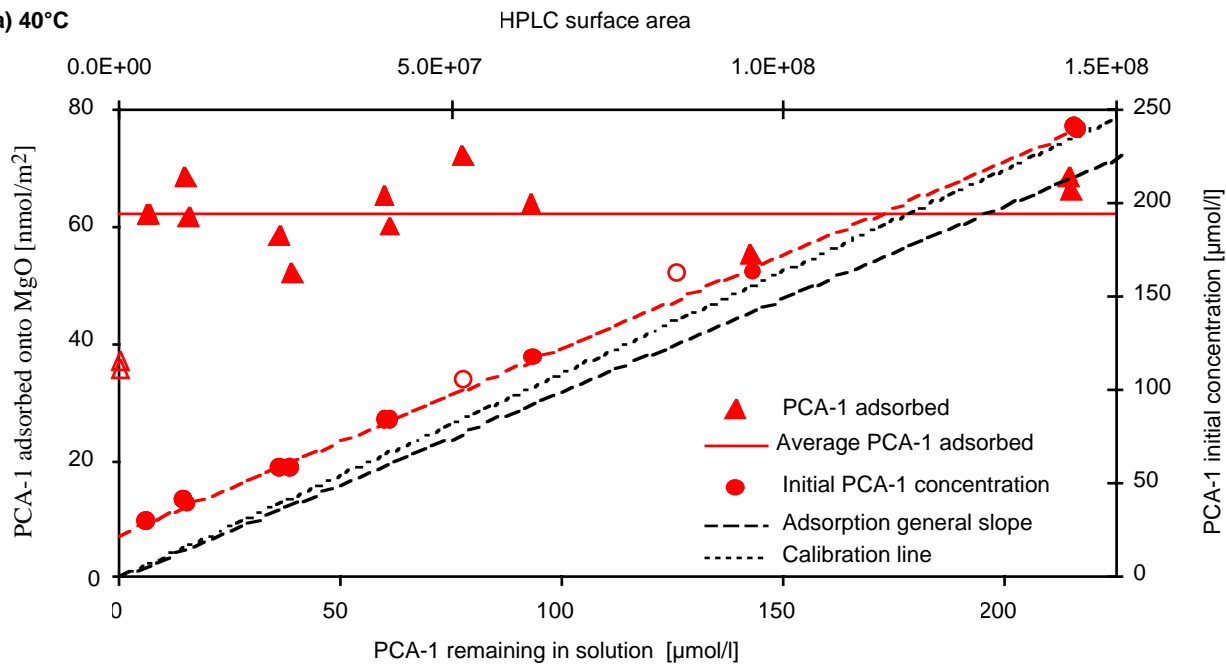
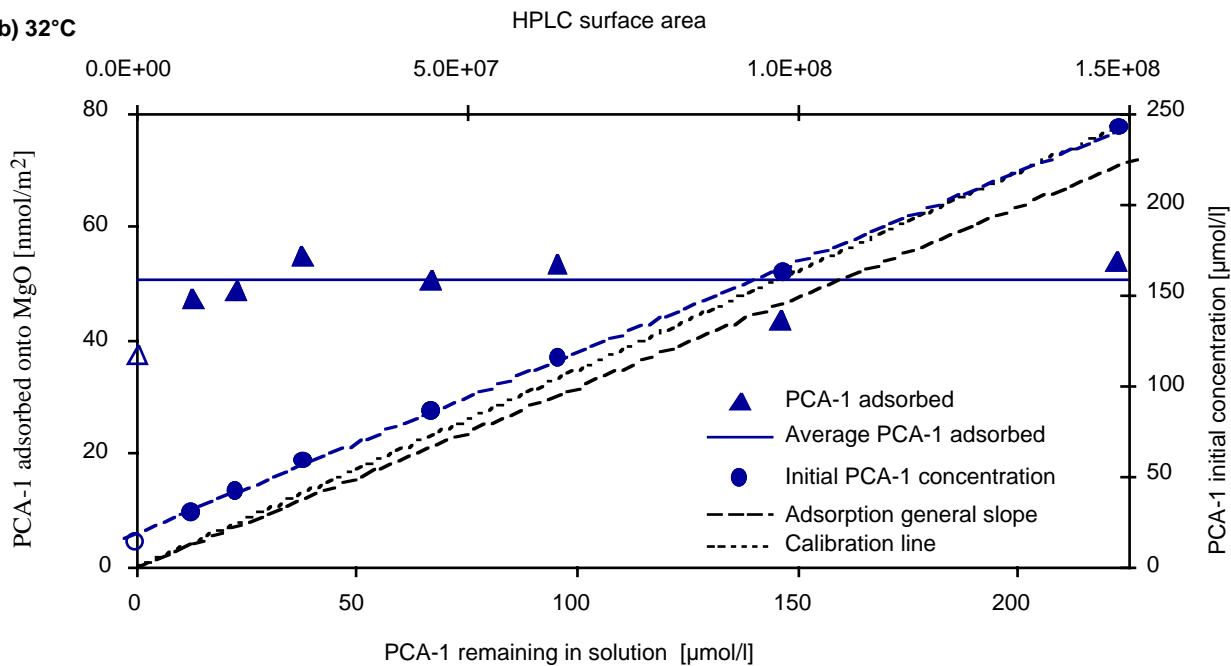


Figure 6-10. Slopes of the regressions of initial concentration versus HPLC surface are shown as a function of temperature, for PCA-1 on MgO. The dotted line (highest one) shows the slope of the calibration line. The three discontinuous lines below show the linear temperature dependence calculated by weighted linear regression as well as 95% confidence intervals. The continuous line shows the temperature independent slope (average value).

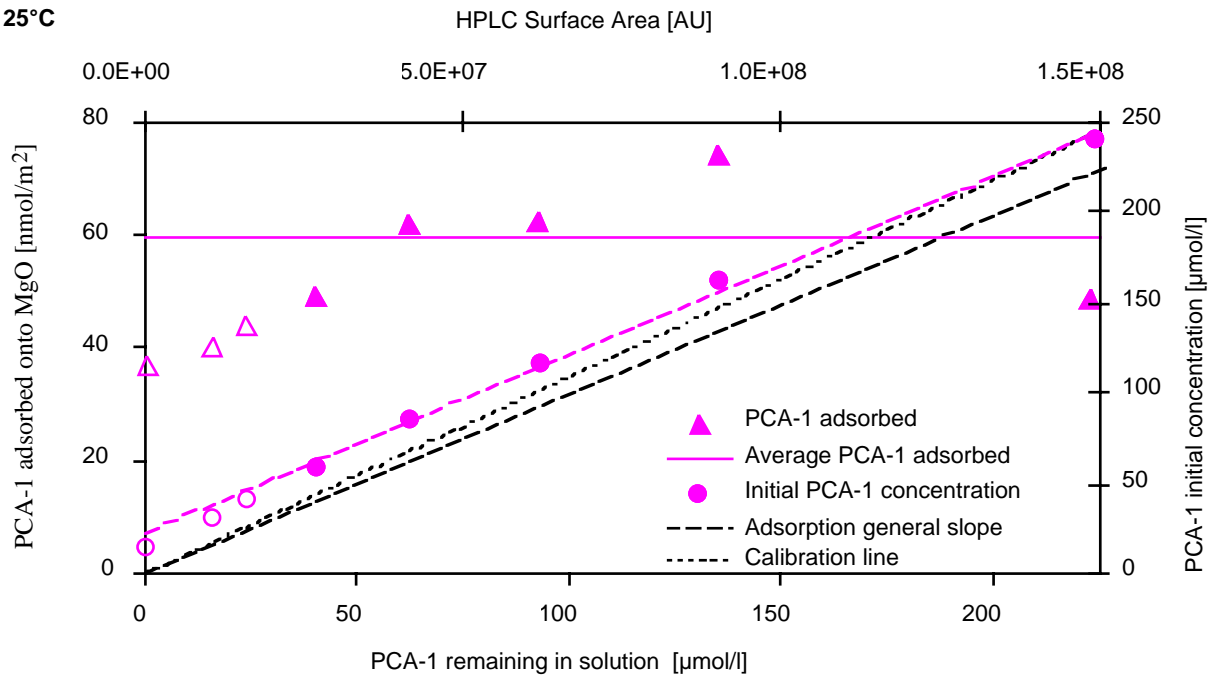
a) 40°C



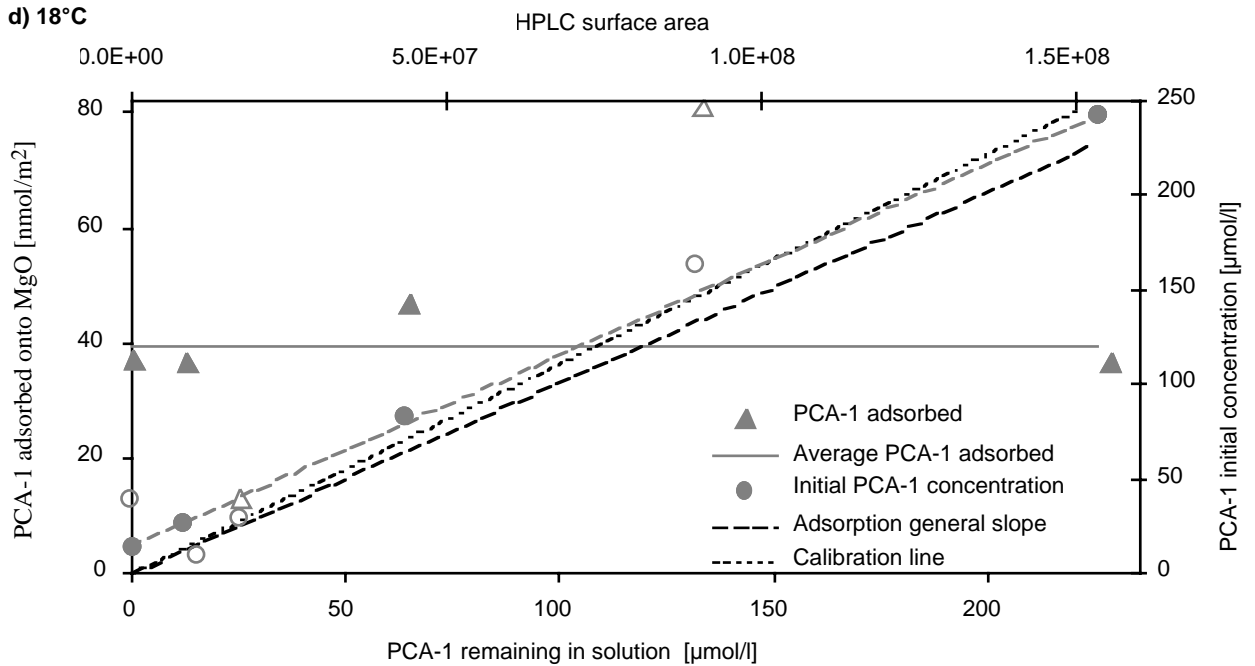
b) 32°C



c) 25°C



d) 18°C



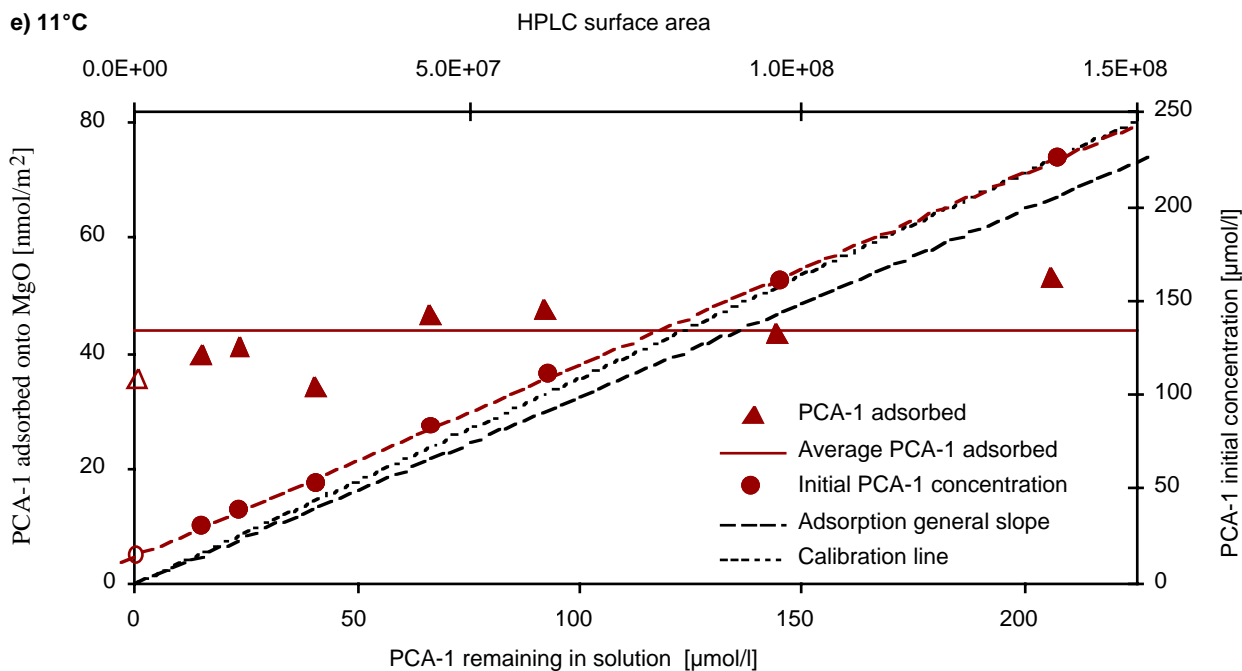


Figure 6-11. Adsorption data of PCA-1 in MgO suspensions at 40°C (a), 32°C (b), 25°C (c), 18°C (d) and 11°C (e). Open symbols indicate data omitted in regressions.

Adsorption plateau values have been calculated by the normal solution depletion method, by taking the intercepts from individual linear regressions and finally by taking intercepts from the general linear regression. The values are shown in Figure 6-12. This figure also gives a temperature effect prediction. It is based on values obtained by the individual regressions. The 95% confidence intervals for this effect are also shown. The level for rejecting the absence of this effect is 98%. Temperature therefore also effects the adsorption of PCA-1 onto MgO. However, the magnitude of this effect is smaller than with PCA-2.

Adsorption of PCE-1 onto MgO

We recall that, due to different qualities of acetonitrile, data at 11°C and 18°C must be treated separately from data at 25, 32 and 40°C. The samples at the lower temperatures (11, 18°C) were measured later with higher purity acetonitrile as mentioned previously (subchapter 6.3.1). For these,

the slopes of adsorption samples and calibration data can be considered identical, since the rejection level for this equality is only 45%.

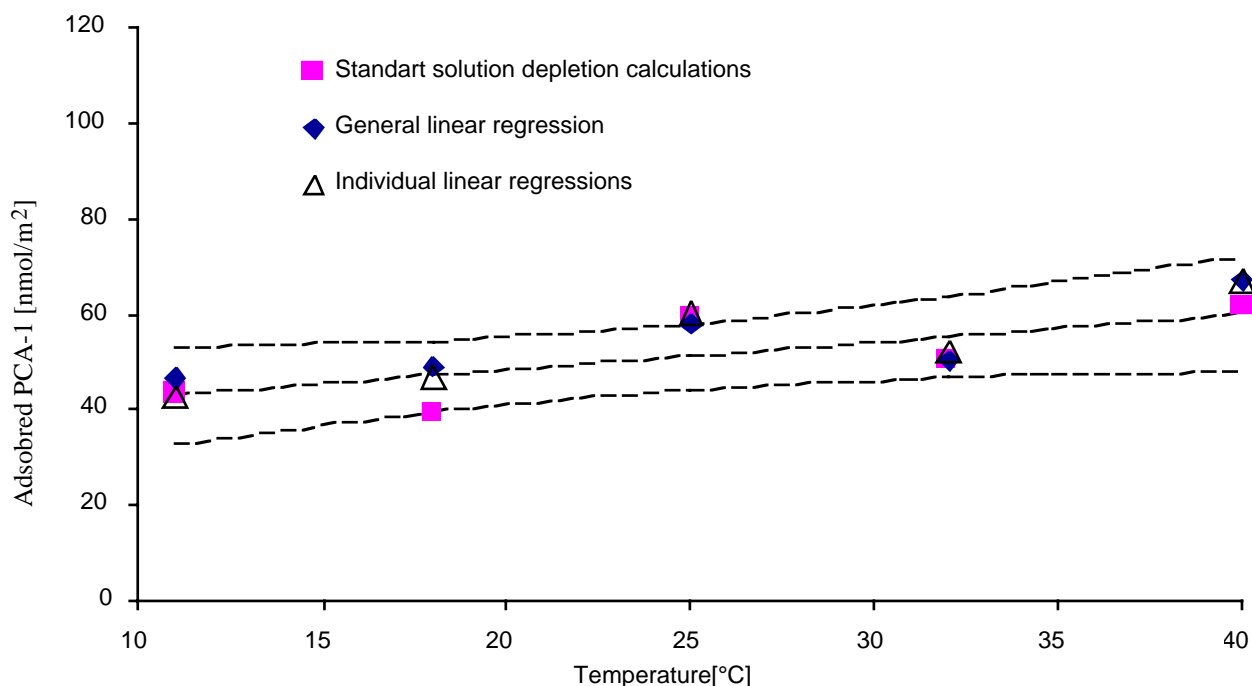
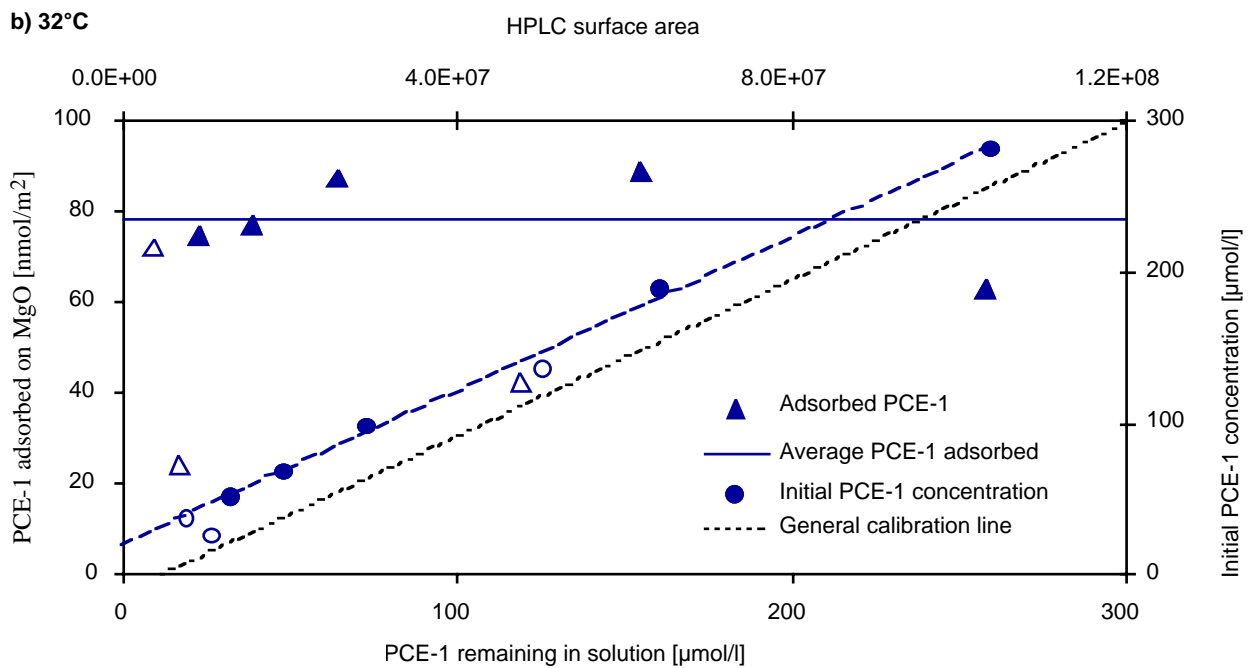
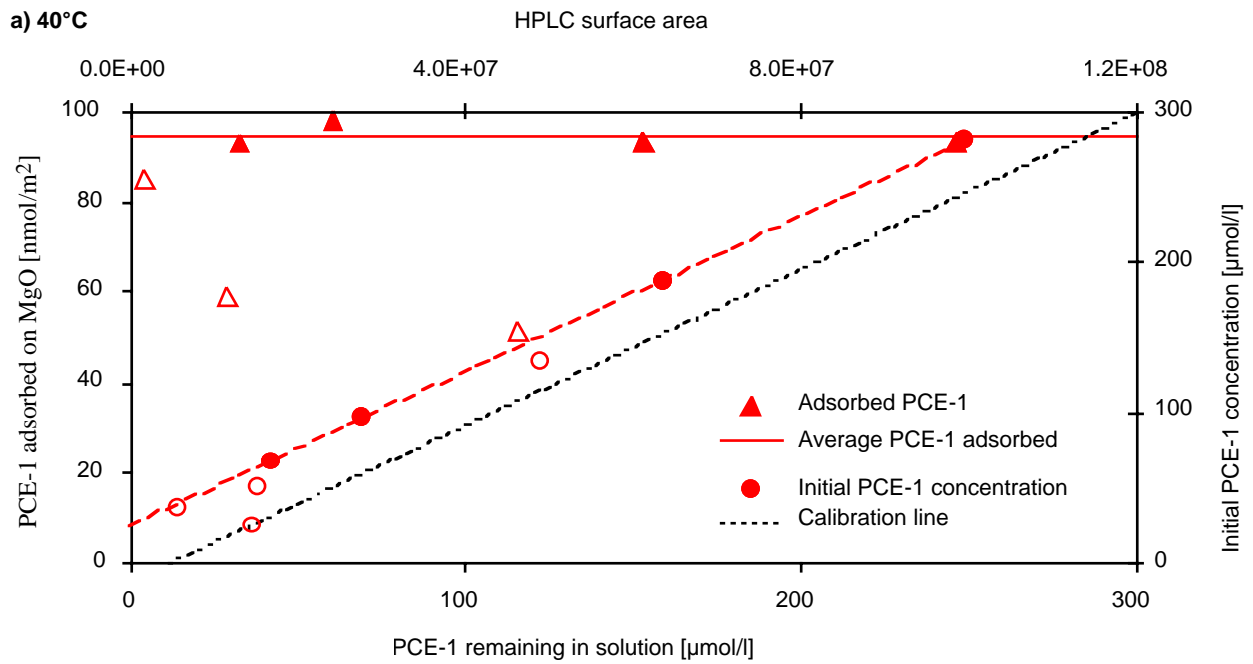
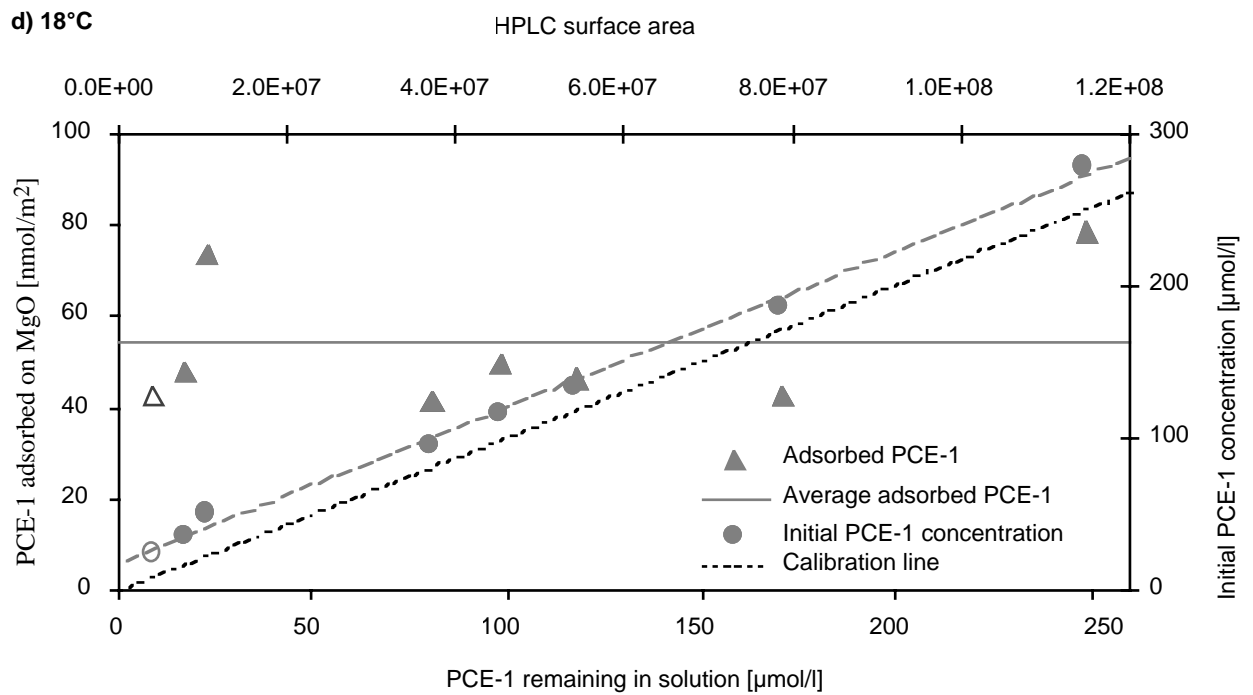
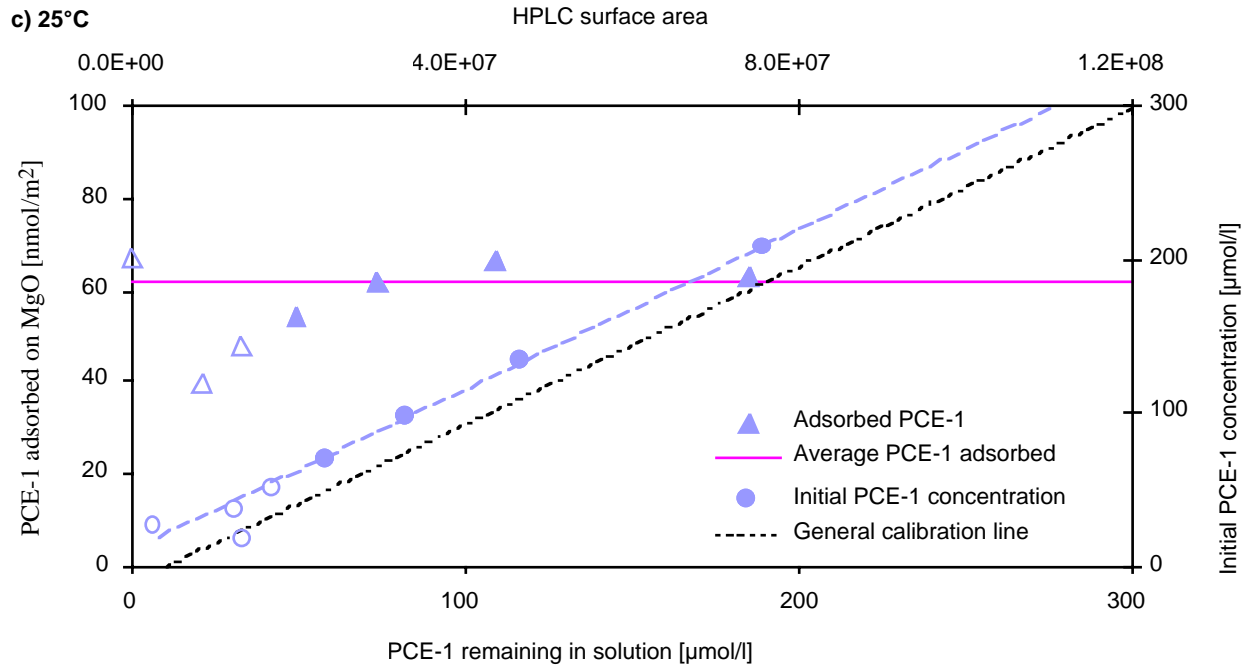


Figure 6-12. Temperature effect on the adsorption of PCA-1 onto MgO. Plateau values are calculated in three different ways. The discontinuous lines show prediction from the values obtained by the individual linear regressions at each temperature, as well as 95% confidence intervals for this prediction.

For the other temperatures (25, 32, 40°C) we can test for the absence of a temperature effect. The rejection level turns out to be 75%. So, the slopes would not be affected by temperature. Note however, that because only three points are available this test is not very reliable.

Nevertheless, we will consider there is no effect of temperature on the slopes computed from adsorption data. At this point, we must determine whether the adsorption data, as well as the one obtained calibration data, all have the same slope. So, we must test the degree of confidence to reject the hypothesis that all these slopes are identical. A value of 53% is obtained, which is considered sufficiently low for calculating a single slope from all these data sets. This optimised slope is the one, which is then used in the solution depletion calculations.





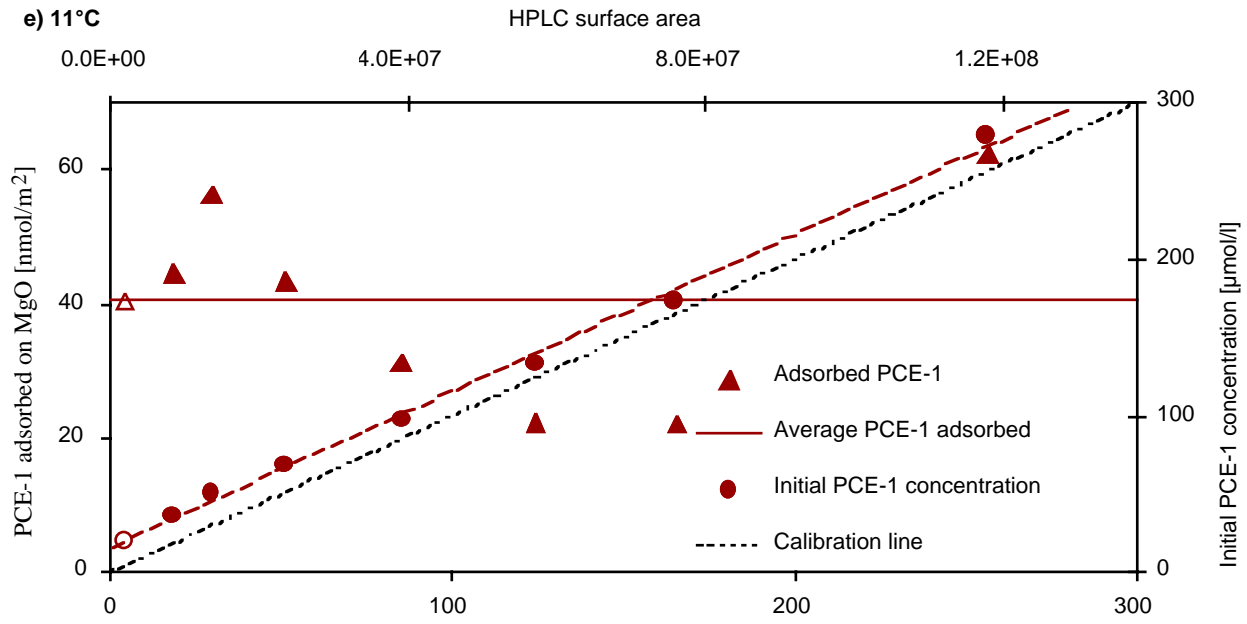


Figure 6-13. Adsorption data of PCE-1 in MgO suspensions at 11, 18, 25, 32, 40°C. Open symbols indicate data omitted in regressions.

Compilation of adsorption data onto MgO

Table 6-1 summarises temperature effects on the adsorption of superplasticizers.

Table 6-1. Compilation of adsorption isotherm plateau values on MgO.

	Adsorbed nmol °C ⁻¹	Adsorbed mg °C ⁻¹
PCE-1	2.00 ± 0.13	19.0 ± 1.2
PCA-2	1.40 ± 0.21	16.1 ± 2.4
PCA-1	0.53 ± 0.13	8.3 ± 1.7

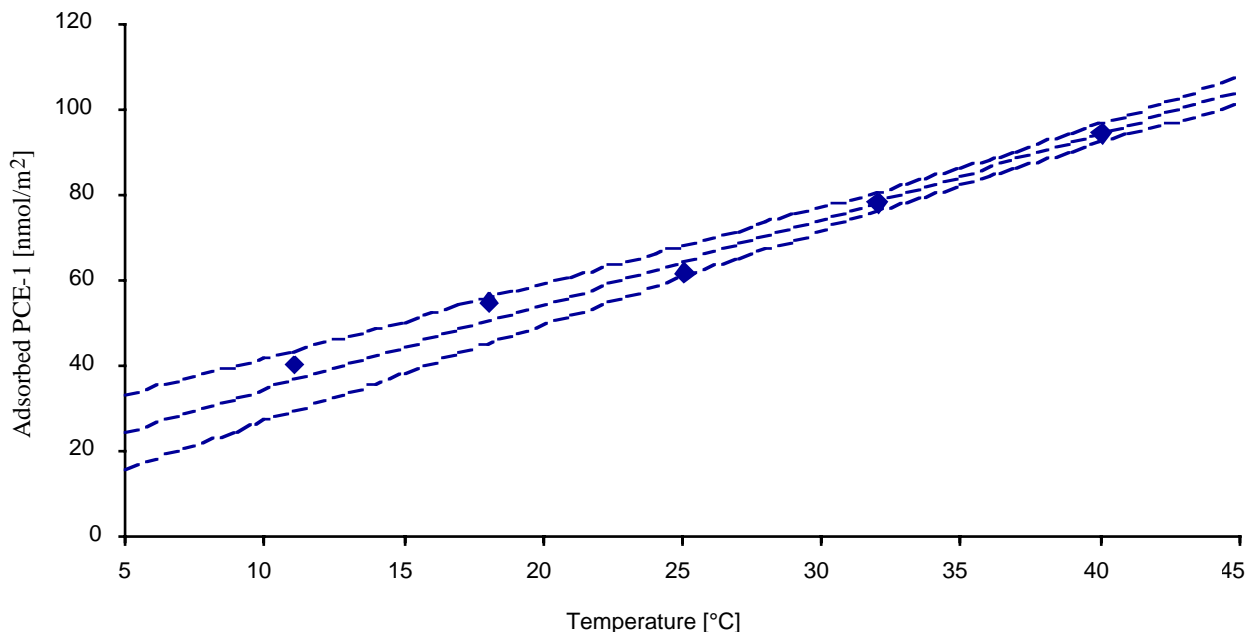
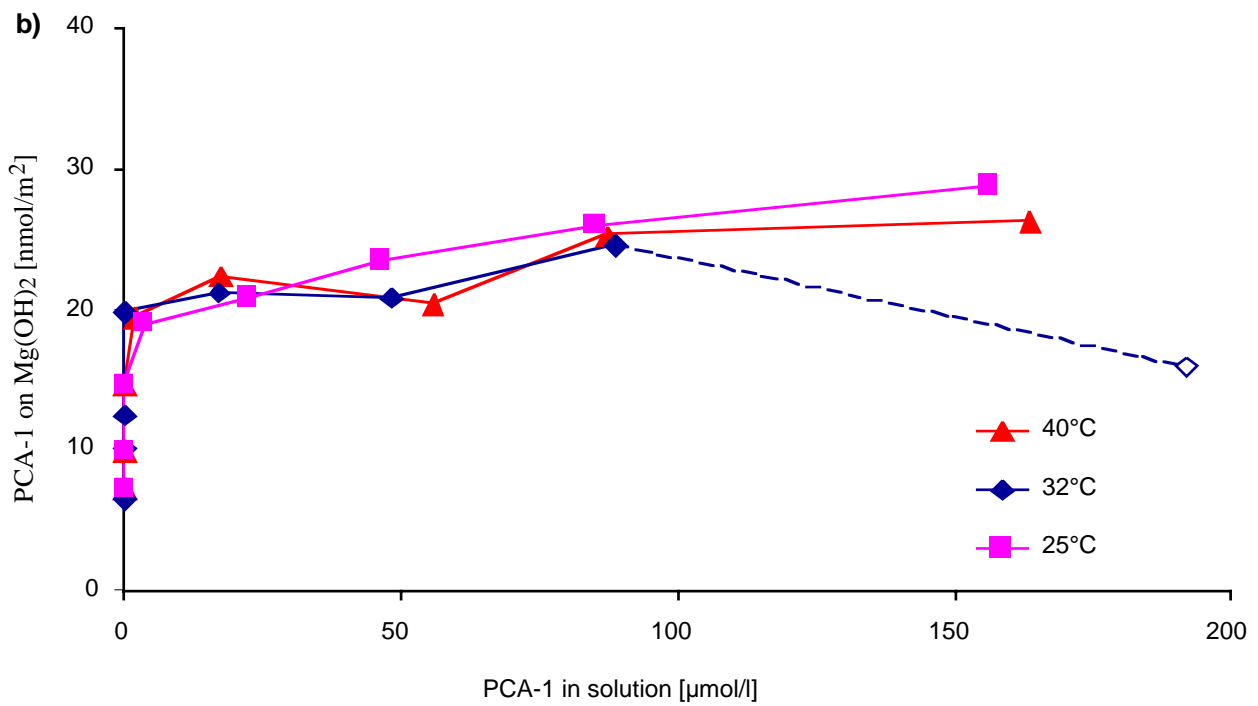
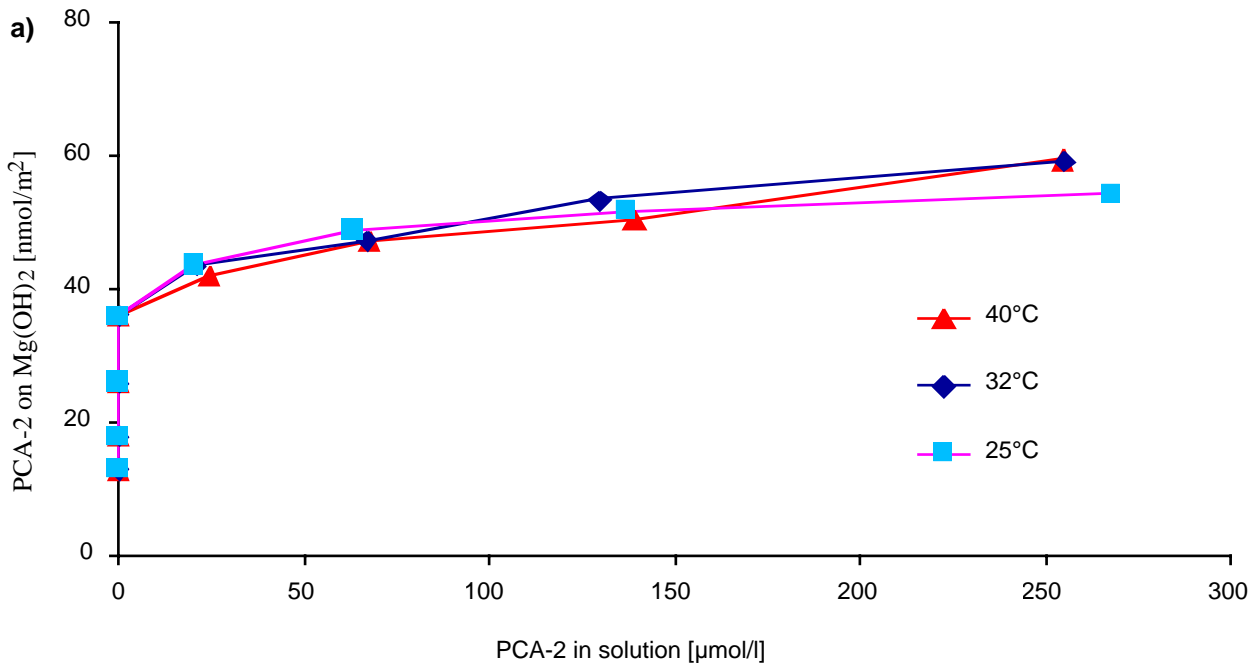


Figure 6-14. Temperature effect on the adsorption of PCE-1 onto MgO. The discontinuous lines show prediction from the values obtained by the individual linear regressions at each temperature, as well as 95% confidence intervals for this prediction.

6.3.3 Adsorption onto Mg(OH)₂

With Mg(OH)₂ as the solid phase, the isotherms exhibit a different functionality than with MgO. In this case, there are two distinct steps: an initial vertical rise (probably an irreversible process). This is followed by a gradual rise to saturation. An illustration of this is given in Figure 6-15.

The data treatment performed for MgO can therefore not be applied to Mg(OH)₂ as easily. The standard solution depletion calculations were used. Plateau value for adsorption are reported in Figure 6-16, for temperatures of 24, 32 and 40°C. No additional temperatures were measured since no temperature effect was apparent.



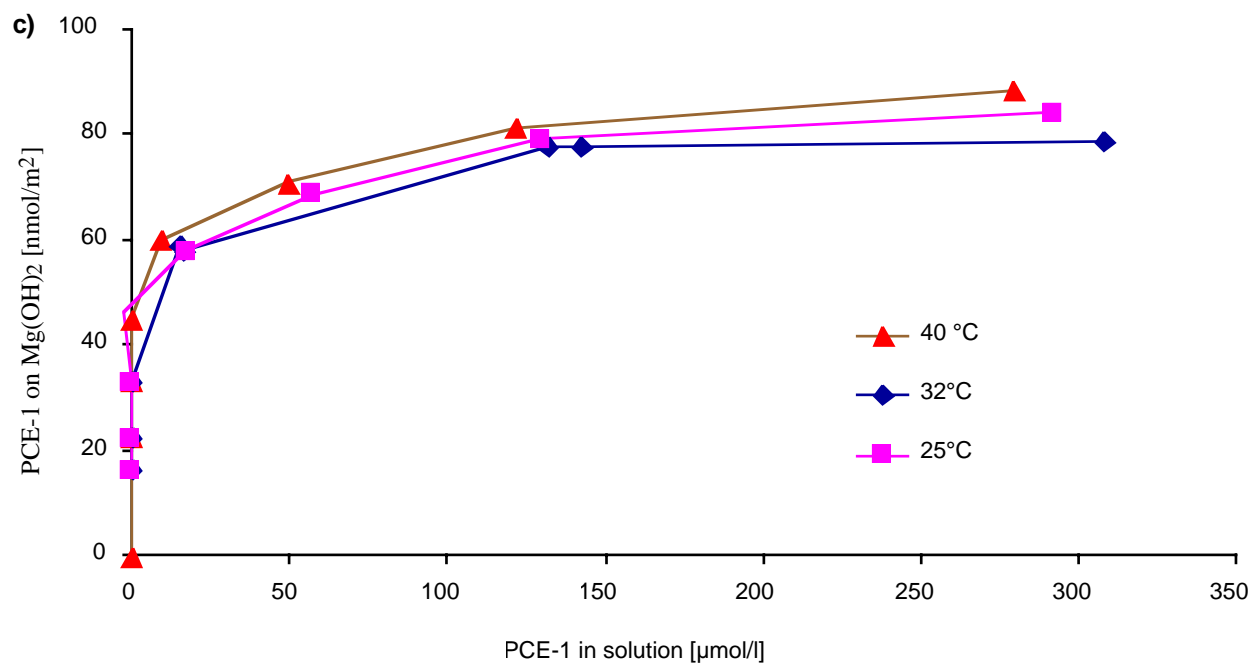


Figure 6-15. Adsorption isotherms of PCA-2, PCA-1 and PCE-1 onto Mg(OH)₂ at 25, 32 and 40°C. The open symbol for PCA-1 at 32°C has not been considered for evaluating the plateau.

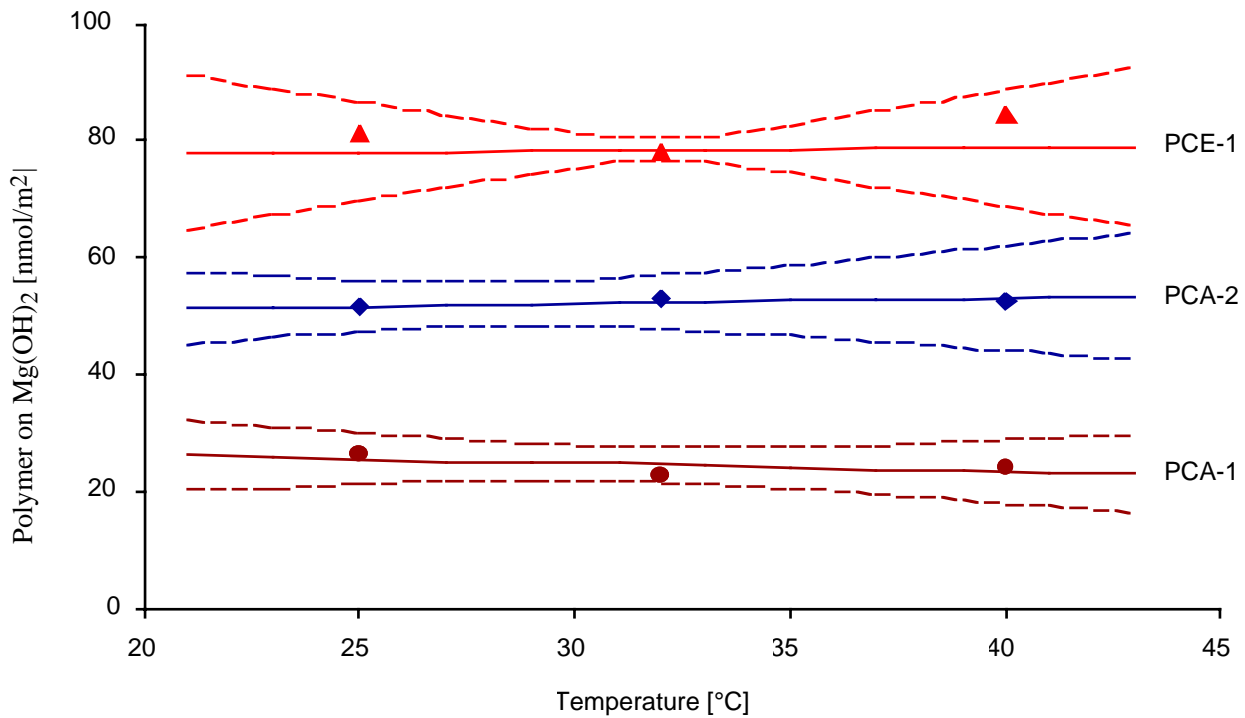


Figure 6-16. Temperature effect on final plateau for adsorption onto $Mg(OH)_2$.

6.4 Rheology

The rheology results presented here have been performed with the polymer PCA-2 and magnesium hydroxide. Possible complications linked to the temperature effect with MgO , to its larger particle size and wider particle size distribution, as well as a limited amount of MgO (sieved and sampled) led to choosing $Mg(OH)_2$. The choice of PCA-2 was made because adsorption errors with this polymer are smaller.

A study of mixtures of $Mg(OH)_2$ and silica fume has led to similar conclusions as those reached previously [Flatt et al (1998b)]. This previous study also contained data relative to PCE-1, which is also consistent with the interpretation given of the results presented below.

6.4.1 General Trends

All flow curves show a linear dependence between stress and shear rate over most of the stress range covered (Figure 6-17). As superplasticizer concentrations are increased, fluids shift from Bingham to Newtonian behaviour. For each type of fluid, there is a different superplasticizer concentration at which the fluid becomes Newtonian. In what follows, we refer to these concentrations as the CSC (Critical Superplasticizer Concentrations).

Above the CSC, sedimentation occurs. At the end of the measurement, the sample holder is opened as shown in Figure 6-18 and a dense sediment can easily be observed or felt at the bottom of the sample holder. In such cases, linear regressions performed over the initial stress ramp (decrease), give negative ordinates (correlation coefficients remain very high). The first data point and occasionally the first two are omitted when deviation from general trend indicates that a stationary regime is not reached.

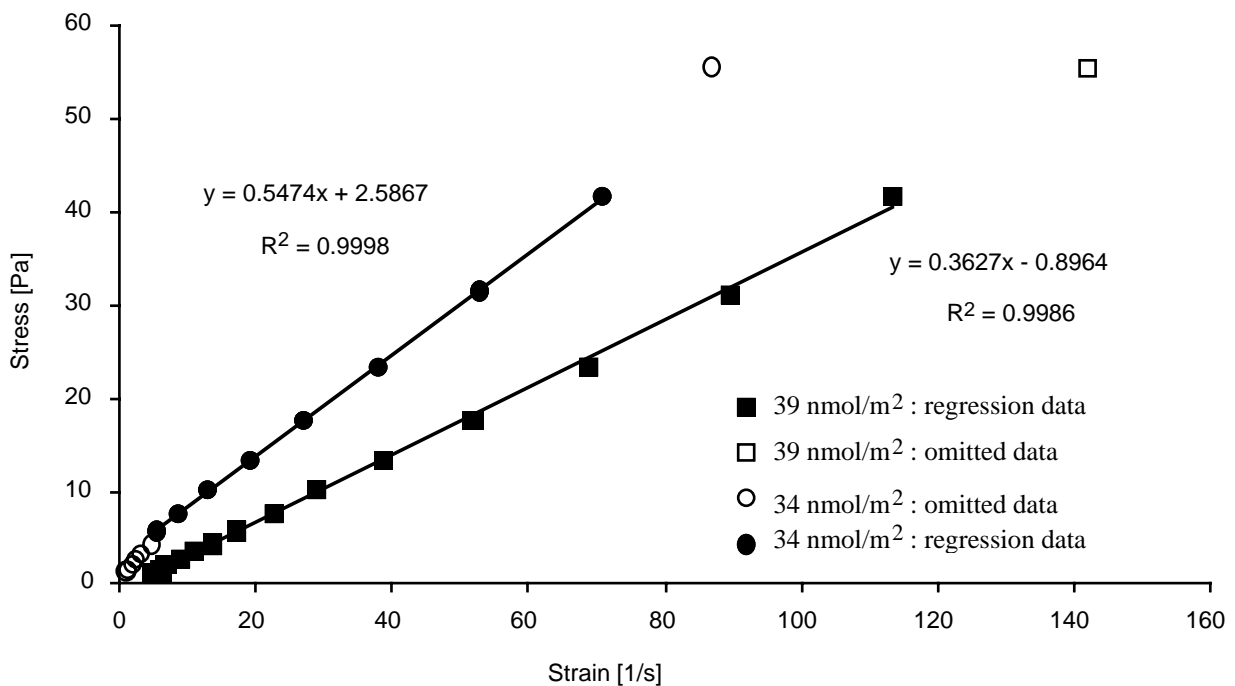


Figure 6-17. Determination of yield stress and viscosity. For suspensions with 41% volume of $Mg(OH)_2$. Higher polymer concentration is above Critical Superplasticizer Concentration (CSC), which results in sedimentation and a negative ordinate at the origin.

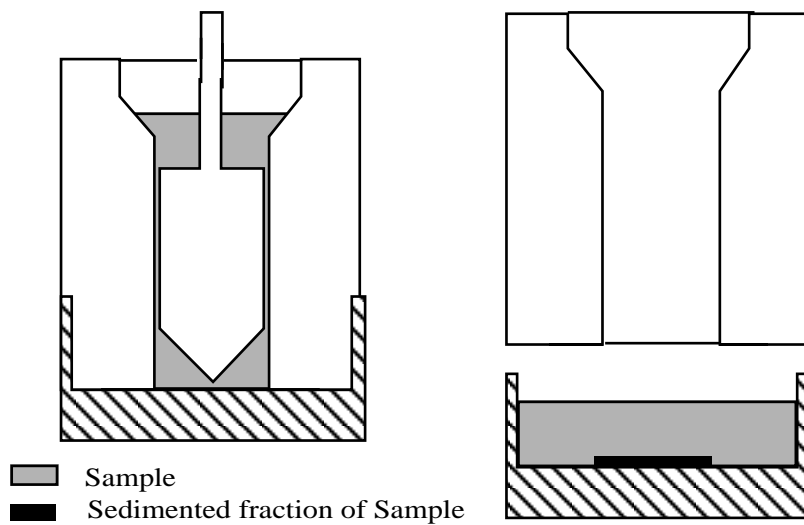


Figure 6-18. Schematic representation of the Z20DIN sample holder. At the end of the measure, the holder can be opened and all the suspension is collected in the lower part. If sedimentation occurs during measurement, it can be observed at the bottom.

As stress is increased back up to its initial value, another main difference is observed between fluids below and above the CSC. Below the CSC, the process is reversible and the final apparent viscosity is identical or occasionally slightly higher than the initial one (Figure 6-19). Above the CSC, when stress is raised, the apparent viscosity is at first larger (at low shear). This could be due either to some sedimented particles being put back into motion or to a slight reagglomeration. At higher shear, apparent viscosity becomes smaller than measured in the beginning (Figure 6-19). This is due to the sedimented particles.

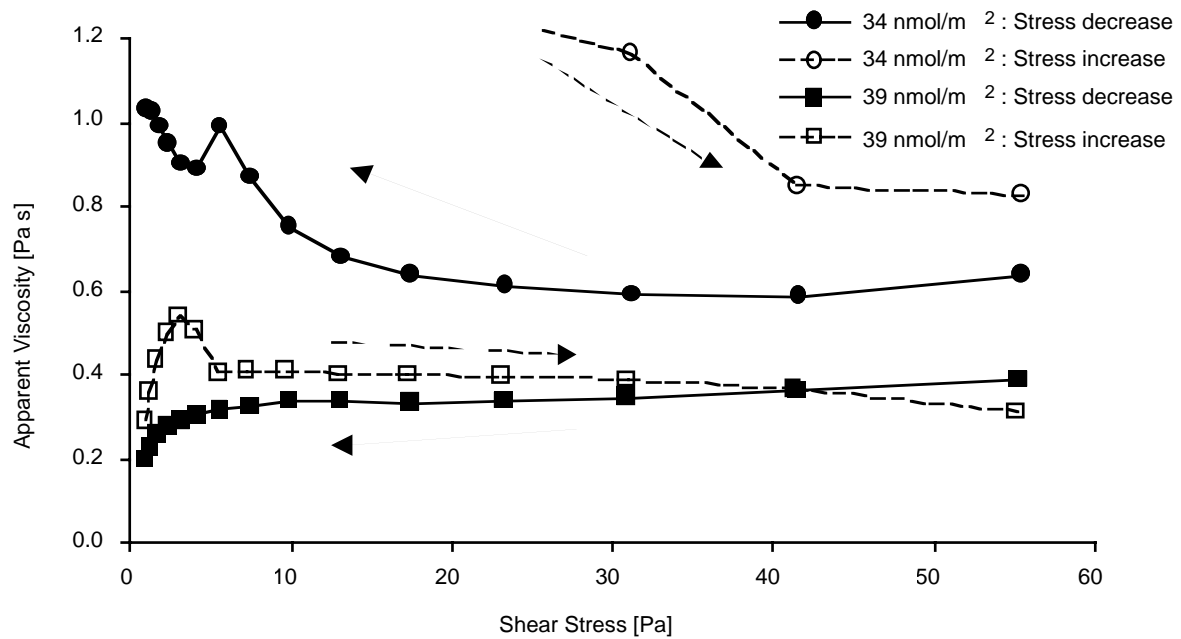


Figure 6-19. Effect of PCA-2 concentration on viscosity curves in suspensions with 41% volume of $Mg(OH)_2$. Full lines show initial stress ramp (decrease) and dotted show final stress ramp (increase) after 30s rest. Apparent viscosity drops if large particles are sufficiently dispersed to sediment (polymer concentration above CSC).

The CSC is obtained by linear interpolation between two samples with different superplasticizer content, one of which has sedimentation and the other not (one has a positive and the other a negative calculated yield stress). Sufficient measurements were made to have both concentrations within less than 15% of one another. An example can be seen in Figure 6-20. Viscosity is obtained in a similar way. The values usually stabilise slightly before yield stress disappears. Viscosity values are therefore reasonably accurate.

6.4.2 Effect of Solid Volume Fraction

As solid fraction is increased, the quantity of polymer per surface of powder necessary to obtain a Newtonian fluid, the CSC, also increases. Figure 6-20 shows yield stress values calculated from the flow curves of $\text{Mg}(\text{OH})_2$ suspensions.

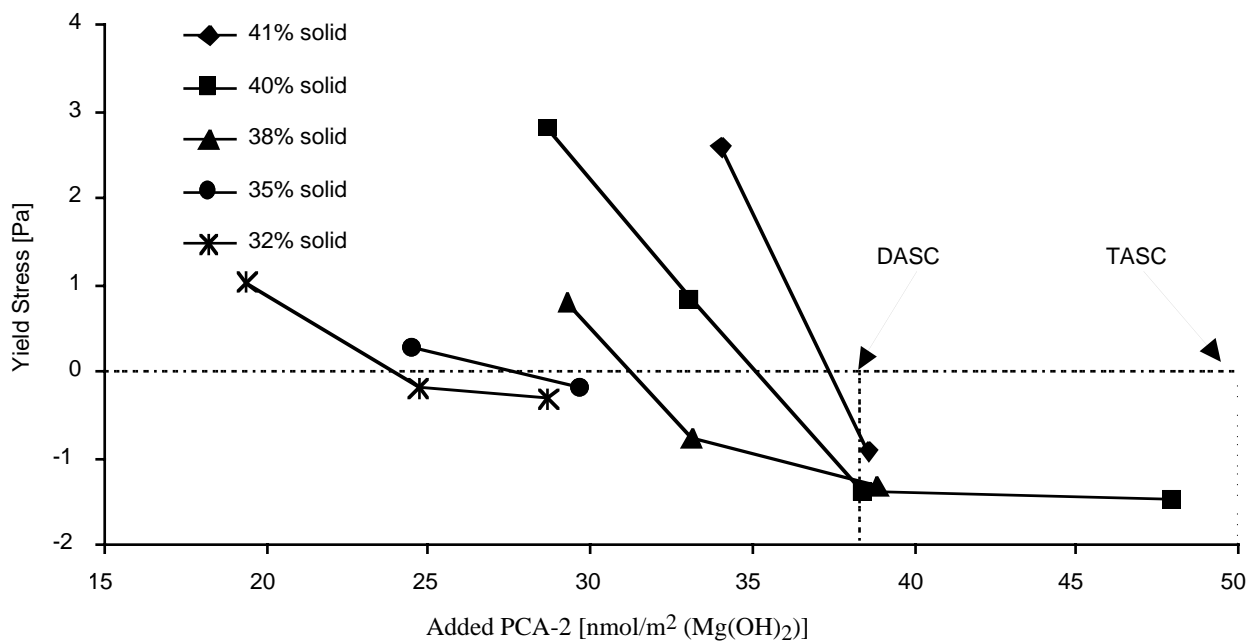


Figure 6-20. Determining Critical Superplasticizer Concentration (CSC) as a function of solid volume fractions in suspensions of $\text{Mg}(\text{OH})_2$. CSC is the concentration for which the calculated yield stress is zero. DASC: Directly Adsorbable Superplasticizer Concentration. TASC: Total Adsorbable Superplasticizer Concentration.

It was not possible to obtain a Newtonian fluid above 41% volume. Above this limit, placing the suspension into the rheometer quickly becomes a problem. So, 41% seems to be the liquid limit of this powder with PCA-2 as dispersant. The amount of PCA-2 required to obtain a Newtonian fluid for this maximum solid loading conditions of 41% volume corresponds to the amount adsorbed at the end of the vertical step of the adsorption isotherm (Figure 6-15). We have termed this dosage the Directly Adsorbable Superplasticizer Concentration (DASC), while the adsorption plateau was termed the Total Adsorbable Superplasticizer Concentration (TASC) [Flatt et al (1998b)].

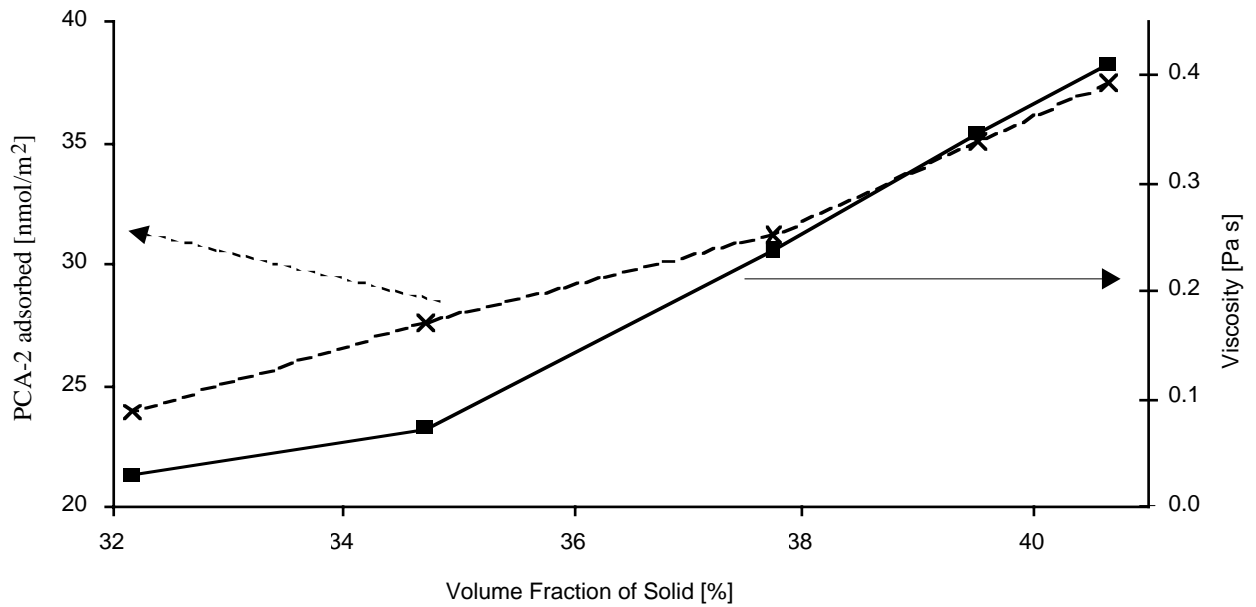


Figure 6-21. Effect of volume fraction on the plastic viscosity and the amount of PCA-2 required for obtaining a Newtonian fluid.

Chapter 7 Discussion of model suspensions

7.1 Zeta potential

Electrostatic repulsion (ER), one of the possible mechanisms involved in dispersion and water reduction, is intimately linked to the potential at the outer Stern layer. This potential can often be identified to zeta potential when the distance of the shear plane to the Stern layer is small. Results in Figure 6-1 shows that one can distinguish two groups of polymers. The first is composed of polymers PCA-1, 2, 3 and SNFC-1, which all induce large and similar final potentials (around -23 mV). The second is composed of polymers PCE-1, 2, 3. They induce lower final potentials and these are wider spread, ranging from -5 to -18 mV. The main reason for these differences is that the first group of polymers are all strong electrolytes, while the others are weak or very weak electrolytes, due to the insertion of PEG-ester units in the polymer backbone. This acts as a charge spacer and decreases the charge density of the PCE-type polymers.

From these results, it is concluded that dispersion by electrostatic repulsion (ER) may be less likely for the PCEs than for the PCAs or the SNFC. However, they can all be successfully used as water reducers in cement applications. Dispersion by PCE-type polymers should therefore involve at least one mechanism other than ER.

Since the surface charge induced by the PCA and SNFC (strong electrolytes) were all found to be very similar, it is expected that dispersion due to electrostatic repulsion will be similar. Any major differences in the dispersion efficiencies would therefore be a consequence of non-electrostatic effects.

The larger negative zeta potential induced by the PCA group polymers as opposed to the PCE polymers is also illustrated for both MgO and Mg(OH)₂ suspensions Figure 6-2 (a and b). The fact that the potential differences between the potentials induced by PCA-2 and PCE-1 are similar for both powders must be linked to the ionicity of the polymers themselves. On the other hand, the fact the the

potentials of the saturated powders are smaller (in absolute value) on MgO than on Mg(OH)₂. This is probably linked to the larger size of the MgO powder, which can lead to a partial loss of acoustophoretic signal. This means that MgO potential (in absolute value) would be more under-evaluated than the potential of Mg(OH)₂. This is one of the reasons why more extensive measurements were carried out with the finer powder of Mg(OH)₂.

Figure 6-2 a and b, indicate that the adsorption continues after the surface has acquired a negative charge. This might be because zeta potential is the potential measured at the shear plane and not the surface, or because of a non-electrostatic interaction involved in the adsorption process. However, the most probable explanation is a surface charge inhomogeneity on the particles. Hoogeveen et al (1996) in their study of the adsorption of cationic polyelectrolytes on oxides (TiO₂ and SiO₂) found experimental indication that this is the most likely explanation.

7.2 Adsorption

7.2.1 Links between adsorption and zeta potential

Zeta potential changes induced by adding polymers can be compared with the adsorption of these polymers by plotting both measurements as a function of the total amount of polymer added. However, because the liquid to solid ratios used in both measurements are not equal, data cannot be correlated directly unless as for PCA-2 on MgO, polymers added adsorb until saturation is reached. This corresponds to a vertical rise in the adsorption isotherms. With Mg(OH)₂, this behavior is observed at first. The isotherms then become incurved, as for PCE-1 on MgO. In these situations, an equilibrium between the adsorbed polymers and polymers in solution may be expected and the ratio between their concentrations should not be greatly influenced by changing the solid to liquid ratio. If the suspension is less concentrated as for zeta potential measurements, more polymer has to be added to achieve the same amount of adsorbed polymer.

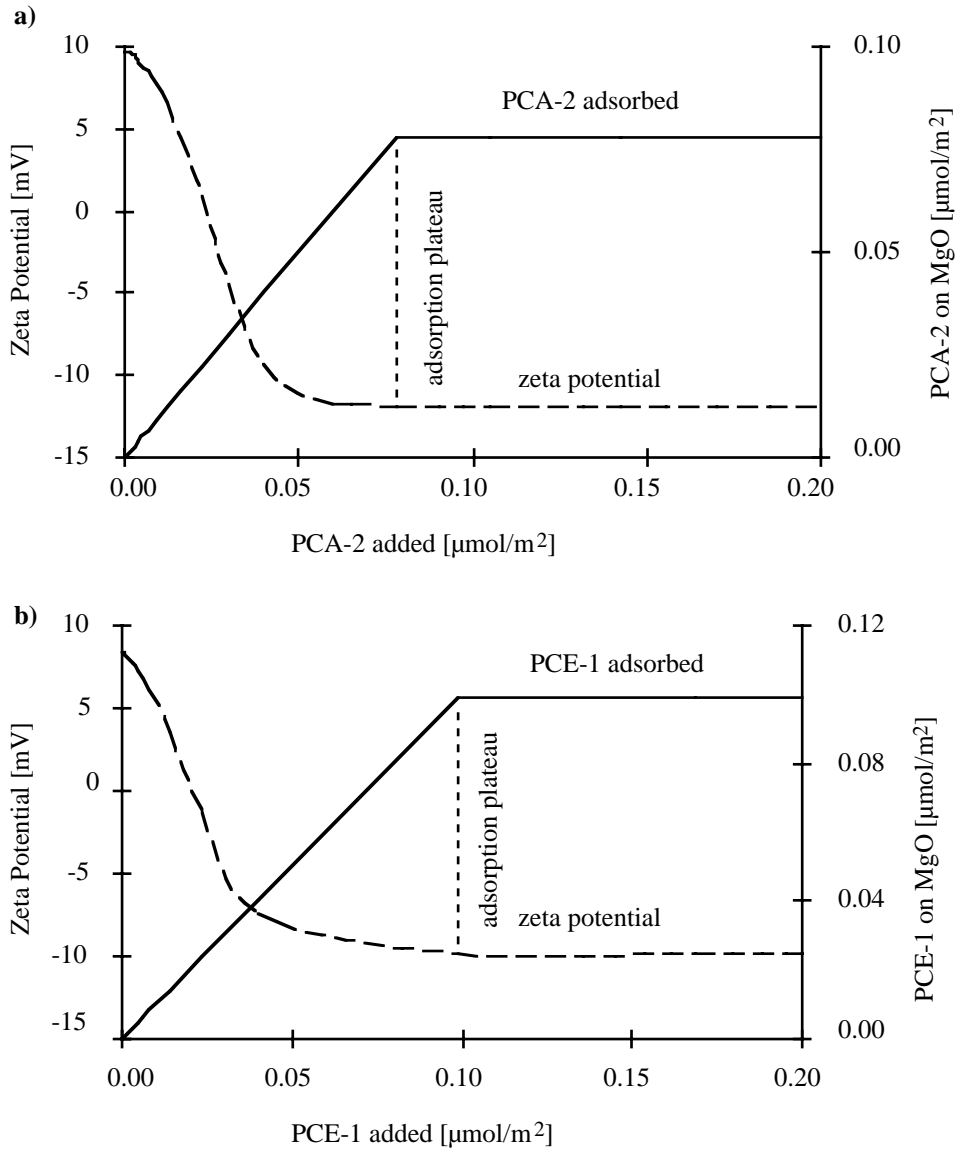


Figure 7-1. Adsorption and zeta potential curves. a) PCA-2 with MgO. b) PCE-1 with MgO.

Figure 7-1 shows zeta potential and adsorption in MgO suspensions for PCA-2 and PCE-1. A similar comparison for $\text{Mg}(\text{OH})_2$ suspensions is given in Figure 7-2. For MgO, it is assumed that all the polymer is adsorbed until the plateau value is reached.

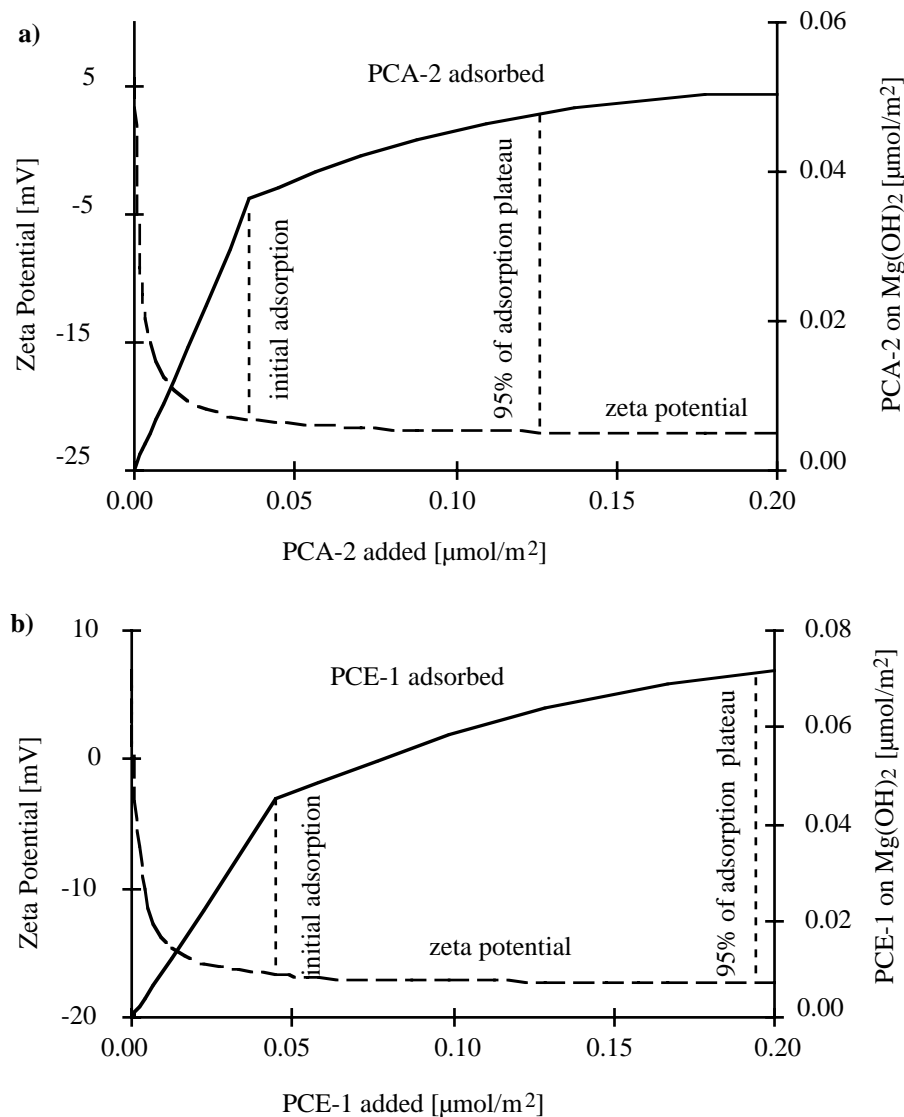


Figure 7-2. Adsorption and zeta potential curves: a) PCA-2 with $Mg(OH)_2$, b) PCE-1 with $Mg(OH)_2$.

Vertical dotted lines show the point where adsorption reaches 95% of the plateau. A fairly good correlation is seen between the adsorption and zeta potential plateaux. For $Mg(OH)_2$, the initial part of the plot is similar to those obtained with MgO corresponding to the vertical segment on the original isotherms. It is followed by a more gradual rise. A first vertical line shows the end of the first segment, while the second corresponds to 95% of plateau value. Between both amounts of added polymer, the zeta potential varies very little. This could indicate that after this step, the additional polymers are adsorbed in difficultly accessible pores, which would not effect zeta potential [Hunter

(1981), p. 284]. Pore size distribution measurements confirm this hypothesis, since we find a non negligible amount of pores smaller than 10 nm in diameter.

7.2.2 Adsorption onto magnesium hydroxide

Adsorption differences with Mg(OH)₂

So far, we have been able to interpret the functionality of the adsorption isotherms of the polymers onto Mg(OH)₂. An absolute comparison of adsorption poses problems due to the uncertainty of the molar mass. So far, results have been calculated using the M_n, the number average molar mass and neglecting its error. This had no consequence as to evaluating trends. However, in order to compare the polymers their adsorption plateau values have been recalculated, as well as the corresponding standard deviations. In Table 7-1, it appears that only when the mass average molar mass used, are the adsorption of PCA-2 and PCE-1 identical. In all other cases adsorption are always different from one polymer to another.

The adsorbed mass seems correlated with the degree of polydispersity of the polymer and inversely correlated with the number average molar mass. The higher the polydispersity, the higher is the mass adsorbed. The lower is the number average molar mass, the higher is the adsorbed mass. This observation is coherent with the previously mentioned possibility of adsorption into the porous network of the Mg(OH)₂ particles.

Such effects could in principle be studied by a more detailed analysis of the HPLC chromatograms. An investigation, which we have not carried out in this case.

Effect of temperature for adsorption onto Mg(OH)₂

For Mg(OH)₂, Figure 6-16 shows that there is no significant effect of temperature on the adsorption of either polymer. It is because no such effect was apparent, no more than three temperatures were measured. A consequence of this choice is that statistical testing is made less reliable. So, for Mg(OH)₂, confidence intervals for rejecting the absence of a temperature, must be treated with a little caution.

Table 7-1. Adsorption plateau values with $Mg(OH)_2$. Values and standard deviations are given for the adsorbed mass of polymer and the amount of adsorbed moles, calculated with both the number and weight average molar mass. Confidence levels refer to the difference between the polymers.

Polymer Type And Comparisons	Mass Adsorbed at 25°C [$\mu\text{g}/\text{m}^2$]	Moles Adsorbed at 25°C (Mn) [nmol/m^2]	Moles Adsorbed at 25°C (Mw) [nmol/m^2]
PCE-1	742 ± 19	78 ± 6	24.7 ± 2.2
PCA-2	593 ± 51	52 ± 6	24.2 ± 3.2
PCA-1	399 ± 70	26 ± 5	9.9 ± 1.8
PCE-1 > PCA-2	99%	99%	55%
PCA-2 > PCA-1	98%	100%	100%
PCE-1 > PCA-1	100%	100%	100%

7.2.3 Adsorption onto magnesium oxide

Adsorption differences with MgO

As explained above, for $Mg(OH)_2$, comparing adsorption in moles for different polymers, is complicated by the determination of the error of the molar mass, and the choice as to which average molar mass to use (number or mass).

In Table 7-2, adsorption onto MgO is calculated at 25°C (this temperature is chosen because it is the one at which all other measurements were performed). Values are given in adsorbed polymer mass and moles of polymer adsorbed, obtained with number and weight average molar masses.

The confidence intervals for rejecting the absence of the difference between the adsorption of the polymers are all quite high. Adsorbed mass of PCE-1 and PCA-2 might be identical, while adsorbed moles using weight average, might be identical for PCE-1 and PCA-2.

Effect of temperature for adsorption onto MgO

The statistical treatment of adsorption data performed in § 6.3, indicates that with magnesium oxide, the adsorption of PCE-1 (Figure 6-14) and of PCA-2 (Figure 6-9) is influenced by temperature. To a much smaller extent, PCA-1 (Figure 6-12) might also be temperature dependent.

Table 7-2. Adsorption plateau values with MgO. Values and standard deviations are given for the adsorbed mass of polymer and the amount of adsorbed moles, calculated with both the number and weight average molar mass. Confidence levels refer to the difference between the polymers.

Polymer type and Comparisons	Mass adsorbed at 25°C [µg/m ²]	Moles adsorbed at 25°C (Mn) [nmol/m ²]	Moles adsorbed at 25°C (Mw) [nmol/m ²]
PCE-1	612 ± 34	64 ± 6	20.4 ± 2.0
PCA-2	843 ± 40	73 ± 7	34.4 ± 3.9
PCA-1	753 ± 61	48 ± 5	18.6 ± 1.9
PCE-1 > PCA-2	100%	82%	100%
PCA-2 > PCA-1	88%	99%	100%
PCE-1 > PCA-1	*97%	97%	73%

* Test performed for PCE-1 < PCA-1.

Up to now, we have performed individual statistical tests in order to decide, polymer by polymer, whether there is an effect of temperature on adsorption. Now, we wish to compare the different effects amongst each other. In order to do this, we need to consider the relative effect of temperature on the adsorption at a given temperature. Because we are considering relative effects, the result is independent of whether we consider adsorbed mass or adsorbed moles, whether these are calculated using number or weight average molar masses. The calculation of the standard deviation is given in detail in (Annex D).

Table 7-3 gives these relative effects and their standard deviations. Data indicates that the most effected polymer is PCE-1, followed by PCA-2 and then PCA-1. The lower part of the table gives the confidence levels for rejecting the absence of these differences. All values confirm the previously mentioned order.

The fact that PCA-2 is less effected by temperature than PCE-1 supports the results of a previous study [Flatt et al (1997b)]. However, in that case, the contrast was much larger. The reason was a 10% computation error for the adsorption plateau of PCA-2 at 32°C, which combined to the less adequate treatment of calibration data than used here, lead to concluding that temperature had no effect on adsorption of PCA-2.

Table 7-3. Effect of temperature on the adsorption of polymers onto MgO. Quantile are given for temperature effects on the individual polymer and on the comparison between the different polymers.

	Relative increase [%/°C]	Quantile of temperature effect
PCE-1	3.1 ± 0.3	100%
PCA-2	1.9 ± 0.3	100%
PCA-1	1.1 ± 0.2	91%
PCE-1 > PCA-2	99%	
PCA-2 > PCA-1	97%	
PCE-1 > PCA-1	100%	

7.2.4 Interpretation of the temperature effect on adsorption

Adsorption of polymers onto surfaces is mainly linked to either polymer-surface, solvent-surface, polymer-polymer or polymer-solvent interactions. One of these factors, or a combination of them, should explain why the plateau concentration of adsorbed PCE-1 onto MgO increases more with temperature than that of PCA-2, which in turn increases more than that of PCA-1. In addition we have found that in presence of Mg(OH)₂, adsorption is not influenced by temperature.

Hoogeveen et al (1996) have shown that adsorption of polycations onto oxide surfaces is mainly influenced by electrostatic attraction. So, for a negative superplasticizer adsorbing onto an initially negative surface, the adsorption enthalpy (ΔH_{ads}) should increase with the number density of ionic groups on the polymer.

Adsorption free energy is given by :

$$\Delta G_{ads} = \Delta H_{ads} - T\Delta S_{ads} \quad [7-1]$$

Where:

ΔG_{ads} is the adsorption free energy

ΔH_{ads} is the adsorption enthalpy

ΔS_{ads} is the adsorption entropy

Because both ΔH_{ads} and ΔS_{ads} should vary little with temperature, any temperature effect should be linked to the $-T\Delta S_{ads}$ term. However, adsorption entropy is negative, since this involves a loss of degree of freedom. In other words, this means that we expect the opposite of the observed behaviour, a desorption with increased temperature.

Up to this point we have considered polymer-surface interactions. But we must also consider solvent-surface interactions. In particular, at a charged interface there is a concentration of oppositely charge ions, which in our system would be the hydroxyls (OH^-). The electrostatic driven adsorption can be viewed as an ion exchange process of the polymer for a larger number of hydroxyl ions. Because hydroxyl ions have a much smaller adsorption enthalpy, they will be much more likely to desorb as temperature is increased than the polymer. There must be a competition for the surface between the polymer and the hydroxyls and a temperature increase should favour the polymer.

We are in presence of an exchange process and its entropy is becoming positive, because the entropy increase due to hydroxyl desorption must be larger than the entropy loss due to the polymer adsorption.

Such a competition may not exist in $\text{Mg}(\text{OH})_2$ suspensions, because of the pH drop (11.3 instead of 12) attributed to the precipitation of hydroxides from dissolved impurities. This pH drop corresponds to a decreasing in of hydroxyl ions concentration by a factor of five.

From a molecular configuration, the heat of adsorption should be:

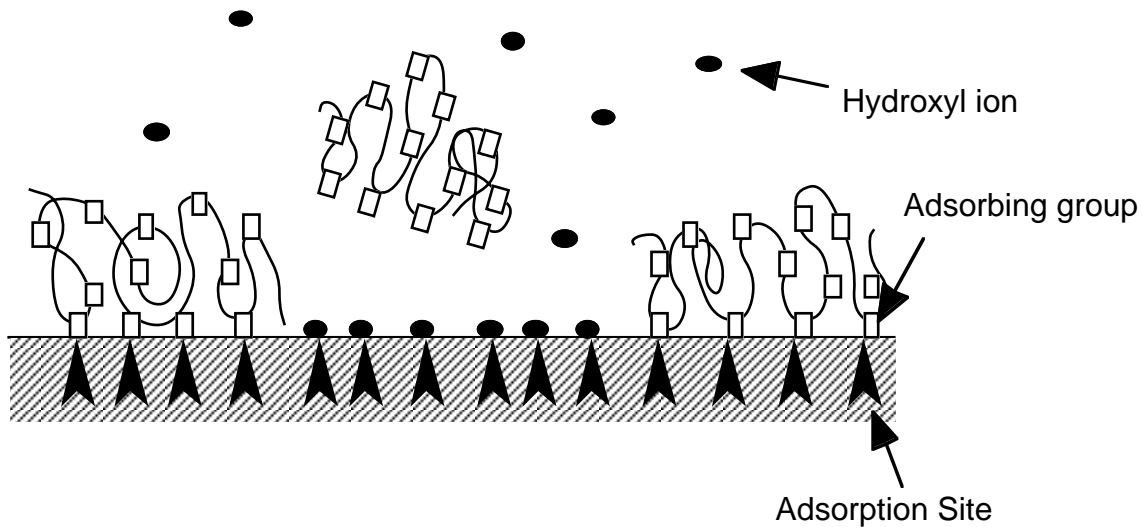
$$\Delta H_{ads(PCA-1)} > \Delta H_{ads(PCA-2)} > \Delta H_{ads(PCE-1)}$$

The higher that heat of adsorption, the competition from the hydroxyls should be less pronounced. This would explain why the adsorption of the PCA-1 polymer onto MgO is fairly independent of temperature. A similar effect could in principle be attributed to a hydrophobic effect in adsorption. However, due to the high solubility of these polymers, it seems improbable.

In Figure 7-3, a very schematic representation of this interpretation is given. The polymers are represented with a certain number of potentially adsorbing groups represented by the open

rectangles. The hydroxyl ions are represented by filled circles and the adsorption sites by the filled arrows. Clearly the scale between the hydroxyl ions and the polymers is not respected. However, this picture might help better understand the suggestion that a temperature increase favours the polymer in its competitive adsorption against hydroxyl ions for adsorption sites.

Low Temperature



High Temperature

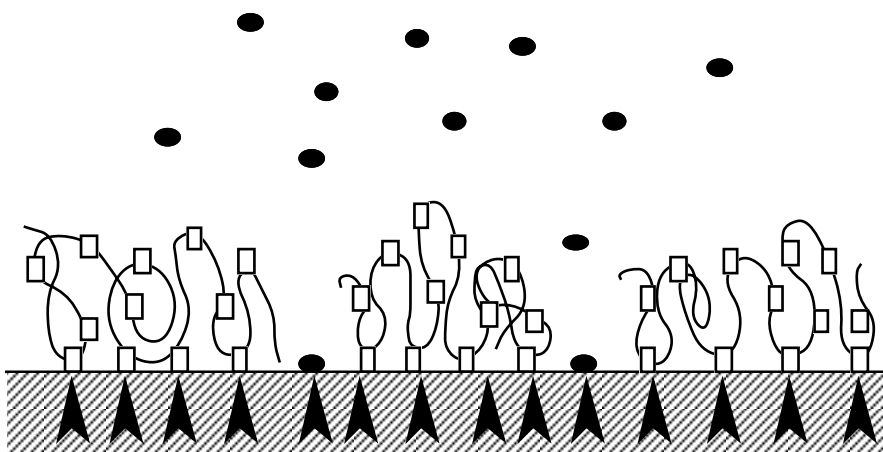


Figure 7-3. Schematic representation of the interpretation of the increased polymer adsorption with temperature. An increase in temperature induces favours the polymer in the competition with hydroxyl ions for adsorption sites.

Finally, it should be noted that at higher temperatures, desorption would be expected. These experiments were not carried out because the polymers are not expected to be very stable at temperature greater than 50°C.

7.3 Surface coverage

Adsorption data allows the calculation of the surface occupied per molecule. Then assuming a certain geometry and packing of the polymers, we can calculate some size factor. For example, we can assume a compact layer of spheres and calculate the radius. This radius could also be the radius of a compact layer of cylinders perpendicular to the surface. In this case we would need a value of the radius to height ratio to get an idea of the adsorbed layer thickness.

Such calculations are not only dependent on the geometry assumed, but also on the molar mass average chosen.

Table 7-4. Diameters a standard deviations of adsorbed polymers, obtained assuming a compact layer of spheres. Values are given using both number and mass average molar mass.

		PCA-1	PCA-2	PCE-1
MgO	Ø(Mw) [nm]	10.2 ± 0.5	7.5 ± 0.4	9.7 ± 0.5
	Ø(Mn) [nm]	6.3 ± 0.3	5.1 ± 0.3	5.5 ± 0.3
Mg(OH) ₂	Ø(Mw) [nm]	14.0 ± 1.3	8.9 ± 0.6	8.8 ± 0.4
	Ø(Mn) [nm]	6.3 ± 0.3	5.1 ± 0.3	5.5 ± 0.3

7.4 Rheology

In most of the following discussions, Critical Superplasticizer Concentration (CSC) will be used. This parameter was defined as the amount of superplasticizer, which must be added to a suspension in order to induce a Newtonian behaviour. Below this dosage, the fluid exhibits a yield stress, consistent with the Bingham rheological model. Above this concentration, the linear regression leads to a negative ordinate at the origin. It is clear that this can not be a negative yield stress, a situation, which

would not have any physical meaning. However, a very important observation was that these negative ordinates at the origin systematically appeared, when at the end of the measurement, a macroscopic sedimentation could be detected. One consequence is a decreased viscosity due to a lower volume fraction of solid in the measured part of the sample. After the critical concentration, acquired data is therefore no more reliable.

For the magnesium hydroxide suspensions, we are under conditions where sedimentation is hindered by even very small yield stress values. This might be linked to the relatively low density of this partially porous powder, as well as to the particle size and size distribution.

The sedimentation is not attributed to flocculation (particle binding due to polymers) since sedimentation volumes decrease as superplasticizers are added [Flatt et al (1998b)].

7.4.1 Effect of Solid Volume Fraction

As the volume fraction of solid is increased, the CSC increases. For volume fractions higher than 41%, PCA-2 can not be used to obtain Newtonian fluids. In fact beyond this limit, the suspensions become very viscous, however much PCA-2 is included.

For this upper bound volume fraction, Figure 6-20 shows that the CSC corresponds to the Directly Adsorbable Superplasticizer Concentration (DASC). This concentration is closely correlated to the effect on zeta potential induced by PCA-2 addition. Above this concentration, PCA-2 continues to be adsorbed but no effect is observed on zeta potential, a fact, which has been related to adsorption into the porous network of the $\text{Mg}(\text{OH})_2$ powder used.

So, it appears that the upper volume limit of a Newtonian behaviour for a $\text{Mg}(\text{OH})_2$ suspension can be reached when the outer surface of this powder is covered. More concentrated suspensions require a higher degree of surface coverage in order for the polymers to be able to disperse the particles and prevent them from reagglomerating. Another way of understanding this result is that Newtonian fluids can be obtained with a degree of agglomeration inversely related to the volume fraction of solid.

The implication of this result is that the maximum performance, as far as solid loading is concerned, requires complete surface coverage. Below total surface coverage, more water is required in order to allow for the agglomerates present to reorient. This is a fact well established in ceramic processing, but is often not considered relevant by concrete practitioners. Indeed, many studies compare

performances for identical dosages, which are kept low for cost reasons. So, results indicate the performances of different polymers at different degrees of undersaturation. They do not yield the information concerning the maximum possible performances of the compared polymers. In some cases, these studies use superplasticizer solutions which do not even contain the same solids content.

What these results point to is that the maximum performance is obtained for total surface coverage. Because adsorption for PCA-2 is complete in this range, we can conclude that the effect is only due to adsorbed polymers. A small uncertainty remains concerning a possible effect of the non adsorbed monomers in presence of adsorbed polymers. However, due to the high degree of polymerisation of PCA-2, this possibility will not be further considered. Effects linked to adsorbed polymers being steric and electrostatic repulsion, these will be the effects considered as responsible for the dispersion of magnesium hydroxide suspensions.

7.5 Implications from model suspension behaviour

The studies on the model suspensions indicate that the dispersing effect of these superplasticizers is linked only to the adsorbed molecules. This result could be obtained unambiguously because of the very strong affinity of the polymer PCA-2 for the $\text{Mg}(\text{OH})_2$ surface (up to total coverage of the outer surface all the added polymer is adsorbed). Therefore, steric and electrostatic repulsion are the mechanisms which must be considered as potentially responsible for dispersion.

Adsorption onto MgO suggests that there is a competition, in alkaline medium, between hydroxyls and polymers for the surface. The higher the adsorption energy of the polymers, the less they are effected by this competition. Because the alkalinity of cement suspension is even higher, it is probable that a similar competition can be found. However, experimental evidence of this would be difficult to obtain. Indeed changing the temperature of a cement suspension would lead to reaction rate changes, which would therefore lead to the superposition of two effects.

So, at this point, we can attribute the dispersion to either steric or electrostatic repulsion or both. Maximum performance is found for total surface coverage. In addition to optimising the dispersion mechanisms, it is also important to obtain a high degree of adsorption. This latter point can become problematic in alkaline suspensions, due to the competition of hydroxyls for adsorption sites.

Chapter 8 Results with cement suspensions

Because it quickly became evident that attempting to provide a full explanation for the cements studied by the partners of Eurêka project would be a too long task, we have chosen to concentrate efforts on studying the two cements obtained from the same clinker. One of these cements was ground with a grinding aid (a triethanol amine acetate) and the other without. The cements not have the same specific surfaces (no significant difference). This surface is about $1\text{m}^2/\text{g}$ (BET).

Let us recall that HPLC allows clear separation of the different polymeric fractions of PCA-1. In the first part of this section, we consider only the overall adsorption of PCA-2 and PCA-1. Then we take a look at the adsorption of the individual fractions of PCA-1. No results for PCE-1 have been obtained with the cement suspensions.

8.1 Adsorption

8.1.1 General trends

In the chapters dealing with model suspensions, we have shown that the adsorption isotherms of the polymers studied exhibit step functionalities. This means that until the surface is saturated, all the polymers added to the suspensions are adsorbed onto surface of the particles. Polymers in excess of this amount remain in the liquid phases. From the analytical point of view, this means that no responses are measured in the supernatants of the suspensions having an initial concentration below the plateau concentration. On the other hand, responses are measured for initial dosages above this specific concentration.

For such behaviours, the graph showing the initial concentration versus the response area is a straight line. If the polymer is not altered by the aqueous phase, then this line is parallel to the calibration line.

This case is illustrated in Figure 8-1 for the adsorption of PCA-2 in a suspension of cement With Grinding Aid, to which the polymer is added after 30 min hydration. The calibration standards were prepared in cement extracts having been hydrated for the same time at the same liquid to solid ratio. This choice turned out very important for PCA-2. Indeed in both samples and standards micellisation was evident because of the apparition of small peaks at higher retention times than that of PCA-2. This is attributed the presence of aluminates. Indeed, the same effect is seen in suspensions of $MgO \cdot Al_2O_3$ but not in suspensions of MgO or $Mg(OH)_2$. This effect was not observed with PCA-1.

An implication of this micellisation effect is that it is important that the standards should be prepared in a solution having a similar ionic composition to the aqueous phase of the suspension. This is a problem for direct addition, because the ionic composition is quickly evolving. So, performing direct regression on adsorption data is probably less misleading than using inadequate calibration data.

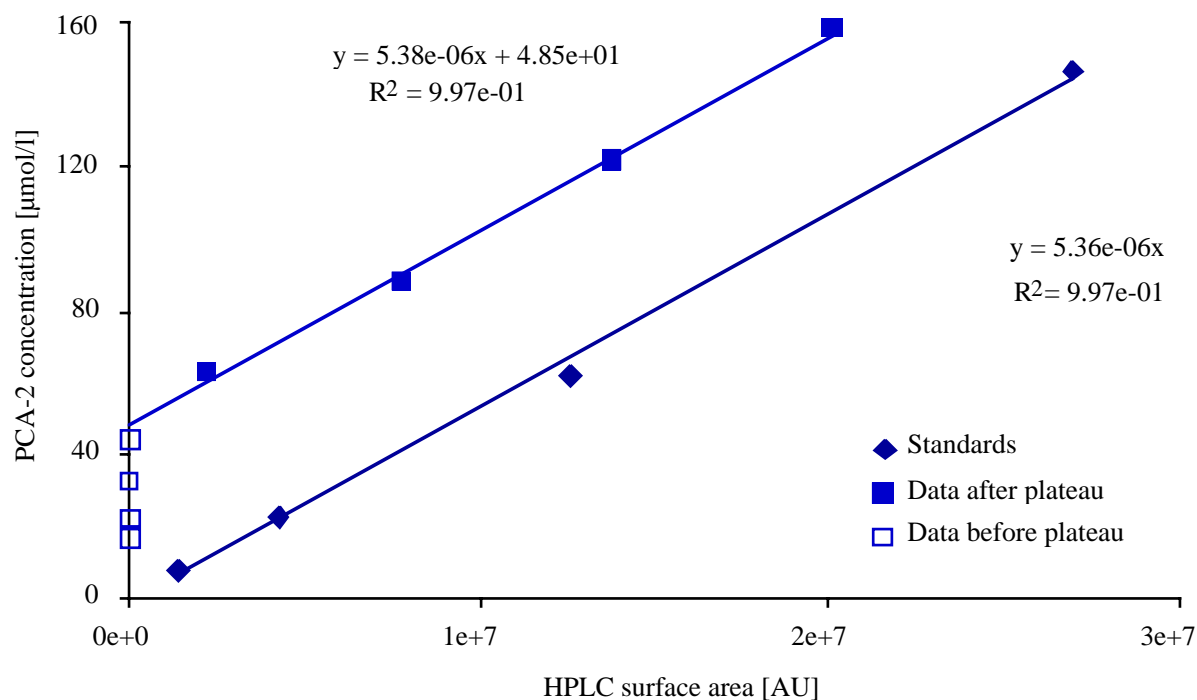


Figure 8-1. Adsorption raw data for polymer PCA-2 and cement ground with a grinding aid.

The open squares represent points below the plateau concentration. No responses are measured in the final liquid phases and all abscissa are equal to zero. The filled squares represent points above the

plateau. Their abscissa are greater than zero. In this figure, the slope obtained from the linear regression over these data (filled squares) appears identical to the one obtained from the standards (filled diamonds). This is confirmed by the confidence level of only 3% for considering that both slopes are not equal. Therefore, experimental data does not allow to differentiate both slopes and these may reasonably be considered as equal.

For step functionalities, the plateau of the adsorption isotherm can therefore be determined without using calibration curves. It is sufficient to take the ordinate at the origin from the linear regression performed over adsorption data, for which responses are greater than zero (Figure 8-1). This requires all suspensions to have almost identical masses of solids and liquids, which was the case in all experiments. No that if the isotherm has another shape, then only data at high initial dosages should be used in the regression, which will provide the plateau value and its slope will be that of a proper calibration line (at the adequate ionic composition of the aqueous phase).

8.1.2 PCA-2

The results of direct addition of PCA-2 are given in Figure 8-2 for adsorption times of 5 and 30 minutes.

Data clearly shows that the cement ground with grinding aid adsorbs more PCA-2 than does the cement ground without. The raw data shows this clearly. Statistical tests are reported in Table 8-1 and Table 8-2 for the slope and optimised ordinates respectively. Because of the little number of data these values are more indicative. Their mode of calculation is detailed below for the global adsorption of PCA-1.

8.1.3 PCA-1

HPLC shows six different identifiable polymeric fractions with PCA-1 (Figure 5-1) instead of one for PCA-2 (Figure 5-2). For the model suspensions, we used the total surface area of these fractions for adsorption calculations, not distinguishing between these fractions. The same procedure is used here at first, in order to test for differences between cements. Then, we turn to an analysis of the individual fractions.

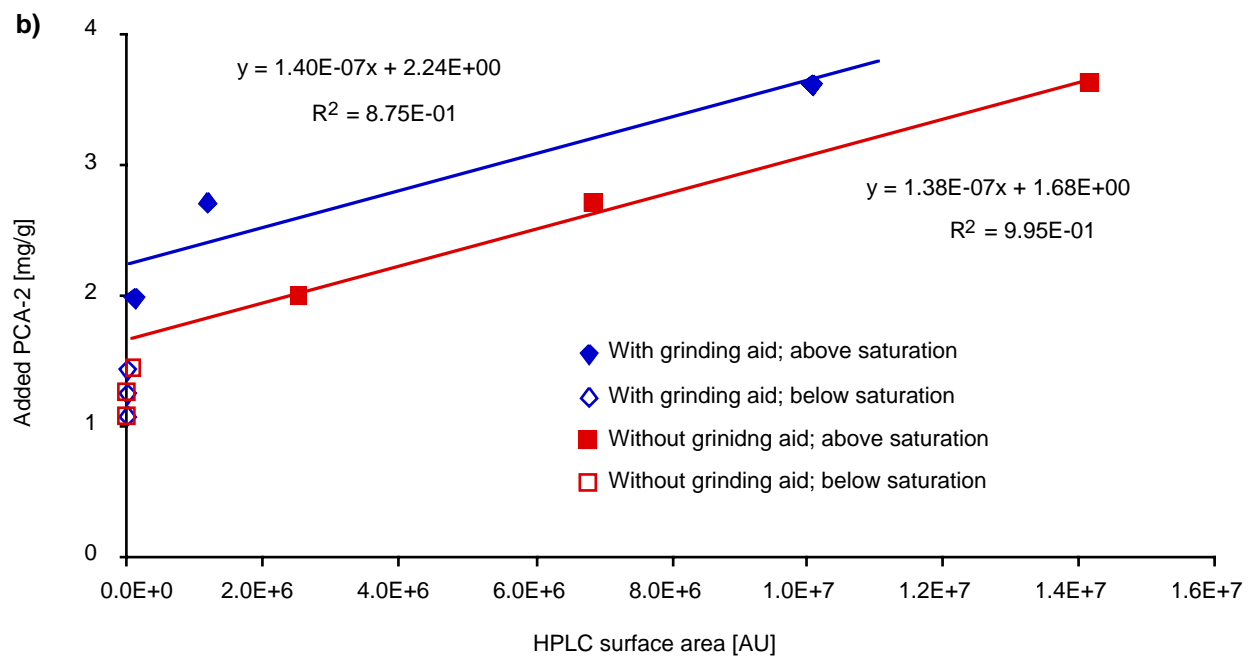
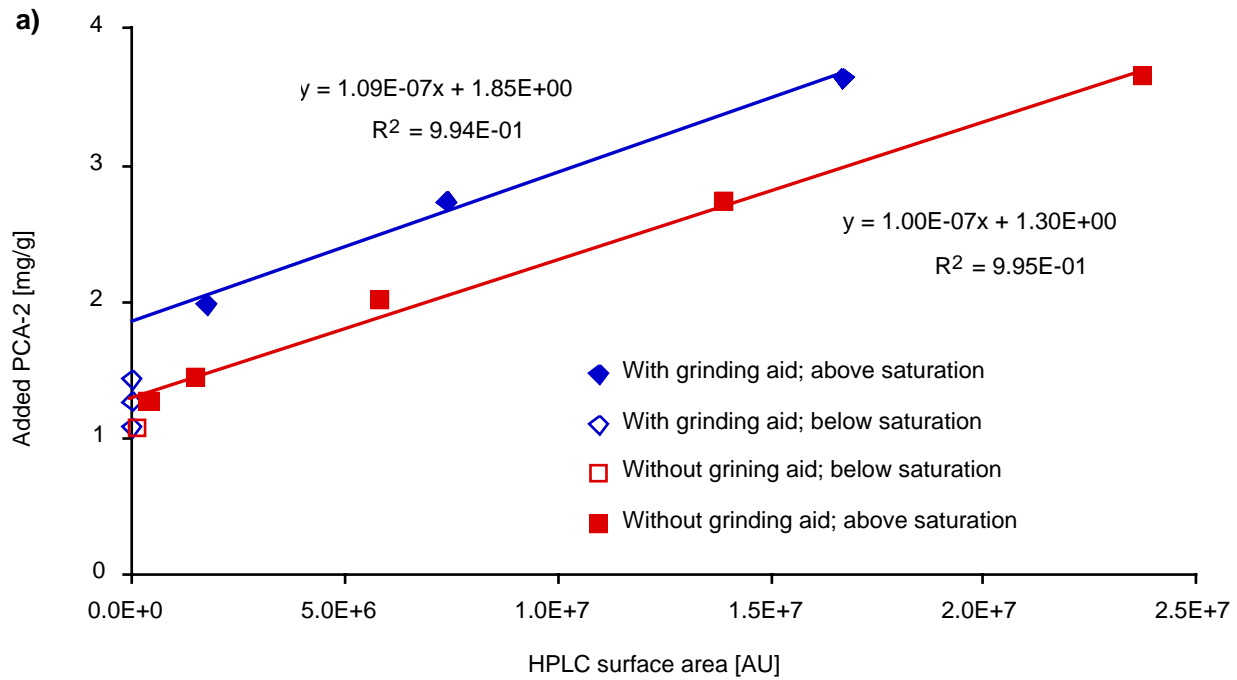


Figure 8-2. Adsorption data for direct addition of PCA-2 to cements with and without grinding aid. Adsorption times are respectively 5 and 30 minutes for figures a and b.

Global adsorption

The raw data for adsorption in the case of direct addition of PCA-1 is reported in Figure 8-3 for adsorption times of 5 and 30 minutes (a and b respectively). The difference between the behaviour of both cements is very small. The ordinate at the origin for the cement with grinding aid is in both cases higher is slightly higher than the one of the cement without grinding aid. In order to decide whether this difference is significant, we perform a statistical test.

The first step is to test whether the slopes of both lines are identical. Values in Table 8-1 indicate that it is not possible to consider the slopes different. At this point, we consider that both lines have the same slope and calculate a single slope for both data sets. This allows to compute more precise ordinates at the origin, which are compared, taking into account the fact that they are no more independent one from the other. Results in Table 8-2 indicate that it is not possible to consider these ordinates different one from the other.

Table 8-1. Confidence intervals to reject the hypothesis that the slopes are equal. For PCA-1 which is not monomodal as PCA-2, the values given are derived from overall polymer response.

Adsorption time	PCA-1	PCA-2
5 min	17%	74%
30 min	28%	6%

Table 8-2. Confidence for rejecting the hypothesis that polymer adsorption is not affected by the type of cement (w/wo grinding aid).

Adsorption time	PCA-1	PCA-2
5 min	84%	100%
30 min	87%	95%

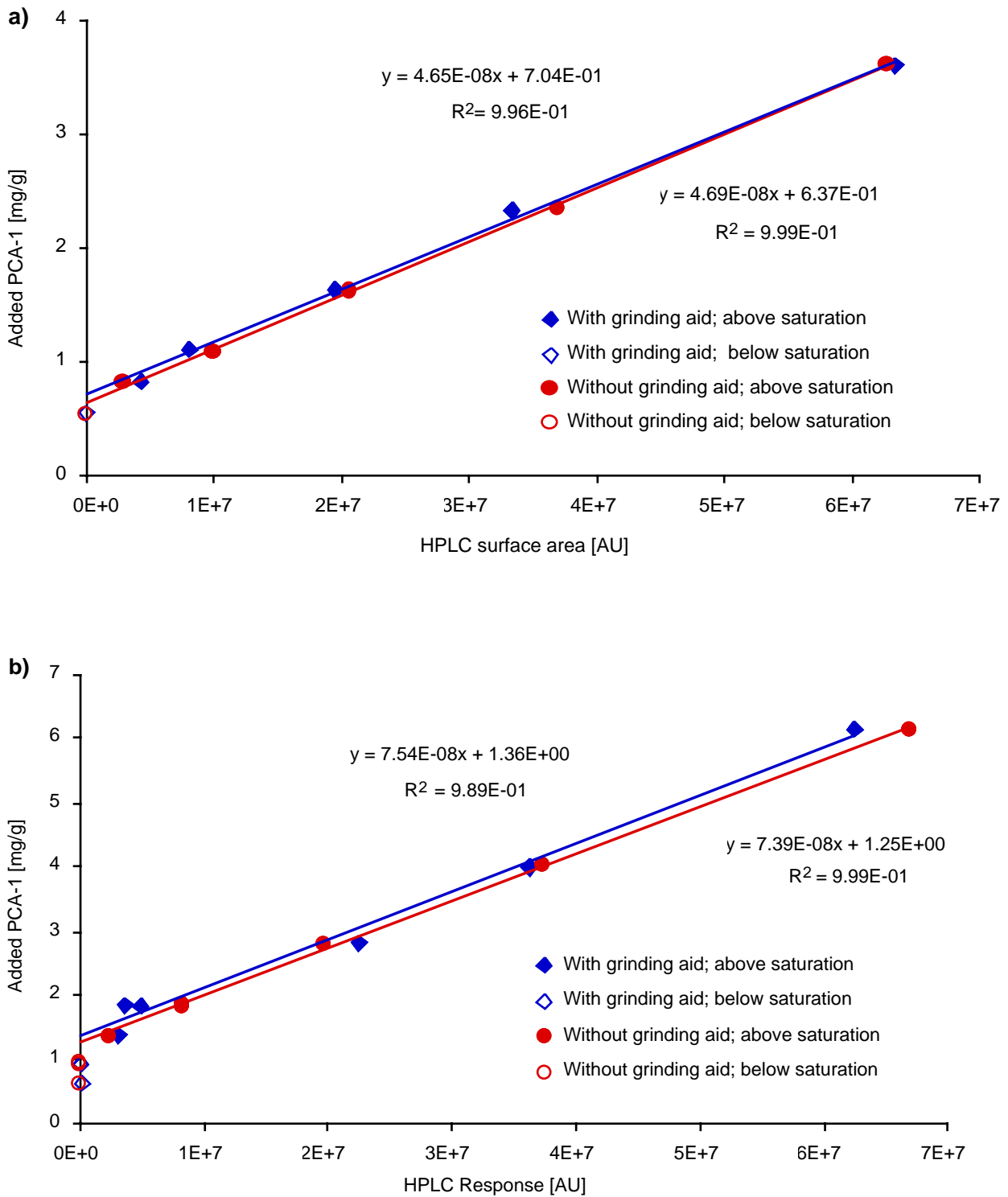


Figure 8-3. Adsorption data for direct addition of PCA-1 to suspensions of cement with and without grinding aid; a) after 5 minutes; b) after 30 minutes.

Adsorption of individual polymeric fractions

The different HPLC peaks of PCA-1 may be due either to fractions of different masses and/or conformations. These fractions appear to adsorb with step like functions. Their plateau values and corresponding errors are determined, as described above, by linear regressions. In this case however, peak heights were used instead of peak surfaces because they provide better correlation for both standards and adsorption samples. The reason behind this is that the chromatographic method cannot totally separate these fractions and that surfaces are partly overlapping.

Plateau values for the various polymeric fractions of PCA-1 have the following physical meaning. They define the concentrations of added superplasticizer beyond which a given fraction stops adsorbing. Though initially all fractions adsorb, it is shown further that they do not all stop adsorbing at the same amount of added polymer. Thus, there is a range over which only some fractions of the added polymer are still adsorbing. In what follows, adsorption of the polymeric fractions of PCA-1 are considered with respect to both cements (without or with grinding aid) and with respect to addition mode (delayed or direct)

Since the specific surfaces between both cements cannot be considered different (confidence interval at most 60%), adsorbed concentrations are given with respect to the mass of cement in the suspensions. Values with respect to surface area are almost the same since these surfaces are very close to $1 \text{ m}^2 \text{ g}^{-1}$.

Effect of polymeric fraction

Figure 8-4 shows adsorption plateau concentrations for the polymeric fractions of PCA-1. Both cements were used and the polymer was in the mixing water (direct addition). All plateau concentrations are plotted along with error bars corresponding to 90% confidence intervals. These values are plotted against retention time.

It appears that the polymeric fractions with larger retention times might have lower plateau values. However, it is difficult from such a graph to decide whether this trend is or not the result of experimental errors. This problem is even greater in Figure 8-5, which shows the case where superplasticizers are added after 30 min hydration (delayed addition).

So, we test whether the slope of plateau values versus retention time is equal to zero ($m_{rt,ads} = 0$?). If $m_{rt,ads} \neq 0$, retention time is correlated with a change in plateau concentration.

Because all plateau concentrations have different errors, they should not be weighted in the same way when calculating $m_{rt,ads}$. Weights are taken as the inverse of the standard deviation of each point. After normalising $m_{rt,ads}$ by its standard deviation, it is possible to determine from a Student law $t_{(1-\alpha; n-2)}$, the confidence level α up to which one can reject $m_{rt,ads} = 0$. In this test, the degree of freedom is $(n-2)(q-2)$, where n is the total number of data points and q is the number of retention times considered.

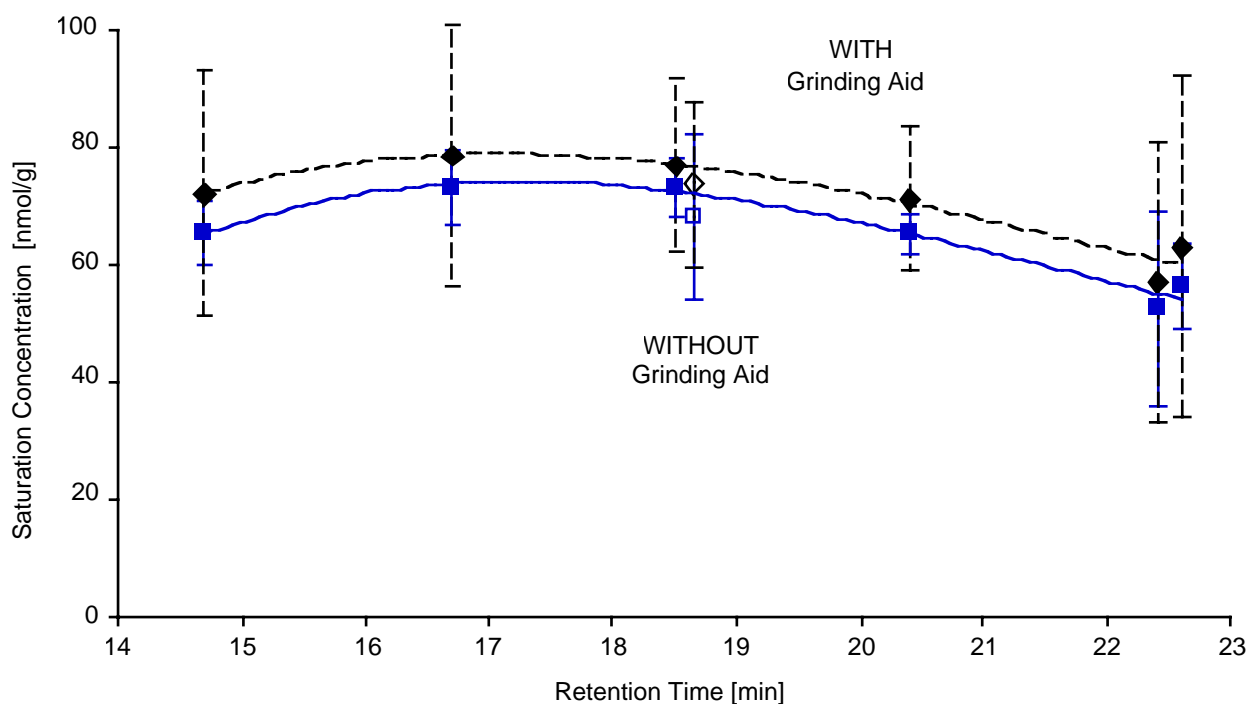


Figure 8-4. Plateau values for polymeric fractions of PCA-1 as a function of retention times. Results are given for both cements and direct addition (hydration time of 0 min). Error bars correspond to 90% confidence intervals. Filled symbols refer to fractions and empty symbols to the overall polymer.

These degrees of confidence are shown in Table 8-3. Values for cement without grinding aid are high. In this case it is possible to consider that retention time is correlated with plateau concentration. In other words, the polymerised part of superplasticizer PCA-1 contains fractions (different mass

and/or conformation) which do not all adsorb in the same way. On the other hand, values for cement with grinding aid are lower. In this case, the correlation might exist but if it does, its effect is too low to be determined with sufficient confidence within the range of experimental errors.

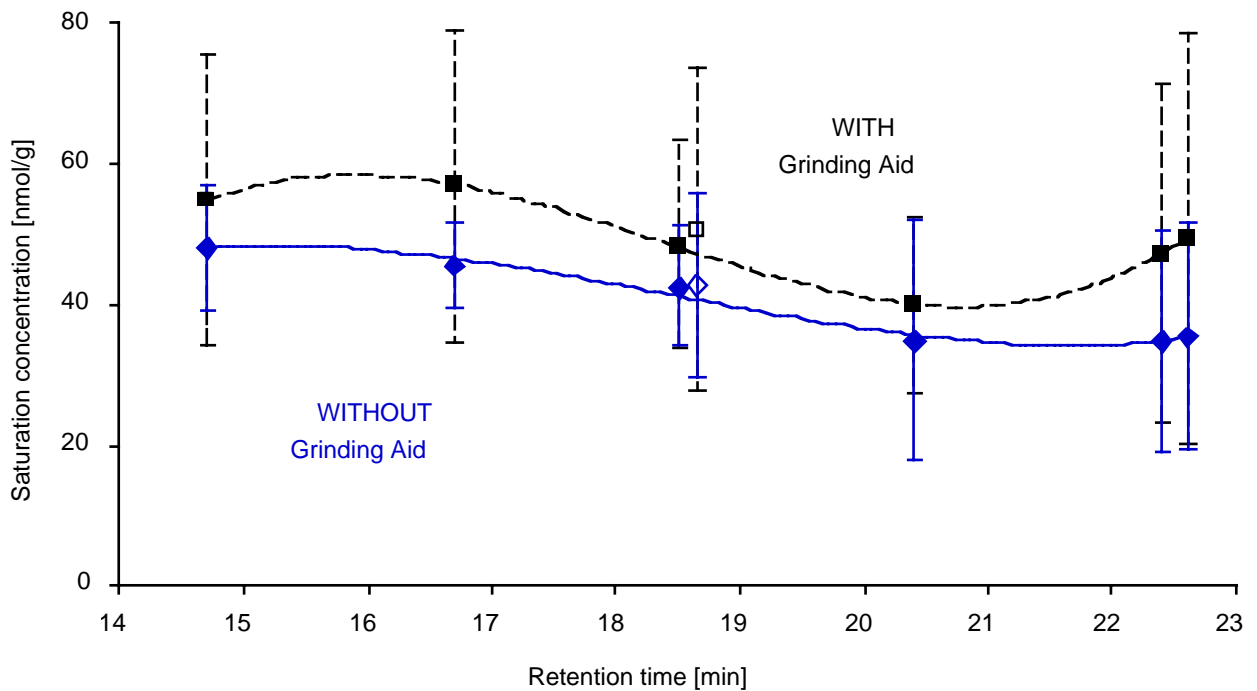


Figure 8-5. TASC values for polymeric fractions of PCA-1 as a function of retention times. Results are given for both cements and delayed addition (hydration time of 30 min). Error bars correspond to 90% confidence intervals. Filled symbols refer to fractions and empty symbols to the overall polymer.

Table 8-3. Confidence intervals for rejecting the absence of a correlation between the amount of PCA-1 for which a given fraction reaches surface saturation and the retention time of these fractions.

	Cement without grinding aid	Cement with grinding aid
Direct addition (hydration time = 0 min)	99%	92%
Delayed addition (hydration time = 30 min)	97%	87%

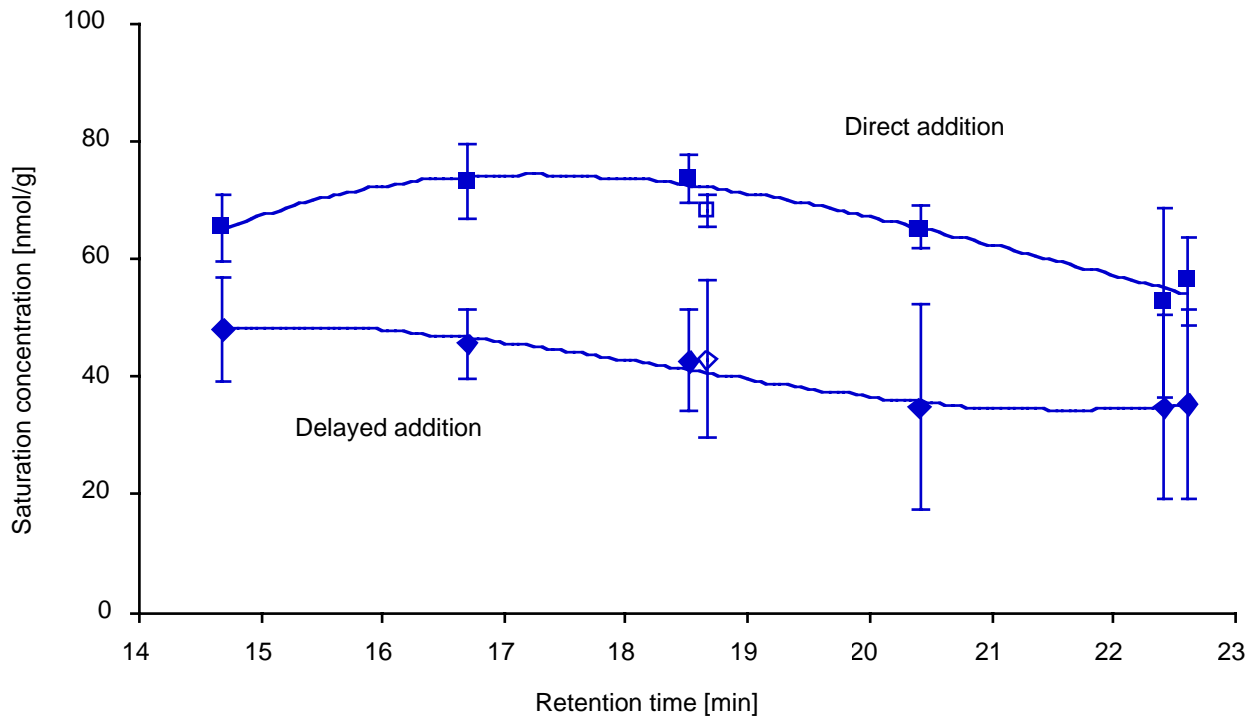


Figure 8-6. TASC values for polymeric fractions of PCA-1 as a function of retention times. Results are given for both cement without grinding aid for direct and delayed addition. Error bars correspond to 90% confidence intervals. Filled symbols refer to fractions and empty symbols to the overall polymer.

Effect of addition time

For each cement, the effect of addition time on adsorption is tested by comparing plateau concentrations obtained for each polymeric fraction. Table 8-4 gives the degrees of confidence up to which :

$$\text{Plateau}_{\text{direct addition, cement x, fraction i}} = \text{Plateau}_{\text{delayed addition, cement x, fraction i}}$$

can be rejected. The correct way to obtain these values is described in [Green and Margerison , 1978 (chapter 14, §6.5.1.)]. Results indicate that hydration decreases the amount of adsorbed polymers in a significant way for both cements. A comparison of the effects of hydration can be seen in Figure 8-6 for cement without grinding aid and in Figure 8-7 for cement with grinding aid.

Effect of Grinding Aid

For each hydration time, the effect of a grinding aid on adsorption is tested. The degrees of confidence up to which

$$\text{Plateau}_{\text{cement without g.a., addition mode m, fraction i}} = \text{Plateau}_{\text{cement with g.a., addition mode m, fraction i}}$$

can be rejected are given in Table 8-5. Values are low and it is concluded that if grinding aid influences adsorption its effect cannot be detected within the range of experimental errors. The effect of grinding can be seen in Figure 8-4 for direct addition and in Figure 8-5 for delayed addition.

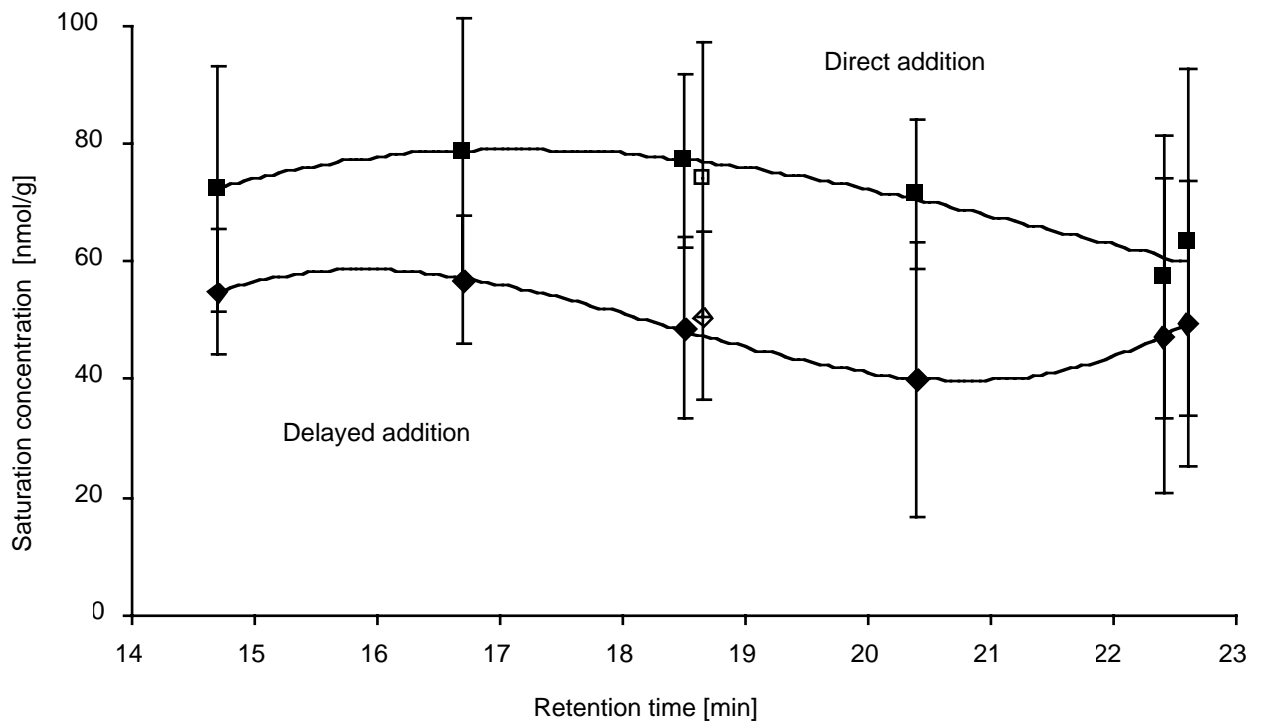


Figure 8-7. TASC values for polymeric fractions of PCA-1 as a function of retention times. Results are given for both cement with grinding aid for both addition modes (hydration times of 0 and 30 min). Error bars correspond to 90% confidence intervals. Filled symbols refer to fractions and empty symbols to the overall polymer.

Table 8-4. Comparison of the effect of hydration on adsorption onto cements 0 and 1. Confidence intervals for rejecting the absence of an effect of hydration on adsorbed amounts. Values are given for each peak (polymeric fraction). The last value is obtained using the total surface of the polymeric fraction of PCA-1.

	peak 1	peak 2	peak 3	peak 4	peak 5	peak 6	Global
Cement without grinding aid	99%	100%	100%	100%	84%	98%	100%
Cement with grinding aid	89%	93%	97%	93%	41%	55%	87%

Table 8-5. Comparison between both cements at direct and delayed addition. Confidence intervals for rejecting the absence of an effect of addition time on adsorbed amounts. Values are given for each peak (polymeric fraction). The last value is obtained using the total surface of the polymeric fraction of PCA-1.

	peak 1	peak 2	peak 3	peak 4	peak 5	peak 6	Global
Direct addition	75%	62%	36%	39%	23%	41%	56%
Delayed addition	53%	75%	61%	46%	70%	69%	67%

8.2 Rheology

8.2.1 General trends

Figure 8-8 to Figure 8-11 show the flow curves obtained for cements with and without grinding aid. Each curve corresponds to a different dosage of superplasticizer, while increasing shear stress.

The first observation is that the functionality of the flow curves changes significantly with superplasticizer dosage. A simple model such as the two parameter Bingham model is insufficient to account for these curves. One can also see that above a certain dosage all curves indicate very similar flow behaviors.

Up to a certain value of shear stress, the shear rate is equal to zero. Then, there is a sudden increase in shear rate. This limiting stress value can be identified as the yield stress. The amplitude of the sudden shear rate increase rises with yield stress magnitude. In some cases, there are a couple of these steps,

indicating that a large particle concentration in one part of the gap causes the rheometer to block. This is probably due either to an inhomogeneous distribution of the particles or to reagglomeration of particles not totally covered by polymers. Nevertheless, it appears that the first yield point can be considered for discussing yield stress.

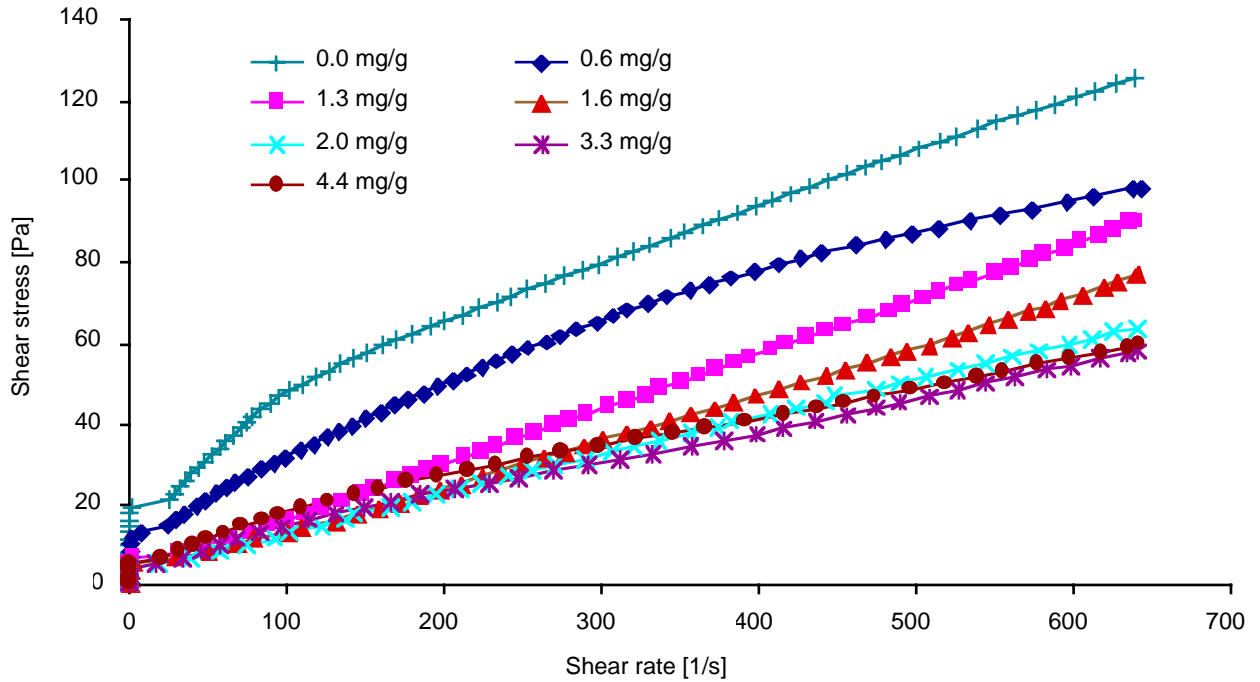


Figure 8-8. Flow curves for increased stress measurements with cement containing grinding aid. The different curves correspond to different dosages of PCA-1.

Most likely, these shear rate discontinuities indicate that hydration causes a bonded network to form between both walls of the cell. The measured yield stress is dependent on the gap size and the time for which the cement is left to hydrate. Nevertheless, this parameter seems to give valuable information on superplasticizer efficiency. It will therefore be extensively used for discussion of the rheology of these suspensions.

At high superplasticizer dosages, some sedimentation took place. Unreliable data was thereby produced.

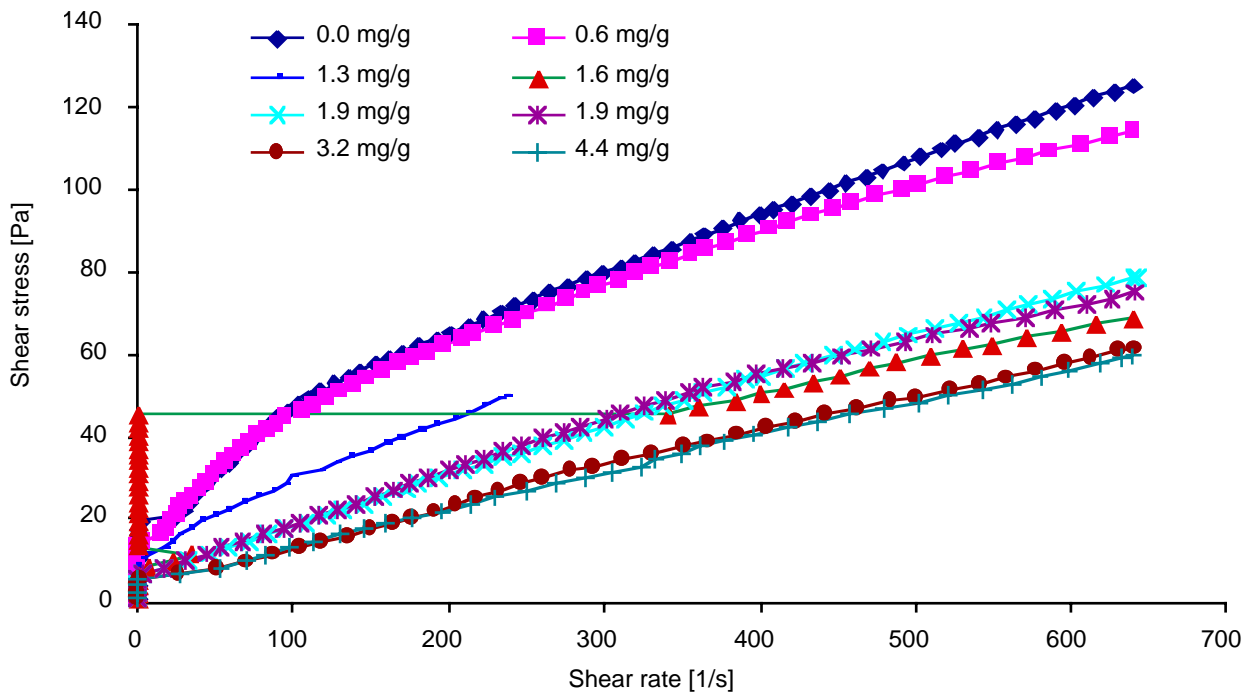


Figure 8-9. Flow curves for increased stress measurements with cement containing grinding aid. The different curves correspond to different dosages of PCA-2.

8.2.2 Yield Stress

Yield stress is determined by taking the first stress value above which shear rate increases suddenly. In figure 10, values obtained for PCA-1 containing suspensions are plotted against PCA-1 dosage. The vertical lines show the amounts of PCA-1 adsorbed after 5 and 30 minutes. An interesting feature is the steeper decrease of yield stress as PCA-1 is added to the cement without the grinding aid. The plateau value of yield stress is reached earlier for this cement.

For suspensions containing PCA-2, the minimal yield stress is reached for dosages slightly lower than the amount adsorbed at 5 minutes for the cement with grinding aid. For the cement without grinding aid, the situation seems to change around the dosage adsorbed after 5 min (figure 12). In the first case at least, it seems that it is not even necessary to cover the cement particles with polymer to obtain a good dispersion. A similar result was obtained for this polymer and model suspensions of $Mg(OH)_2$ (chapter Chapter 1). In that case, it was shown that as solid loading was increased, the polymer requirement increased. The liquid limit was reached more or less once all the powder surface was covered.

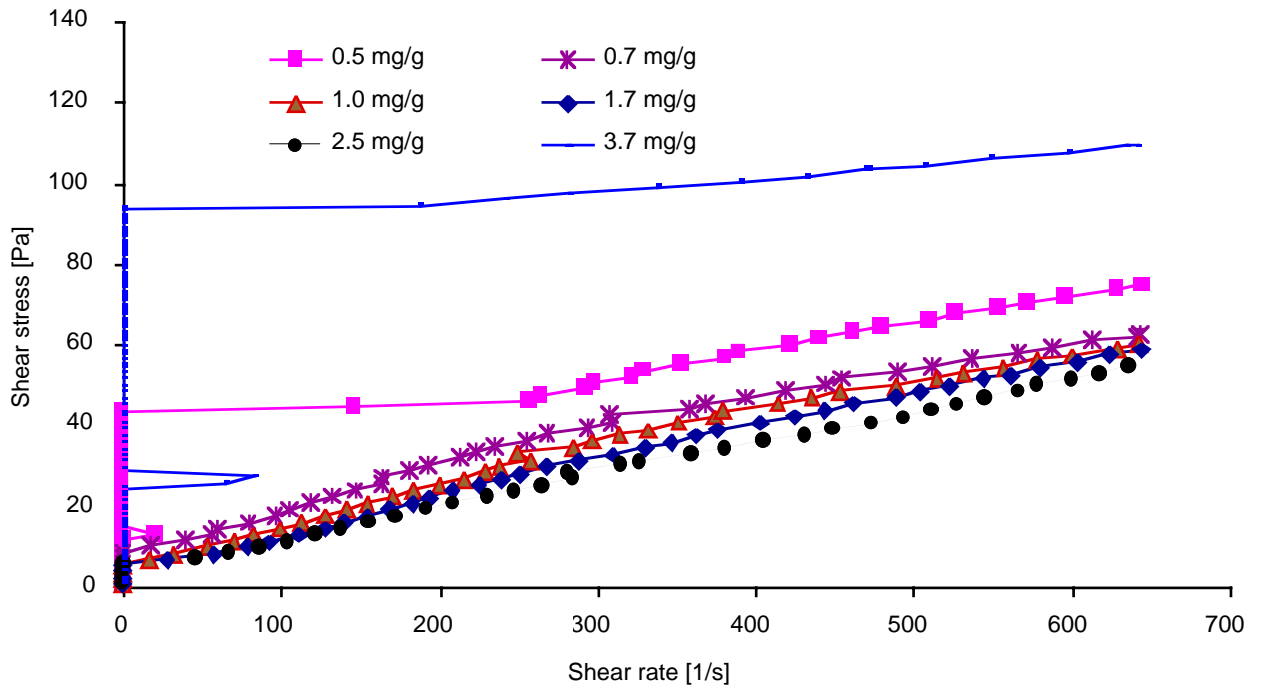


Figure 8-10. Flow curves for increased stress measurements with cement not containing grinding aid. The different curves correspond to different dosages of PCA-1. The high yield stress for 3.7 mg is certainly linked to sedimentation.

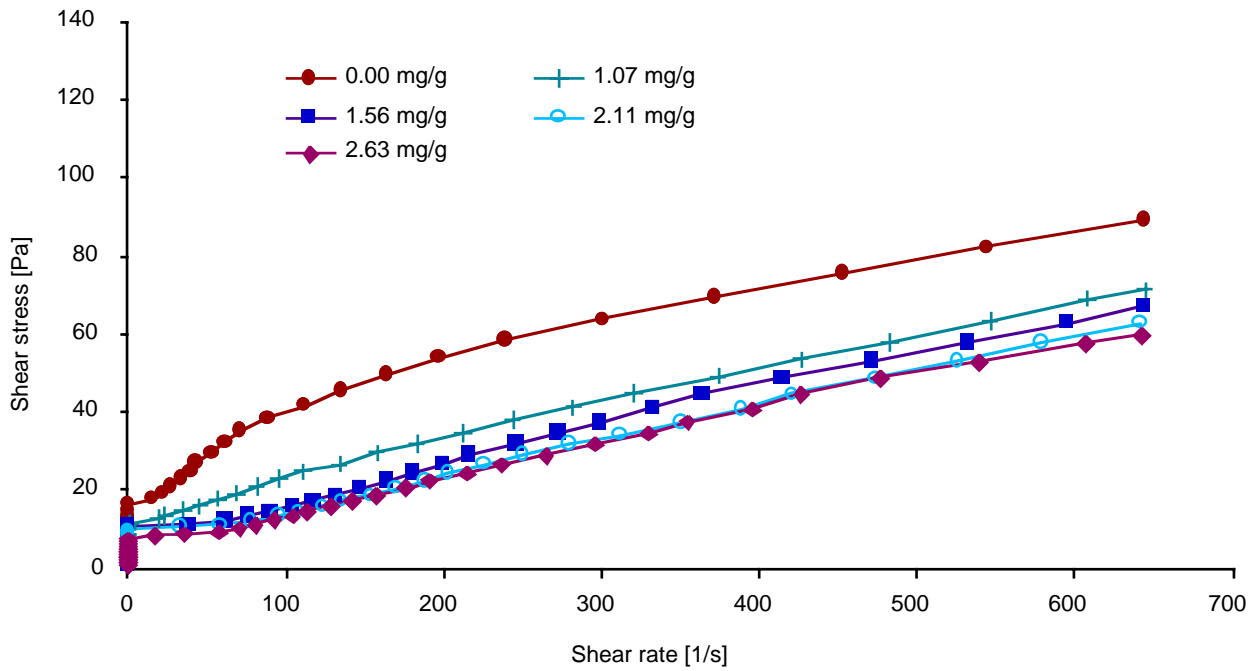


Figure 8-11. Flow curves for increased stress measurements with cement not containing grinding aid. The different curves correspond to different dosages of PCA-2.

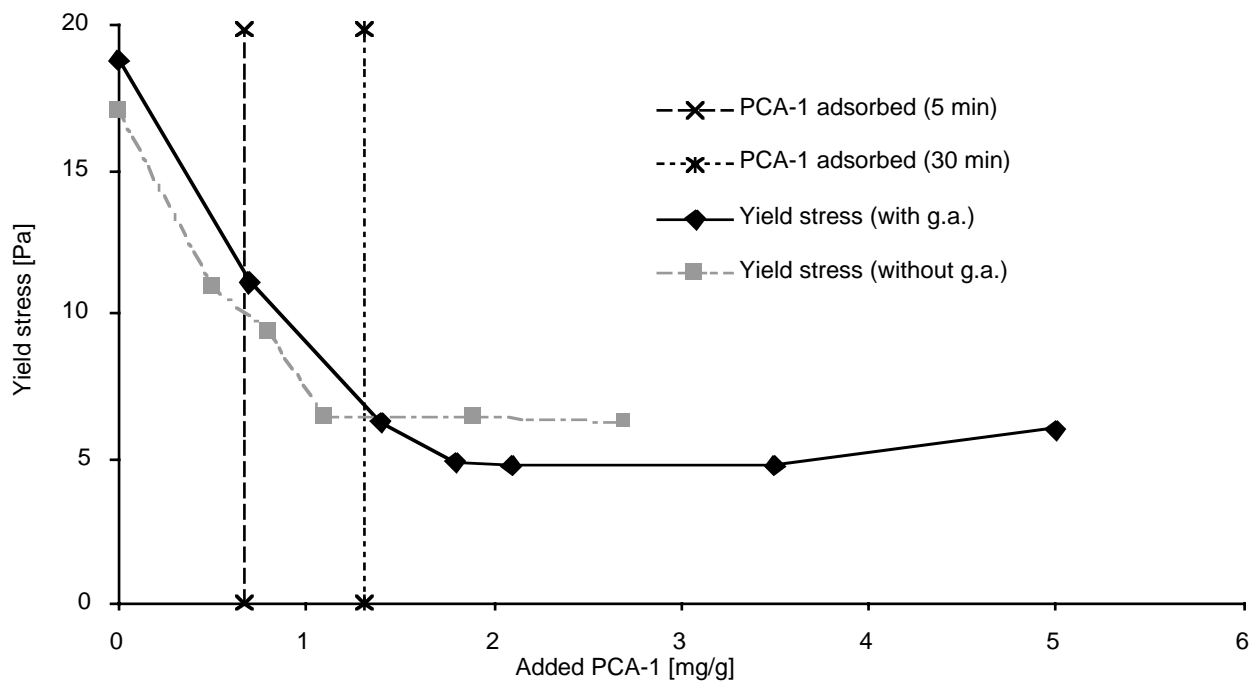


Figure 8-12. Yield stress versus PCA-1 dosage. The vertical lines indicate PCA-1 adsorption.

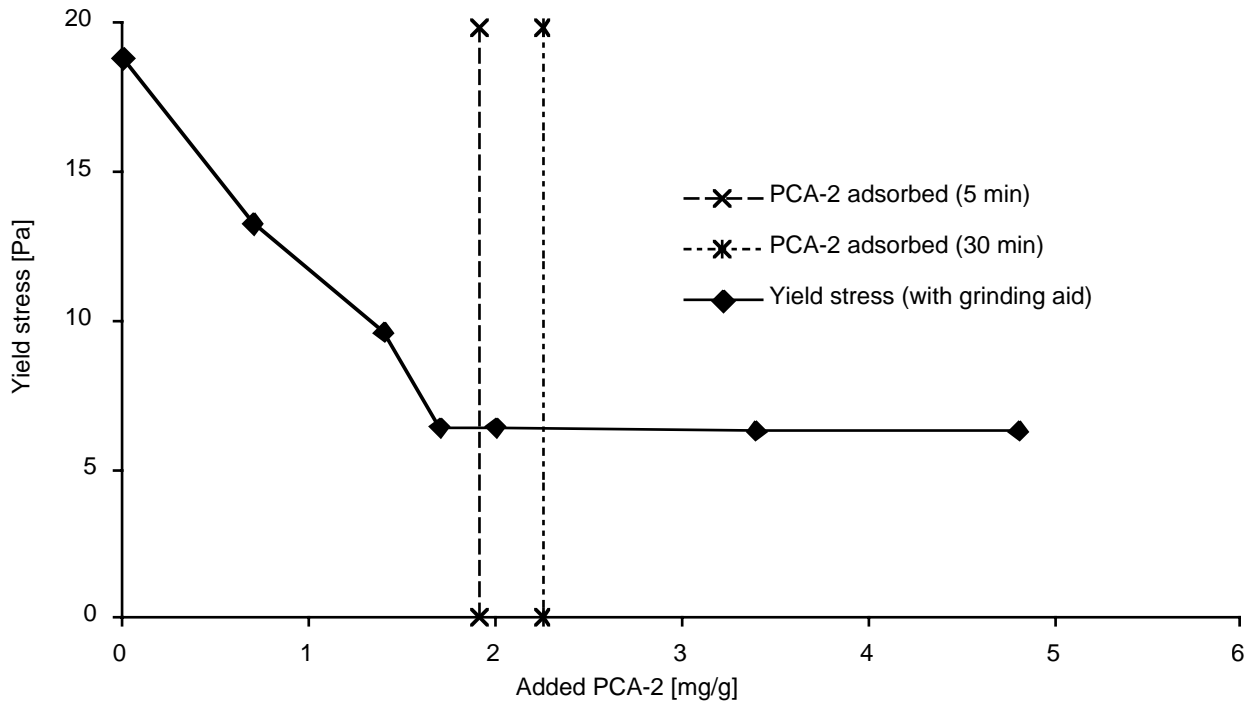


Figure 8-13. Yield stress versus PCA-2 dosage, cement ground with grinding aid.

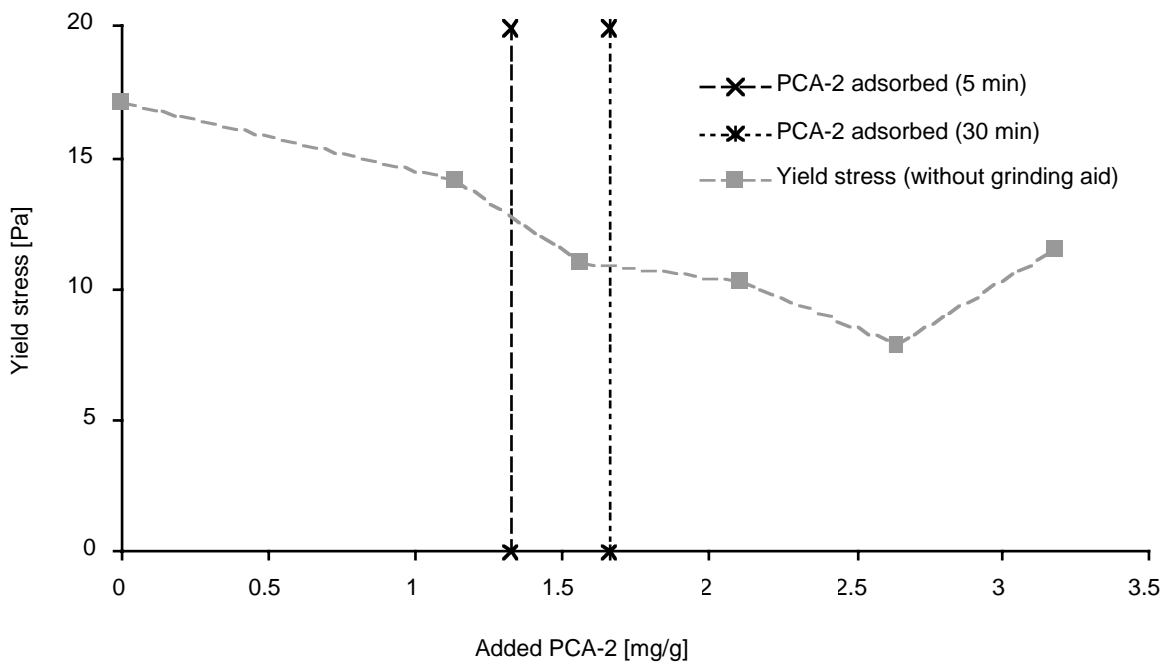


Figure 8-14. Yield stress versus PCA-2 dosage, cement ground without grinding aid

Chapter 9 Discussion of cement suspensions

9.1 Adsorption

9.1.1 Effect of polymeric fraction

Polymer PCA-1 is a test product which presents good superplasticizing properties. However, as is apparent in its chromatogram (Figure 5-1), it contains some products of low molar mass (those at very short retention times). For cost reasons, no separation is done. Because these were not found to adsorb significantly, they are not expected to alter the superplasticizer performance. The very low molar mass products do not have sufficiently strong interactions to adsorb (their adsorption energy may be lower than thermal energy $k_B T$). On the other hand, the polymer fractions adsorb onto the cement particle and they are expected to induce the main fluidifying effects by inducing steric or electrostatic repulsion.

In what follows, we discuss the adsorption of the polymeric fraction of PCA-1. Four different situations are considered: two cements (with and without grinding aid), and two modes of adding superplasticizer (direct or delayed). In order to clarify data analysis, we start with the case of cement without grinding aid, when PCA-1 is included in mixing water (direct addition). Adsorption of the PCA-1 fractions can be seen in Figure 8-4 as a function of the retention times (RT) of these fractions. The values in this figure correspond, for each PCA-1 fraction, to the amount of added PCA-1 below which all the given fraction is adsorbed. For instance, the fraction with RT = 14.7 min (F1) is totally adsorbed until more than 73 nmol/m² PCA-1 are added to the suspension. Above this concentration, the excess of this fraction remains in the aqueous phase. Below it, the entire fraction can be adsorbed onto the surface of the cement particles. On the other hand, the fraction with RT = 22.3 min (F5) is totally adsorbed only until 53 nmol/m² PCA-1 are added. This means that below 53 nmol/m², both F1 and F5 can be totally adsorbed. Between 54 and 73 nmol/m² of added PCA-1, all F1 can be adsorbed,

while an excess of F5 remains in solution. Above 73 nmol/m^2 , both fractions are beyond saturation and their excess remain in the aqueous phase.

However, it is difficult, because of the magnitude of experimental errors to decide whether such differences are statistically significant. In order to solve this uncertainty, we must decide whether retention time and adsorption (plateau) are correlated. This is done by testing the degree of confidence with which one can reject the absence of such a correlation. A high value means there is a correlation. A low value means, that there might be a correlation, but if so, its effect cannot be detected within experimental errors.

When PCA-1 is added in mixing water (Figure 8-4), adsorption turns out to be well correlated with retention time (Table 8-3, first line). The confidence interval for rejecting the absence of such a correlation is higher for cement without grinding aid (99%) than for cement with grinding aid (92%). Both confidence levels decrease when PCA-1 is added after 30 min hydration (Figure 8-5), as indicated in the second line of Table 8-3.

A correlation is clear between retention time and adsorption for cement without grinding aid. For cement with grinding aid, this correlations are lower, because errors are larger. The reason why larger errors are obtained with cement with grinding aid is unclear. However, it appears reasonable to conclude that on both cements, adsorption is correlated with retention time. In other words, the fractions with high retention times reach saturation for lower amounts of added PCA-1.

In order to interpret this correlation, it is necessary to relate retention time to a property of the different PCA-1 fractions. With similar HPLC methods, Piotte *et al.* (1995) found, for PNS, that the fractions containing the largest polymers have the largest retention times. For PCA-1, it is also possible that retention times are linked to conformation differences. In this case, the fractions with the largest retention times would have the highest surface interaction with the HPLC column. It is most likely that these same fractions will also require larger surface areas for adsorption onto the surface of cement particles. Both cases may therefore be united and we can consider that larger retention times can be associated with larger surface requirements for adsorption. In turn, this would mean that the fractions having the larger surface requirements per molecule reach saturation for lower amounts of added superplasticizer (lower surface coverages). Up to a certain amount of added superplasticizer, all fractions adsorb. Then, beyond a certain surface coverage, some fraction can no longer adsorb. The fractions with smaller retention times need less space than the fractions with larger retention times. They can still find adsorption sites when the others cannot.

It should be noted that adsorption of PCA-1 fractions are not found to be correlated with initial peak intensities. Therefore, a straight forward kinetic law linked to polymer availability is insufficient to explain adsorption differences.

The correlation between polymer fractions and adsorption shows that a global analysis of polymer adsorption (by spectrometric UV absorption or total organic content) results in a loss of information. This could lead to misinterpretation of data when trying to relate adsorption properties to rheological data.

An effect of polydispersity is seen with PCA-1 which has a relatively low polydispersity coefficient (2.6). Larger effects could therefore be expected with polymers such as PNS or lignosulphonates which usually have relatively large polydispersity coefficients [Piotte et al (1995), Zhor and Bremmer (1997)]. For instance, the samples of ultrafiltrated lignosulphonate which perform best in the study by Zhor and Bremmer (1997), have dispersities still larger than PCA-1. Separations and better understanding of optimal usage should allow increased performances with lignosulphonates at relatively low cost since (lignosulphonates are a waste product from the paper industry). However, such an approach is not expected to remain cost efficient if performances similar to those of synthetic polymers are required.

9.1.2 Effect of Hydration Time

Superplasticizers can be used either to decrease the amount of required water for a given workability or to increase workability at a given solid loading. In the first case, superplasticizers are added with the mixing water, while in the second, they are added after a given time as concentrated solutions. Various authors have shown that superplasticizers alter the morphology of early hydrates such as ettringite (cubes instead of needles). This is mainly going to affect the applications of the first category. Therefore, when discussing diverse effects of superplasticizers between such systems it is important to introduce chemical dynamics. This also includes considering whether adsorption is influenced by cement hydration.

Results in Figure 8-6 and Figure 8-7 show that hydration decreases adsorption on both cements. The levels of significance are very high for cement without grinding aid and a little lower for the cement with grinding aid (Table 8-4). This decrease might be due to coprecipitation and/or intercalation with ettringite.

9.1.3 Effect of grinding aid (triethanol amine acetate)

No significant difference is seen between both cements at either hydration time (Figure 8-4, Figure 8-5, Table 8-5). It is therefore concluded that if grinding aid alters adsorption, its effect is too small to be detected within experimental errors of these measurements. It must be noted that errors are systematically larger for the cement with grinding aid. This decreases both confidence levels when comparing one cement to another. However, even if an effect due to the grinding aid (triethanol amine acetate) was present, it would remain small.

On the other hand, with PCA-2, there is a clear effect of the grinding aid, which increases adsorption. The fact that PCA-2 is effected by the grinding aid and not PCA-1 must be linked to the chemical effect this product has on the early hydration reactions of cement. Triethanol amine is indeed reported to complex ions from C_4AF phase and thereby enhance their dissolution [Gartner and Myers (1993)]. This molecule therefore increases the amount of aluminates, which might be able to coprecipitate/intercalate the polymer. PCA-1, which does not form micelles (not detected by HPLC) is probably not sensitive to aluminates and therefore almost not effected by the presence of grinding aid. PCA-2 on the other hand, forms micelles with aluminates and is probably highly sensible to the presence of aluminates. We believe this is the reason why with the same specific surface, the cement with grinding aid adsorbs (consumes) more PCA-2 than without grinding aid.

9.2 Rheology

9.2.1 Effect of dosage

For both cements, the minimum yield stress is systematically lower with polymer PCA-1 than with PCA-2. PCA-2 is the fastest adsorbing, as indicated by ordinates at the origin in Figure 8-2 and Figure 8-3. Therefore the lower yield stress induced by PCA-1 is not the result of faster adsorption kinetics of this polymer.

For PCA-2, the fluidification can clearly be attributed only to the adsorbed polymers. For PCA-1, the situation is more complicated. First, there is the effect of polydispersity. Second, there is its important adsorption variation between 5 and 30 minutes. The amount adsorbed at the moment the yield stress is measured must lie in between these two values. So, the amount required is probably close to the adsorbed amount. Because the model systems, as well as the cements with PCA-2 indicate that the

effect is only linked to the adsorbed polymer, we are inclined from these results to extend this conclusion to PCA-1.

9.2.2 Origin of dispersion force

The fact that dispersion seems only linked to adsorbed polymers means that the dispersing effects must be linked to either steric or electrostatic repulsion, or both. Since in model suspensions both PCA-1 and PCA-2 were both found to induce the same zeta potential, this factor cannot account for observed rheology differences.

PCA-1 is larger than PCA-2, so it can most likely induce a larger steric repulsion. In addition, the charge it induces onto the cement particles is farther away from the surface. This means that plane of origin for calculating electrostatic repulsion may be farther away from the plane of origin for the van der Waals forces than for PCA-2.

Differences in planes of origin for interparticle force calculations were found to be responsible for deviations from theory of surface force measurements in silica based systems. Which of these two effects is dominant remains to be determined.

Finally, one sees that the cement with grinding aid is characterized in its dispersed state by lower yield stresses than the polymer ground without grinding aid. Both cements were ground to obtain the same specific surface area. Therefore, more energy (longer time) had to be put into the grinding of the cement without grinding aid, probably causing surfaces to be more reactive. On the other hand, one of the designed effects of this grinding aid is to complex the ions from the C_4AF phase, which is often found around the C_3S . This complexation increases dissolution thereby the setting rate. On smaller time scales, it is possible that this dissolution might help to dissolve some interparticle bridging bonds.

9.3 Conclusions

9.3.1 Adsorption

PCA-1 and PCA-2, two polymers differing mainly from their molar mass distributions have been considered. Polymer PCA-2, which has a narrow molar mass distribution, is used to show how

adsorption can be determined provided adsorption follows a step like function. Polymer PCA-1 is used to show the effect of polydispersity on adsorption.

It is found that the various fractions of its polymeric part do not adsorb in the same way. This is an important result, because it shows the importance of using HPLC when determining polymer adsorption onto powders. With PCA-1, overall analysis such as TOC or UV adsorption might lead to data misinterpretation (50% risk of committing an error larger than 30%).

It has been reported that maximum performance of superplasticizers is often achieved before surface saturation (Ferrari et al (1997), Matsuyama et al (1997)]. This can be due to the polydispersity of the polymers used. For instance, if steric repulsion is a dominant mechanism, the larger polymers would be expected to be most effective. Completing adsorption of these fractions required a lower quantity of PCA-1 than for completing adsorption of the other fractions. This means that if one determines the amount of added polymer required to complete adsorption by an overall analysis of polymer content, the value obtained is larger. Therefore, traditional adsorption methods can lead to overestimating polymer requirements for surface saturation of the most effective polymeric fractions. Comparing such results with rheological data can then lead to believing that the surface does not need to be saturated to reach optimal workability, which is precisely what the above mentioned researchers find. In fact, the surface might have to be saturated with the larger and most effective polymeric fractions.

Another factor which should not be underevaluated is the solid loading. We have shown earlier, using model systems, that superplasticizer dosage and solid ratio are not independent parameters. Furthermore, it appears that the maximal solid loading is reached for total surface coverage. Therefore, with higher solid loadings, polymer requirements might well increase for the above mentioned studies.

Addition time is also shown to alter superplasticizer adsorption, while a grinding aid containing triethanolamine acetate does not have a significant effect. Resolving the question of the effect of a grinding aid is important, since it could be a hidden parameter between cements of different origins. It seems that grinding with triethanolamine (a couple ppm) to achieve the same surface area does not alter polymer adsorption.

9.3.2 Rheology

Dispersion mechanisms are mainly linked to adsorbed polymers. This conclusion has been reached from polymer PCA-2, which is found to adsorb rapidly. In addition its adsorption exhibits a step like function. This means that until the surface is covered, almost all the polymer added is adsorbed.

In this case, it is easy to see whether optimum dispersion is reached with or without needing to over-dose the superplasticizer with respect to the adsorption capacity of the cement in suspension. It was found for PCA-2, that optimum dispersion was reached before plateau in adsorption isotherm. This is in agreement with model systems.

On the other hand, PCA-1, a polymer of the same type as PCA-2 but with a larger molar mass and molar mass distribution, had slower adsorption kinetics. The amount adsorbed at the moment of measuring is however probably close to the amount adsorbed.

9.4 Implication of the behaviour of cement suspensions

Though limited in number, the rheology results presented in chapter 8 are consistent with conclusions reached by the study of model inert systems. It appears that effects are mainly linked to adsorbed polymers. In addition, the presence PCA-2 forms micelles in presence of aluminates and probably is coprecipitated/intercalated in ettringite.

So, dispersion mechanisms must be looked at considering electrostatic and steric repulsion only. In addition, there must be a chemical effect strongly linked to the presence of aluminates.

Chapter 10 Interparticle forces and yield stress

So far, we have shown that, in model suspensions, dispersion influenced by our superplasticizers is linked only to adsorbed polymers. In cement suspensions, the situation appears a little more complicated. Early chemical reactions can lead to coprecipitation or micellisation of a part of the superplasticizers, especially with direct addition. In such a situation, solution depletion gives the amount of consumed polymer, which is the sum of the amount adsorbed and coprecipitated. However, when dosage/performance response of cement suspensions is compared to adsorption (consumption) isotherms, we also reach the conclusion that the maximum performance can be reached without excess polymer in the liquid phase.

In this chapter, we capitalise on this conclusion in order to develop interparticle force calculations for which the polymer contribution is only linked to adsorbed polymers. Because these calculations strongly depend on particle size, we first present a procedure for integrating the wide particle size distribution of cement suspensions. These results are then integrated into a pragmatic model for direct evaluation of yield stress.

10.1 Problem of energy normalisation

In cement suspensions, the interparticle potential only has a primary minimum. Therefore in absence of external forces, cement particles will always tend to agglomerate because of this minimum. The whole purpose of calculating interparticle forces is to determine whether external forces such as shear or Brownian motion can separate these agglomerates.

If they can, then these particles behave individually and have a smaller effective volume than the agglomerated doublet. This means that the viscosity decreases if the external forces overcome the maximum attractive interparticle force.

In what follows, we consider both shear and Brownian motion as possibilities for dispersion from this primary minimum.

10.1.1 Brownian motion

In colloid science, a suspension is usually considered stable if Brownian motion is capable of breaking doublets provided the potential well is not deeper than a certain multiple of the thermal energy $k_B T$. Many values are found in the literature, typically between 2 and 15 $k_B T$.

For a given well depth Φ_{\min} , it is possible to evaluate the time scale for the breaking up of doublets by:

$$t_{break-up} \cong \frac{6\pi\mu a^3}{k_B T} \exp\left(-\frac{\Phi_{\min}}{k_B T}\right) \quad [10-1]$$

Equation [10-1] shows that the time scale is very sensitive to particle size. In pure water, a doublet with $a=1\mu\text{m}$ it would be 34 seconds for a 2 $k_B T$ well and 1.2 days for 10 $k_B T$ well. Note that for the well dispersed cement suspensions studied with $W/C = 0.35$, the viscosity high shear is around 0.2 Pa s. So the break-up times would be about 2 hours and 5.5 years.

In addition, the particle size of $a = 1 \mu\text{m}$ is the low boundary of cement particles. So, only extremely low potential wells could lead to stable dispersions by Brownian motion.

10.1.2 Shear forces

Another way of dispersing agglomerated particles is by applying shear forces. The dimensionless Peclet number Pe evaluates the relative importance of these forces with respect to Brownian forces:

$$Pe = \frac{3\pi\mu a^3}{k_B T} \dot{\gamma} \cong \frac{3\pi a^3}{k_B T} (\tau_0 + \mu_{Bi} \dot{\gamma}) \quad [10-2]$$

For $Pe < 1$, Brownian motion dominates, while for $Pe > 1$ hydrodynamic forces dominate. In pure water, a cement particle with $1 \mu\text{m}$ radius would already have a Pe of 2.3, for a shear rate of 1 s^{-1} . In water, the shear rate giving $Pe = 1$ for this particle is 0.44 s^{-1} .

If we now take into account the higher viscosity of cement suspensions, assuming a Newtonian viscosity of 0.2 Pa , the Pe number becomes 460 for a shear rate of 1 s^{-1} (or 0.002 s^{-1} for $Pe=1$).

In presence of a yield stress the Pe number becomes very large. For instance with 1 Pa yield stress $Pe = 4'290$ for zero shear rate. Note that Bingham model is not relevant in this region, but it allows evaluation of the relative importance of the phenomena under consideration.

These calculations indicate that, in cement suspensions, shear should largely dominate over Brownian motion, even at extremely small shear rates.

Time scales for the break-up of agglomerates should therefore not be discussed in terms of shear forces and not in terms of Brownian motion.

10.2 Interparticle forces

We have just shown that we must consider the stability of cement suspensions with respect to applied shear. We are therefore primarily concerned with determining the maximum attractive interparticle force between any doublet, rather than the depth of a potential well. In this section, we use the equations for the dispersion, electrostatic and steric forces presented in chapter 3. We show that, at small separations, all these forces depend on the harmonic average radius of the interacting particles. This allows us to determine F_{max}/\bar{a} independently of the particle sizes.

10.2.1 Dispersion force

In chapter 3, we showed that for the size range of interest to cement suspensions, the dispersion force could be written as:

$$F_{(a_1, a_2, h)} = -\frac{A_{(h)}}{6} \left(\frac{-\bar{a}}{2h^2} + \frac{-1}{2\bar{a}} + \frac{1}{h} \right) \quad [10-3]$$

For small separations, this simplifies to :

$$F_{(a_1, a_2, h)} \cong A_{(h)} \frac{\bar{a}}{12h^2} \quad [10-4]$$

Because the aqueous phase of cement suspensions is a very concentrated electrolyte, the static term in the dispersion interaction is screened. Retardation, which describes the decrease of the Hamaker constant $A_{(h)}$ with increasing separation is taken into account.

Because proper Hamaker constants of cement components are not yet available at the time of writing this section, the Hamaker constant for magnesium oxide will be used.

10.2.2 Electrostatic force

In chapter 2, we have shown that it is possible to describe the aqueous phase of cement suspensions, which contains many different electrolytes by an equivalent binary electrolyte. We were then able to assess the validity of the Debye-Hückel approximation for the electrostatic repulsion between spheres maintaining an identical and constant potential upon approach. This repulsive force can be written as:

$$F_{ES} \cong -2\pi\epsilon\epsilon_0\bar{a}\psi^2 \frac{\kappa e^{-\kappa h}}{(1 + e^{-\kappa h})} \quad [10-5]$$

With the Debye length given by:

$$\kappa^{-1} = \sqrt{\frac{\epsilon\epsilon_0 k_B T}{2e^2 z_+^2 n_+^b}} \quad [10-6]$$

One of the problems for calculating this force, is the surface potential ψ . This is the potential at the outer bound of the Stern layer, which is the layer in which ions are linked to the surface and not to influenced by Brownian motion. Often, one uses the experimentally determined zeta potential, which is the potential at a shear plane. This plane is situated somewhat farther from the surface than the Stern plane. So, it leads to an under-evaluation of the electrostatic force. In many situations however, this approximation might be valid.

In our case, the charge is induced by adsorption of ionic polymers. Zeta potential measurements are based on relative motion between particles and the surrounding fluid. This motion can compress somewhat the layer of adsorbed polymers, thus modifying the distance at which the potential might be

measured. Polymer layers can be compressed up to a certain extent. There is a limit to how much this layer can be compressed. It is the limit beyond which, in the scaling theory of steric interactions, the steric force goes to infinity.

Let us evaluate this thickness from adsorption data. In order to avoid effects of chemistry (cement) and porosity ($\text{Mg}(\text{OH})_2$), we will use data for MgO. In addition, we will consider PCA-1, the adsorption of which is hardly effected by temperature. The amount of PCA-1 adsorbed onto MgO is $753 \mu\text{g m}^{-2}$. If we assume the density of this layer to be $1400 \mu\text{g mm}^{-3}$ (1.4 g cm^{-3}), and that 75% of the mass can be attributed to the polymer, then we have $1050 \mu\text{g mm}^{-3}$. This leads to the conclusion that the totally compressed thickness would be about 0.7 nm, giving a minimum separation of 1.4 nm.

The Debye length is even smaller. **So, if the potential plane were placed at the surface of the particle, the force would already have dropped by about 88% of its value. Placing the plane of origin of the electrostatic force at the surface of the particle instead of the surface of the compressed layer would therefore lead erroneously to completely neglecting any electrostatic effects.** We emphasise that in reality the plane is probably even further away from the surface, and that electrostatic interactions will contribute to repulsion as soon as adsorbed layers begin to overlap.

In fact, de Gennes (1987) states that the hydrodynamic layer thickness scales in the same way as the adsorbed layer thickness. He mentions that this is confirmed by experimental data, though in some cases the hydrodynamic layer might be even larger. For this reason we will consider that during zeta potential measurements, hydrodynamic forces are not sufficient to significantly compress the adsorbed layer. Therefore we place the plane of origin of electrostatic forces at the surface of the adsorbed layer.

So, we can reformulate the electrostatic force, integrating the adsorbed layer thickness L:

$$F_{ES} = -2\pi\epsilon\epsilon_0\bar{a}\psi^2 \frac{\kappa e^{-\kappa(h-2L)}}{(1 + e^{-\kappa(h-2L)})} \quad [10-7]$$

As the layer gets compressed we will adjust the value of L, thus maintaining the electrostatic force constant during compression. In fact, we will show that compression is negligible in the determination of the maximum attractive force. This approximation therefore does not have major consequences for our calculations.

10.2.3 Steric force

The steric force begins as soon as the adsorbed layers begin to overlap. It increases strongly and reaches infinity as the maximum compression is reached. The functionality of this increase is highly dependent on the adsorption mode (conformation) of the polymer. Pedersen and Bergström (1999), under their experimental conditions, reached the conclusion that PAA adsorbed in a mushroom like conformation under conditions. Though their surface has a significant negative charge, which increases the layer thickness, we consider there are enough similarities with our suspensions to also suppose a mushroom conformation. For such adsorption modes, the scaling theory developed by de Gennes is increasingly used to calculate the steric force. We have for the steric force:

$$F_{Ste} = \bar{a} \frac{6\pi k_B T}{s^2} \left[\left(\frac{2L}{h} \right)^{5/3} - 1 \right] \quad [10-8]$$

Where s is the distance between the centres of two neighbouring mushrooms. This is twice the radius obtained from adsorption data, assuming a compact layer of spheres, disks or mushrooms. L is the maximum length extending into the solvent.

10.2.4 Total interaction

We have indicated that owing to the large sizes of cement particles, shear forces largely dominate over Brownian motion, even at low shear rates. We therefore need to calculate the maximum attractive force between two particles in order to decide whether shear is capable of separating them.

The equations above indicate that at small separations, dispersion, electrostatic and steric forces are all proportional to the interaction radius \bar{a} . We can write:

$$G = \frac{F}{\bar{a}} = \frac{F_{vdW} + F_{ES} + F_{Ste}}{\bar{a}} = \frac{A_{eff}(h)}{12h^2} - 2\pi\epsilon\epsilon_0\psi^2 \frac{\kappa e^{-\kappa(h-2\lambda)}}{(1 + e^{-\kappa(h-2\lambda)})} - \frac{6\pi k_B T}{s^2} \left[\left(\frac{2L}{h} \right)^{5/3} - 1 \right] \quad [10-9]$$

Figure 10-1a and b give the variation of the interparticle force as a function of separation, for three potentials and for polymer layers of 1 and 3 nm respectively. Positive values indicate attraction and negative values repulsion (recall that the force is the derivative of a potential with respect to separation). These figures show clearly that compression is not important at the point where the

maximum attractive force is reached. Indeed, in absence of electrostatic repulsion this maximum is reached for separations of about twice the maximum length of the layer extending from the surface into the solvent. When electrostatic effects come into play, the point of maximum repulsion is beyond this distance. Note that this does not mean that the particles will not come into sufficient contact to lead to layer compression. It means that the maximum force, which we are concerned with for yield stress calculations, is barely effected by the capacity of the layer to be compressed.

So, we can say that there is a definite steric effect. This effect can be significantly complemented by electrostatic repulsion, provided it is reasonable to place the potential (as a measured zeta potential) at the outer bound of the adsorbed layer.

10.2.5 Maximum interparticle force

We have determined numerically for a series of polymer layers and potentials, which is the maximum interparticle force (Annex E). Results using MgO spectral information are given both in Figure 10-2 and Figure 10-3. They show the dominant effect of the adsorbed layer thickness. It also indicates, that for thin layers, the electrostatic contribution must not be overlooked, provided the plane of origin may be placed at the outer-bound of the adsorbed layer.

Figure 10-2 illustrates well the effects of both electrostatic potential ψ and adsorbed layer thickness L . However, it is not convenient for identifying the precise value of G for specific combinations of ψ and L . For this we also plot a projection of this graph in Figure 10-3.

10.3 Problem of wide particle size distribution of cement

We have previously seen that the maximum attractive force between particles is proportional to the harmonic radius average of both particles.

$$\bar{a} = \frac{2a_1a_2}{a_1 + a_2} \quad [10-10]$$

Only in the case of particles of same sizes is this radius equal to the arithmetic average. If both particles have very different sizes ($a_2 \gg a_1$), we get: $\bar{a} \cong 2a_1$.

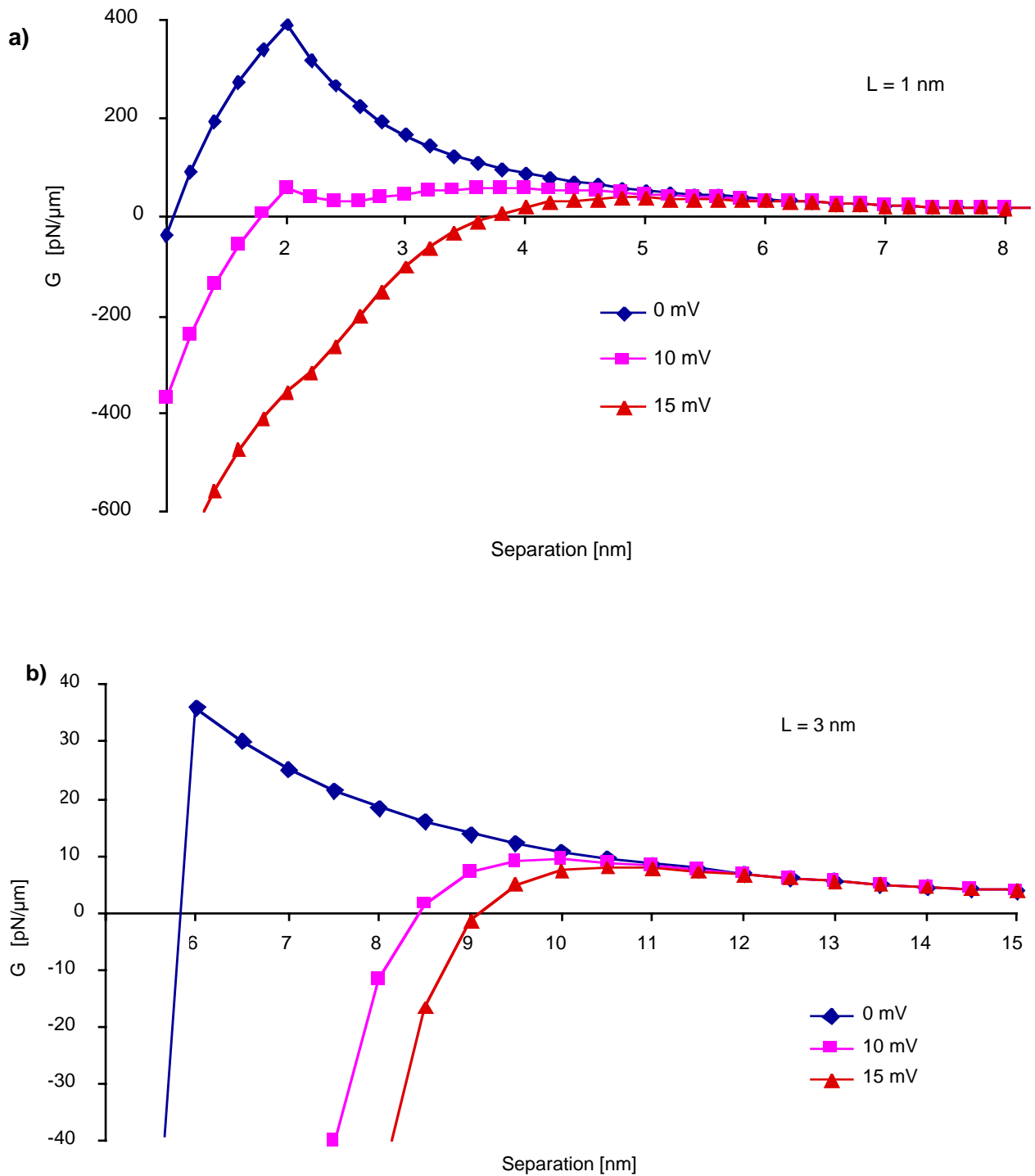


Figure 10-1. Normalised interparticle force as a function of separation, for three different potentials. Positive values indicate attraction and negative values repulsion. Adsorbed layers are 1 nm (a) and 3 nm (b). Computed for MgO particles, in the equivalent symmetric electrolyte representation of a cement suspension.

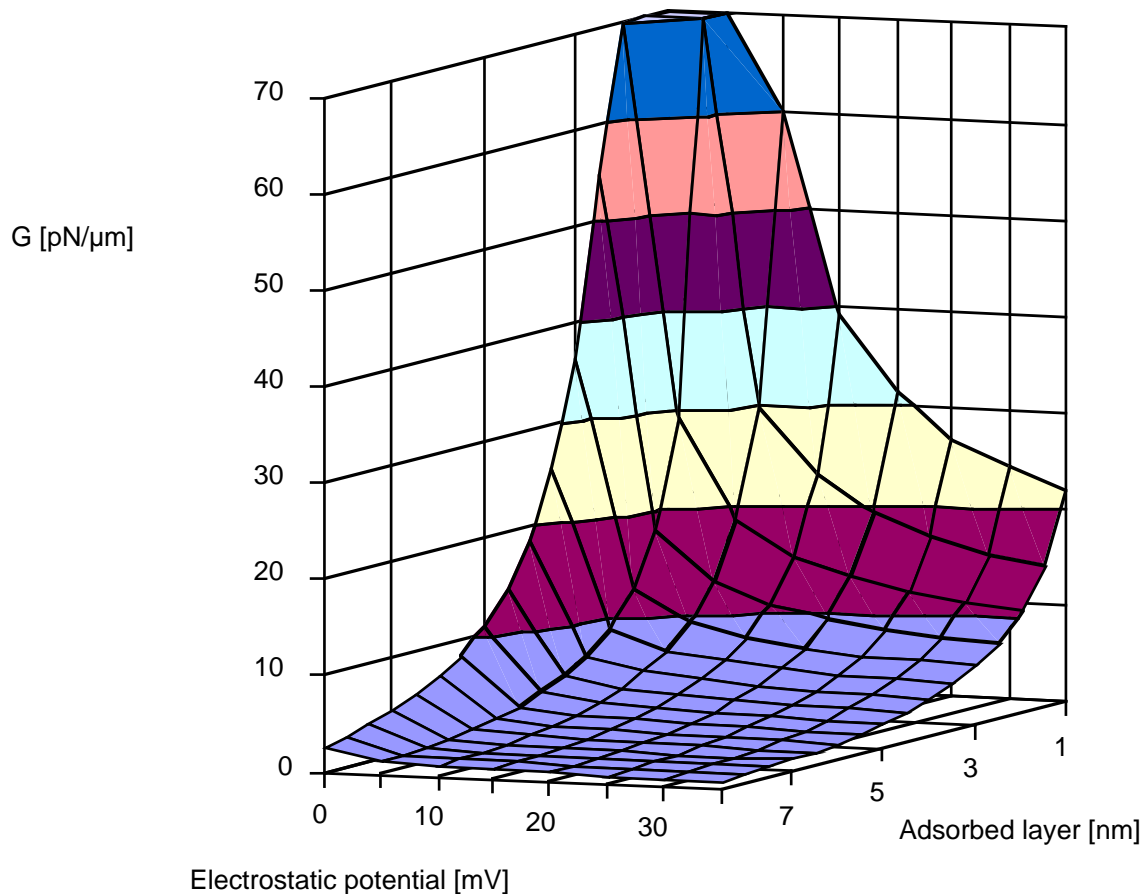


Figure 10-2. Normalised maximum attractive force G , determined using the equivalent symmetric electrolyte representation for a cement suspension and using optical data of MgO particles. All adsorbed layers are considered to have a minimum compressed thickness of 0.7 nm .

Our final objective is to relate interparticle forces to the yield stress of cement suspensions containing superplasticizers. We assume that effects can be related to the pairs of interacting particles. Therefore we need to identify the frequency of interacting particle pairs of different sizes. For cement, the particle size distribution of cement can typically range over two orders of magnitude, so it is important to properly evaluate the interactions between particles of different sizes.

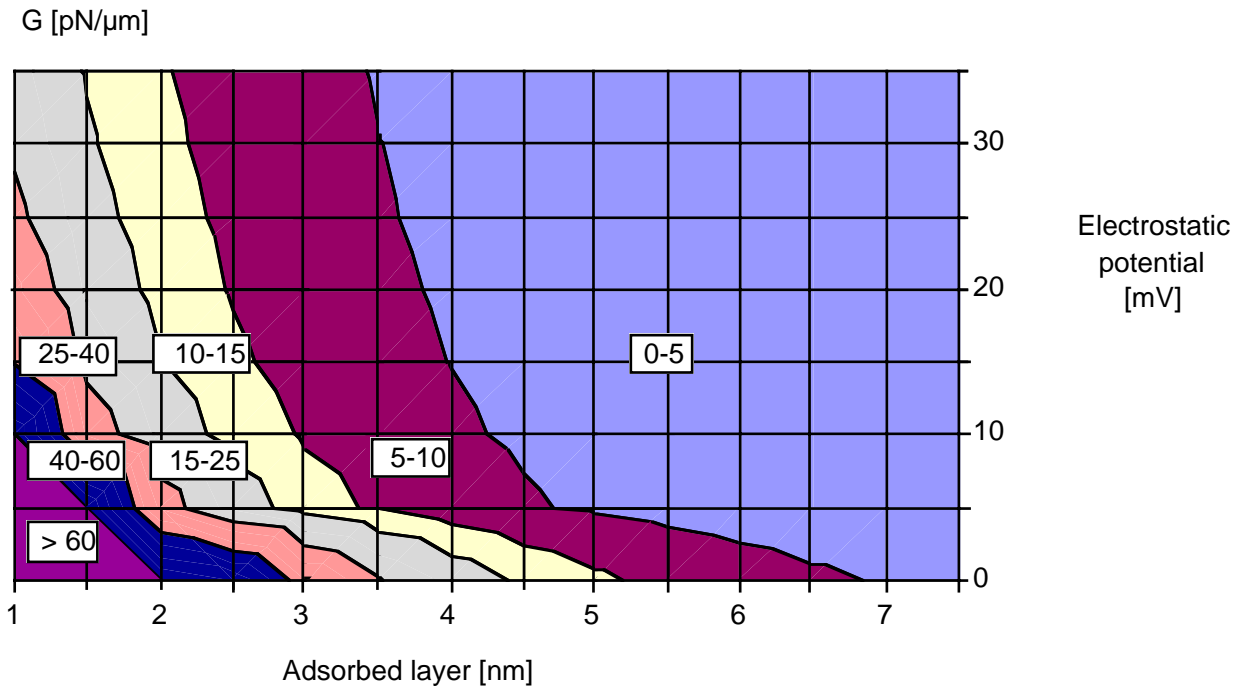


Figure 10-3. Normalised maximum attractive force between two MgO particles. All adsorbed layers are considered to have a minimum compressed thickness of 0.7 nm.

For this we have used a computer program [Roelfstra (1989)], which for a defined particle size distribution places cement particles randomly in a box. It starts with the larger particles and finishes with the smaller ones. If a position is already occupied, the particle is replaced randomly until an available position is found. The algorithm was developed for initialising a computer simulation of cement hydration. Periodic boundary conditions are chosen in order to avoid any edge effects. One limitation is that in the category of the largest particles, only one particle is placed. Therefore we cannot find interactions with the largest class range. However, since their frequency must be low, this does not seem too serious a limitation of this approach.

For illustration, a vertical cut in such a cube is shown in Figure 10-4. Note that the diameter of the circles is only the diameter of the plane cuts the spheres through their centres. We have used the particle size distribution of both Olten and Misubishi cements and a volume fraction of 48% corresponding to a water cement ratio of 0.35, which was used in our rheology measurements. Note that Olten cement with and without grinding aid (triethanol amine acetate) had the same particle size distribution. So we only need to perform a calculation for both these cements.

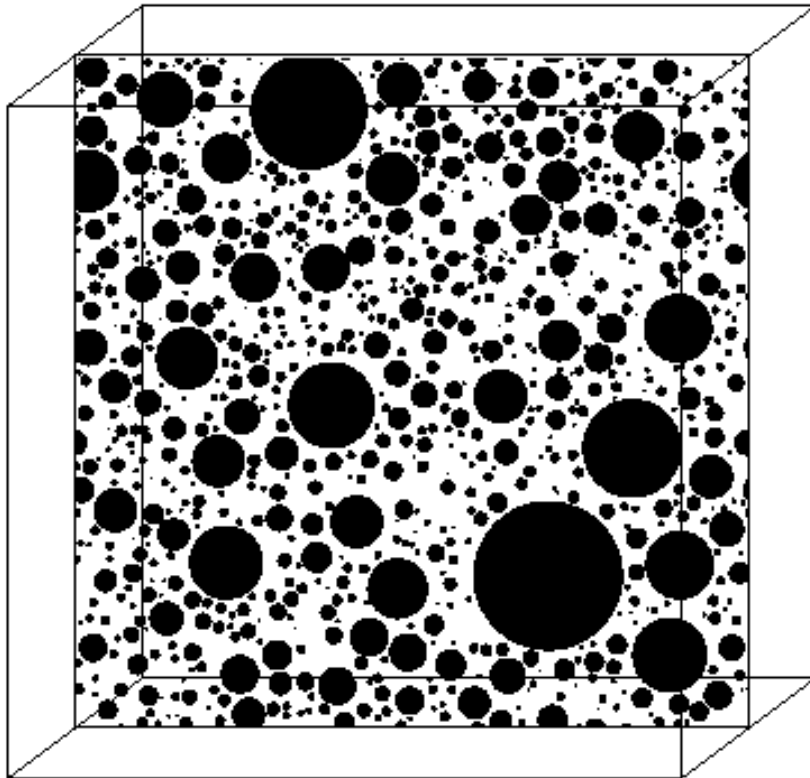


Figure 10-4. Vertical cut in a cube in which spherical particles are placed according to an experimentally determined particle size distribution. Periodic boundary conditions are used in order to avoid edge effects.

At this point, the problem is to decide under which conditions two particles may be considered as interacting. So far, we have decided to define a minimal interparticle distance below which particles are considered to be in contact. This distance was taken once to be the size of the smallest particle and once three times this size. So, if the smallest particle is $1\ \mu\text{m}$. All particle pairs, which have a minimal surface to surface distance smaller than $1\ \mu\text{m}$ (or $3\ \mu\text{m}$ for the second case) will be considered to be in contact. This has been done with the measured particle size distributions of the Olten and Mitsubishi cements used in the Eureka project.

Figure 10-5 and Figure 10-6 give the particle size distributions of these cements. They also give the cumulated frequency of the average diameters of the identified doublets (Annex F gives the Microsoft Excell Macro for this). These average diameters are once the harmonic and once the arithmetic average of the diameters of both particles. These figures clearly show that the using the volume average diameter for interparticle calculations would be incorrect. The best type of average would be a surface average for the Olten cement (Figure 10-5), while it would be a diameter average for the Mitsubishi cement (Figure 10-6). Since the most appropriate type of average to use depends of the

particle size distribution, it is better to determine numerically the average diameter of the interacting particles.

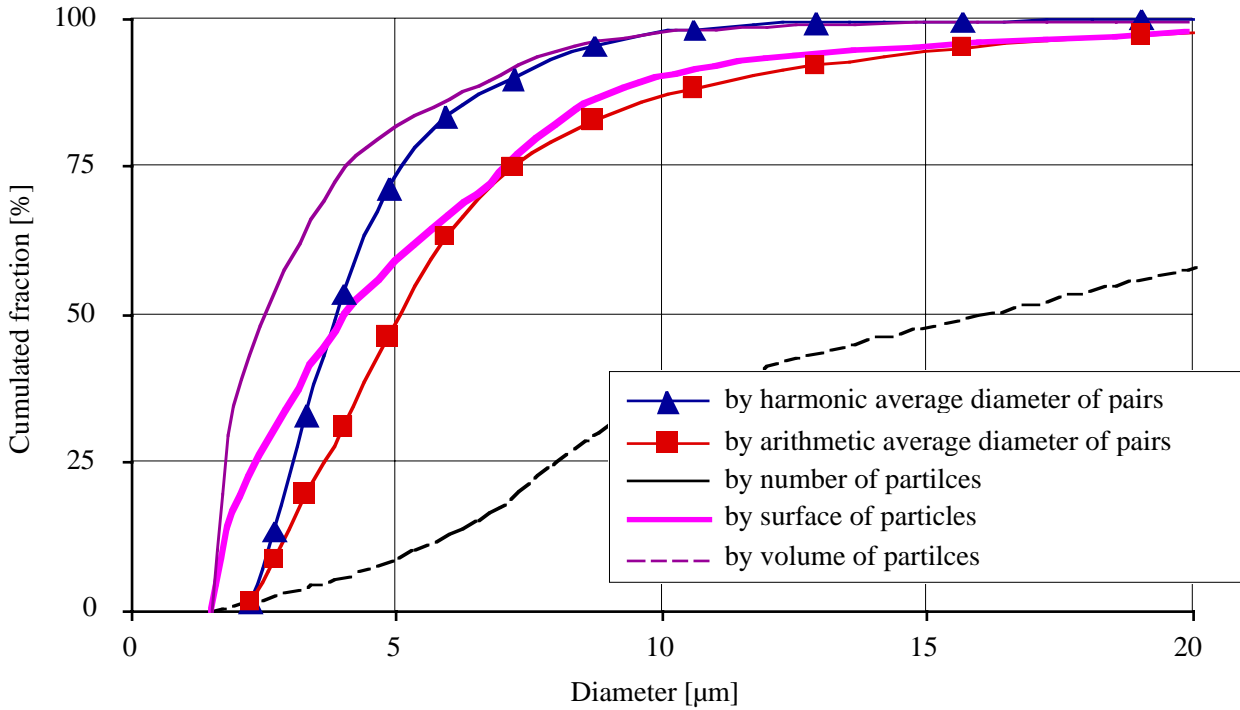


Figure 10-5. Olten cement (without grinding aid). Cumulative distribution of particle size (in volume, surface and number) and of pair interactions. Harmonic and arithmetic averaged diameters are given.

To simplify comparison, we compute the average of all these diameters as follows:

$$\langle \bar{a} \rangle = \frac{\sum_i n_i \bar{a}_i}{\sum_i n_i} = \frac{\sum_k \sum_{l \geq k} n_{k,l} \frac{2a_k a_l}{a_k + a_l}}{\sum_k \sum_{l \geq k} n_{k,l}} \quad [10-11]$$

$$\langle \hat{a} \rangle = \frac{\sum_k \sum_{l \geq k} n_{k,l} \hat{a}_{k,l}}{\sum_k \sum_{l \geq k} n_{k,l}} = \frac{\sum_k \sum_{l \geq k} n_{k,l} \frac{a_k + a_l}{2}}{\sum_k \sum_{l \geq k} n_{k,l}} \quad [10-12]$$

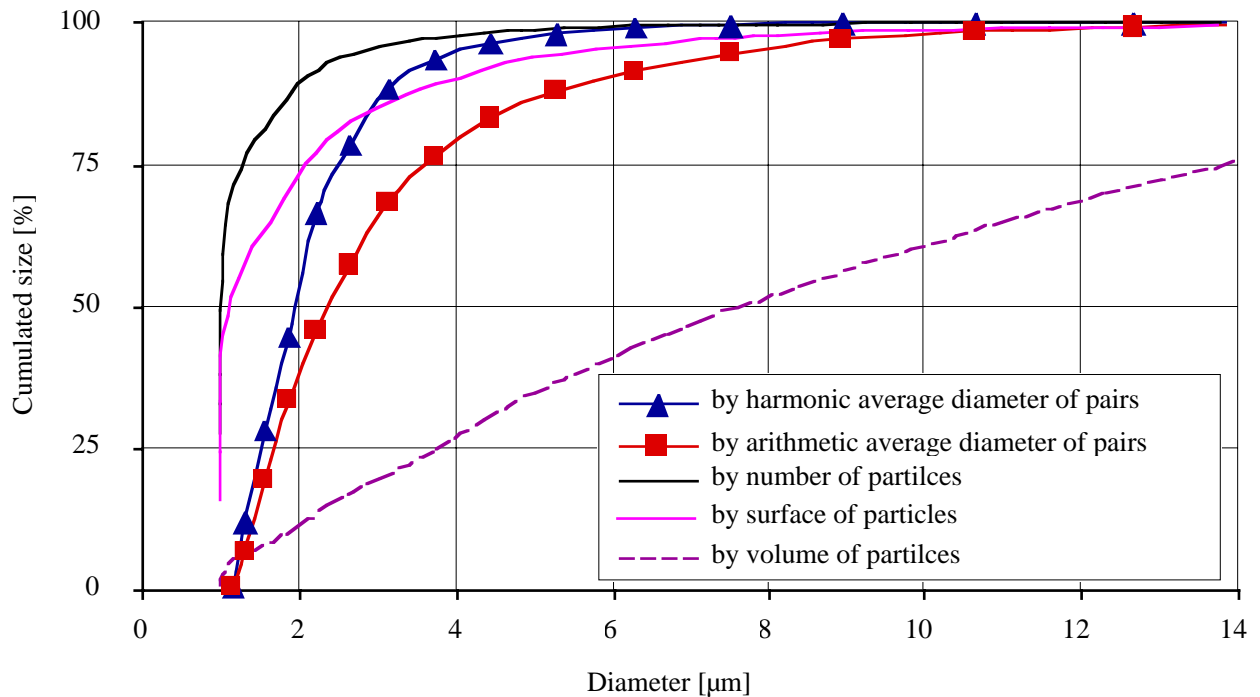


Figure 10-6. Mitsubishi cement. Cumulative distribution of particle size (in volume, surface and number) and of pair interactions. Harmonic and arithmetic averaged diameters are given.

Values are given in Table 10-1. They indicate that the harmonic average is not sensitive to the separation distance chosen. The arithmetic average is however more sensitive. The most sensitive parameter is the average co-ordination number.

10.4 Yield stress calculations

In this section we develop a direct calculation of yield stress values, based on results of interparticle interactions and particle size distributions.

In order to reach this objective, we must know the distribution of forces in the direction of the applied shear. We first develop a force balance between the interparticle forces of randomly oriented doublets. We then show how in a liquid system the applied shear will induce rotation of the doublets, which will reduce the time during which separation can take place.

The actual yield stress calculation is then presented in two parts. We first consider the system as a solid, in which no rotation of the pairs is taking place. This will lead to a relation indicating, for an applied shear stress, what fraction of pair interactions can be broken.

In the second part, we consider an observable time scale during which the solid to liquid transition occurs. The particles must therefore be separated at a given rate. Because this separation takes place in a viscous environment, there is a viscous resistance. We calculate these effects by considering the hydrodynamic interactions between doublets in close contact, using the lubrication analysis presented in chapter 3.

Table 10-1. Summary of pair interaction calculations for cements Olten (without grinding aid) and Mitsubishi. The total number of interactions and number averaged diameter of the harmonic and arithmetic average diameters are given. Cases considered are for separations of one and three radius of the smallest cement particle in the system.

Distance	Olten $\phi_{\min} = 2.05 \mu\text{m}$, cube side = 250 μm number of particles = 52'082			Mitsubishi $\phi_{\min} = 1.09 \mu\text{m}$, cube side = 120 μm number of particles = 49'373		
	Co-ordination Number	Average Interaction Radius		Co-ordination Number	Average Interaction Radius	
		Harmonic	Arithmetic		Harmonic	Arithmetic
1 * ϕ_{\min}	2.7	2.4	3.4	3.0	1.2	1.6
3 * ϕ_{\min}	10.0	2.2	2.9	11.5	1.1	1.4
1.1 μm	1.4	2.4	3.5	3.0	1.2	1.6
2.1 μm	2.7	2.4	3.4	6.0	1.4	1.5
3.3 μm	4.5	2.3	3.2	11.5	1.1	1.4
6.2 μm	10.0	2.2	2.9	36.6	1.0	1.3

10.4.1 Force balances

Projection of interparticle force

Our object is to relate the maximum interparticle forces to the shear stress, which must be applied in order to separate doublets and ultimately induce a solid to liquid transition. In other words, we want to relate these calculations to a yield stress. For this we need to break a certain number of the

interparticle forces. However, the shear stress is applied in a specific direction, while the orientation of the interparticle force is random.

Consider a doublet of spheric particles S_k and S_l , as represented in Figure 10-7a:

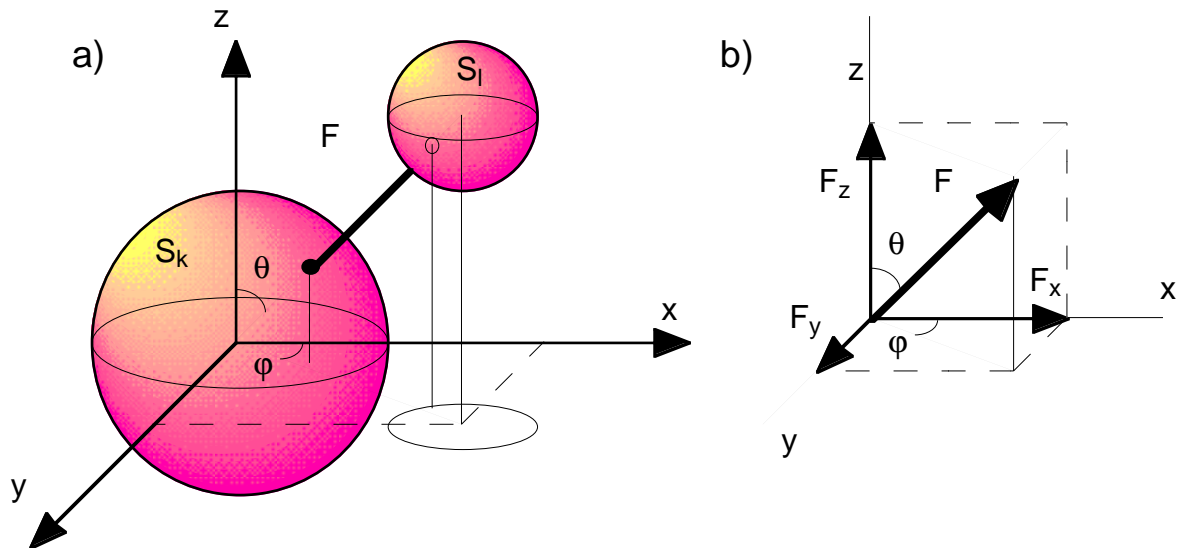


Figure 10-7. Representation of a pair of interacting spheres (a) and of the interparticle force in Cartesian and spherical coordinates (b).

Their interparticle force F is represented in Figure 10-7b. This force is along their line of centres and will cause them to approach one another until they are in contact. At this point a hard sphere interaction will lead to an equal and opposite force applied along the direction of the line of centres. We have:

$$F_x = F \sin \theta \cos \phi$$

$$F_y = F \sin \theta \sin \phi$$

$$F_z = F \cos \theta$$

[10-13]

Movement under shear

Let us consider a sheared system in which the force is applied in the positive direction of the x-axis. We assume that there is a constant shear gradient in the z direction. In absence of other forces, we can distinguish the following cases:

Case I.	$0 < \theta < 90$	and	$-90 < \varphi < 90$	S_1 moves away from S_k
Case II.	$0 < \theta < 90$	and	$90 < \varphi < 270$	S_1 moves towards S_k
Case III.	$90 < \theta < 180$	and	$-90 < \varphi < 90$	S_1 moves towards S_k
Case IV.	$90 < \theta < 180$	and	$90 < \varphi < 270$	S_k moves away from S_1

In what follows, we will assume that the doublets have a random orientation, which is not influenced by Brownian motion or gravity. A treatment of these factors has previously been carried out by Velleghol (1997), for doublets in an electrophoretic field.

Let us consider case I. We apply a shear force to S_1 , such that it will be equal and opposite F_x , the x-projection of the interparticle force felt by S_1 . Now, we have a situation in which the F_y and F_z can no more be balanced by a hard sphere interaction, because this force can only be along the line of centres. These unbalanced forces will result in the rotation of the doublet along both θ and φ angles. Rotation along φ should lead to an alignment into the x-z plane ($\varphi=0$).

For rotation along θ , the situation is more complicated once $\theta=0$ is reached, the shear force cancels. However, due to inertia the doublet should go to values of θ larger than 90. Contrary to the φ rotation situation, the shear will not induce a rotation in the opposite direction. At this point, it is the sphere S_k and no more S_1 , which will have the largest velocity along the x-axis. We have passed from case I to case III.

In case IV, the hard sphere force is increased to resist the shear force pushing S_k towards S_1 . As previously we are left with an unbalanced force system leading to rotation.

The final result is a rotation of the doublet around the y-axis (θ rotation) and an alignment into the x-z plane ($\varphi=0$). Only for the initial situation of $\theta=0$, will no rotation occur.

This rotation reduces the time during which the applied shear can lead to particle separation. The calculations we will perform to determine whether shear can separate particles must take this into

account. In the solid regime however, the doublets will not rotate, because the surrounding continuous media, ultimately provides the forces opposing the unbalanced projections of the interparticle forces.

Nevertheless, we must therefore deal with the initial random orientation of particles, which is somewhat similar to considering a set of particles all rotating at the same speed.

Rupture Stress per doublet

Let us now consider our suspension, while it can still be considered in the solid regime. For a randomly oriented doublet, the shear stress, we consider that from the macroscopic stress, the stress, which can effectively be used to separate the doublet is given by:

$$\tau_{k,l,\theta} = \tau_{k,l} \cos \theta \quad [10-14]$$

This indicates the stress is equal to zero if the doublet is aligned in the direction in which stress is applied, while it is maximum if the doublet is perpendicular to this direction.

This can be equated to the x-axis projection of the interparticle force [10-13], normalised by the average surface $\overline{\Omega}_{k,l}$, over which the stress is applied:

$$\tau \cos \theta = \frac{F \sin \theta \cos \varphi}{\overline{\Omega}_{k,l}} \quad [10-15]$$

Replacing the force by the maximum attractive interparticle force and using relations [10-9] and [10-10], we get:

$$\frac{G}{\tau_{k,l}} = \frac{\overline{\Omega}_{k,l} \frac{\cos \theta}{\sin \theta} \cos \varphi}{\bar{a}} \quad [10-16]$$

The average of $\cos(\varphi)$ can be obtained by:

$$\langle \cos \varphi \rangle = \frac{\int_0^{\pi/2} \cos \varphi \, d\varphi}{\int_0^{\pi/2} d\varphi} = \frac{2}{\pi} \quad [10-17]$$

Now we need to determine the average surface over which the shear stress must be applied per each doublet. We have chosen to first calculate the average intersection surface of a shear plane with each sphere:

$$\bar{\Omega}_i = \frac{\int_{-a_i}^{a_i} \pi(a_i^2 - h^2) dh}{\int_{-a_i}^{a_i} dh} = \frac{\pi}{2a_i} \left(2a_i^3 - \frac{2a_i^3}{3} \right) = \frac{2}{3} \pi a_i^2 \quad [10-18]$$

We have chosen to take the average of $\bar{\Omega}_k$ and $\bar{\Omega}_l$ both these surface to determine $\bar{\Omega}_{k,l}$:

$$\bar{\Omega}_{k,l} = \frac{\bar{\Omega}_k + \bar{\Omega}_l}{2} = \frac{\pi}{3} (a_k^2 + a_l^2) \quad [10-19]$$

Replacing [10-17], [10-18] and [10-19] in [10-16], we get:

$$\frac{G}{\tau_{k,l}} = \frac{2(a_k^2 + a_l^2) \cos \theta}{3\bar{a} \sin \theta} \quad [10-20]$$

Fraction of broken bonds

Care must be taken when evaluating an average value of the θ term, because values can vary between 0 and infinity. Assume we fix the value of G/τ , where τ here is the applied yield stress. Then, for each doublet, we have a critical angle θ_c , which satisfies the above equation and which will depend on the doublet. We can write this as:

$$\tan \theta_c = \left\{ \left(\frac{G}{\tau_{k,l}} \right)^{-1} \frac{2(a_k^2 + a_l^2)}{3\bar{a}} \right\} \quad [10-21]$$

This angle θ_c can be used to determine the fraction of bonds $f_{k,l}(G/\tau)$, which will not be broken for the fixed value of G/τ .

$$f_{k,l}(G/\tau) = \frac{\pi/2 - \theta_c}{\pi/2} = 1 - \frac{2\theta_c}{\pi} \quad [10-22]$$

We can calculate the total fraction of broken bonds as:

$$\frac{1}{2} \frac{\sum_k \sum_{l \geq k} n_{k,l} \left(1 - \frac{2\theta_c}{\pi}\right)}{\sum_k \sum_{l \geq k} n_{k,l}} \quad [10-23]$$

The 1/2 factor in front is to take into account the fact that only half the orientations can lead to separation, the others lead to compression.

Effective volume

Knowing the fraction of doublets, which must be separated to allow a liquid behavior, it is possible to judge the efficiency of a superplasticizer. In a polydisperse system, the dispersion of different doublets will not have the same effect on rheology. Non dispersed doublets have a larger effective volume than the individual particles. We choose to use this in order to evaluate the importance of the degree of dispersion, which must be reached in order to get a given yield stress.

This degree of dispersion will depend on the volume fraction of solids. We consider that there is a maximum effective volume fraction, which can be reached, for instance 59% ($E/C = 0.22$), for which a suspension can be expected of being able to take on a fluid behavior. If we start with a suspension in which we have 48% volume of particles ($E/C = 0.35$) then we can have an additional effective volume due to non-dispersed doublets of 11%. So, we can determine whether or not a given superplasticizer satisfies this condition for a desired yield stress, by extending [10-23] as:

$$\Delta\Theta = \frac{\sum_k \sum_{l \geq k} n_{k,l} \left(1 - \frac{2\theta_c}{\pi}\right) \Delta V_{k,l}}{d^3} \quad [10-24]$$

Where $\Delta V_{k,l}$ is the increase of the effective volume due to a pair of agglomerated particles of radius a_k , a_l . The volume of the cube used to determine the values of $n_{k,l}$ is d^3 . Because the movement of these particles might be partly co-ordinated and because the degree of co-ordination is not unity, it is not advisable to determine $\Delta V_{k,l}$ based on the inscribed sphere. We have chosen to use the truncated cone which is tangent to both spheres and has its base at the tangency points of these spheres, as shown in Figure 10-8.

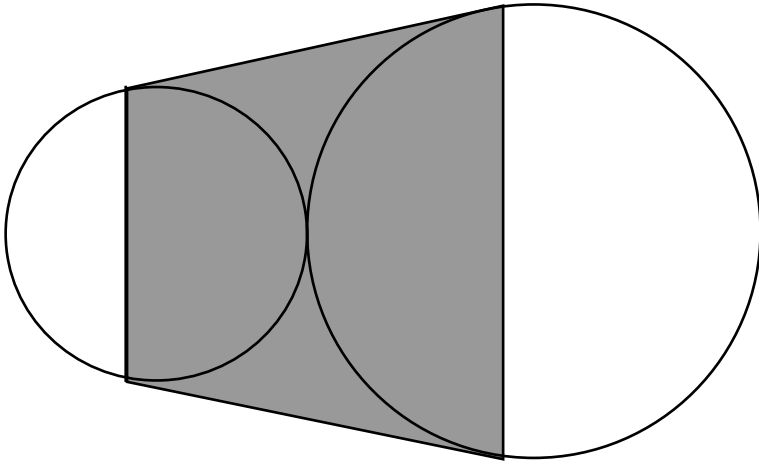


Figure 10-8. Truncated cone used to determine the effective volume increase due to a doublet.

This volume is given by (Annex E):

$$\Delta V_{k,l} = \frac{2\pi}{3} \hat{a}^2 (4\hat{a} - \bar{a}) \quad [10-25]$$

We have determined this volume for each doublet (Figure 10-9).

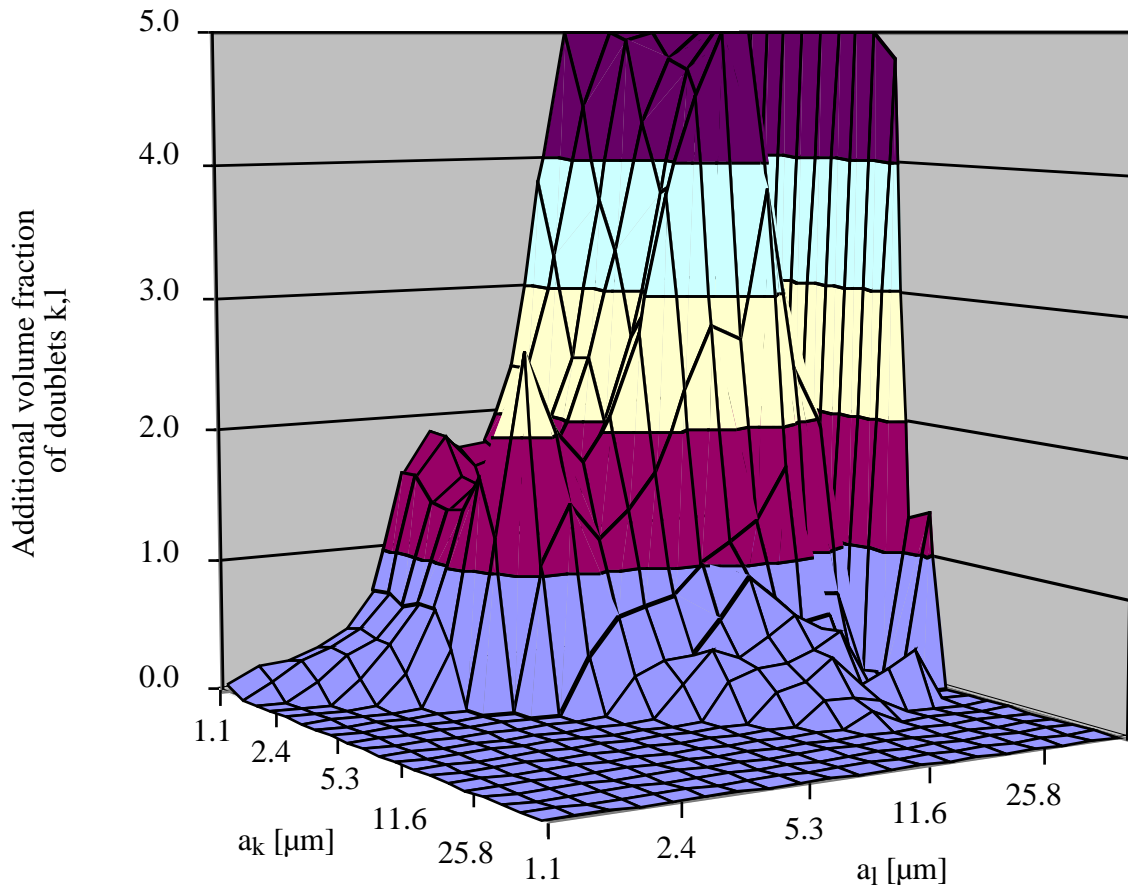


Figure 10-9. Effective volume increase due to the presence of non-dispersed doublets, as a function of the radius of the particles (logarithmic scale for a_k and a_l). The relative values are given for a suspension of W/C of 0.35.

Assume, we know the effective volume increase which a suspension can undergo, while remaining fluid, then we can use an iteration to determine G/τ , from [10-23]-[10-25]. Our rheology testing was done for volume fractions of 48% ($E/C=0.35$). If we assume the maximum volume fraction is 59% ($E/C=0.22$), then we conclude that the volume fraction increase can be 11%. For the Olten cement, this leads to a value of G/τ of 0.96. For this condition, the distribution of the additional effective volumes due to non dispersed doublets are plotted in Figure 10-10.

For other values of G/τ , we G/τ plot the total additional volume fraction in Figure 10-11. The linear dependence arises from the fact that we are in a domain where considered, most angles are large and $(1-2*\theta_c/\pi)$ is inversely proportional to $\tan(\theta_c)$. Since $\tan(\theta_c)$ is itself inversely proportional to G/τ , we get a linear dependence between the majority of non dispersed fractions and G/τ . The higher the

shear stress (τ) or the lower the interparticle attractive force parameter (G), the lower the additional volume fraction. This is expected. The fact that the dependence is linear makes further calculations easier.

For the Olten cement, we can write:

$$\frac{G}{\tau} \cong 0.088\Delta\Theta_{[\%]} \quad [10-26]$$

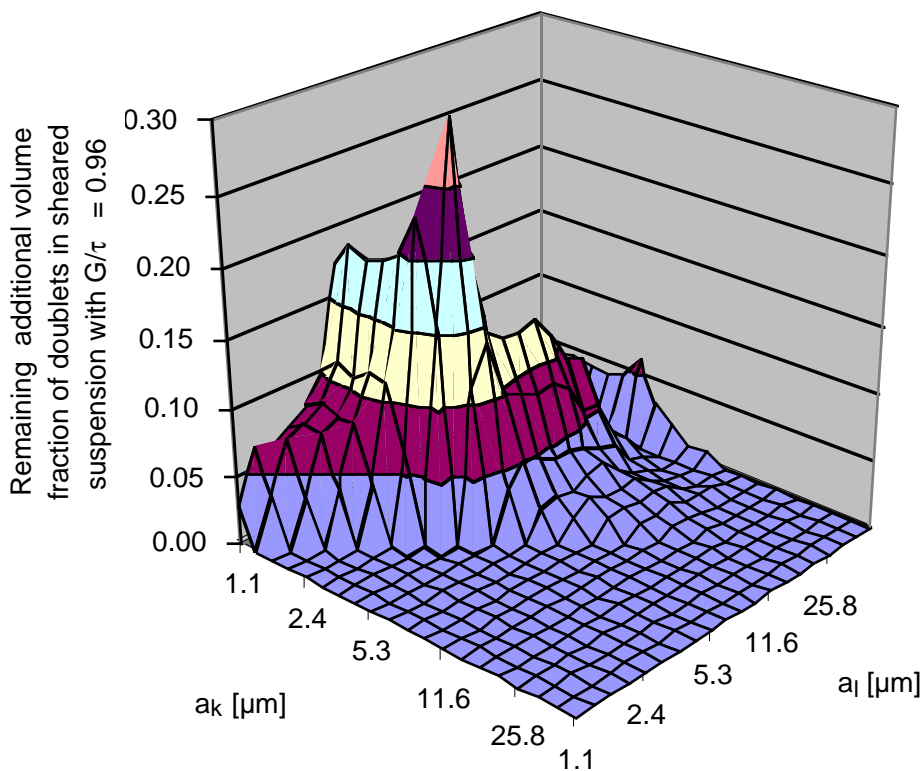


Figure 10-10. Effective volume increase due to the presence of non-dispersed doublets, as a function of the radius of the particles (logarithmic scale for a_k and a_i). Only doublets leading to a value of $G/\tau = 0.96$ ($\Delta V_{tot} = 11\%$) are considered. The relative values are given for a suspension of W/C of 0.35.

Maximum packing fraction of solids

Nolan and Kavanagh (1994) have calculated the maximum packing density of solids for powders having *log-normal* particle size distributions (Table 10-2). Because the particle size distribution of the Olten cement follows a *log-normal* distribution (correlation coefficient of 0.994), we can use these results to estimate the maximum effective volume of solids in a suspension of Olten cement. The normalised standard deviation of the distribution is 1.5, so a random close packed corresponds to a volume fraction of 65%, while a loose packed situation corresponds to 53%. We will consider two situations for the maximum packing density. The first will be random close packed (65%) and the second will be the average between the random close packed and the loose packed (59%). This later situation can be considered as a way of taking into account the effect of the non-spherical cement particles, which should decrease the random close packed figure expected for spheres.

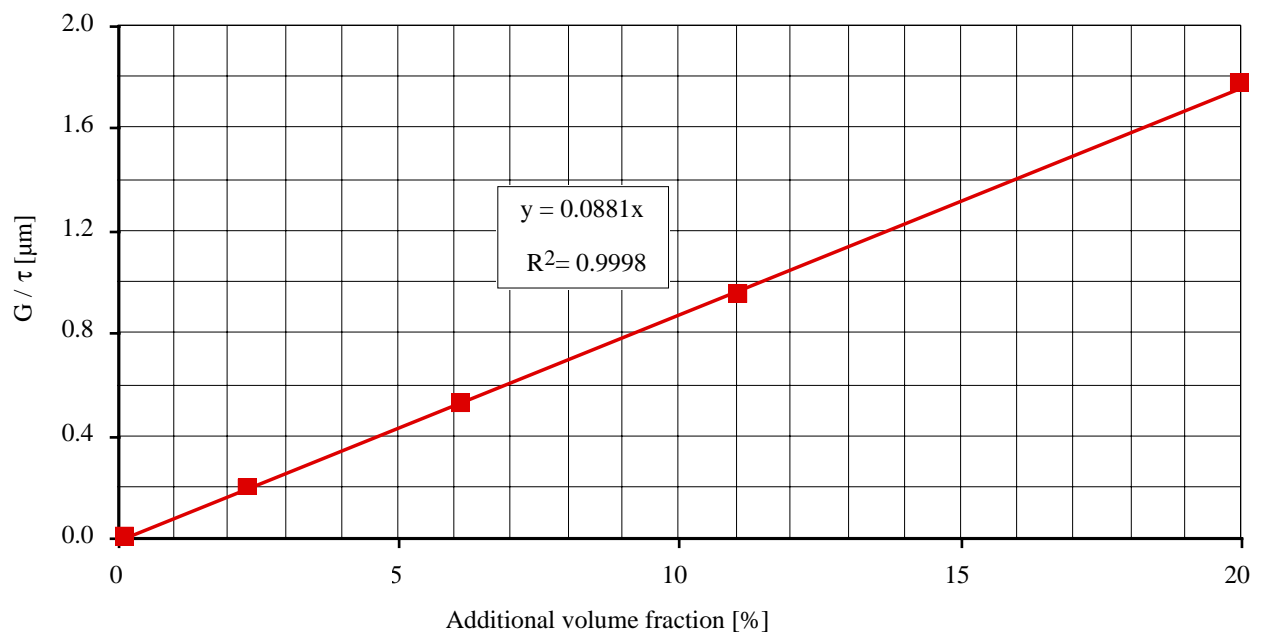


Figure 10-11. Total additional volume fraction due to the presence of doublets, given as a function of the ratio between the interparticle force parameter G and the yield stress τ .

Estimation of polymer layer thickness

So far, we have used the particle size distribution of the Olten cement to calculate the frequency of interactions between particles of different sizes. For each pair of particles we then estimated what the increase in effective volume fraction would be if this pair could not be dispersed. By calculating a balance between interparticle forces and the yield stress required to disperse each doublet, we obtained a linear relation between a dispersion factor G/τ and the total increase in effective volume fraction (Figure 10-11). G is the interparticle force parameter. It decreases when the superplasticizer efficiency increases. τ is the applied stress.

Table 10-2. Maximum packing densities for powders having log-normal particle size distributions, from Nolan and Kavanagh (1994)

Normalised standard deviation	Packing Density	
	Random Close Packed [%]	Loose Packed [%]
0	64.2	51.6
0.1	64.3	52.3
0.2	65.7	54.0
0.31	68.1	57.8
0.41	68.7	62.3
0.52	71.2	61.3
0.62	70.1	62.0
0.84	76.7	65.0

We assume that the solid-liquid transition occurs if the total effective volume is lower or equal to a maximum volume fraction, which depends on the nature of the solid. Using the packing approach above, we estimate this fraction to be 65% (or 59% in the second situation).

The measurements we performed were made for W/C ratios of 0.35, corresponding to a solid volume fraction of 48%. So the additional volume fraction, which can be allowed due to non-dispersed pairs, is between 17% (or 11%). With equation [10-26] or Figure 10-11 we can determine that a dispersion parameter G/τ lower or equal to 1.36 (or 0.96) is required to obtain a solid to liquid transition. Experimentally, we have determined the yield stresses for suspensions dispersed with superplasticizer

PCA-1 and PCA-2 to be 6 and 10 Pa respectively. So, the interparticle force parameter must be between 8.2 (or 5.8) and 13.6 (or 9.6) pN/ μm respectively.

Using the solver of Excell with the interpolating macro in Annex F and values of G listed in Annex E (for MgO), we obtain different combinations of layers and thickness, which give that value of G. For a layer without any electrostatic potential, the targeted values of G are reached for layers of 5.4 nm (or 6.5 nm) and 4.4 nm (or 5.3 nm), for PCA-1 and PCA-2 respectively. For 10 mV, the layers would have to be of 3.1 nm (or 3.9 nm) and 2.3 nm (or 3.0 nm). These values are summarised in Table 10-3.

Table 10-3. Estimation of the required adsorbed layer thickness giving the yield stress measured on the Olten cement either with PCA-1 or PCA-2. Two values for the effective volume increase are considered, corresponding to a close and a loose packed situation for the particle size distribution of the Olten cement.

Polymer	Effective volume increase 17% (random close packed)		Effective volume increase 11% (average random close packed and loose packed)	
	PCA-1	PCA-2	PCA-1	PCA-2
Yield Stress [Pa]	6	10	6	10
G_{IP} [pN/ μm]	8.2	13.6	5.8	9.6
L ($\psi = 0$ mV) [nm]	5.4	4.4	6.5	5.3
L ($\psi = 10$ mV) [nm]	3.1	2.3	3.9	3.0

These results indicate that an adsorbed layer thickness of slightly more than half of the distance between adsorption points as determined from adsorption isotherms is estimated for a 0 mV potential (Table 7-4). For 10 mV potential, this thickness is about a third of that diameter.

These values remain in a physically relevant range, provide the surface-polymer interaction is strong. The presence of calcium could be responsible for this compression of the layer. Nevertheless, with only physically relevant parameters, this model begins to account for measured yield stresses.

Limitations

Being able to calculate a yield stress from polymer and cement parameters makes it possible to develop at least semi-quantitative predictions of superplasticizer performances. However, in order to reach this objective the limitations mentioned below deserve further investigation:

- The exact determination of the maximum allowable effective volume fraction increase due to non dispersed doublets.
- The measurement of the real parameters for the steric force. In particular, the layer thickness.
- The position of the plane of origin for electrostatic forces.
- The importance of hydrodynamic forces. This contribution will be evaluated below.
- Proper dielectric data for the different cement phases (calculations done here with MgO data).

10.4.2 Hydrodynamic interactions

So far, we have considered that we were dealing with a solid at rest. We have calculated the yield stress required to break sufficient bonds so that enough particles could move independently one from another so that the solid to liquid transition could be reached. Now, we must consider that this transition must take place over an observable time scale. While attempting to separate one particle from another, there are lubrication forces, which resist this separation. As indicated in chapter 3, these forces depend on the particle sizes, the separation distance between particles and the velocity of separation.

In chapter 3, we gave the relation between the force which resists the separation of particles in close contact and the velocity at which this separation takes place. When the velocity is along the line of centres we have a so-called squeeze resistance. On the other hand, if the velocity is perpendicular to this line, one has a shear resistance. These two situations allow calculation the hydrodynamic resistance to the separation of a doublet having a random orientation, provided the velocity is decomposed into two velocities parallel and perpendicular to the line of centres.

Let us first consider the situation in which $0 < \theta < 90$ and $-90 < \phi < 90$ (Case I). In this situation, S_1 moves away from S_k .

If we define a new Cartesian co-ordinate system such that the \mathbf{z}_2 axis is along the line of centres (Figure 10-12):

$$\mathbf{z}_2 = \begin{bmatrix} \sin \theta \cos \varphi \\ \sin \theta \sin \varphi \\ \cos \theta \end{bmatrix} \quad [10-27]$$

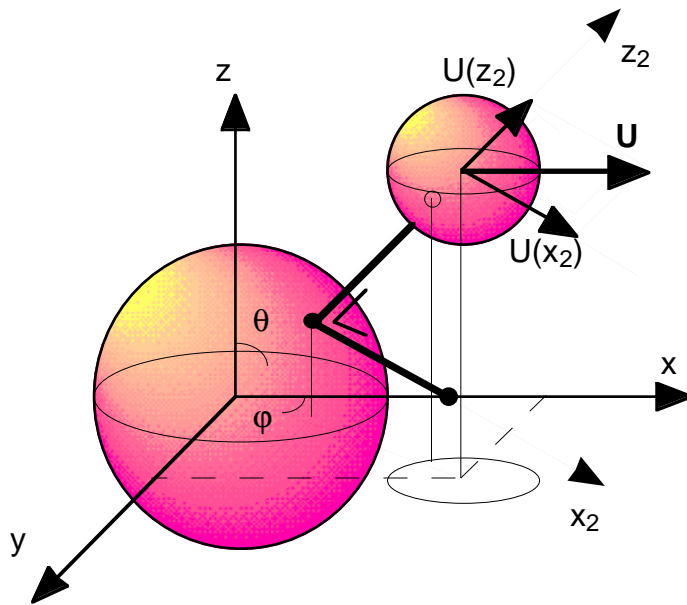


Figure 10-12. Representation of two interacting spheres. The upper sphere has a velocity $\mathbf{U}(\mathbf{x})$ in the positive \mathbf{x} direction, while the other one is at rest. This velocity is decomposed into a velocity $\mathbf{U}(\mathbf{z}_2)$ along the direction of the line of centres and a velocity $\mathbf{U}(\mathbf{x}_2)$ perpendicular to it. This allows calculations of the lubrication squeeze and shear forces, $\mathbf{F}(\mathbf{z}_2)$ and $\mathbf{F}(\mathbf{x}_2)$ respectively.

The \mathbf{x}_2 axis is defined so that it is in the \mathbf{z}_2, \mathbf{U} plane. We have:

$$U(\mathbf{z}_2) = \mathbf{z}_2 \cdot \mathbf{U} = \begin{bmatrix} \sin \theta \cos \varphi \\ \sin \theta \sin \varphi \\ \cos \theta \end{bmatrix} \cdot \begin{bmatrix} U \\ 0 \\ 0 \end{bmatrix} = U \sin \theta \cos \varphi \quad [10-28]$$

$$\mathbf{U}(\mathbf{x}_2) = \mathbf{U} - \mathbf{U}(\mathbf{z}_2) = \begin{bmatrix} U \\ 0 \\ 0 \end{bmatrix} - U \sin \theta \cos \varphi \begin{bmatrix} \sin \theta \cos \varphi \\ \sin \theta \sin \varphi \\ \cos \theta \end{bmatrix} = U \begin{bmatrix} 1 - \sin^2 \theta \cos^2 \varphi \\ -\sin^2 \theta \sin \varphi \cos \varphi \\ -\sin \theta \cos \theta \cos \varphi \end{bmatrix} \quad [10-29]$$

So the norm of this vector is given by:

$$\begin{aligned} U(\mathbf{x}_2) &= U \sqrt{(1 - \sin^2 \theta \cos^2 \varphi)^2 + (-\sin^2 \theta \sin \varphi \cos \varphi)^2 + (-\sin \theta \cos \theta \cos \varphi)^2} \quad [10-30] \\ &= U \sqrt{1 - 2 \sin^2 \theta \cos^2 \varphi + \sin^4 \theta \cos^4 \varphi + \sin^4 \theta \sin^2 \varphi \cos^2 \varphi + \sin^2 \theta \cos^2 \theta \cos^2 \varphi} \\ &= U \sqrt{1 + \sin^2 \theta \cos^2 \varphi (-2 + \sin^2 \theta (\cos^2 \varphi + \sin^2 \varphi) + \cos^2 \theta)} \\ &= U \sqrt{1 + \sin^2 \theta \cos^2 \varphi (-2 + \sin^2 \theta + \cos^2 \theta)} \\ &= U \sqrt{1 - \sin^2 \theta \cos^2 \varphi} \end{aligned}$$

The unit vector \mathbf{x}_2 is given by:

$$\mathbf{x}_2 = \frac{1}{\sqrt{1 - \sin^2 \theta \cos^2 \varphi}} \begin{bmatrix} 1 - \sin^2 \theta \cos^2 \varphi \\ -\sin^2 \theta \sin \varphi \cos \varphi \\ -\sin \theta \cos \theta \cos \varphi \end{bmatrix} \quad [10-31]$$

We can now decompose the velocity of sphere S_2 into a velocity $\mathbf{U}(\mathbf{x}_2)$ transverse to the line of centres and a velocity $\mathbf{U}(\mathbf{z}_2)$ along the line of centres. Using the equations above it is possible to calculate the hydrodynamic interaction force along \mathbf{x}_2 and \mathbf{z}_2 .

From the squeeze resistance, we have for $\mathbf{F}(\mathbf{z}_2)$:

$$\mathbf{F}(\mathbf{z}_2) = 6\pi\mu a_l W_{(\varepsilon, \beta)} \mathbf{U}(\mathbf{z}_2) \quad [10-32]$$

While as for the shear resistance, we have for $\mathbf{F}(\mathbf{x}_2)$:

$$\mathbf{F}(\mathbf{x}_2) = 6\pi\mu a_l V_{(\varepsilon, \beta)} \mathbf{U}(\mathbf{x}_2) \quad [10-33]$$

We are concerned with the projection onto \mathbf{x} of the sum of both these forces:

$$\begin{aligned}
F(\mathbf{x}) &= \mathbf{F}(\mathbf{x}_2)\mathbf{x}_2 \cdot \mathbf{x} + \mathbf{F}(\mathbf{z}_2)\mathbf{z}_2 \cdot \mathbf{x} \\
&= 6\pi\mu a_l V_{(\varepsilon,\beta)} \mathbf{U}(\mathbf{x}_2) \cdot \mathbf{x} + 6\pi\mu a_l W_{(\varepsilon,\beta)} \mathbf{U}(\mathbf{z}_2) \cdot \mathbf{x} \\
&= 6\pi\mu a_l V_{(\varepsilon,\beta)} U \sqrt{1 - \sin^2 \theta \cos^2 \varphi} + 6\pi\mu a_l W_{(\varepsilon,\beta)} U \sin \theta \cos \varphi
\end{aligned} \tag{10-34}$$

This is the force needed to separate a doublet in absence of interparticle forces.

Since we are applying a shear field, we may replace the velocity U by the velocity difference between both spheres, which is given by:

$$U = U(S_k) - U(S_l) = \dot{\gamma}(a_k + a_l + h) \cong \dot{\gamma}(a_k + a_l) \tag{10-35}$$

So the force along x becomes:

$$\begin{aligned}
F(\mathbf{x}) &= 6\pi\mu a_l V_{(\varepsilon,\beta)} \dot{\gamma}(a_1 + a_2) \cos \theta \sqrt{1 - \sin^2 \theta \cos^2 \varphi} + \\
&\quad 6\pi\mu a_l W_{(\varepsilon,\beta)} \dot{\gamma}(a_1 + a_2) \cos \theta \sin \theta \cos \varphi
\end{aligned} \tag{10-36}$$

In the flow the spheres doublets will undergo rotation, according to angle θ . Therefore, we need to determine the angle θ , which gives the maximum force along x . Because we intend to separate particles, we are only interested in

$$-\frac{\pi}{2} \leq \varphi \leq \frac{\pi}{2}$$

So, the average values of $\cos \varphi$ and $\cos^2 \varphi$ are respectively $2/\pi$ and $1/2$.

$$F(\mathbf{x}) = 6\pi\mu a_l V_{(\varepsilon,\beta)} \dot{\gamma}(a_k + a_l) \cos \theta \sqrt{1 - \frac{\sin^2 \theta}{2}} + \frac{12\pi\mu a_l}{\pi} W_{(\varepsilon,\beta)} \dot{\gamma}(a_k + a_l) \cos \theta \sin \theta \tag{10-37}$$

Let us define G_H , which gives is the above hydrodynamic resistance, normalised by \bar{a} . We have:

$$G_H = 3\pi \frac{(a_k + a_l)^2}{a_k} V_{(\varepsilon,\beta)} \mu \dot{\gamma} \cos \theta \sqrt{1 - \frac{\sin^2 \theta}{2}} + 6 \frac{(a_k + a_l)^2}{a_k} \mu \dot{\gamma} W_{(\varepsilon,\beta)} \cos \theta \sin \theta \tag{10-38}$$

In case IV, the equation is the same, except that a_l is replaced by a_k .

To determine these resistances, we have taken the viscosity of water and shear rates of 0.2, which is the average shear rate at which the solid to liquid transition was observed. We took the viscosity of water, because we considered that the dominant effects was the viscous behaviour of the fluid around the spheres. At these low shear rates, we considered to the lubrication resistances of each doublet to be independent of the others.

We have selected two doublets. The first is the one, which has the maximum potential volume contribution in Figure 10-9. It concerns particles of radius 45.6 and 1.1 μm . The second situation is the doublet which has the maximum final contribution to the effective volume increase in Figure 10-10. In this situations the particle radii are 4.4 and 3.6 μm . For both these situations, we have calculated the value of G_H for $\theta=45^\circ$. Independently of this choice the shear resistance gives values of G_H , which are negligible with those obtained from interparticle force calculations (8-14 $\text{pN}/\mu\text{m}$). This component does therefore not play an important part in the measured yield stress.

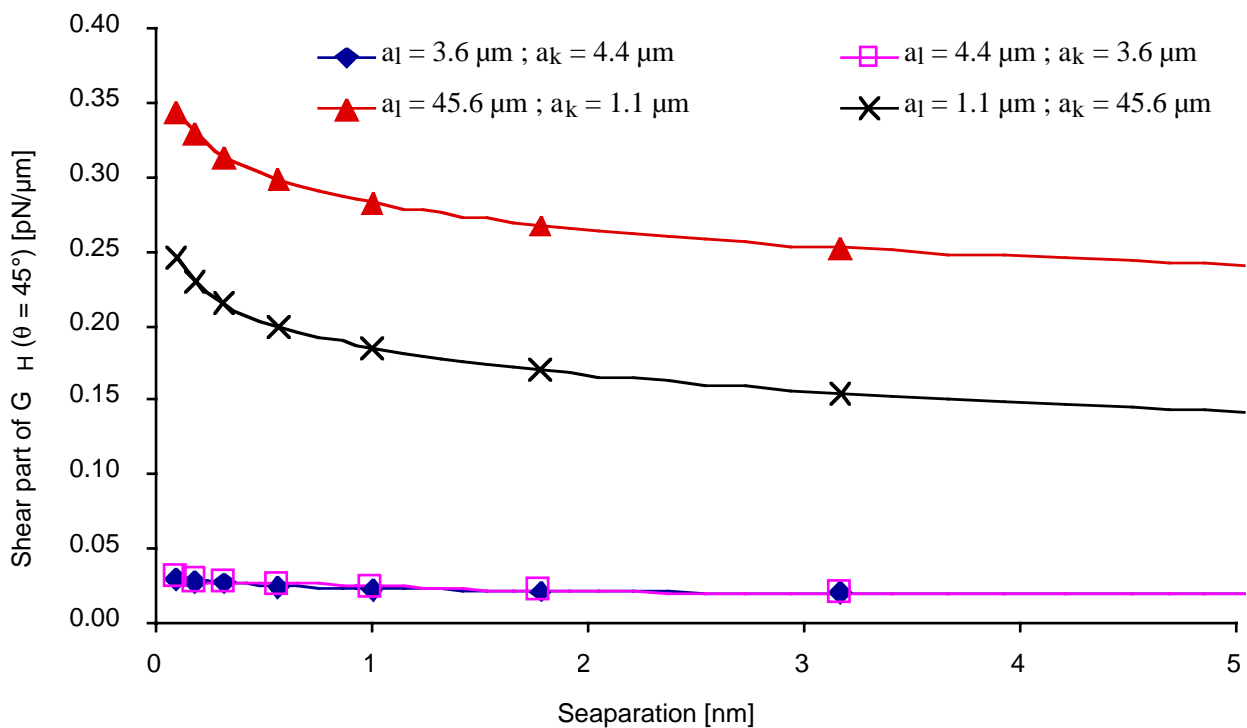


Figure 10-13. Shear component of the reduced hydrodynamic resistance G_H in the direction of applied shear. The angle θ is taken to be 45° .

On the other hand the squeeze components (resistance along the line of centres) are much higher as indicated in Figure 10-14. For separation of about 2-3 nm, they are of the order of the values determined from interparticle potentials. So this component can bring in an additional resistance to separation which must be significant. An interesting aspect of Figure 10-14 is that this resistance is relatively independent of which sphere is being moved away.

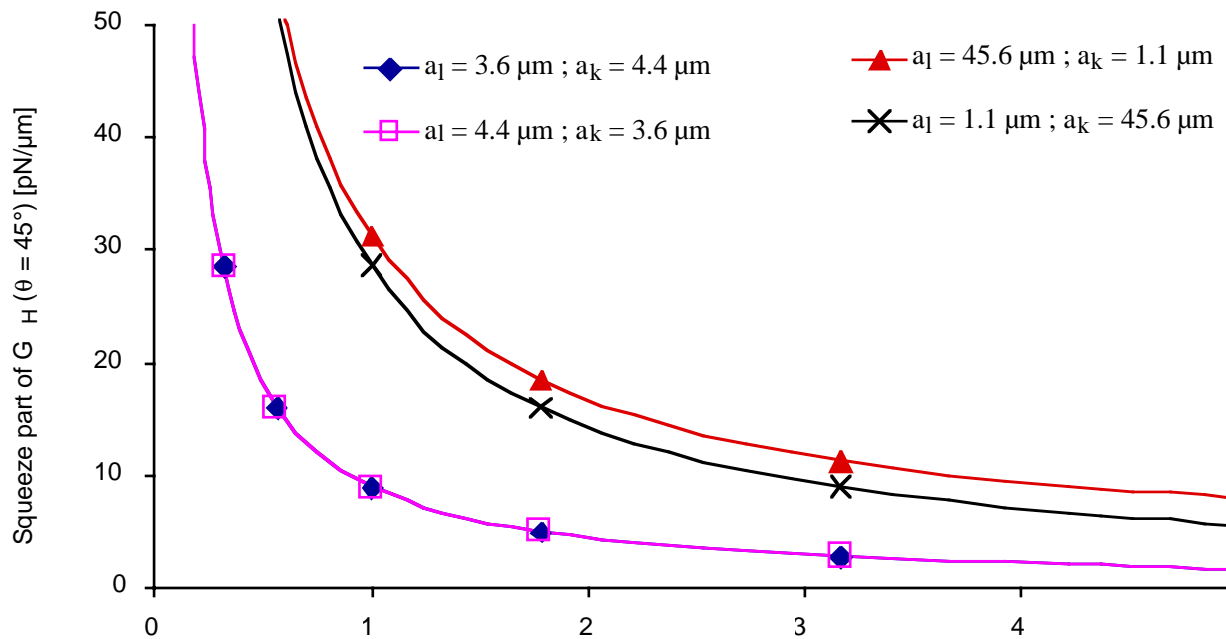


Figure 10-14. Squeeze component of the reduced hydrodynamic resistance G_H in the direction of applied shear. The angle θ is taken to be 45° .

We can reformulate the G_H only taking in the squeeze term:

$$G_H \cong 6 \frac{(a_k + a_l)^2}{a_k} \mu \dot{\gamma} \mathcal{W}_{(\varepsilon, \beta)} \cos \theta \sin \theta \quad [10-39]$$

Because G_H depends on the particle sizes, and because it does not have the same θ dependence as G_{ip} , developing the probability of bond breaking for different conditions is a more tedious task than without hydrodynamic interactions. Each doublet would require a separate numerical iteration to solve for θ . This would have to be done for a set of values of G_{ip} , and separation distances.

Another solution is to determine what the order of magnitude of yield stress would be for the maximum squeeze resistance, if particles were perfectly dispersed. We call this yield stress τ_H and

deduce it from the measured yield stress τ . This difference gives a yield stress corrected τ_{ip} , which can then be used in [10-26] to calculate G_{ip} .

For a separation of 1 nm, we calculate the number average of the maximum yields for each pair and get a value for τ_H of about 3 Pa. This would lead to values of G_H of 3.5 and 8.3 pN/ μm . In the absence of electrostatic potential, for the random close packed situation, this would be reached for layers of 7.1 and 5.1 nm, respectively. For 10 mV the layers would have to be of 4.5 and 2.8 nm.

This is a very rough approximation of the hydrodynamic effects. Much more detailed calculations would be required to get a more quantifiable comparison. The problem will be the evaluation of the initial particle separation. We chose 1 nm because this is about 3 water molecules, which seemed a physically relevant minimal distance to consider. These estimations of hydrodynamic interactions suggest that layer thickness would have to be about 30% larger when hydrodynamic interactions are not neglected.

Results are summarised in Table 10-4 for the situation where the maximum allowable increase of the effective volume is 17% (random close packed), corresponding to $W/C_{\text{max}} = 0.173$). If this value is only of 11% (average between random close packed and loose packed), corresponding to $W/C_{\text{max}} = 0.22$, then the layer thicknesses are larger, as indicated in Table 10-5.

Table 10-4. Summary of yield stress calculations for the Olten cement at $E/C = 0.35$. The allowable increase in effective volume fraction is estimated to be of 17% of the total volume of suspension (random close packed).

Polymer	Without Hydrodynamic Interactions		With Hydrodynamic Interactions (3Pa)	
	PCA-1	PCA-2	PCA-1	PCA-2
Corrected Yield Stress τ_{ip} [Pa]	6	10	3	7
G_{ip} [pN/ μm]	8.2	13.6	4.5	10.5
L ($\psi = 0$ mV) [nm]	5.4	4.4	7.1	5.1
L ($\psi = 10$ mV) [nm]	3.1	2.3	4.5	2.8

The general picture from this data is that the layer thickness would be smaller, particularly with a small electrostatic potential than what might be expected from a compact layer of spheres. This can be

linked to a relatively strong interaction with the surface, leading to rather compressed mushrooms, almost more like pancakes.

These values strongly contrast with the contour length of both PCA-1 (59 nm) and PCA-2 (38 nm), obtained using average bond length for polystyrene (0.154 nm) and M_w . These expectations contrast with the study by Pedersen and Bergstöm (1999) of polyacrylic acid of M_w 10'000 on zirconia, in which the adsorbed layers were measured by AFM to be of about 20 nm into the solution. In addition, to polydispersity, this can rise from the fact that both the polymer and the surface are negatively charged, which should increase the extension length.

Table 10-5. Summary of yield stress calculations for the Olten cement at E/C= 0.35. The allowable increase in effective volume fraction is estimated to be of 11% of the total volume of suspension (average between random close packed and loose packed).

Polymer	Without Hydrodynamic Interactions		With Hydrodynamic Interactions (3Pa)	
	PCA-1	PCA-2	PCA-1	PCA-2
Corrected Yield Stress τ_{IP} [Pa]	6	10	3	7
G_{IP} [pN/ μ m]	5.8	9.6	2.9	6.7
L ($\psi = 0$ mV) [nm]	6.5	5.3	8.4	6.1
L ($\psi = 10$ mV) [nm]	3.9	3.0	5.6	3.6

Recently Klein (1999) has given results of AFM measurements with PVP⁺Br⁻, in which it appears that the layer thickness in highly ionic medium would be of the order of 3.5 nm. This situation might be more relevant to cement, since the polymer and surface are oppositely charged. In the section below, we extrapolate recently published data of comb-type superplasticizer adsorption layer thickness to obtain an estimation of the layer thickness of the backbone of this polymer. The value of 3.8 nm obtained is consistent with Klein's results.

10.4.3 Experimental data for estimating of layer thickness

Measurements by AFM or surface force would be required to get a proper estimation of the thickness of this adsorbed layer. However, there is another method of estimating this parameter. It consists of

adsorbing a polymer into the pores of a filter of known pore diameter (100 nm and 200 nm for instance). Once the polymers are adsorbed, the effective thickness of the pores is reduced and a higher pressure must be applied to force fluid flow through the filter. Using the Hagen-Poiseuille relation, it is then possible to calculate the thickness of the adsorbed polymer.

This method was used by Sakai and Daimon (1997) with comb-type superplasticizers, having a polycarboxylate backbone onto which side chains of poly(ethylene oxide) were grafted. The filter was made of alumina and they used three superplasticizers, with different numbers of ethylene oxide units in the side chains. Their results are reported in Figure 10-15 and show an excellent linear relation between the number of units and the length of ethylene oxide. The slope of this line is 0.130 nm/unit, which is close to the length of an individual unit of ethylene oxide, 0.148 nm [Russel et al (1991), subchapter 6.2]. This difference indicates an average tilting angle of 30°, either from an average orientation of the chain or from a forced orientation in the flow field.

The most interesting information for us in this data is the ordinate at the origin in Figure 10-15, since it gives an indication of the thickness of the adsorbed polymeric backbone alone (3.8 nm). If we accept the important hypothesis that the backbone conformation is not significantly affected by the presence of side chains, this gives an indication of thickness of our layer. Indeed, the backbone used by Sakai and Daimon is within a similar class of polymers to those we have studied. However, the presence of a pyrrolidone group in PCA-1 (Figure 4-6a) and of a propyl aldehyde group in PCA-2 (Figure 4-6b) must slightly increase the thickness of the adsorbed layer, since they are both expected to be non-adsorbing [Napper (1983)].

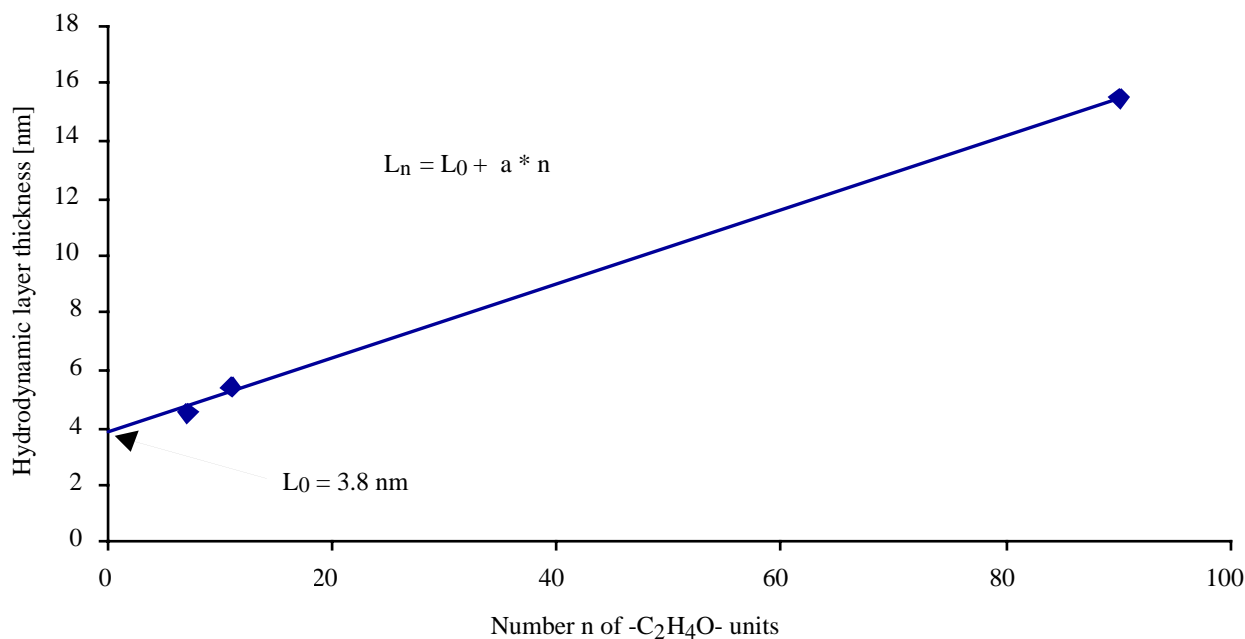


Figure 10-15. Thickness of layers of comb copolymers determined by Sakai and Daimon (1997).

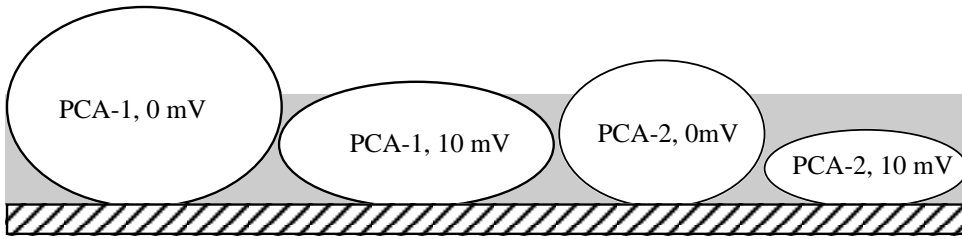
So, the thickness of 3.8 nm obtained from the data of Sakai and Daimon (1997) probably slightly underestimates the thickness of adsorbed PCA-1 and PCA-2. Nevertheless, it suggests that these layers will not be much larger, which in turn would indicate that there is a contribution of electrostatic repulsion according to the situations considered in Table 10-4 and Table 10-5.

Along with the results by Klein (1999), the above estimation suggests that our estimation of the layer thickness are in a good range. The difference between PCA-1 and PCA-2, would be linked to different molar masses, and possibly the pyrrolidone group, which could be making adsorption conformation less compressed than the propyl aldehyde group of PCA-2.

In order to make the comparison of the different thicknesses more visual, we have reported these as the small diameter of ellipses in Figure 10-16. For comparison, the thickness estimated from the data by Sakai and Daimon (1997) is shown by the light grey band.

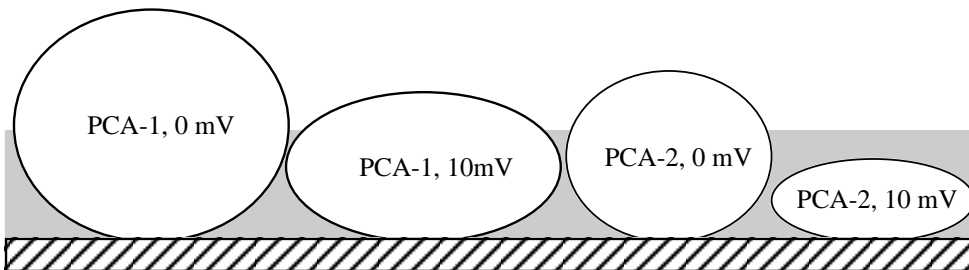
Hydrodynamic interactions considered

Maximum packing fraction = random close packed



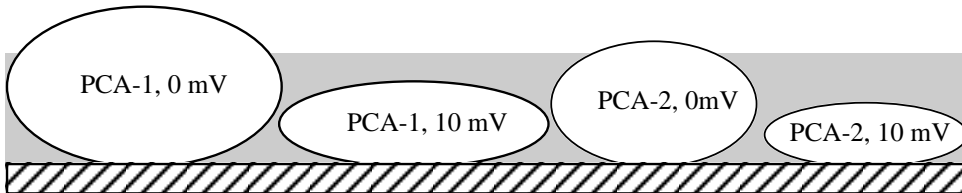
Hydrodynamic interactions considered

Maximum packing fraction = average (random close packed, loose packed)



No Hydrodynamic interactions

Maximum packing fraction = random close packed



No Hydrodynamic interactions

Maximum packing fraction = average (random close packed, loose packed)

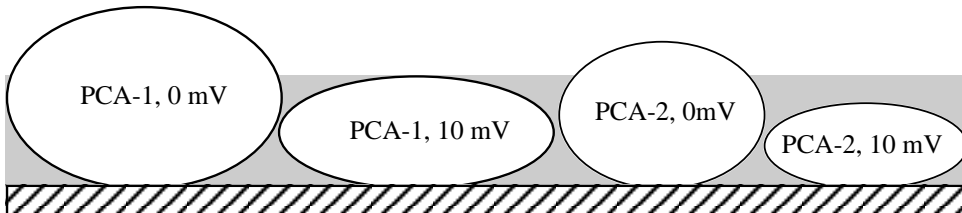


Figure 10-16. Schematic representation of the estimated layers, for the four situations considered. The gray layer corresponds to the estimate based on data by Sakai and Daimon (1997).

10.5 Implications of interparticle force calculations

We have attempted to link results of interparticle force calculations to experimentally determined values of yield stress. Many unknowns appear along this development. The major ones are

- The maximum solid volume fraction (geometric packing).
- The minimum separation of the particles (hydrodynamic interactions).
- The thickness of the adsorbed layer (interparticle forces).
- Use of Magnesium dielectric data instead of pure cement phases.

Choosing values that seem physically relevant for the first two parameters we can calculate the thickness of the layer required in order to obtain the measured yield stress. For a maximum packing leading to a suspension with W/C between 0.173 and 0.28, as well as for minimum separation of 3 water molecules, we calculate layer thicknesses, which are of the order of half the distance between adsorption sites determined experimentally. This calculation suggests that polymers are adsorbed in a mushroom or pancake conformation.

It is not the object of this development to perform a fitting procedure. Rather it is to show that a detailed development of interparticle forces can lead, with physically relevant values for the parameters needed, to estimating yield stresses within the range of those measured experimentally. This is in itself an important achievement, which stresses the importance of this microstructural approach. Further quantification, will require precise determination of the variables of the model. In addition it will require a more thorough estimation of the effect of hydrodynamic interactions.

Finally, let us point out that Sakai and Daimon (1997) gave a value of a non-retarded, non-screened Hamaker constant for C_3S of 4.55×10^{-6} J/mol. This value was not obtained using the proper dielectric data of water compiled by Roth and Lenhoff (1996). If we use the same dielectric data of water as Sakai and Daimon (1997), we calculate for MgO a non-retarded and non-screened Hamaker constant of 4.2 J/mol. Since both values are close, MgO certainly is a good model for calculating the retarded and screened dispersion forces as was done in this chapter.

Chapter 11 General discussion

11.1 A brief overview

The main theme of this thesis has been to evaluate the modification of interparticle forces induced by superplasticizers in cement suspensions. By reducing the number and size of agglomerates, dispersants reduce the effective volume of solid in a suspension. This is illustrated schematically in Figure 11-1, in which we show two doublets for which the effective volume is assumed to be the sphere surrounding each doublet. In this situation, the doublets could move more independently one from another (physical volume exclusion and hydrodynamic interactions exist). Assume an ensemble of $2N$ particles of radius a . When dispersed the effective solids volume would be: $2N\left(\frac{4}{3}\pi a^3\right) = \frac{8}{3}N\pi a^3$. If agglomerated as doublets, the effective solid volume would be: $N\left(\frac{4}{3}\pi(2a)^3\right) = \frac{32}{3}N\pi a^3$. So, the effective volume fraction of a suspension in which particles are agglomerated as doublets would be 4 times larger than the effective volume of the perfectly dispersed system. This simple example illustrates the importance of being able to desagglomerate particles in order to increase the workability of a suspension.

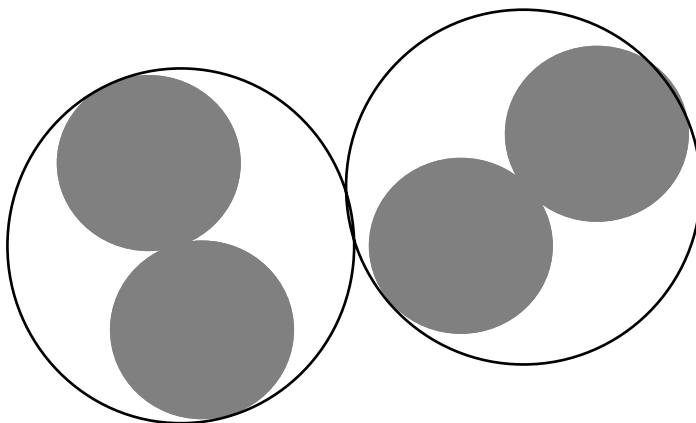


Figure 11-1. Effective volume of two doublets.

Such an effect is undoubtedly present in cement suspensions. However, cement is not an inert system and reactions begin as soon as water gets in contact with the cement particles. As hydration proceeds, the paste thickens and sets before hardening much later. Modifying early hydration reactions could in principle modify the rheology of cement suspensions. This means that unlike inert systems (in our case $\text{Mg}(\text{OH})_2$ and MgO), the effect of a superplasticizer is always potentially the superposition of dispersion and a chemical effect. There are many reasons to believe that dispersion is the dominant contribution. For instance, addition of sugar, a very powerful retarder of the chemical reactions, does not substantially increase workability. Nevertheless, it remains impossible to obtain a clear separation of these effects unless inert systems are used.

It is important to point out again, that the main theme of this thesis has been to evaluate the importance of dispersion effects in the increase of the workability of cement suspensions. It is our belief, that it is indispensable to reach a thorough understanding of these mechanisms before attempting a comparative study of the performance of superplasticizers in different cements. Otherwise the risk is higher to begin attributing all kinds of chemical effects in order to account for the difference between the performance of a given superplasticizer in different cements.

Most of this thesis has been oriented towards obtaining both the theoretical tools and experimental results necessary to develop a relevant model for evaluating the importance of dispersion effects in cement suspensions. A key section of this thesis is chapter 3. It contains a presentation of *state of the art* knowledge of interparticle forces, to which we have added many further developments needed in order to make the application of these theories relevant to cement suspensions. These developments are critical to allow correct interpreting of experimental data. They provide the basis of our approach to studying dispersion effects in cement suspensions.

The next section deals specifically with the interpretation of the results as far as dispersion effects are concerned. As mentioned previously, superplasticizers also modify chemistry of cement suspensions. This is addressed in the third and last section of this chapter. Our understanding of these effects is based on some of our results and on a personal interpretation of some recent data from the literature.

11.2 Role of physico-chemical effects

11.2.1 Agglomeration

Agglomeration can occur when the total attractive force between particles is larger than total repulsive force. Dispersion, electrostatic and depletion forces can predominantly induce attraction. Attractive depletion forces occur with non-adsorbing polymers and are not present in our system. Attractive electrostatic forces occur when the potentials (or charges) of the two interacting particles are of opposite sign (or not of identical value). It can also originate from ion correlation due to divalent or trivalent cations. We have considered that all particles have the same potential, induced by adsorbed polyelectrolytes, and that ion correlation attraction can be neglected. In addition, we considered this potential to remain constant upon approach.

Electrostatic forces

Because cement suspensions have strong concentrations of electrolytes, the repulsive force only acts significantly on a very short range. The decay length depends on the ion concentration as well as on the ion valences. The decay length varies with the inverse of the valence, but only with the inverse square root of concentration. So, ions of high valences contribute strongly to screening. In particular, for the negative charges induced by superplasticizer adsorption, the decay length is expected to decrease strongly with calcium concentration. This is true. However, at the pH and electrolyte concentrations of cement suspension only 50% of the calcium in solution is found to be present in its divalent form. The other 50% is distributed as $\text{Ca}(\text{OH})^+$ and CaSO_4 . Using the calculated ion distributions, we have determined an equivalent symmetric electrolyte, which leads to the same Poisson-Boltzmann relationship. Over a limited range of potentials, this allowed us to establish approximations in order to evaluate the magnitude of the electrostatic repulsion.

Dispersion forces

The dispersion force is always attractive between particles of same nature. It can be written as the product between a term depending on the dielectric properties of the interacting particles and of the intervening medium (the Hamaker constant), and a term depending on the geometries of the interacting particles. The geometric term decays strongly with distance. This explains why, avoiding

close approach, for instance with adsorbed polymers, decreases the maximum driving force of agglomeration. Although the dispersion force decreases with distance, it is dominated by the geometric term, we must also consider that the Hamaker constant, which should rather be called the Hamaker parameter, also decays with increasing separation. This is called retardation. We have shown that with a separation of 10 nm (twice the average polymer thickness estimated in absence of hydrodynamic interactions), the force is 60% smaller than would be expected if retardation were overlooked. In addition the Hamaker parameter is sensitive to high electrolyte concentrations. Indeed this parameter describes the degree of correlation between the dipoles in both particles, over the whole electromagnetic range. This includes a static term, which is non-retarded, but can be screened at high electrolyte concentrations. The aqueous phase of the cement suspension, as well as the layers of adsorbed strong electrolytes, meets this requirement. So the dispersion interaction must be screened in cement suspensions. If calculations are performed without this an error of 17% on the interaction force is made.

Steric Forces

With the model system $\text{Mg}(\text{OH})_2$, we have obtained experimental evidence that the dispersion effects of superplasticizers can be linked directly to the amount of adsorbed polymers. Therefore, we have to focus on steric and electrostatic forces.

In order to calculate the steric forces, we have used the scaling theory developed by de Gennes, assuming that the conformation of the adsorbed polymers was mushrooms-like. This model contains three parameters. One of these is the distance between the centre of the mushrooms and can be obtained from adsorption data.

Our adsorption data was obtained by solution depletion, which is based on determining the difference between the amount of polymer introduced and the amount remaining in the aqueous phase after a given time. In absence of chemical reactions, this difference gives the amount adsorbed. If there is a chemical reaction leading a coprecipitate of the polymer, then this difference is the combination of the amounts adsorbed and coprecipitated. In cement suspensions, the existence of such coprecipitations, is illustrated by the difference between direct and delayed addition modes. In direct addition, the polymer is in the mixing water. It is therefore present when the precipitation of ettringite reaches its maximum rate. In delayed addition, most of the ettringite has precipitated once the superplasticizer is added. So, fewer polymers are consumed by the reaction with aluminates (coprecipitation or intercalation or micellisation, etc.). Nevertheless, in delayed addition, some polymer might still be coprecipitated. For this reason, we have used adsorption data on MgO in order

to determine the polymer to polymer distance on the surface. Data with $\text{Mg}(\text{OH})_2$ was not used because, we found that the porosity of our powder influences adsorption, making interpretation of absolute surface coverage much more complicated.

For the two other parameters in the model for describing the steric force, we do not have experimental data. Determination of these would require curve fitting of AFM or surface force measurements. However, the fit can not strictly use the de Gennes model, since for these polymers, electrostatic interactions must be taken into account. Because we do not have such data, the following choices have been made.

For the second parameter of the de Gennes model, which is minimum thickness to which the polymer can be compressed before it behaves as a hard wall, we have assumed that the adsorbed layer would have a density of 1400 g/m^3 and that the polymer represents 75% of the mass. This allows us with adsorption data to estimate that this fully compacted layer would be 0.7 nm thick. In fact this parameter is not an extremely sensible one, in the range of compressions which can be reached under the attractive interparticle forces of our systems.

The last parameter is the adsorbed layer thickness and is the most sensitive. We have calculated the effect for various layer thickness in order to show the expected trends. We have found that in order to account for experimentally determined yield stresses, the layer thickness would be between 30% and 85% of the centre to centre distance between the adsorbed polymers.

Electrosteric forces

The adsorption of the strongly ionic polymers induces an electrostatic charge or potential. At very small separation, where the dispersion force is maximum, this will not be without effect on the total interparticle force. A complete model should take into account the charge distribution on the polymer, the ion-ion interactions, the ion-polymer interactions and the polymer-polymer interactions. One approach could be to use an appropriate Monte-Carlo simulation for instance. The situation is complicated, but is the only method, which might allow a proper evaluation of bridging by divalent calcium ions. Development of such a model is far beyond the scope of this work. Nevertheless, we feel that at this point the best approximation, which can be made, is to place the plane of origin of the electrostatic charge/potential at the outer layer of the adsorbed layer. We have used constant potential conditions, which lead to the existence of a finite force at zero separation. This force was considered to remain constant from the point on during compression. As a consequence having a plane of origin

for the electrostatic potential at the surface of the polymer layer, the maximum interparticle force occurs before the layer overlap begins, even for very small potentials.

Total interaction

Experimental data on model systems has pointed to the importance of adsorbed polymers. The calculations performed illustrate the dominant effect of the adsorbed layer thickness. The larger the layer, the lower the attractive force. On the other hand, in order to quantify this force, we must also include the electrostatic force, particularly for thin layers. This is important for developing relevant yield stress calculations. It is also a very important piece of information for tracking cement/superplasticizer incompatibilities. Indeed, our calculations suggest that a relatively small change in the potential can modify the yield stress in a critical range. Incompatibilities may therefore be linked to changes in electrostatic potential, surface layer thickness or chemistry. Considering chemistry and adsorbed layer thickness only might lead to misinterpretation. This is of particular importance for polymers such as SNFC, which are of small molar mass and should have relatively thin adsorbed layers. For polymers in which there is significant electrostatic contribution, we can expect that increasing ionic strength might reduce this effect, even if the ionic strength is already very high. For cement, the ionic strength should increase with solid loading. So, we expect electrosteric type polymers to lose efficiency faster with an increase in W/C compared to non-ionic polymers.

Because adsorbed polymers are of great importance in dispersion, it is of primary importance that they adsorb onto the particle surfaces. We found with MgO that this adsorption can be strongly influenced by temperature, possibly linked to a competition with hydroxyl ions for the positive surface. In addition, we showed that polydispersity in the polymeric fraction of the superplasticizer influences adsorption, even for polydispersities of only 2.6, which remain much lower than most data reported for SNFC or lignosulfonates, for instance. For other polymers, which can not be either well separated or detected, one does not really know what the polydispersity is. Consequently, any relation between average molar mass data and parameters for calculating steric repulsion is highly hazardous. For this reason and for several situations, we preferred using PCA-2, which has the narrowest distribution of molar masses (polydispersity of 2.2).

Effect of particle size

Within reasonable approximation, the total interaction force in a doublet is proportional to the harmonic average radius of the two interacting particles larger than $1\mu\text{m}$. This radius is always smaller or equal to the arithmetic average ratio. Cement has a broad particle size distribution and one must therefore determine the harmonic average radius and the frequency of interactions between particles of different sizes. In the program used to calculate these interactions, we use a minimum separation distance. When particles are closer than this distance, we consider that they are agglomerated. The average ratio is not very sensitive to this distance, but the number of interactions is. We have performed calculations with different values, but the most reasonable seems to be the minimal distance equal to the size of the smallest particle in the distribution.

11.2.2 Desagglomeration

Cement suspensions are not stable in a colloidal sense. They do not have a potential barrier resisting agglomeration. The potential curves only have a primary minimum. Its depth decreases strongly with increasing adsorbed layer thickness and to a lesser extent with increasing electrostatic potential.

The concept of Brownian motion as a means providing the energy necessary to separate these particles does not seem relevant to cement suspensions, since even the smallest cement particles are too large to be significantly effected by Brownian motion. On the other hand, shear forces, even at very low shear rate are capable of providing the forces needed to separate the agglomerated particles.

Yield stress is used to define the stress, which induces a transition between a solid and a liquid behaviour. There are serious limitations in using this parameter, because the transition is not as clear as it may seem. However, for cement suspensions, which can only undergo extremely small deformations before leaving the linear viscoelastic regime, this parameter should provide reasonable insight into the microstructure of the suspension.

The force, which can be transferred to a doublet from an applied stress, varies roughly with the square of the arithmetic radius of the particles. On the other hand the interparticle force increases with the harmonic average ratio of these particles. So, at low stresses only doublets composed of large particles can be dispersed. As stress is increased, the particles of smaller doublets can be separated.

The problem for calculating yield stress is to determine which fraction of doublets must be broken in order to obtain the desired solid-liquid transition. One solution that has a physical basis, is to estimate (may be calculate) the maximum solid fraction, which can be reached with a given particle size distribution. We then consider that this maximum solid fraction is the sum of the solids and the additional effective volume due to agglomerates. For a given solid loading, we can therefore calculate what the additional effective volume of agglomerates can be in order to reach the maximum solid loading of this system. We can then calculate the yield, which will disperse enough doublets to induce an effective volume fraction smaller or equal to this maximum solid loading.

The limitation of this approach is precisely the determination of the maximum volume fraction. We consider agglomerates to act only through an increase of the effective solid loading. However, we consider that the maximum loading remains constant. In addition, this calculation relies strongly on the accuracy of interparticle force calculations. For this reason, it is paramount for the further development of this method to obtain precise values for the thickness of the adsorbed layers. In addition, there is need to develop a rigorous analysis of the role of electrostatics in the interactions of layers of adsorbed polyelectrolytes. The last sensitive parameter is the minimum distance, which can be used to identify doublet in the particle-packing program.

Despite all these limitations, the yield stresses that are calculated with data having reasonable physical basis, lead to values similar to those determined experimentally. We believe this is a promising approach, which deserves further developments and which could be applied to many other systems in which the particle sizes are sufficiently large to neglect restabilisation by Brownian motion.

Finally, it is important to point out that these agglomeration calculations are based on the assumption that the adsorbed layer does not contribute to the dispersion force. It is important that future work seriously addresses this issue. Indeed, if the polymer contributes to the dispersion force, then the effective plane of origin of the dispersion force is shifted outwards. If the adsorbed layer thickness is L and the plane of origin shift is P , then the agglomeration force varies roughly with $1/(L-P)^2$ instead of $1/L^2$. So that the maximum interparticle force would change by a factor $L^2/(L-P)^2$. If $P=L/2$, the force would be about 4 times larger and 1.8 times larger if $P=L/4$.

11.3 Role of chemical effects

Grinding aid effect

The two cements we studied were produced by grinding the same clinker. One of the cements was ground with a triethanol amine acetate, a common grinding aid, and the other without grinding aid. Both were ground sufficient time in order to obtain the same final specific surface. At the end, the particle size distributions were quasi identical.

We found that the adsorption of PCA-2 was significantly effected by the grinding history of the cement. On the other hand, PCA-1 was not significantly effected. Triethanol amine has been reported to increase the solubility of the C_4AF phases, by complexing the iron ions. This increases the availability in solution of aluminates makes coprecipitation with polymers more probable. In fact, it seems from HPLC that PCA-2 and aluminates form micelles even at low concentrations.

So, we are led to believe that there is a chemical reaction, which acts as a sink for part of the added polymer. This reaction can be coprecipitation or micellisation or intercalation. For this reason, it is too restrictive to interpret solution depletion results strictly in terms of adsorption. We propose the term of polymer consumption instead, so that we group adsorption and chemical reactions in the same term.

The grinding history also seems to effect the yield stress. We found that values for the cement with grinding aid was lower than those of the cement without grinding aid, for both polymers. Though significant, this difference remains small (about 25%). It is possible that this difference comes from small variations in the particle size distributions. It might also originate from the fact that in order to obtain the same final specific surface; longer grinding times are required in absence of the grinding aid. More energy must be put into the system and the final surface must contain more defects. This probably enhances somewhat the initial reactivity (first hour or so). Here, we talk of reactivity in the general sense and not restrictively to the reactions which are of concern for superplasticizer consumption.

In the remaining paragraphs of this section, we will argue that other data in the literature also point towards the existence of a chemical sink for part of the added polymer. The interpretation of these results does not involve the authors who collected the experimental data.

Etringite a chemical sink for superplasticizers

Uchikawa et al (1997a,b) reported AFM results in which the force between a cement compact and a platinum tip was measured in presence of different polymers. Comb copolymers induced the strongest repulsion and these authors conclude on the importance of steric effects. However, they did not comment the fact that the interaction began at distances at least ten times larger than what might be expected from the polymers they were using. More recently, in a review paper, Uchikawa (1999) determined by Auger spectrometry the carbon profiles in these compacts. This time however, he performed this measurement in both direct and delayed adsorption modes. A striking result was that the depth of the layer in which carbon was found varied by a factor about ten between both addition modes. In fact, the depth was compatible with the polymer size, in the case of delayed addition. In the case of direct addition, the depth was ten times larger, making it compatible with his previously mentioned AFM results. In a schematic way, these results could suggest the situation shown schematically in Figure 11-2.

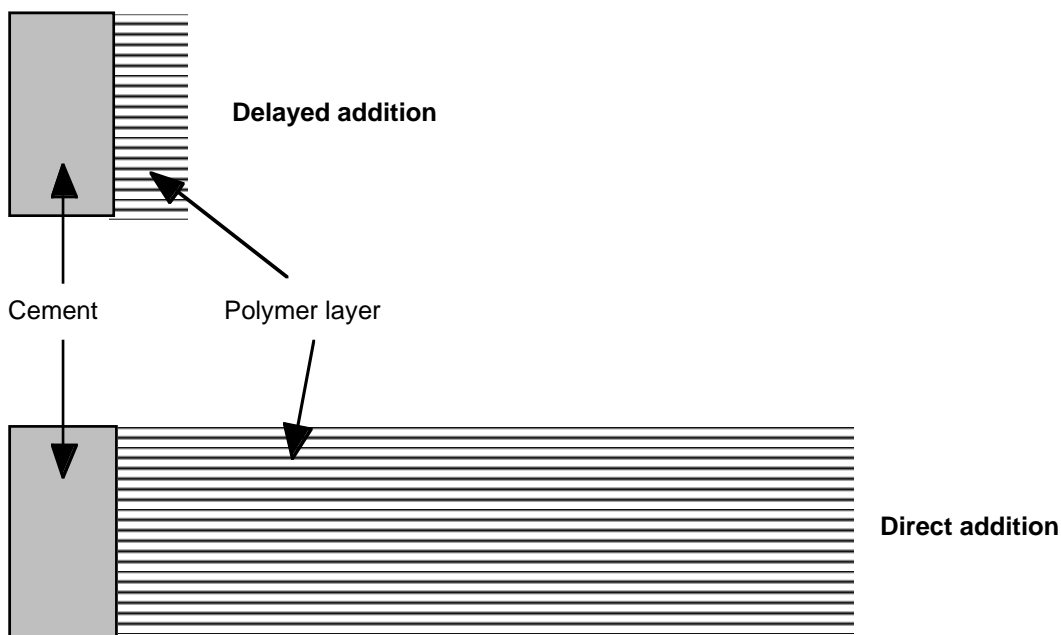


Figure 11-2. Schematic representation of adsorbed polymer thickness differences, which are suggested by the Auger spectroscopy measurements by Uchikawa (1999).

In fact we can take this schematisation a step further and explicitly integrate the effect of aluminates. In delayed addition most aluminates would form ettringite, before polymer is added. In direct addition, a first layer of coprecipitate (or micelles, or gel) would be formed. This layer might be expected to have dielectric properties similar to cement. Therefore, it could not be considered as a layer inducing a steric repulsion, since the plane of origin of the dispersion forces would be shifted outwards. Provided enough polymers are added an ultimate layer might be able to adsorb onto this ill-defined layer. Only this fraction of the polymer would be able of inducing steric repulsion. This idea is schematised in Figure 11-3.

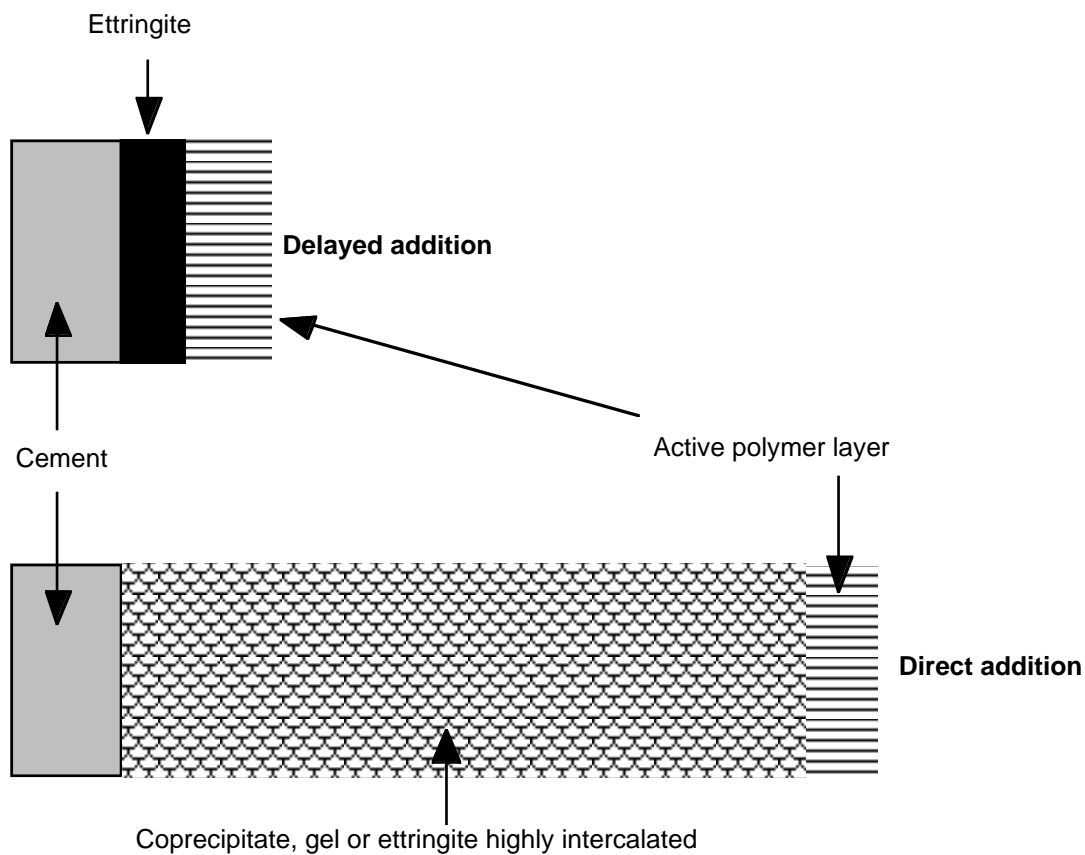


Figure 11-3. Schematic illustration of the chemical sink effect of ettringite precipitation. In the case of direct addition, many polymers are consumed uselessly. The plane of origin for the van der Waals force would be shifted from the surface towards the basis of the polymer layer.

The existence of coprecipitation has been shown by Fernon et al (1997) for oligomers of SNFC. Based on these observations, they proposed a model for the intercalation of SNFC into calcium aluminate hydrates (Figure 11-4). In fact, it appears that the counter ion of SNFC can play a controlling role in this process. Piotte (1993) found that if magnesium was used as a counter-ion to SNFC, the suspensions thickened strongly. However, this does not occur with the polymers we used. We have found this involves precipitation in the strongly alkaline pH of $\text{Mg}(\text{OH})^+/\text{SNFC}^-$ type coprecipitate. For this reaction to occur, magnesium should arrive as a dissociated divalent cation in the alkaline medium. SNFC, which can contain non-linear polymer, leads to a gel, while the linear polymers used in this study do not. The structure of this coprecipitate is illustrated in Figure 11-5. It is an adaptation of the model proposed by Fernon et al (1997) to explain the coprecipitation of calcium aluminates and SNFC oligomers.

However, if MgCl_2 is added to the cement, the precipitation of $\text{Mg}(\text{OH})_2$ is almost instantaneous, much less SNFC is coprecipitated and the suspension is much more fluid. So, the counter-ions can have a strong effect, provided it interacts in a specific way with the polymer. Because we do not have this type of interaction with the polymers we studied, we do not have to consider this effect in our model systems.

Role of sulphates and alkalis

At this point we must consider factors capable of reducing the amount of polymers lost in the chemical sink. This could be done, for instance, by increasing the sulphate content. If more sulphates are available, more ettringite will be formed and consequently fewer polymers should be consumed and *lost*. This idea explains the results by Pagé et al (1999). They found, using direct addition, that including small amounts of 0.2% Na_2SO_4 in the polymer solution decreased the apparent adsorption, or rather consumption, and improved the rheology. Therefore, at equal dosage of superplasticizer, more polymers are available for adsorption and a better workability can be obtained. Kim et al (1999) found very similar results when they compared high and low alkali cements. There is confusion when one talks of alkalis in cement. The chemical analysis gives them as Na_2O and K_2O . However, most comes in the form of Na_2SO_4 and K_2SO_4 . The sulphate precipitates during ettringite formation and leaves 2KOH and either 2NaOH in solution. This gives the impression that Na_2O and K_2O have been hydrolysed. So, the results by Kim et al (1999) are more than likely also comparing a high and a low sulphate situation. The trends they observe are the same than those of Pagé et al. (1999) as illustrated in Figure 11-6.

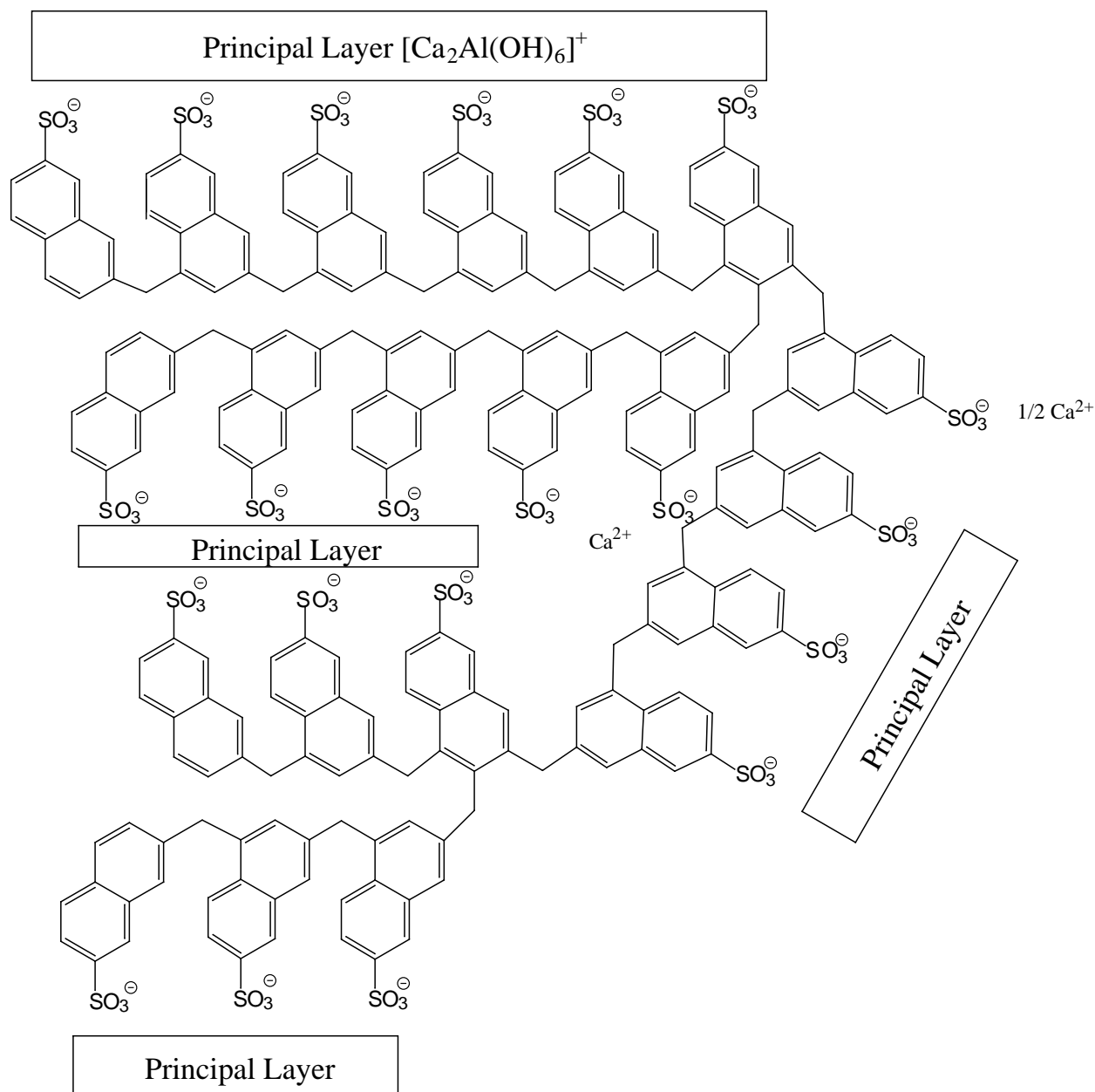


Figure 11-4. Calcium aluminate layers intercalated with SNFC [Feron et al (1997)].

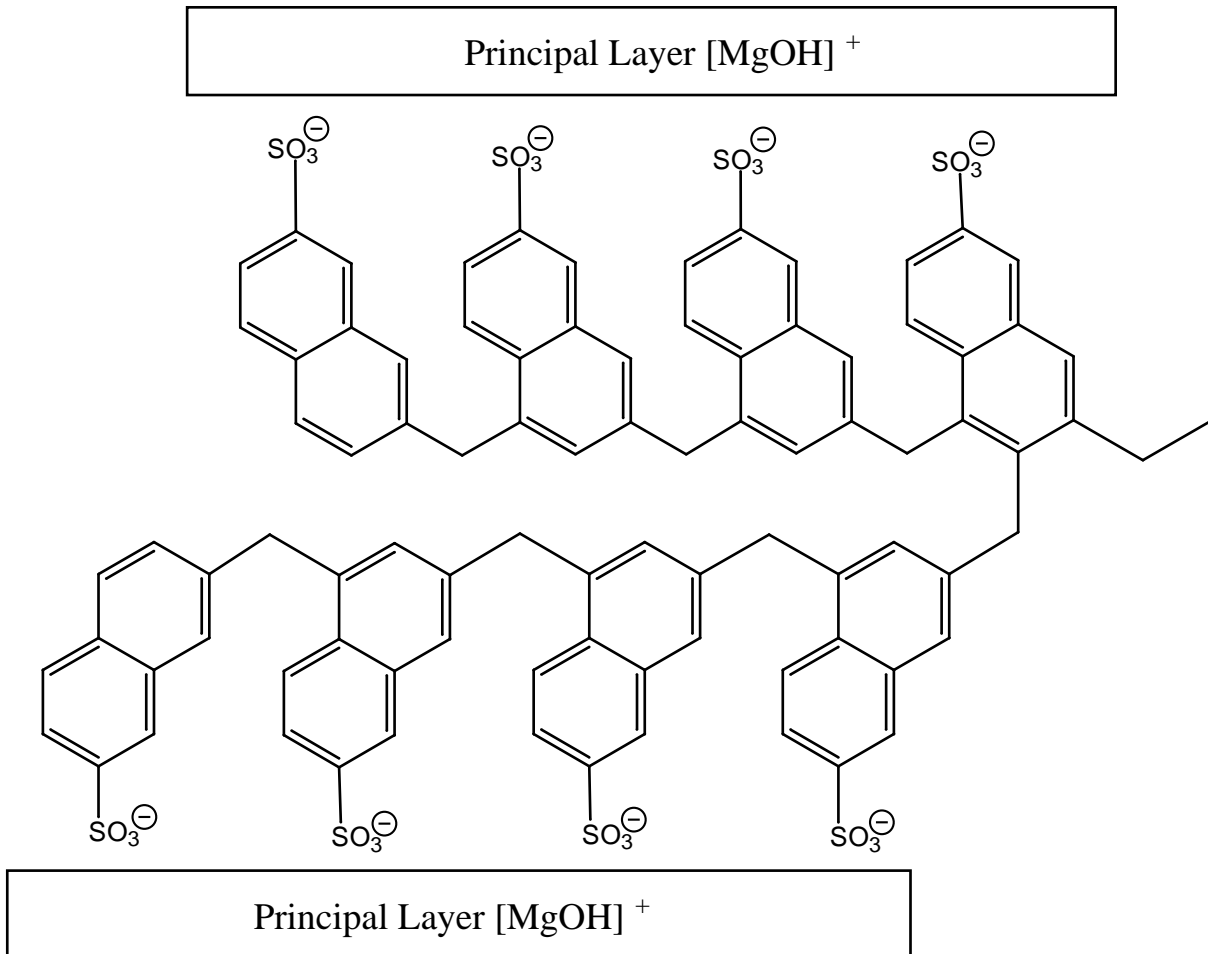


Figure 11-5. Schematic representation of the compound formed when MgSNFC is placed in a highly alkaline environment. The figure is adapted from the one presented by Fernon et al (1997) for the coprecipitated of SNFC and calcium aluminates.

With the model proposed here, what in fact happens is that the “consumption” of polymer is decreased by higher availability of sulphate ions, whether directly added or coming from the cement. This minimises the coprecipitation, micellisation or intercalation so that at equal dosage the superplasticizer efficiency is higher.

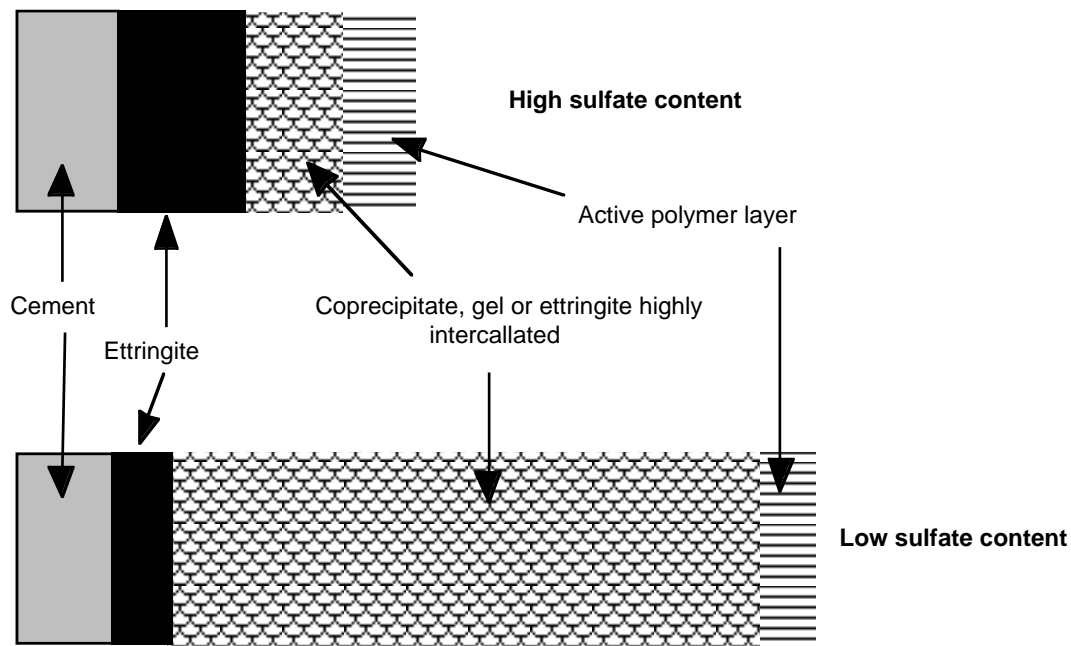


Figure 11-6. Schematic representation of the effect of sulphate content in cement. With high amounts of sulphate less polymer is lost in the chemical sink.

Reactivity towards superplasticizers

We can bring these results together with the ones showing the effect of the grinding aid. Let us use the term reactive cement to designate the reactivity towards the polymer. That is, a very reactive cement would consume a lot of polymer by coprecipitation type reactions, therefore giving a lower workability at equal dosages. We illustrate this in Figure 11-7. A misinterpretation of this mechanism could lead to the conclusion that the higher the adsorption, the worse the dispersion! From this we could expect that NaOH should produce effects similar to those with Na_2SO_4 , since Na_2O increases early reactivity [Hewlett (1999), subchapter 8.3.3]. On the other hand, we do not expect significant effects due to the addition of NaCl. Perhaps at every high additions, there might be an ionic strength effect.

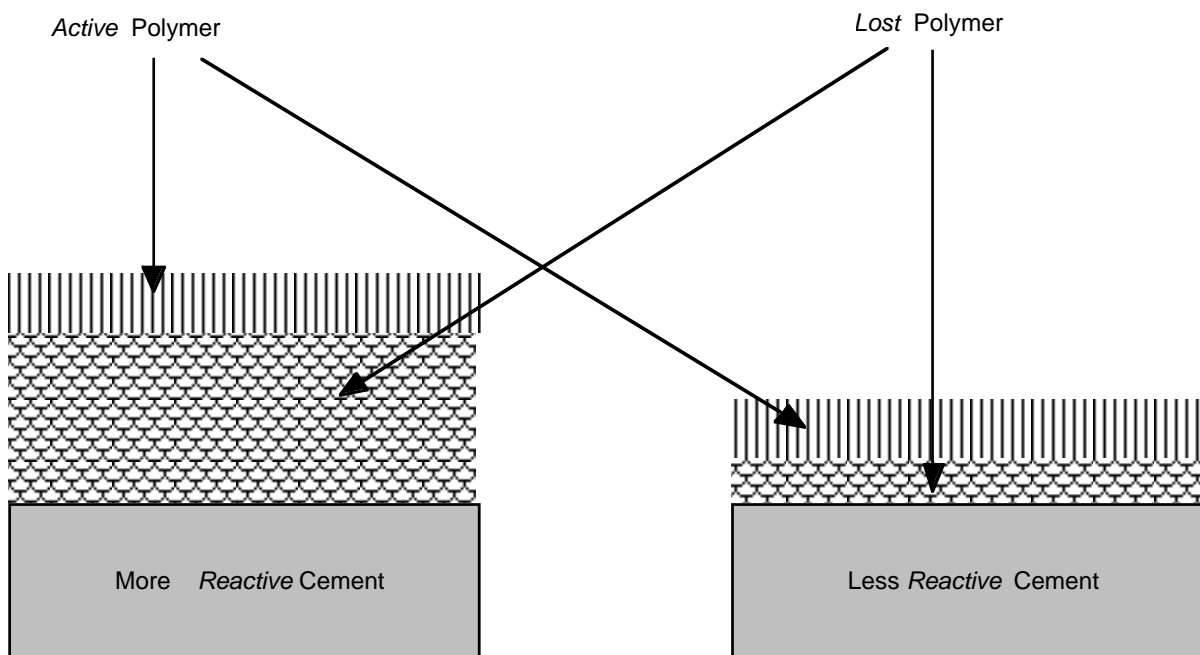


Figure 11-7. Schematic representation of the concept of reactivity of a cement towards a polymer. Higher reactivity leads to a higher consumption of polymer in side-reactions and lower availability of the polymer for dispersion. As a result more polymer is required for equal performance.

The amount of polymer, which is consumed by the early reactions, depends both on the polymer and the cement. This is well illustrated by the fact that PCA-1 is not effected significantly by grinding history, while adsorption of PCA-2 is.

For economic reasons, we must maintain a good dosage-efficiency response. Therefore, we must avoid uselessly consuming part of the added polymer. For this reason, delayed addition should be preferred. This procedure will become limited in particular at low water-cement ratios, where dispersion is required to make mixing possible. Furthermore, delayed addition is often not possible for practical reasons on construction sites. Therefore, it will be necessary to use polymers, which do not quickly lose their efficiency. Comb copolymers, for which the side chains usually are polyethylene oxides, maintain workability over a long range of time. Sakai and Daimon (1997) attribute this to the fact that these side chains can stretch out and induce a steric effect while hydration layers grow from the surface. We illustrate this in Figure 11-8.

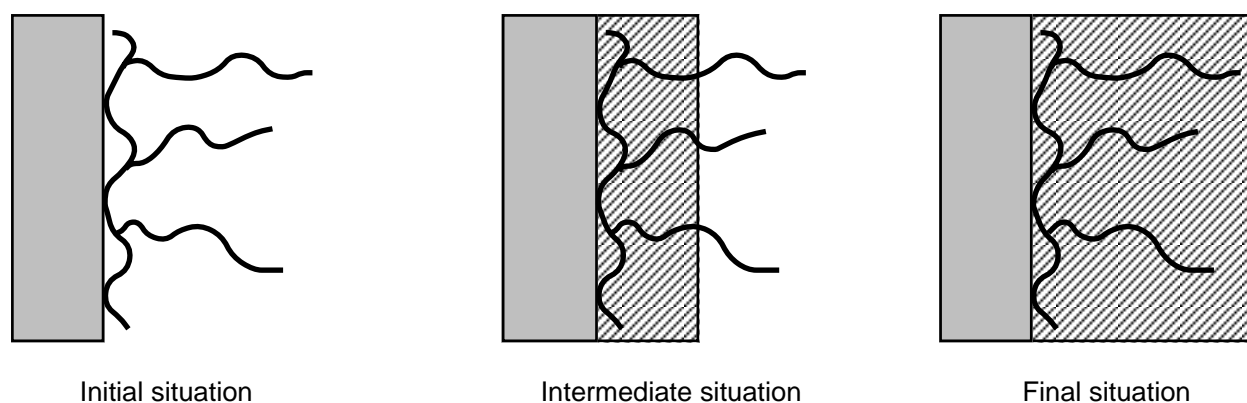


Figure 11-8. Illustration of one explanation of the longer induced workability in presence of comb copolymers, with polyethylene oxide as side chains. Adapted from Sakai and Daimon (1997).

Finally, we can point out that in order to maintain workability over a very long time, the presence of polymers capable of readsorbing onto the surface would be necessary. Tanaka et al (1999) have presented some molecules, which are devised to “open-up” or “unfold” before being able to adsorb.

This limited interpretation of chemical effects stresses the importance of differentiating between polymer adsorption and polymer consumption. We have shown that optimal dispersion requires total surface coverage. For a given dosage, depending on the importance of coprecipitation, this coverage will or will not be reached. From this it is evident that comparing efficiencies of polymers at equal dosages on only a limited range of dosages cannot provide sufficient data for mechanistic interpretation. The agglomeration effects become much more complicated. This frequently used experimental procedure is useful if one seeks a desired effect for the lowest dosage of polymer. It is not valid for seeking the maximum performance.

Chapter 12 Conclusions

The main theme of this thesis has been to study the optimum dispersion, which polyelectrolyte superplasticizers can induce in cement suspensions. It turned out that these effects can be related to the adsorption of the polymeric molecules on to the surface of particles. This decreases the attractive forces leading to agglomeration, by a steric repulsion, possibly complemented by an additional electrostatic contribution.

In order for this dispersion to take place it is therefore essential for the superplasticizers to adsorb efficiently onto the surface. This has been studied in detail both with cements and model systems (MgO and Mg(OH)₂).

Provided the superplasticizers can adsorb, a dispersion effect will be observed. The question is then to determine what the magnitude of this effect might be, depending on the molecular structure of the polymers.

A model was developed in order to relate quantitatively interparticle force calculations to the rheology of cement suspensions at low shear rate. Though this model still presents a number of limitations, it provides a good correlation with experimental data, using realistic parameters such as:

- adsorbed layer thickness compatible with adsorption data
- maximum effective volume fractions compatible with particle packing fractions expected for the particle size distribution of the measured cement
- electrostatic potentials low due to the high electrolyte concentrations.

This model opens very interesting perspectives for comparing microstructural differences between cement suspensions with similar workability, but dispersed with different superplasticizers.

Additional complications arise in cement suspensions, because the superplasticizers can interfere with the on-going hydration reactions. In particular, an important amount of superplasticizers can be consumed during the early formation of ettringite. Implications with respect to the chemical composition of cements and the consequence on the performance attainable for a given dosage are discussed.

12.1 Adsorption

Results

As mentioned above, adsorption of polymeric molecules is a very important step in order to develop a steric or electrosteric repulsion capable of avoiding intimate contact between particles, which otherwise would be strongly agglomerated.

With cement suspensions, the full potential of HPLC has been exploited to analyse the effect of polydispersity in adsorption (consumption). It was possible to show that within the polymeric fraction, the adsorption is correlated with increasing retention time of the fraction but not with its initial concentration. So segregation during adsorption, which can be attributed to molar mass. Larger molar masses adsorb less than the lower ones. However, the difference decreases when the polymer is not included in the mixing water, but added later. This might point to a preferential consumption of low molar mass products by coprecipitation, intercalation or micellisation during the formation of ettringite.

The main result of this is that the proportions of the polymeric fractions consumed and remaining in solution are not the same. Therefore, if adsorption data is to be used in interparticle force calculations, it is paramount either to work with polymers having a narrow molar mass distribution or to have the ability of separating and analysing these fractions, to know what parts adsorb and to what extent.

With MgO model suspensions, temperature was found to effect adsorption, depending on the nature of the polymer. This has been interpreted as the result of a competitive adsorption between the anionic polymers and hydroxyl groups, which are present in large amounts at the pHs investigated. Such an effect could have important implications for the adsorption of polymers in cement suspensions. However, getting experimental evidence of this is complicated by the consumption of

superplasticizers during the early formation of ettringite. To avoid this difficulty, it would be possible to add the polymer as a concentrated solution a few minutes after mixing, once the ettringite formation has passed its maximum rate. In addition, temperature changes will change the kinetics of hydration. However, it would be conceivable to study the effect of different concentrations of added hydroxides on the adsorption of polymer in delayed addition.

Perspectives

Understanding effects of polydispersity is of great practical importance for superplasticizer producers. If only one part of the molar mass distribution, probably the largest, is really giving the desired effect, then different choices can be devised. The first is to have enough analytic resolution to decide if the polymers synthesised have enough of the critical molar mass fraction. The second could be to blend a polymer with a narrow molar mass distribution, more costly to synthesise, with a much more polydisperse polymer of the same type, but with a definitely lower average molar mass, not overlapping with the critical mass fraction. This other polymer would just have the function of allowing a good final coverage of the surface, probably also hindering some reactions.

The possibility that hydroxyl groups might be in competition for surface sites, with the polymers must be looked into more thoroughly. The difficulty in modifying the hydroxyl content is that the zeta potential might also change. Nevertheless, with MgO there is probably a range in which it is possible to study this effect, without reaching too negative zeta potentials, which would clearly hinder polymer adsorption. If temperature effects are studied for two hydroxyl concentrations, it is expected that the one having the least hydroxyls would be the less temperature dependent. In addition, it would have higher adsorption, but the difference would decrease with increasing temperature.

Solving this problem of competitive adsorption represents an important information for the design of polymers. Indeed, if there are effects, they would increase with decreasing adsorption energies. Therefore, there would be a limit to inclusion of side chains in comb-type copolymers, since they act as charge spacers and decrease the density of adsorbing groups.

12.2 Rheology

Results

Interpreting of the rheology of cement suspensions is a complex issue. One of the main problems is that because of the important amount of large particles in cement, sedimentation takes place even before zero yield stress. There seems to be a degree of agglomeration above which, sedimentation is hindered because the effective size of agglomerates is space filling. At lower degrees of agglomeration, sedimentation can take place without being spacially hindered. So, if one wants to observe the optimum dispersion effect of a superplasticizer, one must increase the volume fraction of solids, so that hindered settling by dispersed particles will be sufficient to avoid sedimentation. At very high volume fractions however, one can expect interparticle friction effects to modify the behaviour.

With a rheometer using concentric cylinder geometry, the macroscopic effect of sedimentation is somewhat lowered since particles will also be coming down from the liquid above the gap. Measurements point to the existence of a minimal yield stress, which depends both on the polymer and the cement.

With model suspensions, sedimentation appeared as soon as the suspensions became Newtonian in behaviour. This must be a fortuitous combination of the particle size distribution and effective density of the material. However, this combination, allowed understanding the major role of adsorbed polymers much better than could have been possible with cement suspensions. Dispersion of the highest volume fraction required saturation of the surface by adsorbed polymers, without any additional polymers remaining in solution. This strongly suggests that the dispersing capacity of these superplasticizers is indeed exclusively linked to the adsorbed polymers.

Perspectives

It is important to find the most adequate method for measuring the rheology of cement suspensions. The first question to address is, does one ultimately look for an application in which settling hindering agents are used. For instance, self-levelling concrete often contains organic molecules, which increase the intrinsic viscosity without modifying the yield stress, thus hindering sedimentation but not flow at very low shear rates. Use of such an agent would bring in an additional parameter, capable of interacting with the numerous other factors contributing to the rheologic behaviour. However, it would make the rheology measurements easier, allowing for instance the use of cone and plate or

plate and plate geometries. Without such molecules, these experimental configurations are much too sensitive to sedimentation to allow the study of the maximum performance of superplasticizers.

Another important question to address is to know whether one looks for the maximum performance of a superplasticizer, or whether one wants to reach a given effect for the least amount of added polymer. For many applications, the effects sought do not require total dispersion of the cement particles. Therefore, it is possible to maintain a certain degree of agglomeration. This makes interpretation very complicated because rheology will not only depend on the optimal dispersion capacity of the polymer, but also on surface coverage and the rate of interparticle bridging by superplasticizers due to badly covered surfaces. Copolymers containing both adsorbing and non-adsorbing groups are therefore expected to perform better at a low surface coverage, since they will induce less bridging by crossed adsorption.

The other major consideration is to know what type of shear rates the cement will ultimately experience in mortars or concrete. It was considered that it is mainly in the low shear regime that the effects of superplasticizers can be analysed. In addition many field tests are done with methods such as slump, in which the dominant factor is yield stress. What the situation is in a mixed, poured or pumped concrete is another issue.

If in the future, it is confirmed that the low shear behaviour is the most important to study, then one must choose between measuring the paste by oscillation, creep and recovery or stress ramps. The latest rheometers, might allow sufficiently small deformations to measure cement suspensions, without rupturing their microstructure. Creep and recovery also seems a method, which could open new perspectives in understanding and quantifying the effect of superplasticizers. These methods require however, a larger amount of experimental work or less straight forward interpretation and extrapolation. It is therefore important to judge whether the additional information is sufficiently important to warrant a more time consuming approach. For yield stress measurements by stress ramps, the use of a paddle could offer a way of avoiding the problem of wall-slip. However, this method only gives yield stress as a physically based parameter and not viscosity. Further quantitative modelling of rheology including behaviour at higher shear will therefore not be possible with only such data.

The rheology of cement suspensions is a complex issue and one must define what type of information one seeks. Experimental set-ups and procedures can then be chosen more judiciously. Our belief is that in order to understand superplasticizer behaviours, it is important to make these choices in order to obtain data, which can in principle be quantitatively linked to the microstructure of the cement suspension.

12.3 Interparticle forces

Results

Calculations suggest that the dominant effect in dispersion is linked to the adsorbed layer thickness. For polyelectrolytes, this thickness can also have an importance in the electrostatic effect, since it shifts outwards the plane of origin of the electrostatic charge or potential. The exact position of this plane of origin is debatable. It was argued that zeta potential measurements will not significantly compress this layer and that this plane should be near the extremity of the adsorbed layer.

In cement suspensions, the aqueous phase is a very concentrated electrolyte in which ion pair associations take place and activities are not unity, which leads to deviations from the Poisson-Boltzmann equation derived for ideal solutions. An equivalent symmetric electrolyte representation was developed to allow the use of existing solutions for calculating the electrostatic repulsion between charge surfaces in an ideal electrolyte. In addition, the static term involved in the dispersion force is screened the high electrolyte concentration and must therefore not be taken into account when calculating the attractive dispersion force. Preventing close contact by adsorbed polymers reduces the maximum attractive force. This is possible because these polymers do not contribute (or at least little) to the dispersion attractive force. Since this force strongly decreases with distance, the maximum force is reduced. The decrease of the dispersion force is dominated by a geometric term, which is multiplied by the Hamaker constant. However, this Hamaker constant, which should rather be called Hamaker parameter, also decreases with distance. This is called retardation and must be taken into account in order to obtain correct values for the dispersion force. Neglecting retardation would lead to an error of 60% for the estimated polymer thickness.

The interparticle force calculations indicate that cement particles, even with superplasticizers will tend to agglomerate. Because of their large size, cement particles are not efficiently separated by Brownian motion. However, even very low shear rate is capable of transferring to the agglomerates the forces (or moments) required to separate pairs. For this reason, a model was developed seeking to relate the magnitude of the maximum interparticle force to yield stress.

These interparticle forces depend on the sizes of the interacting particles and so does the efficiency of shear transfer to the pairs. So, particle size comes into the attractive and the separating shear force. Separation becomes increasingly feasible as the size increases. For precise determination of the

probability of separating two particles, both sizes must be taken into account. This rises a difficulty for cement suspensions since it has a large particle size distribution. To solve this, a computer simulation was used to determine the frequency of contacts between particles of different sizes, for the measured particle size distribution of the cement used.

Using this approach, the probability of separating pairs of particles was determined with respect to the particle sizes, the superplasticizer nature and the applied shear. So, for an applied shear, there is for each type of particle pair a fraction, which remains agglomerated, and increases the effective volume of the suspension. This increase in the effective volume must not lead to a final effective volume larger than the maximum random compact packing density of the cement, which can be determined based on its particle size distribution. Conversely, this argument can be used to calculate the yield stress of a suspension by inputting the cement particle size distribution and superplasticizer characteristics.

Numerical results are in good agreement with experimentally determined values of yield stress, for polymer layers with a thickness compatible with both adsorption data and rather compressed mushroom-type conformation of the adsorbed molecules. The major achievement of this approach is that all parameters are within physically relevant ranges. Further characterisation of the polymer conformation and wider studies of rheology, should allow to optimise this for direct quantitative predictions of superplasticizer efficiencies in cement.

Perspectives

Hamaker constants of pure cement phases must be determined to calculate all the possible pair interactions between these phases. This will also lead to better understanding how the multimineral cement grains might be interacting with one another.

Another interesting avenue might be to determine the dielectric properties of polymer films in a very concentrated electrolytic medium. In order to quantify the maximum attractive interparticle force it is important to know to what extent the adsorbed layer contributes to the dispersion interaction. In absence of electrostatic effects, this force decreases with about $1/L^2$, where L is the adsorbed layer thickness. A contribution to the dispersion interaction from the polymer would effectively decrease L and consequently increase the maximum interparticle force.

The adsorbed layer thickness is the most important parameter. It is also difficult to determine. AFM and surface force measurements could be made with clean surfaces in a concentrated electrolyte environment in order to evaluate this. These methods however, rely on a fitting procedure, which can be more or less well adapted to integrating electrostatic effects. An important complement to this therefore seems to determine the adsorbed polymer conformation at surfaces. In this procedure, the most complicated step could well be determining the dominant characteristics of the surface in adsorption (defects, solid solutions, etc.).

Electrostatics is probably the most complicated interaction. In cement suspensions, there is the possibility that divalent calcium could bridge negative surfaces by ion correlation. This could have an effect in polymer adsorption, but also in polymer-polymer interactions. In addition one should take into account the interactions of all the different ionic groups with all those of the other polymer layers as well as the dissociated ions in solution. Finite ion volume effects should be considered as well as thermodynamics for non-ideal solutions. This is a challenging task for an interesting fundamental work having major practical implications. Indeed, for tracing cement / superplasticizer incompatibilities, it is important to know whether or not dispersion also depends on electrostatic repulsion.

The approach for direct calculation of yield stress deserves further development. Moreover, it would be interesting to test its predictions in concentrated suspensions of spherical particles. The distribution of these does not have to be narrow, since it is taken into account in the model. It only needs to have a size above which Brownian effects are negligible. By limiting the number of large particles, sedimentation problems would be decreased. In addition high electrolyte concentrations should be used, so that screening and double layer compression is the same as in cement. Nice spherical calcite powders have been synthesised at the LTP and could be an interesting model system for such studies. The pH would however have to be lower than that of cement, in order not to hinder adsorption.

To conclude these perspectives linked to interparticle forces it is important to consider whether the trend of superplasticizer development is to reach good effects at dosages so low that surface saturation is not achieved. If such is the case, the correlation of polymer characteristics to the macroscopic effects on rheology will be more complicated than the treatment here. This topic has been addressed for polymer brushes, either adsorbed or grafted. It needs an extension for the mushroom, pancake or train and loop adsorption modes expected for superplasticizers studied in this thesis.

12.4 Chemical effects

Interpretation

Some mechanisms, which increase polymer consumption, have been described. They are linked, in presence of aluminates, to either coprecipitation, micellisation, or intercalation. It seems that higher sulphate concentrations favour the direct precipitation of ettringite, leading to a lower consumption of added polymers. For this reason, high alkali cements, and superplasticizers containing additional Na_2SO_4 give a better workability at low dosages.

Perspectives

A more detailed study of the above mentioned mechanisms would lead to understanding how to avoid loosing a lot of polymer in these reactions, particularly in direct addition. This mode of addition is the most convenient and probably the most widely used. So, such information has a lot of practical relevance. It was mentioned that in the case of PCA-2, HPLC showed, in presence of aluminates, the apparition of peaks at large retention times, most probably micelles. If the supernatant is contacted with a cation exchange resin (loaded with Na), these peaks are no longer present. However, it might be that the micelles are adsorbed onto the resin. A more detailed study by HPLC could provide interesting information about micelle formation and stability. A limitation could be the difficulty in separating high molar mass polymeric fractions and micelles at large retention times. Photon correlation spectroscopy might be a method allowing detection of these micelles, provided enough are formed.

Addition of sodium sulphate to control the ettringite precipitation can be problematic for concrete in which there is a risk of alkali silica reactions. One possibility could be to introduce cheap low molar mass products, which have a strong reaction with aluminates. These low molar masses would have poor adsorption, thus not competing with other polymers intended to give the dispersion effect.

12.5 Perspectives for durability

A major implication of the use of superplasticizers is to improve the durability of concrete. Producing concrete with less water leads in general to a lower final porosity. This will lead to less carbonation,

chloride ingress or sulphate attack. In fact the real objective is to lower the permeability and diffusivity of concrete.

Let us assume, that the water / cement ratio has been fixed. In such a situation one would have the choice between using an excellent polymer at low dosage or a less good polymer at higher dosage. In both cases, a degree of agglomeration would remain. In the first situation, agglomerates would be relatively independent of particle sizes. In the second situation, the remaining agglomerates would be predominantly between the small particles. The consequences on the final permeability should be evaluated.

This can be done experimentally, but also numerically. Indeed, the program, which was used to determine the frequency of contacts between particles of different sizes can simulate hydration of C_3S . It allows calculation of the development of a microstructure based on the progress of the chemical reactions. These simulated microstructures have been used recently for simulating mercury intrusion porometry, showing this approach is a way of numerically evaluating permeability.

In order to evaluate the effect of different degrees of agglomeration on the final permeability, a routine could be integrated in the initial placing of particles, taking into account interparticle interactions. This routine could exploit information on the nature of the superplasticizer and its dosage. Hydration simulations will then lead to microstructures, in which the effect on permeability of different types of residual agglomeration could be evaluated. One could calculate the consequence of choosing either to under-dose an effective but expensive polymer, or to over-dose a less effective but cheaper polymer. This could be a powerful tool for addressing this typical construction site choice, in terms of durability, the ultimate objective of using superplasticizers.

References

- Aïtcin P.-C., Jolicoeur C. and MacGregor J.G. (1994) « Superplasticizers: how they work and why They occasionally don't », *Concrete International*, **16** [5], pp. 45-52.
- Batchelor G.K. (1972) « Sedimentation in a dilute dispersion of spheres », *J. Fluid. Mech.*, **52**, pp. 245-268.
- Bergström L., Schilling C.H. and Aksay I.A. (1992) « Consolidation behavior of flocculated alumina suspensions », *J. Am. Ceram. Soc.*, **75** [12], pp. 3305-3314.
- Bergström L. (1997) « Hamaker constants of inorganic materials », *Adv. Colloid Interface Sci.*, **70**, pp. 125-169.
- Bürge T.A., Widmer J., Schoeber I. and Sulser U. (1992) « Water soluble copolymers, a process for their preparation and their use as fluidizers in suspensions of solid matter », US Patent 5, 100, 984.
- Chapuis J. (1986) « Physical elementary mechanisms of fluidification by superplasticizers or water-reducing agents », *Proc. 8th ICCG, Rio de Janeiro*, **6**, pp. 544-549.
- Chapuis J. (1990) « Rheological measurements with cement paste in viscosimeters: a comprehensive approach », *Rheology of fresh cement and concrete* (P.F.G. Banfill, Ed.), E. & F.N. SPON, London, etc., pp. 3-12.
- Claesson P.M., Kjellander R., Stenius P. and Christenson H.K., (1986) « Direct measurement of temperature-dependent interactions between non-ionic surfactant layers », *Journal of the Chemical Society, Faraday Transactions 1*, **82**, pp. 2735-2746.
- Costa U., Corazza F., Colombet P., Fernon V. and Vichot A. (1997) « Mechanisms of cement - admixture interaction », *Proceedings of the 10th International Congress on the Chemistry of Cement*, V. 3, (editor: H.J. Justness), paper 3iii003.
- Damidot D., Sorrentino D. and Guinot D. (1997) « Factors influencing the nucleation and growth of the hydrates in cementitious systems: an experimental approach », in 2nd RILEM Workshop on Hydration and Setting, To be published.
- Davidson R.L. (1980) « Handbook of water-soluble gums and resins », McGraw-Hill Book Company, New York etc., pp. 3-8.
- Evans F.D. and Wennerström H. (1994) « The colloidal domain - where physics, chemistry, biology and technology meet », VCH Publishers, Inc., New York,.

- Fernon V., Vichot A., Le Goanvic N., Colombet P., Corazza F. and Costa U. (1997) « Interaction between portland cement hydrates and polynaphtalene sulfonates », *Proceedings of the 5th Canmet/ACI International Conference on superplasticizers and Other Chemical Admixtures in Concrete* (editor: Malhotra V.M.), American Concrete Institute, Detroit, SP-173, pp. 225-248.
- Ferrari G., Cerulli T., Clemente P. and Dragoni M. (1997) « Adsorption of naphtalene sulfonate superplasticizers by cement particle through gel permeation chromatography », *Proceedings of the 5th Canmet/ACI International Conference on Superplasticizers and Other Chemical Admixtures in Concrete* (editor: Malhotra V.M.), American Concrete Institute, Detroit, SP-173, pp. 869-892.
- Ferraris C (1996) « Measurement of rheological properties of high performance concrete: state of the art report », National Institute of Standards and Technology, Gaitherburgh, USA, NIST 5869.
- Fischer E.W. (1958) *Kolloid-Z.* **160**, pp. 120-.
- Flatt R.J., Houst Y.F., Bowen P., Hofmann H., Widmer J., Sulser U., Maeder U. and Bürge T.A., (1997a) « Adsorption of superplasticizers on model powders: temperature dependence, effect on zeta potential and role of chemical structure », *Proceedings of the 10th International Congress on the Chemistry of Cement*, V. 3, (editor: H.J. Justness), 1997, paper 3iii002.
- Flatt R.J., Houst Y.F., Bowen P., Hofmann H., Widmer J., Sulser U., Maeder U. and Bürge T.A., (1997b) « Interaction of superplasticizers with model powders in a highly alkaline medium », *Proceedings of the 5th Canmet/ACI International Conference on Superplasticizers and Other Chemical Admixtures in Concrete* (editor: Malhotra V.M.), American Concrete Institute, Detroit. SP-173. pp. 743-762.
- Flatt R.J., Houst Y. F., Oesch R., Bowen P., Hofmann H., Widmer J., Sulser U., Maeder U. and Bürge T.A. (1998a) « Analysis of superplasticizers in concrete », *Analisis* **26** [2], 1998 pp. M28-M35.
- Flatt R.J., Houst Y.F., Bowen P., Hoffmann H., Widmer J., Sulser U., Maeder U. and Bürge T.A. (1998b) « Effect of superplasticizers in a highly alkaline model suspensions containing silica fume », *Proceedings of the 6th Canmet/ACI International Conference Fly-Ash, Silica Fume, Slag and Natural Pozzolans in Concrete*, (editor: Malhotra V.M.), American Concrete Institute, Detroit. 1998. SP-178. pp. 911-930.
- Fritz B. (1975) « Etude thermodynamique et modélisation des réactions entre minéraux et solutions. Application à la géochimie des altérations et des eaux continentales. », *Sci. Géol. Mém. Univ. Louis Pasteur*, vol. 41.
- Gartner E. and Myers D. (1993) « Influence of tertiary alkanolamines on portland cement hydration », *J. Am. Ceram. Soc.*, **76** [6], pp. 1521-1530.
- De Gennes P.-G. (1987) « Polymers at an interface: a simplified view ». *Advances in Colloid and Interface Science*, **27**, pp. 189-209.
- Girod G., Lamarche J.M. and Foissy A. (1988) « Adsorption of partially hydrolyzed polyacrylamide on titanium dioxide », *Journal of Colloid and Interface Science*, **21** [1], pp. 265-272.

- Green J.R. and Margerison D. (1978) « Physical sciences data 2: statistical treatment of experimental data », Elsevier, Amsterdam, p. 322.
- Hoogeveen, N.G., Stuart, M.A.C. and Fleer, G.J. (1996) « Polyelectrolyte adsorption on oxides. I. Kinetics and adsorbed amounts », *J. Colloid and Interfaces Sci.*, **182**, pp. 133-145 and “II. Reversibility and Exchange”, *ibid.*, pp. 146-157.
- Horn R.G. (1990) « Surface forces and their Action in Ceramic Materials », *J. Amer. Cer. Soc.*, **73** [5], pp. 1117-1135.
- Houst Y. F., Flatt R.J., Bowen P., Hofmann H., Widmer J., Sulser U., Maeder U. and Bürge T.A. (1999) « Influence of superplasticizer adsorption on the rheology of cement pastes » *Proceedings of the RILEM international symposium on the role of admixtures in high performance concrete*. RILEM Publications s.a.r.l., Cachan, France, PRO 5, pp. 387-402.
- Hunter, R.J. (1981) « Zeta Potential in colloid science: principles and applications », Academic Press, London, England.
- Israelachvili J. (1990) « Intermolecular & surface forces », Academic Press, London, England.
- Jolicoeur C., Nkinamubanzi P.C., Simard M.A. and Piote M. (1994) « Progress in understanding the functional properties of superplasticizers in fresh concrete », Proc. of the 4th CANMET/ACI International Conference on Superplasticizers and Other Chemical Admixtures, Montreal, ACI SP 148, Detroit, pp. 63-87
- Kim B.-G., Jiang S.P. and Aïtcin P.-C. (1999) « Influence of molar mass of polynaphtalene sulfonate superplasticizers on the properties of cement pastes containing different alkali contents », *Proceedings of the RILEM international symposium on the role of admixtures in high performance concrete*. RILEM Publications s.a.r.l., Cachan, France, PRO 5, pp. 97-111.
- Kim S. and Karrila S.J. (1991) « Microhydrodynamics: principles and selected applications. », Boston: Butterworth-Heinemann.
- Kendall M.G. and Stuart A. (1969-76) « The advanced theory of statistics.; Vol. 1: distribution theory », Griffin, London, 2nd ed..
- Klein J. (1999) Oral presentation given at the «18TH JOURNEE DES MATERIAUX TRIBOLOGIE - Approche système », EPFL, Lausanne, Switzerland, 4-5th MARS 1999.
- Kumacheva E., Klein J., Pincus P. and Fetters L.J (1993) « Brush formation from mixtures of short and long end-functionalized chains in a good solvent », *Macromolecules*, **26**, pp. 6477-6482.
- Langbein D. (1974) « Theory of the van der Waals attraction », *Springer Tracts in modern physics*. Springer.
- Lifshitz E. M. (1956) « The theory of molecular attractive forces between solids ». *Soviet Physics JETP* **2**, pp. 7-83.
- Mahanty J. and Ninham B. W. (1976) « Dispersion forces », Academic Press, London, England.

- Marlow B.J., Fairhurst D. and Pendse H.P. (1988) « Colloid vibration potential and the electrokinetic Characterization of Concentrated Colloids », *Langmuir*, **4**, pp. 611-626.
- Matsuyama H., Lewis J.A. and Young J.F. (1997) « Dispersion mechanism in processing cement paste », Proceedings of the 2nd RILEM Workshop on hydration and setting - Why does cement set? An Interdisciplinary approach, Dijon, France, to be published.
- Mehta P.K. (1986) « Concrete: structure, properties and Materials », Prentice-Hall Inc., Englewood NJ, USA, p. 450.
- Mehta P.K. (1998) « Role of pozzolanic and cementitious material in sustainable development of the concrete industry », *Proceedings of the 6th Canmet/ACI International Conference Fly-Ash, Silica Fume, Slag and Natural Pozzolans in Concrete*, (editor: Malhotra V.M.), American Concrete Institute, Detroit.. SP-178. pp. 1-20.
- Morgenthaler S. (1997) « Introduction à la statistique », Presses polytechniques et universitaires romandes, Lausanne, Switzerland..
- Nachbaur L. (1997) « Etude de l'influence d'électrolytes sur l'hydratation et la prise du silicate tricalcique, composant principal du ciment portland. Caractérisation des interactions à l'origine de la prise. », PhD. Thesis. University of Bourgogne, Dijon, France. 141p.
- Naper D.H. (1983) « Polymeric stabilization of colloidal dispersions », Academic Press, London, 428p.
- Neubauer C.M., Yang M. and Jennings H.M. (1998) « Interparticle potential and sedimentation behavior of cement suspensions: effects of admixtures », *Advn. Cem. Bas. Mat.*, **8**, pp. 17-27.
- Nkinamubanzi, P.-C. (1994) « Influence des dispersants polymériques (superplastifiants) sur les suspensions concentrées et les pâtes de ciment », Ph.D. thesis, University of Sherbrooke, Canada.
- Nolan G.T. and Kavanagh P.E. (1994) « The size distribution of interstices in random packing of spheres », *Powder Technology*, **78**, pp. 231-238.
- Ogden A.L and Lewis J.A. (1996) « Effect of nonadsorbed polymer on the stability of weakly flocculated suspensions », *Langmuir*, **12**, pp. 3413-3424.
- Ottenwil R.H. and Walker T. (1974) *Kolloid-Z. Z. Polymere*, **227**, pp.108-.
- Pagé M., Nkinamubanzi P.-C. and Aïtcin P.-C. (1999) « The cement / superplasticizer compatibility: a headache for superplasticizer manufactures » *Proceedings of the RILEM international symposium on the role of admixtures in high performance concrete*. RILEM Publications s.a.r.l., PRO 5, Cachan, France, pp. 48-56.
- Pailthorpe B. A. and Russel W. B. (1982) « The retarded van der Waals interaction between spheres », *J. Colloid Interface Sci.* **89**, pp. 563-566.
- Parks G.A. (1965) « The isoelectric points of solid oxides, solid hydroxides and aqueous hydroxo complex systems », *Chemical Review*, **67**, pp. 177-198.

- Pedersen H.G. and Bergström L. (1999) « Forces measured between zirconia surfaces and poly(acrylic acid) solutions », *J. Am. Ceram. Soc.*, **82** [5], pp. 1137-1145.
- Pierre A., Carquille C., Lamarche J.M., Foissy A. and Mercier R. (1988) « Adsorption d'un polycondensat d'acide naphthalène sulfonique (PNS) et de formaldéhyde sur le dioxyde de titane », *Cement and Concrete Research*, **18** [1], pp. 18-28.
- Piotte M. (1993) "Caractérisation du polynaphtalènesulfonate)-Influence de son contre-ion et de sa masse moléculaire sur son interaction avec le ciment", Thesis, University of Sherbrooke, Canada, pp. 149-152.
- Piotte M., Bossányi F., Perreault F. and Jolicoeur C. (1995) « Characterization of poly(naphtalenesulfonate) salts by ion-pair chromatography and ultrafiltration », *J. Chrom. A*, **704**, pp. 377-385.
- Pitzer K.S. (1991) « Activity coefficients in electrolyte solutions », 2nd Ed., CRC Press, Boca Raton, FL, U.S.A.
- Peterson H.G. and Bergström (1999) « Forces between zirconia surfaces in poly(acrylic acid) solutions », *J. Am. Ceram. Soc.*, **82** [5], pp. 137-1145.
- Pfefferkorn E., Carroy A. and Varoqui R. (1985) *J. Colloid Interface Sci.* **86**, pp. 1997-.
- Press W.H., Teukolsky, S.A., Vetterling, W.T. and Flannery, B.P., (1992) « Numerical recipes in C - the art of scientific computing », Cambridge University Press, Cambridge, 2nd Ed., pp. 661-663
- Ramachandran V.S., Malhotra V.M., Jolicoeur C. and Spiratos N. (1998) « Superplasticizers: properties and applications in concrete », CANMET Publication MTL 97-14 (TR), Ottawa, Canada.
- Roelfstra P.E. (1989) « A numerical approach to investigate the properties of concrete numerical concrete », PhD. Thesis no. 788, EPFL, Lausanne, Switzerland.
- Roth C.M. and Lenhoff A.M. (1996) « Improved parametric representation of water dielectric data for Lifshitz theory calculations », *J. Colloid Interface Sci.*, **39**, pp. 637-639.
- Russel, W. B., Saville D. A. and Schowalter W. R. (1991) « Colloidal Dispersions », Cambridge University Press.
- Sakai E. and Daimon M. (1995) « Mechanisms of Superplastification », *Materials Science of Concrete IV* (Skalny J. and Mindess S, Eds.), The American Ceramic Society, Westerville, OH, pp. 91-111.
- Sakai E. and Daimon M., (1997) « Dispersion Mechanisms of Alite Stabilized by Superplasticizers Containing Polyethylene Oxide Graft Chains », *Proceedings of the 5th Canmet/ACI International Conference on Superplasticizers and Other Chemical Admixtures in Concrete* (editor: Malhotra V.M.), American Concrete Institute, Detroit, SP-173, pp. 187-202.
- Scales P.J. and Jones, E. (1992) « Effect of Particle Size Distribution on the Accuracy of Electroacoustic Mobilities », *Langmuir*, **8**, pp. 385-389.
- Schramm G. (1994) « A practical Approach to Rheology and Rheometry », Haake, Karlsruhe, Germany.

- Schultz M.A. and Struble L.J. (1993) « Use of Oscillation shear to study flow behavior of fresh cement paste », *Cement and Concrete Research*, **23** [2], pp. 273-282.
- Sigmund W.M., Bell N.S. and Bergström L. (1999) « Novel powder processing methods for advanced ceramics », *J. Am. Ceram. Soc.* (submitted June 1999).
- Struble L.J. and Schultz M.A. (1993) « Using creep and recovery to study flow behavior of fresh cement paste », *Cement and Concrete Research*, **23**, pp. 1369-1379.
- Swiss society for cement, lime and gypsum producers (1988) « L'industrie du ciment », Edited by *Société suisse des fabricants de ciment, chaux et gypse*, Zurich.
- Tanaka Y., Ohta A. and Sugiyama T. (1999) « Polycarbonate-based advanced superplasticizers for high performance concrete », *Proceedings of the International RILEM Conference on the Role of Admixtures in High Performance Concrete*, (editors: J.G. Cabrera and R. Rivera-Villarreal), RILEM Publications s.a.r.l, Cachan, France, pp. 135-142.
- Uchikawa H. (1999) « Function of Organic Admixture Supporting High Performance Concrete », *Proceedings of the International RILEM Conference on the Role of Admixtures in High Performance Concrete*, (editors: J.G. Cabrera and R. Rivera-Villarreal), RILEM Publications s.a.r.l, Cachan, France, pp. 69-96.
- Uchikawa H., Hanehara S. and Sawaki D. (1997a) « The role of steric repulsive force in the dispersion of cement particles in fresh paste prepared with organic admixtures », *Cement and Concrete Research*, **27** [1], pp. 37-50.
- Uchikawa, H., Hanehara S. and Sawaki D., (1997b) « Effect of electrostatic and steric repulsive force on the dispersion of cement particles in fresh cement paste », *Proceedings of the 10th International Congress on the Chemistry of Cement*, V. 3, (editor: H.J. Justness), paper 3iii001.
- Vellegrol D. (1997) « Determining the forces between colloidal particles using differential electrophoresis » PhD thesis Carnegie Mellon University, Pittsburgh, U.S.A.
- Yang M., Neubauer C.M. and Jennings H.M. (1997) « Interparticle potential and sedimentation behavior of cement suspensions » *Advn. Cem. Bas. Mat.*, **5**, pp. 1-7
- Yoshioka K., Sakai E. and Daimon M. (1997) « Role of steric hindrance in the performance of superplasticizers in concrete », *J. Am. Ceram. Soc.*, pp. 2667-2671.
- Zhor J. and Bremmer T.W. (1997) « Influence of molecular weight fractions on the properties of fresh cement », *Proceedings of the 5th Canmet/ACI International Conference on Superplasticizers and Other Chemical Admixtures in Concrete* (editor: Malhotra V.M.), American Concrete Institute, Detroit, SP-173, pp. 781-805.

Annex A Cement nomenclature

Notation	Chemical composition	Chemical name
CH	Ca(OH)_2	Calcium hydroxide
C_3S	$3\text{CaO}\cdot\text{SiO}_2$	Tricalcium silicate
C_3A	$3\text{CaO}\cdot\text{Al}_2\text{O}_3$	Tricalcium aluminate
H	H_2O	Water
CSH	$\text{CaO}\cdot\text{SiO}_2\cdot\text{H}_2\text{O}$	Calcium silicate hydrate

Annex B Notations

Annex B.1 Greek Symbols

Notation	Signification	Value	SI units
ϵ_0	Permittivity of vacuum	8.854×10^{-12}	$C^2N^{-1}m^{-2}$
ϵ_r	Relative dielectric permittivity		—
c_k	Concentration of species k		mol/kg _{water}
γ_k	Activity coefficient of species k		
$\dot{\gamma}$	Shear rate		1/s
μ	True viscosity		Pa s
μ_{Bi}	Intrinsic viscosity (Bingham model)		Pa s
μ_{H-B}	Herschel Buckley parameter		
μ_k^*	Electrochemical potential		
$\rho^{(e)}$	Total density of charges		$C m^{-3}$
$\rho^{(f)}$	Free charge density		$C m^{-3}$
σ	Stress tensor		
τ	Shear Stress		Pa
τ_0	Yield Stress		Pa
ψ	Electrostatic potential		

Annex B.2. Latin Symbols

Notation	Signification	Value	SI units
a_k	Activity of k		—
A_{D-H}	First Debye-Hückel parameter		
$A_{(h)}$	Hamaker constant for a separation h		J
B_{D-H}	Second Debye-Hückel parameter		
c_k	Concentration of species k		mol/kg _{water}

C_{D-H}	Third Debye-Hückel parameter		
C_k	Species specific 3 rd Debye-Hückel parameter		
e	Charge of a electron	1.60210×10^{-19}	C
E	Electrostatic field		N/C
F	Force		N
h	Separation distance between interacting spheres		m
h	Planck's constant	6.6256×10^{-34}	J s
$H_{(a1,a2,h)}$	Geometric term in the dispersion interaction		—
K	Equilibrium constant		—
k_B	Boltzmann's constant	1.38054×10^{-23}	J/°K
N_a	Avodgadro's number	6.02552×10^{23}	Molecules/mole
n_k	Concentration of k		Molecules m ⁻³
Q	Charge of a particle		C
T	Temperature		°K
$u(y)$	Velocity of fluid		m s
z_k	Charge number of ion k		—
ΔG_{ads}	Adsorption free energy		J mol ⁻¹
ΔH_{ads}	Adsorption enthalpy		J mol ⁻¹
ΔS_{ads}	Adsorption entropy		J °K ⁻¹ mol ⁻¹

Annex C Hamaker constant calculations

The retarded and non retarded Hamaker constants were calculated using Visual Basic Macros developed in Excel and listed below.

For these calculations we pass parameters *solid* and *water*, which are a vector and a matrix characterising the dielectric properties of the solid and of water respectively.

The **water matrix** is given by the section of the table below within the dark frame. Values are also given in Table 3-6.

	UltraViolet Range		Infra Read Range			Permanent Dipoles	
C (UV)	omega (UV)	g (UV)	C (IR)	omega (IR)	g (IR)	B	1/ Tau (MW)
1	1E+16	1E+15	1	1E+14	1E+15	1	1E+11
	rad/s	rad/s		rad/s	rad/s		rad/s
0.0484	1.25	0.957	1.46	0.314	2.29	76.8	1.08
0.0387	1.52	1.28	0.737	1.05	5.78		
0.0923	1.73	3.11	0.152	1.40	4.22		
0.344	2.07	5.92	0.0136	3.06	3.81		
0.360	2.70	11.1	0.0751	6.46	8.54		
0.0383	3.83	8.11					

The vector **solid**, is given by the four values in any line of Table 3-7.

There are two separate functions.

The first gives non-retarded Hamaker constant. It can be or not screened. The formulation is

Hamaker_nrt(solid, water, screening, T)

If *Screening* is equal to zero then the static term is removed. If not specified, the static term is included.

T is the temperature in °K. If not specified the temperature is taken to be 298.15°K.

The difference between the case with and without screening provides the value of the static term.

The second function for obtaining Hamaker constants, calculates the non static terms as a function of separation (given in nm). The formulation is:

Hamaker_screened_rt(separation, solid, water, T)

Separation is the closest distance between both surfaces. It must be given in nanometers.

T is the temperature in °K. If not specified the temperature is taken to be 298.15°K.

The macros used for this are listed below:

Public c(11), omega(11), g(11) ' UV and IR terms for water permittivity
 Public B, Tau_MW ' microwave terms for permittivity of water
 Public epsilon_0_s, C_UV, omega_UV, no, C_IR, omega_IR ' parameters for permittivity of solids

Public kB, h, epsilon_0, c_light, gzeta_c, limiting_factor

Function hamaker_screened_rt(D, solid, water, Optional T)

' Method is taken from paper by Pailthorpe and Russel (1982) in J. Colloid Interface Sci.

If IsMissing(T) Then T = 273.15 + 25

```

' Convert interparticle distance from nanometers to meters
D = D / 1000000000#

' Initialise global parameters
physical_coefficients
solids_data (solid)
water_data (water)

' Define Norm factor of imaginay frequency
gzeta_m_factor = (4 * Application.Pi() ^ 2 * kB * T / h)

' Initialise incremented function
integral_0 = 0
integral = 0

'This loop sums over frequencies
m = 1
max_added_part = 0
Do
    gzeta_m = gzeta_m_factor * m

    ' Evaluate the maximum value for integration to infinity
    p_sup = evaluate_integral_limit(D, gzeta_m)

    ' This calculates the integral to "infinity" by Romberg method
    added_part = Romberg_integration(D, gzeta_m, p_sup)
    integral = integral + added_part

    If Abs(added_part) > Abs(max_added_part) Then
        max_added_part = added_part
    Else
        If Abs(added_part / integral) < (limiting_factor / m) Then Exit Do
    End If
    integral_0 = integral
    m = m + 1
If m > 500 Then Exit Do

```

Loop

hamaker_screened_rt = 3 / 2 * kB * T * integral

End Function

Function Romberg_integration(D, gzeta_m, p_sup)

strips = 2

'Evaluate trapeze integration terms

T1_n = trapeze_increment(D, gzeta_m, p_sup, 1) / 2

T1_2n = T1_n / 2 + trapeze_increment(D, gzeta_m, p_sup, 2)

T2_2n = (16 * T1_2n - T1_n) / 15

'This loop integrates until sufficient accuracy is obtained

Do

' increment strips

strips = strips * 2

' increment trapeze integrations

T1_n = T1_2n

T1_2n = (T1_2n / 2) + trapeze_increment(D, gzeta_m, p_sup, strips)

'increment Romberg approximations for second order evaluations

T2_n = T2_2n

' Romberg evaluations

T2_2n = (16 * T1_2n - T1_n) / 15

T3_2n = (64 * T2_2n - T2_n) / 63

If Abs((T1_2n - T2_2n) / T1_2n) < limiting_factor Or Abs((T2_2n - T3_2n) / T2_2n) < limiting_factor Then Exit Do

Loop

Romberg_integration = T1_2n

End Function

Function trapeze_increment(D, gzeta_m, p_sup, steps)

```

trap_integral = 0

dp = (p_sup - 1) / steps
If steps = 1 Then factor = 0 Else factor = 1
p_no1 = 1 + factor * dp
p_final = p_sup - factor * dp

For p = p_no1 To p_final Step (dp * 2)

    trap_integral = trap_integral + integral_term_Ham_sc_rt(D, gzeta_m, p)
Next p
'Formula for trapeze integration
trapeze_increment = trap_integral * dp

End Function
Function trapeze_integration(D, gzeta_m, p_sup, steps)
    trap_integral = 0
    trap_0 = integral_term_Ham_sc_rt(D, gzeta_m, 1)
    trap_n = integral_term_Ham_sc_rt(D, gzeta_m, p_sup)

    dp = (p_sup - 1) / steps
    For p = 1 + dp To p_sup - dp Step dp

        trap_integral = trap_integral + integral_term_Ham_sc_rt(D, gzeta_m, p)
    Next p
    'Formula for trapeze integration
    trapeze_integration = (trap_0 + 2 * trap_integral + trap_n) / 2 * dp

End Function
Function evaluate_integral_limit(D, gzeta_m)

    'physical_coefficients
    'solids_data
    'water_data

    increment = 2
    integral_term_0 = integral_term_Ham_sc_rt(D, gzeta_m, 1)

```

Do

integral_term_loop = integral_term_Ham_sc_rt(D, gzeta_m, increment)

If Abs(integral_term_loop) > Abs(integral_loop_0) Then

integral_loop_0 = integral_term_loop

Else

If Abs(integral_term_0) > Abs(integral_term_loop / limiting_factor) Then Exit Do

End If

increment = increment * 2

Loop

evaluate_integral_limit = increment

End Function

Function integral_term_Ham_sc_rt(D, gzeta_m, p)

' Function to calculate the terms in the integral for screened Hamaker related constant

' Calculate permittivities of continuous phase and spheres

eps_1 = solids_permittivity(gzeta_m)

eps_0 = water_permittivity(gzeta_m)

gzeta_c = c_light / (2 * D * eps_0 ^ 0.5)

S1 = (p ^ 2 - 1 + eps_1 / eps_0) ^ 0.5

ln_term_1 = 1 - ((S1 * eps_0 - p * eps_1) / (S1 * eps_0 + p * eps_1)) ^ 2 * Exp(-gzeta_m / gzeta_c * p)

ln_term_2 = 1 - ((S1 - p) / (S1 + p)) ^ 2 * Exp(-gzeta_m / gzeta_c * p)

integral_term_Ham_sc_rt = p * Application.Ln(ln_term_1 * ln_term_2) * (gzeta_m / gzeta_c) ^ 2

End Function

Function hamaker_nrt(solid, water, Optional screening, Optional T)

' check whether salting is considered to cancel out the static term

```

If IsMissing(screening) Then screening = 0.5

If screening = 0 Then
    static_factor = 0
Else
    static_factor = 0.5
End If

If IsMissing(T) Then T = 273.15 + 25

physical_coefficients
solids_data (solid)
water_data (water)

'Define Norm factor of imaginay frequency
gzeta_m_factor = (4 * Application.Pi() ^ 2 * kB * T / h)

hamaker_sum = 0
For m = 0 To 3000
    gzeta_m = m * gzeta_m_factor
    For s = 1 To 4

        'difference in dielectric response (eq.15)
        eps_1 = solids_permitivity(gzeta_m)
        eps_3 = water_permitivity(gzeta_m)

        delta_13 = (eps_1 - eps_3) / (eps_1 + eps_3)

        hamaker_sum = hamaker_sum + (delta_13 ^ 2) ^ s / s ^ 3
    Next s

    If m = 0 Then hamaker_sum = hamaker_sum * static_factor ' coefficient 1/2 for m=0 term
Next m

hamaker_nrt = 3 * kB * T / 2 * hamaker_sum

End Function

```

Function permittivity(material, m, solid, water, Optional T)

If IsMissing(T) Then T = 273.15 + 25

kB = 1.38054E-23 ' Boltzmann's constant in J/K

h = 6.6256E-34 ' Plank's constant in J s

epslion_0 = 0.000000000008854 ' Permittivity of vaccum in C^2 / N m^2

' Values for these physical constants are taken from Russel et al (1991), page xvii

'Define Norm of imaginay frequency

gzeta_m = m * (4 * Application.Pi() ^ 2 * kB * T / h)

If material = "water" Then

water_data (water)

permittivity = water_permittivity(gzeta_m)

ElseIf material = "solid" Then

solids_data (solid)

permittivity = solids_permittivity(gzeta_m)

Else

permittivity = "what material"

End If

End Function

Sub water_data(water)

' Read Parameters for Microwave terms (due to orientation of permanent dipoles)

B = water(1, 7)

tau_inv = water(1, 8) * 1000000000000#

Tau_MW = 1 / tau_inv

' Read Parameters for UV and IR terms

For uv = 1 To 6

c(uv) = water(uv, 1)

```

    omega(uv) = water(uv, 2) * 1E+16
    g(uv) = water(uv, 3) * 1E+15
Next uv

For ir = 1 To 5
    c(ir + 6) = water(ir, 4)
    omega(ir + 6) = water(ir, 5) * 1000000000000000#
    g(ir + 6) = water(ir, 6) * 1E+15
Next ir

End Sub

Function water_permitivity(gzeta_m)

'Compute microwave term(due to orientation of permanent dipoles)
microwave = B / (1 + gzeta_m * Tau_MW)

'Evaluate the sum of the damped oscillators
summation = 0
For j = 1 To 11
    denominator = 1 + (gzeta_m / omega(j)) ^ 2 + g(j) * gzeta_m / omega(j) ^ 2
    summation = summation + c(j) / denominator
Next j

' return value
water_permitivity = 1 + microwave + summation

End Function

Sub solids_data(solid)

' Read Parameters for Microwave terms (due to orientation of permanent dipoles)

C_UV = solid(1, 1)
omega_UV = solid(1, 2) * 1E+16
C_IR = solid(1, 3)
omega_IR = solid(1, 4) * 1000000000000000#

```

End Sub

Function solids_permitivity(gzeta_m)

$$\text{IR_term} = C_{\text{IR}} / (1 + (\text{gzeta_m} / \text{omega_IR})^2)$$

$$\text{UV_term} = C_{\text{UV}} / (1 + (\text{gzeta_m} / \text{omega_UV})^2)$$

$$\text{solids_permitivity} = 1 + \text{IR_term} + \text{UV_term}$$

End Function

Sub physical_coefficients()

limiting_factor = 0.01 / 1000 'fixes difference between maximum and minimum increment

' Values for these physical constants are taken from page xvii in "Colloidal Dispersions"

kB = 1.38054E-23 ' Boltzmann's constant in J/K

h = 6.6256E-34 ' Plank's constant in J s

epsilon_0 = 0.00000000008854 ' Permittivity of vaccum in C^2 / N m^2

c_light = 299790000# ' speed of light

End Sub

Annex D Statistical treatment of data

Annex D.1 Testing the identity of lines

Adsorption data led to graphs in which the plot of added polymer versus polymer detected after adsorption was linear. This is compatible with a step type isotherm, in which all is adsorbed until saturation is reached. The ordinate at the origin of the above mentioned graph gives the amount of polymer adsorbed at surface saturation. The slope of these lines is linked to the response of the polymer in the aqueous phase and would be the slope of the calibration line, of which the ordinate at the origin should be zero (expect as for PCE-1 if an impurity in the solvent is eluted at the same time as the polymer).

We have developed a procedure in which we first test, a set of isotherms, whether they all have the same slope. If this is the case, then we calculate from all data sets a single slope. This then allows to calculate different ordinates at the origin with higher precision.

So, we have a procedure to obtain more precise adsorption plateau values. However, these values are no more independent one of another. Therefore if we want to decide whether plateaus are significantly different one from the other, we must perform a more complicated statistical test.

For the case of the adsorption data on cement, we studied two similar cements at two different adsorption times. We found the cement type did not effect the slope, but could effect the ordinate at the origin. So, at each adsorption time, we could determine an optimised slope characterising the response of the polymer in solution. We then were interested in comparing the slopes at different adsorption times, in order to see whether the response changed, for instance due to hydrolysis.

Annex D.1.1 Use of the macros

The procedures are as follows:

Test whether slopes are identical by using :

`compare_lines (pt_ou_ord, x1, y1, x2, y2, x3, y3, x4, y4, x5, y5)`

`pt_ou_ord` 1 to test the slope, 2 to test the non-optimised ordinates at the origin.

`xi, yi` are vectors giving the data of x and y respectively for set i. At least two sets must be given.

The function returns the degree of confidence to reject the equality (confidence to accept difference).

If slopes are different then determine whether the optimised ordinates are or not one same value:

`compare_opt_ords (x1, y1, x2, y2, x3, y3, x4, y4, x5, y5)`

The function returns the degree of confidence to reject the equality (confidence to accept difference).

Determine the optimised slope and its standard deviation:

For the slope: `weighted_parameter (1, x1, y1, x2, y2, x3, y3, x4, y4, x5, y5)`

For its std. dev.: `weighted_std_dev (1, x1, y1, x2, y2, x3, y3, x4, y4, x5, y5)`

Again at least two sets of data are required, the other 3 are optional.

Determine the **optimised ordinate** and its standard deviation:

For the optimised ordinate: `optimised_ordinate (1, x, y, slope, er_pente)`

x, y are the data vectors of the set of which one determines the optimised ordinate.

Slope is the optimised slope obtained by `weighted_parameter (1, x1, y1, x2,y2, ...)`

Er_pente is the optimised slope obtained by `weighted_parameter (2, x1, y1, x2,y2, ...)`

For its standard deviation: `optimised_ordinate (2, x, y, slope, er_pente)`

If the optimised ordinates are the same then determine the unique ordinate and its standard deviation by:

For the general ordinate: `weighted_parameter (2, x1, y1, x2, y2, x3, y3, x4, y4, x5, y5)`

For its std. dev.: `weighted_std_dev (2, x1, y1, x2, y2, x3, y3, x4, y4, x5, y5)`

To test if the optimised slope of two sets of two lines are identical, we use:

`compare_opt_slopes(x1a, y1a, x1b, y1b, x2a, y2a, x2b, y2b, x1, y1, x2, y2)`

x1a, y1a and x2b,y2b identify the data sets for the first adsorption time

x1b, y1b and x2a,y2a identify the data sets for the second adsorption time

The function returns a probability for rejecting the equality of both optimised slopes.

Annex D.1.2. Microsoft Excell Macro listing

Function `compare_lines(pt_ou_ord, x1, y1, x2, y2, Optional x3, Optional y3, Optional x4, Optional y4, Optional x5, Optional y5)`

' comparison of two general straight lines not

' calculation from "statistical treatment of experimental data" by Green and Margerison (1978)

' pages 298 and following

r = 2

r_max = 5

ReDim n(r_max), Val(r_max), er_val(r_max), w(r_max), d2(r_max)

```

n(1) = Application.CountA(x1)
Val(1) = Application.Index(Application.LinEst(y1, x1, 1, 1), 1, pt_ou_ord)
d2(1) = Application.Index(Application.LinEst(y1, x1, 1, 1), 5, 2)
w(1) = weight(pt_ou_ord, x1)

```

```

n(2) = Application.CountA(x2)
Val(2) = Application.Index(Application.LinEst(y2, x2, 1, 1), 1, pt_ou_ord)
d2(2) = Application.Index(Application.LinEst(y2, x2, 1, 1), 5, 2)
w(2) = weight(pt_ou_ord, x2)

```

```

If IsMissing(x3) = False And IsMissing(y3) = False Then

```

```

  r = 3
  n(3) = Application.CountA(x3)
  Val(3) = Application.Index(Application.LinEst(y3, x3, 1, 1), 1, pt_ou_ord)
  d2(3) = Application.Index(Application.LinEst(y3, x3, 1, 1), 5, 2)
  w(3) = weight(pt_ou_ord, x3)

```

```

End If

```

```

If (Not IsMissing(x4)) And (Not IsMissing(y4)) Then

```

```

  r = 4
  n(4) = Application.CountA(x4)
  Val(4) = Application.Index(Application.LinEst(y4, x4, 1, 1), 1, pt_ou_ord)
  d2(4) = Application.Index(Application.LinEst(y4, x4, 1, 1), 5, 2)
  w(4) = weight(pt_ou_ord, x4)

```

```

End If

```

```

If (Not IsMissing(x5)) And (Not IsMissing(y5)) Then

```

```

  r = 5
  n(5) = Application.CountA(x5)
  Val(5) = Application.Index(Application.LinEst(y5, x5, 1, 1), 1, pt_ou_ord)
  d2(5) = Application.Index(Application.LinEst(y5, x5, 1, 1), 5, 2)
  w(5) = weight(pt_ou_ord, x5)

```

```

End If

```

```

val_av = Application.SumProduct(w, Val) / Application.Sum(w)

```

```

ntot = Application.Sum(n)

numérateur = 0

For bcl2 = 1 To r
    numérateur = numérateur + w(bcl2) * (Val(bcl2) - val_av) ^ 2
Next

t = (numérateur / (r - 1)) / (Application.Sum(d2) / (ntot - 2 * r))
compare_lines = 1 - Application.FDist(t, r - 1, ntot - 2 * r)

End Function

Function weighted_parameter(pt_ou_ord, x1, y1, x2, y2, Optional x3, Optional y3, Optional x4,
Optional y4, Optional x5, Optional y5)
    r = 2
    r_max = 5

    ReDim Val(r_max), er_val(r_max), w(r_max)
    Val(1) = Application.Index(Application.LinEst(y1, x1, 1, 1), 1, pt_ou_ord)
    Val(2) = Application.Index(Application.LinEst(y2, x2, 1, 1), 1, pt_ou_ord)

    w(1) = weight(pt_ou_ord, x1)
    w(2) = weight(pt_ou_ord, x2)

    If IsMissing(x3) = False And IsMissing(y3) = False Then
        r = 3
        Val(3) = Application.Index(Application.LinEst(y3, x3, 1, 1), 1, pt_ou_ord)
        w(3) = weight(pt_ou_ord, x3)
    End If

    If (Not IsMissing(x4)) And (Not IsMissing(y4)) Then
        r = 4
        Val(4) = Application.Index(Application.LinEst(y4, x4, 1, 1), 1, pt_ou_ord)
    End If
End Function

```

```
w(4) = weight(pt_ou_ord, x4)
```

```
End If
```

```
If (Not IsMissing(x5)) And (Not IsMissing(y5)) Then
```

```
  r = 5
```

```
  Val(5) = Application.Index(Application.LinEst(y5, x5, 1, 1), 1, pt_ou_ord)
```

```
  w(5) = weight(pt_ou_ord, x5)
```

```
End If
```

```
weighted_parameter = Application.SumProduct(w, Val) / Application.Sum(w)
```

```
End Function
```

```
Function weighted_std_dev(pt_ou_ord, x1, y1, x2, y2, Optional x3, Optional y3, Optional x4,  
Optional y4, Optional x5, Optional y5)
```

```
  r = 2
```

```
  r_max = 5
```

```
  ReDim Val(r_max), n(r_max), w(r_max), d2(r_max)
```

```
  Val(1) = Application.Index(Application.LinEst(y1, x1, 1, 1), 1, pt_ou_ord)
```

```
  w(1) = weight(pt_ou_ord, x1)
```

```
  d2(1) = Application.Index(Application.LinEst(y1, x1, 1, 1), 5, 2)
```

```
  n(1) = Application.CountA(x1)
```

```
  Val(2) = Application.Index(Application.LinEst(y2, x2, 1, 1), 1, pt_ou_ord)
```

```
  w(2) = weight(pt_ou_ord, x2)
```

```
  d2(2) = Application.Index(Application.LinEst(y2, x2, 1, 1), 5, 2)
```

```
  n(2) = Application.CountA(x2)
```

```
If IsMissing(x3) = False And IsMissing(y3) = False Then
```

```
  r = 3
```

```
  n(3) = Application.CountA(x3)
```

```
  Val(3) = Application.Index(Application.LinEst(y3, x3, 1, 1), 1, pt_ou_ord)
```

```
  d2(3) = Application.Index(Application.LinEst(y3, x3, 1, 1), 5, 2)
```

```
  w(3) = weight(pt_ou_ord, x3)
```

End If

If (Not IsMissing(x4)) And (Not IsMissing(y4)) Then

 r = 4

 n(4) = Application.CountA(x4)

 Val(4) = Application.Index(Application.LinEst(y4, x4, 1, 1), 1, pt_ou_ord)

 d2(4) = Application.Index(Application.LinEst(y4, x4, 1, 1), 5, 2)

 w(4) = weight(pt_ou_ord, x4)

End If

If (Not IsMissing(x5)) And (Not IsMissing(y5)) Then

 r = 5

 n(5) = Application.CountA(x5)

 Val(5) = Application.Index(Application.LinEst(y5, x5, 1, 1), 1, pt_ou_ord)

 d2(5) = Application.Index(Application.LinEst(y5, x5, 1, 1), 5, 2)

 w(5) = weight(pt_ou_ord, x5)

End If

ntot = Application.Sum(n)

weighted_std_dev = (Application.Sum(d2) / (ntot - 2 * r) / Application.Sum(w)) ^ 0.5

End Function

Function optimised_ordinate(desired_value, x, y, slope, er_pente)

 n = Application.CountA(x)

 If desired_value = 1 Then

 ' The ordinate at the origin is returned

 somme_ord = Application.Sum(y) - slope * Application.Sum(x)

 optimised_ordinate = 1 / n * somme_ord

 ElseIf desired_value = 2 Then

 ' The standard deviation of the ordinate at the origin is returned

```
optimised_ordinate = (1 / n ^ 2 * Application.Sum(x) ^ 2 * er_pente ^ 2) ^ 0.5
```

```
Else
```

```
optimised_ordinate = "???"
```

```
End If
```

```
End Function
```

```
Function compare_opt_ords(x1, y1, x2, y2, Optional x3, Optional y3, Optional x4, Optional y4,
Optional x5, Optional y5)
```

```
    r = 2 ' number of lines
```

```
    r_max = 5
```

```
    ReDim ord(r_max), w(r_max), SCe(r_max), n(r_max), sig_2(r_max), x_moyen(r_max),
ord_bcl(r_max))
```

```
    If (Not IsMissing(x5)) And (Not IsMissing(y5)) Then
```

```
        r = 5
```

```
        slope_opt = weighted_parameter(1, x1, y1, x2, y2, x3, y3, x4, y4, x5, y5)
```

```
        er_opt_slope = weighted_std_dev(1, x1, y1, x2, y2, x3, y3, x4, y4, x5, y5)
```

```
        n(5) = Application.CountA(x5)
```

```
        x_moyen(5) = Application.Average(x5)
```

```
        ord(5) = optimised_ordinate(1, x5, y5, slope_opt, er_opt_slope)
```

```
        w(5) = weight(2, x5)
```

```
    Else
```

```
        If IsMissing(x4) = False And IsMissing(y4) = False Then
```

```
            r = 4
```

```
            slope_opt = weighted_parameter(1, x1, y1, x2, y2, x3, y3, x4, y4)
```

```
            er_opt_slope = weighted_std_dev(1, x1, y1, x2, y2, x3, y3, x4, y4)
```

```
            n(4) = Application.CountA(x4)
```

```
            x_moyen(4) = Application.Average(x4)
```

```
            ord(4) = optimised_ordinate(1, x4, y4, slope_opt, er_opt_slope)
```

```
            w(4) = weight(2, x4)
```

```
        ElseIf IsMissing(x3) = False And IsMissing(y3) = False Then
```

```

r = 3
slope_opt = weighted_parameter(1, x1, y1, x2, y2, x3, y3)
er_opt_slope = weighted_std_dev(1, x1, y1, x2, y2, x3, y3)
n(3) = Application.CountA(x3)
x_moyen(3) = Application.Average(x3)
ord(3) = optimised_ordinate(1, x3, y3, slope_opt, er_opt_slope)
w(3) = weight(2, x3)

Else
slope_opt = weighted_parameter(1, x1, y1, x2, y2)
er_opt_slope = weighted_std_dev(1, x1, y1, x2, y2)
End If
End If

n(1) = Application.CountA(x1)
x_moyen(1) = Application.Average(x1)

n(2) = Application.CountA(x2)
x_moyen(2) = Application.Average(x2)

ord(2) = optimised_ordinate(1, x2, y2, slope_opt, er_opt_slope)
' Take individual ordinates at the origin
ord(1) = optimised_ordinate(1, x1, y1, slope_opt, er_opt_slope)

w(1) = weight(2, x1)
w(2) = weight(2, x2)

ord_av = Application.SumProduct(w, ord) / Application.Sum(w)
' weighted average ordinate at the origin

SCe(1) = 0 ' initialise variables for the F test
SCe(2) = 0 ' see Morgenthaler (1997) pg. 161

ord_bcl(1) = ord_av ' initially, tests with one ordinate at the origin only
ord_bcl(2) = ord_av

```

```

For bcl0 = 1 To 2                                ' the squares of the errors from the models
  For bcl1 = 1 To n(1)
    SCe(bcl0) = SCe(bcl0) + (y1(bcl1) - (ord_bcl(1) + slope_opt * x1(bcl1))) ^ 2
  Next

  For bcl2 = 1 To n(2)
    SCe(bcl0) = SCe(bcl0) + (y2(bcl2) - (ord_bcl(2) + slope_opt * x2(bcl2))) ^ 2
  Next

  ord_bcl(2) = optimised_ordinate(1, x2, y2, slope_opt, er_opt_slope) ' Take individual ordinates
  ord_bcl(1) = optimised_ordinate(1, x1, y1, slope_opt, er_opt_slope)
Next

ntot = Application.Sum(n)

p = r                                            ' r+1 = max number of parameters evaluated
q = 1                                           ' q+1 = min number of parameters evaluated
' remark: the model 2 introduces p-q additional parameters

numérateur = (SCe(1) - SCe(2)) / (p - q)
dénominateur = SCe(2) / (ntot - p - 1)

t = numérateur / dénominateur

compare_opt_ords = 1 - Application.FDist(t, p - q, ntot - p - 1)

```

End Function

Function compare_opt_slopes(x1a, y1a, x1b, y1b, x2a, y2a, x2b, y2b, x1, y1, x2, y2)

```

'This function calculates the degree of confidence to reject the hypothesis according to which
'two lines, with different ordinates at the origin have the same slope
' each of these lines is the combination of two other lines (cement with or without grinding aid)
' They have the same slope, but not the same ordinate at the origin

```

```

r = 2                ' number of lines
p = r                ' r+1 = max number of parameters evaluated
q = 1                ' q+1 = min number of parameters evaluated
' remark: the model 2 introduces p-q additional parameters

```

```

ReDim n(r), ord(r), w(r), SCe(r), sig_2(r), x_moyen(r), ord_bcl(r), ordinate_opt(r, 2), slope_opt(r)

```

```

n(1) = Application.CountA(x1a) + Application.CountA(x1b)

```

```

n(2) = Application.CountA(x2a) + Application.CountA(x2b)

```

```

'calculate average ordinate at each time

```

```

slope = weighted_parameter(1, x1a, y1a, x1b, y1b)

```

```

ordinate_opt(1, 1) = (Application.Sum(y1a) - slope * Application.Sum(x1a)) /
Application.CountA(y1a)

```

```

ordinate_opt(1, 2) = (Application.Sum(y1b) - slope * Application.Sum(x1b)) /
Application.CountA(y1b)

```

```

slope = weighted_parameter(1, x2a, y2a, x2b, y2b)

```

```

ordinate_opt(2, 1) = (Application.Sum(y2a) - slope * Application.Sum(x2a)) /
Application.CountA(y2a)

```

```

ordinate_opt(2, 2) = (Application.Sum(y2b) - slope * Application.Sum(x2b)) /
Application.CountA(y2b)

```

```

'calculate average slope for all data

```

```

slope_opt(1) = weighted_parameter(1, x1, y1, x2, y2)

```

```

slope_opt(2) = slope_opt(1)

```

```

SCe(1) = 0

```

```

SCe(2) = 0

```

```

For bcl0 = 1 To 2                ' square of errors of models

```

```

    For bcl1 = 1 To Application.CountA(x1a)

```

```

    SCe(bcl0) = SCe(bcl0) + (y1a(bcl1) - (ordinate_opt(1, 1) + slope_opt(1) * x1a(bcl1))) ^ 2
Next

```

```

For bcl1 = 1 To Application.CountA(x1b)

```

```

    SCe(bcl0) = SCe(bcl0) + (y1b(bcl1) - (ordinate_opt(1, 2) + slope_opt(1) * x1b(bcl1))) ^ 2
Next

```

```

For bcl2 = 1 To Application.CountA(x2a)

```

```

    SCe(bcl0) = SCe(bcl0) + (y2a(bcl2) - (ordinate_opt(2, 1) + slope_opt(2) * x2a(bcl2))) ^ 2
Next

```

```

For bcl2 = 1 To Application.CountA(x2b)

```

```

    SCe(bcl0) = SCe(bcl0) + (y2b(bcl2) - (ordinate_opt(2, 2) + slope_opt(2) * x2b(bcl2))) ^ 2
Next

```

```

'Calculate optimized slopes at each temperature

```

```

slope_opt(1) = weighted_parameter(1, x1a, y1a, x1b, y1b)

```

```

slope_opt(2) = weighted_parameter(1, x2a, y2a, x2b, y2b)

```

```

Next

```

```

ntot = Application.Sum(n)

```

```

numérateur = (SCe(1) - SCe(2)) / (p - q)

```

```

dénominateur = SCe(2) / (ntot - p - 1)

```

```

t = numérateur / dénominateur

```

```

compare_opt_slopes = 1 - Application.FDist(t, p - q, ntot - p - 1)

```

```

'compare_opt_slopes = x1(3)

```

```

End Function

```

```

Function weight(ord_ou_pente, x)

```

```

If ord_ou_pente = 2 Then

```

```

    weight = Application.CountA(x) * Application.DevSq(x) / Application.SumSq(x)

```

```

ElseIf ord_ou_pente = 1 Then
    weight = Application.DevSq(x)
Else
    weight = 0
End If
End Function

```

Annex D.2. Testing an effect on a series of values, all having their own uncertainty

The effect of temperature T on the amount of adsorbed polymer y , was evaluated for each combination of polymer and powder using a linear regression. At each temperature T , n_T measurements of y were performed, giving an average y_T and an uncertainty $\sigma(y_T)$, the standard deviation of y at temperature T . All values of T are known exactly. The slope b and its variance $\text{var}(b)$, the ordinate a and its variance $\text{var}(a)$, as well as the covariance of slope and the ordinate $\text{cov}(a,b)$ can be calculated by well established methods [Press et al (1992)].

The standard deviation $\sigma(\mu_T)$ for the prediction μ_T , of the expectation y_T , is given by:

$$\sigma(\mu_T) = \sqrt{\text{var}(\mu_T)} = \sqrt{\text{var}(b T + a)} = \sqrt{\text{var}(a) + T^2 \text{var}(b) + T \text{cov}(a,b)} \quad [\text{D-1}]$$

Because at each temperature a finite number of measurements are used to calculate σ_T , these values are approximations. This is taken into account by correcting when calculating the confidence intervals Δy_T on a prediction μ_T . Bilateral Student factors are used instead of a the normal law. The number of degree of freedom is the total number of measurements minus two (number of parameters estimated in the regression) minus the number of temperatures studied (number of $\sigma(\mu_T)$ estimated). Confidence intervals of 95% were systematically used. The p-value of the temperature effect is obtained with a unilateral Student law, the ratio $\sigma(b)/b$ and the same number of degree of freedom given above.

The relative importance of temperature was reported as the ratio between the slope, obtained by the linear regression, and the predicted amount of adsorbed polymer for a temperature of 25°C. When calculating the error associated with this ratio, we must take into account the fact that these parameters

are not independent of each other. The error for such a ratio is given by [Kendall, M.G. and Stuart, p. 325]:

$$\sigma\left(\frac{b}{\mu_{25^\circ C}}\right) = \sqrt{\text{var}\left(\frac{b}{\mu_{25^\circ C}}\right)} = \frac{b}{\mu_{25^\circ C}} \sqrt{\frac{\text{var}(b)}{b^2} + \frac{\text{var}(\mu_{25^\circ C})}{\mu_{25^\circ C}^2} - \frac{2 \text{cov}(b, \mu_{25^\circ C})}{b \mu_{25^\circ C}}} \quad [\text{D-2}]$$

Where:

$$\text{cov}(b, \mu_T) = \text{cov}(b, a + b T) = \text{cov}(a, b) + T \text{cov}(b, b) = \text{cov}(a, b) + T \text{var}(b) \quad [\text{D-3}]$$

Annex D.2.2 Listing of Microsoft Excell macro

The Macro is called as follows: tendency (choice, x, y, y_std_dev, n, nb_ev_pars_per_series)

Choice	0- for the degree of confidence to reject absence of an effect
	1- for the slope of the regression
	2- for the variance of the slope
	3- for the ordinate at the origin
	4- for the variance of the ordinate at the origin
	5- for the covariance of the slope and the ordinate at the origin
	6- for the correlation coefficient
x,y	are the vectors with values of the series
y_std_dev	is a vector containing the standard deviation of each value of y
n	is a vector containing, for each value of y, the number of data points used to determine y.
nb_ev_pars_per_series	is a vector containing for each value of y, the number of parameters which have estimated by the regression leading y.

.....

```
Function tendency(choice, x, y, y_std_dev, n, nb_ev_pars_per_series)
```

```
'This function can return different values linked to making a decision of a dependence
```

```
' of a series of values on a parameter (ex: adsorption on temperature)
```

```
' Each value has itself been evaluated in a previous treatment
```

```
' the last parameter asks how many parameters were evaluated in that procedure
```

```
  'define the choices
```

```
    reject_probability_chosen = 0
```

```
    slope_chosen = 1
```

```
    slope_variance_chosen = 2
```

```
    ordinate_chosen = 3
```

```
    ordinate_variance_chosen = 4
```

```
    covariance_chosen = 5
```

```
    correlation_coeff_chosen = 6
```

```
'check how many values are given
```

```
nb_series = Application.CountA(x)
```

```
'create a dimension for 1/sigma^2
```

```
ReDim one_over_sigma2(nb_series), xx(nb_series), xy(nb_series)
```

```
'Calculate the sums necessary for the statistical treatment
```

```
S = 0
```

```
Sx = 0
```

```
Sy = 0
```

```
Sxx = 0
```

```
Sxy = 0
```

```
For bcl1 = 1 To nb_series
```

```
  sigma_2 = y_std_dev(bcl1) ^ 2
```

```
  S = S + 1 / sigma_2
```

```
  Sx = Sx + x(bcl1) / sigma_2
```

```
  Sy = Sy + y(bcl1) / sigma_2
```

```
  Sxx = Sxx + x(bcl1) ^ 2 / sigma_2
```

$$S_{xy} = S_{xy} + x(\text{bc11}) * y(\text{bc11}) / \text{sigma}_2$$

Next bc11

$$\text{delta} = S * S_{xx} - S_x^2$$

$$\text{ordinate} = (S_{xx} * S_y - S_x * S_{xy}) / \text{delta}$$

$$\text{variance_ordinate} = S_{xx} / \text{delta}$$

$$\text{slope} = (S * S_{xy} - S_x * S_y) / \text{delta}$$

$$\text{variance_slope} = S / \text{delta}$$

$$\text{covariance} = -S_x / \text{delta}$$

$$\text{correlation_coefficient} = -S_x / (S * S_{xx})^{0.5}$$

If choice = reject_probability_chosen Then

$$\text{slope_over_error} = \text{Abs}(\text{slope}) / \text{variance_slope}^{0.5}$$

$$\text{degrees_of_liberty} = \text{Application.Sum}(n) - \text{nb_ev_pars_per_series} * \text{nb_series} - 2$$

$$\text{tendency} = 1 - \text{Application.TDist}(\text{slope_over_error}, \text{degrees_of_liberty}, 1)$$

ElseIf choice = slope_chosen Then

$$\text{tendency} = \text{slope}$$

ElseIf choice = slope_variance_chosen Then

$$\text{tendency} = \text{variance_slope}$$

ElseIf choice = ordinate_chosen Then

$$\text{tendency} = \text{ordinate}$$

ElseIf choice = ordinate_variance_chosen Then

$$\text{tendency} = \text{variance_ordinate}$$

ElseIf choice = covariance_chosen Then

$$\text{tendency} = \text{covariance}$$

ElseIf choice = correlation_coeff_chosen Then


```
tendency = correlation_coefficient
```

```
Else
```

```
tendency = delta
```

```
End If
```

```
End Function
```


Annex E Interparticle force parameters

In this annex we give numerical values for the interparticle parameter G between spheres in the symmetric electrolyte representation developed for simulating cement suspensions. The interparticle force is obtained by the product of G and the harmonic average of both radii of interacting particles, given by $\bar{a} = \frac{2a_k a_l}{a_k + a_l}$. The tables below have been calculated by the following Microsoft Excell

Macro.

Annex E.1 Numerical values

The first column gives the electrostatic potential. The first line gives the adsorbed layer thickness. The of G are given in $pN/\mu m$. The compacted layer thickness was 0.7 nm and the polymer spacing 10 nm.

Magnesium Oxide

Potential [mV]	Adsorbed layer thickness L [nm]																
	1.0	1.5	2.0	2.5	3.0	3.5	4.0	4.5	5.0	5.5	6.0	6.5	7.0	7.5	8.0	8.5	11
0	393	166	89	54	36	25	19	14	11	8.6	6.9	5.7	4.7	3.9	3.3	2.8	1.41
5	310	83	29	18	13	9.2	7.0	5.5	4.4	3.6	2.9	2.5	2.1	1.8	1.5	1.3	0.72
10	60	30	19	13	9.4	7.1	5.6	4.4	3.6	3.0	2.5	2.1	1.8	1.6	1.4	1.2	0.65
15	39	23	15	11	8.1	6.2	4.9	4.0	3.3	2.7	2.3	1.9	1.7	1.4	1.3	1.1	0.61
20	31	19	13	10	7.3	5.7	4.5	3.7	3.0	2.5	2.1	1.8	1.6	1.4	1.2	1.0	0.56
25	27	17	12	8.9	6.8	5.3	4.3	3.5	2.9	2.4	2.0	1.8	1.5	1.3	1.1	1.0	0.49
30	24	16	11	8.3	6.4	5.0	4.1	3.3	2.8	2.3	2.0	1.7	1.4	1.2	1.0	0.9	0.41
35	22	15	10	7.8	6.1	4.8	3.9	3.2	2.7	2.2	1.9	1.6	1.3	1.1	0.9	0.8	0.31

α -Alumina

Potential [mV]	Adsorbed layer thickness L [nm]																	
	1.0	1.5	2.0	2.5	3.0	3.5	4.0	4.5	5.0	5.5	6.0	6.5	7.0	7.5	8.0	8.5	11	
0	749	270	142	85	56	38	28	21	16	12	10	7.9	6.5	5.4	4.5	3.8	1.8	
5	666	187	59	31	20	14	11	8.1	6.4	5.1	4.1	3.4	2.9	2.4	2.1	1.8	0.93	
10	416	56	32	21	15	11	8.3	6.5	5.2	4.2	3.5	2.9	2.4	2.1	1.8	1.6	0.84	
15	77	40	25	17	13	9.4	7.3	5.7	4.6	3.8	3.1	2.6	2.2	1.9	1.7	1.4	0.79	
20	58	33	22	15	11	8.5	6.6	5.3	4.3	3.5	2.9	2.5	2.1	1.8	1.6	1.4	0.74	
25	48	29	19	14	10	7.9	6.2	5.0	4.0	3.3	2.8	2.4	2.0	1.7	1.5	1.3	0.67	
30	42	26	18	13	10	7.4	5.9	4.7	3.9	3.2	2.7	2.3	1.9	1.7	1.4	1.2	0.58	
35	38	24	17	12	9.1	7.1	5.6	4.5	3.7	3.1	2.6	2.2	1.8	1.6	1.3	1.1	0.49	

Calcite

Potential [mV]	Adsorbed layer thickness L [nm]																
	1.0	1.5	2.0	2.5	3.0	3.5	4.0	4.5	5.0	5.5	6.0	6.5	7.0	7.5	8.0	8.5	11
0	244	104	56	34	23	16	12	9.1	7.1	5.7	4.6	3.8	3.2	2.7	2.3	2.0	1.04
5	160	28	16	10	7.4	5.6	4.3	3.5	2.8	2.3	2.0	1.7	1.4	1.2	1.1	1.0	0.55
10	29	16	11	7.6	5.7	4.4	3.5	2.9	2.4	2.0	1.7	1.5	1.3	1.1	1.0	0.86	0.50
15	21	13	8.9	6.5	5.0	3.9	3.2	2.6	2.2	1.8	1.6	1.3	1.2	1.0	0.90	0.80	0.47
20	17	11	7.9	5.9	4.5	3.6	2.9	2.4	2.0	1.7	1.5	1.3	1.1	1.0	0.85	0.75	0.41
25	15	10	7.2	5.4	4.2	3.4	2.8	2.3	1.9	1.6	1.4	1.2	1.0	0.90	0.78	0.68	0.35
30	13	9.2	6.7	5.1	4.0	3.2	2.6	2.2	1.8	1.6	1.3	1.1	1.0	0.82	0.70	0.60	0.26
35	12	8.6	6.3	4.8	3.8	3.1	2.5	2.1	1.7	1.5	1.2	1.0	0.86	0.72	0.60	0.50	0.16

Quartz

Potential [mV]	Adsorbed layer thickness L [nm]																
	1.0	1.5	2.0	2.5	3.0	3.5	4.0	4.5	5.0	5.5	6.0	6.5	7.0	7.5	8.0	8.5	11
0	144	60	32	19	13	8.9	6.5	4.8	3.7	2.9	2.3	1.9	1.6	1.3	1.1	0.93	0.45
5	61	12	7.2	4.8	3.4	2.6	2.0	1.6	1.3	1.0	0.85	0.71	0.60	0.52	0.45	0.39	0.21
10	13	7.5	5.0	3.5	2.6	2.0	1.6	1.3	1.0	0.86	0.72	0.61	0.52	0.45	0.39	0.34	0.19
15	9.4	6.0	4.1	3.0	2.3	1.8	1.4	1.1	0.94	0.79	0.66	0.56	0.48	0.41	0.36	0.31	0.15
20	7.8	5.2	3.6	2.7	2.1	1.6	1.3	1.1	0.88	0.73	0.61	0.51	0.43	0.36	0.30	0.25	0.10
25	6.9	4.6	3.3	2.5	1.9	1.5	1.2	1.0	0.81	0.66	0.54	0.44	0.36	0.29	0.23	0.19	0.03
30	6.2	4.3	3.1	2.3	1.8	1.4	1.1	0.91	0.73	0.58	0.46	0.36	0.28	0.21	0.15	0.10	0.00
35	5.7	4.0	2.9	2.2	1.7	1.3	1.0	0.81	0.63	0.48	0.36	0.26	0.18	0.11	0.05	0.00	0.00

Spinel

Potential [mV]	Adsorbed layer thickness L [nm]																	
	1.0	1.5	2.0	2.5	3.0	3.5	4.0	4.5	5.0	5.5	6.0	6.5	7.0	7.5	8.0	8.5	11	
0	425	178	95	57	38	26	19	14	11	8.6	6.9	5.6	4.6	3.8	3.2	2.7	1.3	
5	342	95	31	19	13	9.3	7.0	5.4	4.3	3.5	2.9	2.4	2.0	1.7	1.5	1.3	0.67	
10	92	32	20	13	9.6	7.2	5.5	4.4	3.5	2.9	2.4	2.0	1.7	1.5	1.3	1.1	0.61	
15	42	24	16	11	8.2	6.2	4.9	3.9	3.2	2.6	2.2	1.9	1.6	1.4	1.2	1.0	0.57	
20	33	20	14	9.8	7.3	5.7	4.5	3.6	3.0	2.5	2.1	1.8	1.5	1.3	1.1	0.98	0.51	
25	28	18	12	9.0	6.8	5.3	4.2	3.4	2.8	2.3	2.0	1.7	1.4	1.2	1.06	0.91	0.44	
30	25	16	11	8.4	6.4	5.0	4.0	3.2	2.7	2.2	1.9	1.6	1.3	1.1	0.97	0.83	0.36	
35	23	15	11	7.9	6.1	4.8	3.8	3.1	2.6	2.1	1.8	1.5	1.2	1.0	0.87	0.73	0.26	

Silica

Potential [mV]	Adsorbed layer thickness L [nm]																
	1.0	1.5	2.0	2.5	3.0	3.5	4.0	4.5	5.0	5.5	6.0	6.5	7.0	7.5	8.0	8.5	11
0	31	13	6.91	4.18	2.75	1.91	1.38	1.03	0.79	0.62	0.50	0.40	0.33	0.27	0.23	0.19	0.09
5	2.6	1.5	1.03	0.73	0.54	0.41	0.33	0.26	0.21	0.17	0.14	0.12	0.10	0.09	0.08	0.07	0.03
10	1.6	1.1	0.75	0.56	0.42	0.33	0.26	0.21	0.18	0.14	0.12	0.10	0.08	0.06	0.05	0.04	0.01
15	1.3	0.88	0.64	0.48	0.37	0.29	0.23	0.18	0.14	0.11	0.08	0.06	0.04	0.03	0.01	0.00	0.00
20	1.1	0.77	0.57	0.43	0.32	0.24	0.17	0.12	0.08	0.05	0.03	0.01	0.00	0.00	0.00	0.00	0.00
25	1.0	0.70	0.50	0.36	0.25	0.17	0.11	0.06	0.02	0.00	0.00	0.00	0.00	0.00	0.00	0.00	0.00
30	0.90	0.62	0.42	0.27	0.17	0.08	0.02	0.00	0.00	0.00	0.00	0.00	0.00	0.00	0.00	0.00	0.00
35	0.80	0.52	0.32	0.18	0.07	0.00	0.00	0.00	0.00	0.00	0.00	0.00	0.00	0.00	0.00	0.00	0.00

Annex E.2 Microsoft Excell Macro Listing

The function for determining the total attractive force is called by :

total_force(choice, choice_screening, choice_retardation, mineral, c_ionique, valence, potential_mV, compact_layer_nm, extended_layer_nm, center_center_nm)

The macro uses a simple step by step evaluation going from a minimum separation distance of twice the compacted layer to twice the sum of the extended layer and five Debye lengths ($1/\kappa$). The Step taken is 0.005 nm.

```

permitivite_vide = 8.854188E-12          ' permitivity of vacum [C^2/J/m]
permitivite_rel = 78.5                  ' relative permitivity of water [-]
k_boltzmann = 1.3807E-23                ' Boltzmann's constant [J/°K]
charge_elec = 1.60219E-19              ' charge of an electron [C]

somme_Nixzi2 = 2 * Na * 1000 * c_ionique * valence ^ 2 ' Sum of ni x zi^2

num_kapa = permitivite_rel * permitivite_vide * k_boltzmann * temperature
den_kapa = charge_elec ^ 2 * somme_Nixzi2
kapa = ((num_kapa / den_kapa) ^ 0.5) ^ -1

max_force = 0
separation_max_force = 0
For separation_nm = 2 * compact_layer_nm To 2 * extended_layer_nm + 10 * (1 / kapa *
1000000000#) Step 0.005

    VDW = attraction(choice_screening, choice_retardation, mineral, separation_nm)

    ES = electro_stat(c_ionique, valence, separation_nm, potential_mV, extended_layer_nm, kapa)

    Ster = steric(separation_nm, extended_layer_nm, center_center_nm, compact_layer_nm)

    force = VDW + ES + Ster

    If force > 0 Then
        If force >= max_force Then
            max_force = force
            separation_max_force = separation_nm
        End If
    End If
Next separation_nm

If choice = 1 Then
    total_force = max_force
ElseIf choice = 0 Then

```

```

If separation_nm <= 2 * extended_layer_nm Then
    effective_separation_m = 0
Else
    effective_separation_m = (separation_nm - 2 * extended_layer_nm) / 1000000000#
                                ' separation given in nm is converted to m
End If

potential_V = potential_mV / 1000                                ' convert mV to V

If IsMissing(kapa) Then
    k_boltzmann = 1.3807E-23                                ' Boltzmann's constant [J/°K]
    temperature = 298.15                                ' default temperature est de 25°C
    Na = 6.02225E+23                                ' Avogadro's number
    charge_elec = 1.60219E-19                                ' charge of an electron [C]

    somme_Nixzi2 = 2 * Na * 1000 * c_ionique * valence ^ 2 ' Sum of ni x zi^2

    num_kapa = permitivite_rel * permitivite_vide * k_boltzmann * temperature
    den_kapa = charge_elec ^ 2 * somme_Nixzi2
    kapa = ((num_kapa / den_kapa) ^ 0.5) ^ -1
End If

' the first condition for this equation is that the curvature is small with respect to the double layer
' the second is that zeta is smaller than 25 mV (linearised Poisson Boltzmann)
num_electro_1 = 2 * Application.Pi() * permitivite_vide * permitivite_rel * potential_V ^ 2
num_electro_2 = kapa * Exp(-kapa * effective_separation_m)
den_electro = (1 + Exp(-kapa * effective_separation_m))

electro_stat = -num_electro_1 * num_electro_2 / den_electro

End Function

Function steric(separation_nm, extended_layer_nm, center_center_nm, compact_layer_nm)
    If separation_nm < 2 * compact_layer_nm Then
        steric = -1E+70
    
```

```
ElseIf separation_nm > 2 * extended_layer_nm Then
    steric = 0
Else

    k_boltzmann = 1.3807E-23           ' Boltzmann's constant [J/°K]
    temperature = 298.15              ' default temperature est de 25°C

    extended_layer_m = extended_layer_nm / 1000000000#           ' convert nm to m
    center_center_m = center_center_nm / 1000000000#           ' convert nm to m

    separation_m = separation_nm / 1000000000#                   ' convert nm to m

    terme1 = 6 * Application.Pi() * k_boltzmann * temperature / center_center_m ^ 2
    terme2 = ((2 * extended_layer_m / separation_m) ^ (5 / 3) - 1)

    steric = -terme1 * terme2
End If
End Function
```



```
For bcl1 = 1 To 20

  For bcl2 = 1 To bcl1
    If interaction_matrix(bcl1, bcl2) >= a1 And interaction_matrix(bcl1, bcl2) < a2 Then
      total = total + number_matrix(bcl1, bcl2)
    End If
  Next
Next
setup_PSD = total
End Function
```


Annex G Interparticle force parameters

In order to get quickly values of the interparticle force parameter to study polymer effects, we used the following Macro to interpolate between the values of a matrix containing previously calculated values of G for various electrostatic potentials and layer thickness (given in Annex E). The interpolation is a simple linear interpolation.

The macro is called by: `F_by_a(potential, layer, vct_potentials, vct_layers, mtx_F_by_a)`

Potential is the electrostatic potential for which G must be evaluated

Layer is the polymer layer thickness for which G must be evaluated

Vct_potentials is a vector of dimension v , containing the electrostatic potentials in mV for which G has previously been evaluated.

Vct_layers is a vector of dimension L , containing the layers in nm for which G has previously been evaluated.

Mtx_F_by_a is a matrix with v lines and L columns containing the values of G .

The value is indeterminate if the potential or layer are smaller than the smallest of their values in their respective vectors. If they are larger than the largest, the macro returns an error message.

.....
Function `F_by_a(potential, layer, vct_potentials, vct_layers, mtx_F_by_a)`

`index_pot = Application.WorksheetFunction.Match(potential, vct_potentials, 1)`

`index_lay = Application.WorksheetFunction.Match(layer, vct_layers, 1)`

```
If index_pot = Application.CountA(vct_potentials) Then
```

```
  F_by_a = "potential out of range"
```

```
ElseIf index_layer = Application.CountA(vct_layers) Then
```

```
  F_by_a = "thickness out of range"
```

```
Else
```

```
  delta_pot = vct_potentials(index_pot + 1) - vct_potentials(index_pot)
```

```
  delta_layer = vct_layers(index_layer + 1) - vct_layers(index_layer)
```

```
  multiply_pot = (potential - vct_potentials(index_pot)) / delta_pot
```

```
  multiply_layer = (layer - vct_layers(index_layer)) / delta_layer
```

```
  F_a_x1y1 = mtx_F_by_a(index_pot, index_layer)
```

```
  F_a_x2y1 = mtx_F_by_a(index_pot, index_layer + 1)
```

```
  F_a_x1y2 = mtx_F_by_a(index_pot + 1, index_layer)
```

```
  increment_layer = (F_a_x2y1 - F_a_x1y1) * multiply_layer
```

```
  increment_pot = (F_a_x1y2 - F_a_x1y1) * multiply_pot
```

```
  F_by_a = F_a_x1y1 + increment_pot + increment_layer
```

```
End If
```

```
End Function
```

Annex H Additional effective volumes

We want to equate the volume of which a cut is shown in Figure H-1. For this, we need h_k , h_l , d and h .

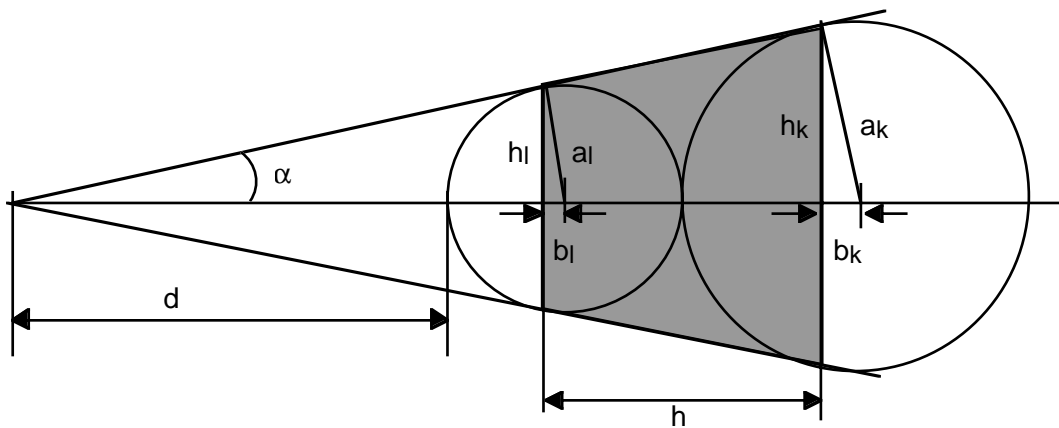


Figure H-1. Truncated cone inscribed in the common tangents to spheres S_k and S_l .

We can write $\sin(\alpha)$ as :

$$\sin \alpha = \frac{a_k}{a_k + 2a_l + d} = \frac{a_l}{a_l + d} \quad [\text{H-1}]$$

Which gives for d :

$$\begin{aligned}
 a_k a_l + a_k d &= a_k a_l + 2a_l^2 + a_l d \\
 d &= \frac{2a_l^2}{a_k - a_l}
 \end{aligned}
 \tag{H-2}$$

We can rewrite $\sin(\alpha)$ as :

$$\begin{aligned}
 \sin \alpha &= \frac{a_k}{a_k + 2a_l + d} = \frac{a_k}{a_k + 2a_l + \frac{2a_l^2}{a_k - a_l}} \\
 &= \frac{a_k(a_k - a_l)}{a_k^2 - a_k a_l + 2a_k a_l - 2a_l^2 + 2a_l^2} \\
 &= \frac{a_k(a_k - a_l)}{a_k(a_k + a_l)} = \frac{a_k - a_l}{a_k + a_l}
 \end{aligned}
 \tag{H-3}$$

However, $\sin(\alpha)$ is also given by b_l/a_l , so we get :

$$b_l = a_l \frac{a_k - a_l}{a_k + a_l}
 \tag{H-4}$$

This allows us to determine the radius h_l of the upper base of the cone :

$$\begin{aligned}
 h_l &= \sqrt{a_l^2 - b_l^2} = a_l \sqrt{1 - \left(\frac{a_k - a_l}{a_k + a_l}\right)^2} = \frac{a_l}{a_k + a_l} \sqrt{(a_k + a_l)^2 - (a_k - a_l)^2} \\
 &= \frac{2a_l \sqrt{a_k a_l}}{a_k + a_l}
 \end{aligned}
 \tag{H-5}$$

In a similar way we can get h_k , since $\sin(\alpha)$ is also given by b_k/a_k :

$$h_k = \sqrt{a_k^2 - b_k^2} = a_k \sqrt{1 - \left(\frac{a_k - a_l}{a_k + a_l}\right)^2} = \frac{2a_k \sqrt{a_k a_l}}{a_k + a_l}
 \tag{H-6}$$

Note that $h_k/h_l = a_k/a_l$ as expected.

We now need the volume of the truncated cone having circular end surface , with radius h_k and h_l respectively.

The height h of this volume is given by :

$$\begin{aligned} h &= \frac{a_k - a_l}{a_k} (a_k + 2a_l + d) = \frac{a_k - a_l}{a_k} \left(a_k + 2a_l + \frac{2a_l^2}{a_k - a_l} \right) & [\text{H-7}] \\ &= \frac{1}{a_k} (a_k^2 - a_k a_l + 2a_k a_l - 2a_l^2 + 2a_l^2) = \frac{1}{a_k} (a_k^2 + a_k a_l) \\ &= a_k + a_l \end{aligned}$$

$$\begin{aligned} V &= \frac{\pi}{3} (a_k + a_l) (a_k^2 + a_k a_l + a_l^2) = \frac{\pi}{3} (a_k + a_l)^3 - \frac{\pi}{3} (a_k + a_l) a_k a_l & [\text{H-8}] \\ &= \frac{8\pi}{3} \hat{a}^3 - \frac{2\pi}{3} \hat{a}^2 \bar{a} = \frac{2\pi}{3} \hat{a}^2 (4\hat{a} - \bar{a}) \end{aligned}$$

Curriculum

Robert Johann FLATT

Date of Birth July 23rd 1969

Nationality Swiss and British

Background 1989 - 1994 Chemical Engineering, Swiss Federal Institute of Technology (S.F.I.T), Lausanne, Switzerland.

- Third year at Carnegie Mellon University (C.M.U), Pittsburgh PA, U.S.A.
- Academic distinction : Dean's list Mellon College of Science
- Undergraduate research project at the Research Center on the Materials for the Artist and Conservator, Mellon Institute, C.M.U. Title: **“Paint pigment analysis by reflective visible range spectroscopy in paintings by Andy Warhol”**.
- Undergraduate thesis done at the *Centre de Géochimie de la Surface* of the *Centre National de la Recherche Scientifique* in Strasbourg, France. Title: **“Modelling of the alteration of the Bern sandstone and the Jaumont limestone: role of sulfur dioxide and fly-ash”**

1986 - 1989 *Gymnase de la Cité*, Lausanne, Switzerland.

- Drawing prize for sculpture portfolio, summer class competition.
- Academic award for final exam results.

Professional experience 1996(2) – 1999(9) Laboratory of powder technology, department of materials science, S.F.I.T, , Lausanne, Switzerland

Ph.D thesis - **“Interparticle forces and superplasticizers in cement suspensions”**.

- Within European Eureka Program « Interaction of Cements with high range water reducers ».
- Knowledge applied with success to developing superfluid injection mortars for repair of roman mosaics.
- Attended the **advanced European course** on the “Sciences and technologies of the materials and environment for the protection of stained glasses and stone monuments” given within the European Commission program on Environment and Climate.

1995(7) – 1996(1) Laboratory of stone conservation, department of materials science, S.F.I.T, , Lausanne, Switzerland

Research Grant - **“Determination of alteration risks for *in-situ* conservation of roman mosaics”**.

- Funded by the department of archeology of the Canton of Vaud.

1994(7) – 1994(12) Laboratory of technical chemistry, department of chemistry, S.F.I.T, Lausanne, Switzerland.

Research Grant - “**Synthesis and study of stationary phases for ion exchange chromatography**”.

Special interests

Sculpture

- Attended university level classes in sculpture, using stone, plaster, bronze, aluminum, wax and clay.
- Presented two sculptures for a collective exhibition in 1997 at the art gallery *Gallerie de la Poste* in Riex, Switzerland.

Languages

English – Excellent knowledge (first language)

French – Excellent knowledge (mother tongue)

German – Good knowledge

Italian – Good knowledge

Spanish – Beginner’s level

Objectives

To develop a wide theoretical and practical knowledge of colloid science.

To apply this knowledge to the study of construction materials, looking at durability and restoration issues, in particular for the conservation of cultural heritage.

Interest in producing durable materials and repair materials.

Undergraduate projects supervised

“Elaboration of an injectable mortar for the restoration of a roman mosaic of the IIIrd century.”, Yan Huet and Benoit Petit, winter term 1998.

“*In Situ* conservation of the roman mosaics at the villa of Boscéaz (Orbe, Switzerland): preparation of an injectable repair mortar”, Stéphane Essade and Vincent von Niderhausern, spring term 1997.

“Synthesis of a γ -2CaO.SiO₂ powder”, Luciano Perez, winter term, 1997.

“Determination of the optimal conservation conditions for the roman mosaics of Orbe”, Jean François Despois and Collin Sanctuary, spring term 1996.

Oral presentations

« Influence of superplasticizer adsorption on the rheology of cement pastes » *RILEM international symposium on the role of admixtures in high performance concrete*, Monterrey, Mexico, 1999.

« In-situ conservation of roman mosaics at the villa of Boscéaz (Orbe, Switzerland) » *advanced European course on the “Sciences and technologies of the materials and environment for the protection of stained glasses and stone monuments”*, Paris, France, 1998.

« Mg-polynaphthalene sulfonate and its (adverse) role in cement processing », *72nd ACS Colloid & Surface Science Symposium*, University Park, U.S.A., 1998.

« Effect of superplasticizers in a highly alkaline model suspensions containing silica fume », *6th Canmet/ACI International Conference on Fly-Ash, Silica Fume, Slag and Natural Pozzolans in Concrete*, Bangkok, Thailand, 1998.

« Analysis of superplasticizers in concrete » *Annual Meeting of the "Groupe d'analyse chimique"*, Lausanne, Switzerland, 1997.

« In-situ conservation of the roman mosaics at the villa of Boscéaz (Orbe, Switzerland): a diagnosis of risks involved. » *Fall Meeting 1996 of the Materials Research Society, Materials Issues in Art and Archeology*, Boston, U.S.A., 1996.

« Interaction of superplasticizers with model powders in a highly alkaline medium », *5th Canmet/ACI International Conference on Superplasticizers and Other Chemical Admixtures in Concrete*, Rome, Italy, 1997.

« Adsorption of superplasticizers on model powders: temperature dependence, effect on zeta potential and role of chemical structure », *10th International Congress on the Chemistry of Cement*, Gothenburg, Sweden, 1997.

« Modelling of sulfur dioxide deposition on the Bern sandstone » *1995 LCP Congress on Preservation and Conservation of Cultural Heritage*, Montreux, Switzerland, 1995.

Publications

Houst Y. F., Flatt R.J., Bowen P., Hofmann H., Widmer J., Sulser U., Maeder U. and Bürge T.A. (1999), « New superplasticizers: from research to application », in *Modern concrete materials: binders additions and admixtures*. (editors Dhir R.K. and Dyer T.D.), Thomas Telford, London, pp. 445-456.

Houst Y. F., Flatt R.J., Bowen P., Hofmann H., Widmer J., Sulser U., Maeder U. and Bürge T.A. (1999), « Influence of superplasticizer adsorption on the rheology of cement pastes » *Proceedings of the RILEM international symposium on the role of admixtures in high performance concrete*. RILEM Publications s.a.r.l., Cachan, France, PRO 5, pp. 387-402.

Houst Y. F., Flatt R.J., Bowen P., Hofmann H., Widmer J., Sulser U., Maeder U. and Bürge T.A. (1999), « Optimisation of superplasticizers: from research to application » *Proceedings of the RILEM international symposium on the role of admixtures in high performance concrete*. RILEM Publications s.a.r.l., PRO 5, Cachan, France, pp.121-134.

Flatt R.J., Houst Y. F., Oesch R., Bowen P., Hofmann H., Widmer J., Sulser U., Maeder U., Bürge T.A. (1998) « Analysis of superplasticizers in concrete » *Analisis* **26** [2], pp. M28-M35.

Flatt R.J., Houst Y.F., Bowen P., Hoffmann H., Widmer J., Sulser U., Maeder U., Bürge T.A. (1998) « Effect of superplasticizers in a highly alkaline model suspensions containing silica fume », *Proceedings of the 6th Canmet/ACI International Conference Fly-Ash, Silica Fume, Slag and Natural Pozzolans in Concrete*, (editor: Malhotra V.M.), American Concrete Institute, Detroit, SP-178. pp. 911-930.

Flatt R. J., Girardet F.J., Weidmann D.C. (1997) « In-situ conservation of the roman mosaics at the villa of Boscéaz (Orbe, Switzerland): a diagnosis of risks involved. » *Mat. Res. Soc. Symp. Proc.* **462**, pp. 317-322.

Flatt R.J., Houst Y.F., Bowen P., Hofmann H., Widmer J., Sulser U., Maeder U., Bürge T.A. (1997) « Interaction of superplasticizers with model powders in a highly alkaline medium », *Proceedings of the 5th Canmet/ACI International Conference on Superplasticizers and Other Chemical Admixtures in Concrete* (editor: Malhotra V.M.), American Concrete Institute, Detroit, SP-173. pp. 743-762.

Flatt, R.J., Houst, Y.F., Bowen, P., Hofmann, H., Widmer, J., Sulser, U., Maeder, U., Bürge, T.A., (1997) « Adsorption of superplasticizers on model powders: temperature dependence, effect on zeta potential and role of chemical structure », *Proceedings of the 10th International Congress on the Chemistry of Cement*, V. 3, (editor: H.J. Justness), paper 3iii002.

Flatt R.J., Girardet F.J., Crovisier J.-L. (1996) « Modelling of sulfur dioxide deposition on the Bern sandstone » *Proceedings of the 1995 LCP Congress on Preservation and Conservation of Cultural Heritage* (editor: Pancella R.), Atelier de Reprographie EPFL, Lausanne, pp. 401-406.

Weidmann D., Flatt R.J., Félix C., Girardet F.J., Glauser A. (1996) « Analyse des altérations et déformation des mosaïques à Orbe-Boscéaz (Canton de Vaud, Suisse). » *Proceedings of the Sixth International Committee for the Conservation of Mosaics*, (to be published).